UNIVERSITY OF LIVERPOOL

Climatological Controls on Stratification and Phytoplankton Variability in a Temperate Continental Shelf Sea

Thesis submitted in accordance with the requirements of the University of Liverpool for the degree of

Doctor in Philosophy

by

Jennifer Elizabeth Jardine

May 2020

in the
Faculty of Science and Engineering
School of Environmental Sciences
Department of Earth, Ocean and Ecological Sciences

ABSTRACT

Climatological Controls on Stratification and Phytoplankton Variability in a Temperate Continental Shelf Sea

Jennifer Elizabeth Jardine

Continental shelf seas are some of the most valuable ecosystems on the planet, sustaining half of the world's fisheries and acting as a significant contributor to the biological carbon pump. During the winter months, the combination of convection, wind and tidal stresses results in a homogenous water column, where phytoplankton growth is limited by light. Only towards spring, when positive buoyancy inputs outcompete mixing from winds, waves and tides, will the spring bloom occur. On the Northwest European Shelf, the current paradigm is that the buoyancy control on water-column structure is dominated by thermal inputs. Yet, despite its position beneath the North Atlantic Storm Track, there has been little investigation into the buoyancy inputs from rain.

The aim of this thesis is to fully assess the role of rainfall, and by extension the large-scale climatological controls, on the seasonal stratification of a temperate continental shelf sea, and the associated implications on phytoplankton variability and ecosystem functioning.

In this thesis, we present a new physical trigger mechanism for the onset of seasonal stratification. A quantitative assessment of the energy budget revealed seasonal stratification to be initially triggered by a positive buoyancy input from rain. Multidecadal analysis from 1982 to 2015 further demonstrated that seasonal stratification in 30 out of 34 years were triggered by similar storm events. A twofold increase in the variability of stratification onset dates from the mid-1990s is observed, coinciding with a phase shift from a negative to a positive Atlantic Multidecadal Oscillation.

We further show that sporadic winter rain events can produce short-lived periods of ephemeral stratification, only persisting up to two days. Despite the short duration of these events, the

formation of a non-limiting light environment resulted in patches of enhanced phytoplankton growth. A gradual increase in chlorophyll concentrations throughout February and March 2015 eludes that such winter stratification events may act to sustain phytoplankton populations throughout the winter period.

Finally, analysis of multidecadal, coupled model data from 1998 to 2015 displays established periods of stratification that are sustained for up to two weeks, supporting enhanced phytoplankton growth. This stratification is both formed and eroded by extreme storms, yet such events allow phytoplankton populations to be maintained until seasonal stratification is triggered. Up to 22% of spring phytoplankton growth can occur in these prebloom periods, before the onset of seasonal stratification. Future work will continue to study the climatological controls on bio-physical interactions upon the shelf, especially in relation to cross-shelf fluxes between contrasting climatological modes.

Contents

List of Figures

List of Tables

Acknowledgements

I would like to thank my supervisors, Matthew Palmer, Claire Mahaffey and Jason Holt, for their continued guidance and support throughout my PhD. Special thanks to Matthew, for all your enthusiasm, help and continued patience in all aspects of my PhD. Claire, thank you for all your guidance with the nitty-gritty aspects of shelf sea biogeochemistry, and with my seemingly endless questions about nutrient stoichiometry. Special thanks also go to Jason and Sarah Wakelin, not only for your support with the ins and outs of NEMO-ERSEM, but also for your continued patience both throughout my PhD and with my current postdoctoral position, which I started before my thesis submission. Thank you for the sponsorship from Adam Mellor, at the Agri-Food and Biosciences Institute, throughout my PhD.

Thanks also to my collaborators: André Düsterhaus for your guidance on the large-scale climatological modes, the MARS glider team for the technical aspects of glider deployments, Charlotte Williams for the glider data processing, and Tom Hull for the Smartbuoy data and all my questions that came with it. Huge thanks also go to Juliane Wihsgott, for your continued help with air-sea fluxes and ECMWF data.

I would also like to thank my PhD colleagues, both in and out of Nicholson Office 205, for all the laughs, drinks and burritos over the last few years. Thanks also to Julie Samson, for your continued support outside of working hours, and DTP karaoke nights.

I am incredibly grateful to my parents, who have supported me throughout my PhD and beyond. And finally, thanks to Adrian, who never failed to make me laugh after a long day.

Declaration

I hereby certify that this thesis constitutes my own product, that where the language of others is set forth, quotation marks so indicate, and that appropriate credit is given where I have used the language, ideas, expressions or writings of another.

I declare that the thesis describes original work that has not previously been presented for the award of any other degree of any institution.

Jennifer Elizabeth Jardine

1. Introduction to continental shelf seas

Continental shelf seas are arguably one of the most important ecosystems on the planet. Covering a global area of 25 million km^2, they only account for 7-9% of the total surface area of the ocean yet support up to 30% of the global oceanic primary productivity (Wollast, 1998; Tweddle et al 2013). Shelf seas also have a large economic and societal importance by supporting over 90% of the global fisheries (Pauly et al, 2002). Globally, approximately 50% (e.g. Field et al, 1998) of all oxygen production is a result of phytoplankton: microscopic algae that, like all plants, use a combination of light and nutrients for photosynthesis. Forming the base of all oceanic food webs (Fenchel, 1988; Sherr and Sherr, 1991; Frederiksen et al, 2006), phytoplankton underpin the US$143 billion of the global fishing industry (FAO, 2018), providing sustenance for the 4.5 billion people who rely on fish for 15% of their protein intake (Béné et al, 2015). As the global demand for fish is predicted to increase 20% over the next decade (FAO, 2018), a multi-disciplinary approach to understanding this dynamic environment is pivotal for understanding how anthropogenic activity will impact shelf sea regimes in the future.

In this chapter, the climatological controls that underpin the physical and biogeochemical processes in temperate shelf seas will be introduced.

1.1 What are the physical controls on shelf seas?

Conventionally, shelf seas are defined as the transition between the continental shelf and the deep ocean. The outer edge of shelf seas is typically defined by a ~200m isobath, forming the boundary of an area of steep topography known as the shelf break, which acts to separate the relatively shallow coastal seas from the deep ocean in as little distance as 4km (Simpson and Sharples, 2012). As such, shelf seas act as a buffer between land and the deep ocean, dissipating a high proportion of oceanic energy that results in vigorous mixing at the shelf break (Pingree

and Mardell, 1997; Green et al 2008; Sharples et al, 2009) and mediating the flux of nutrients (e.g. nutrients, carbon) between the two boundaries (Huthnance 1995, Liu et al 2000).

In temperate regions, the vertical density structure of a shelf sea is controlled by the delicate balance of buoyancy, from surface heating and freshwater inputs, and mixing process driven by convection, wind and tidal stresses. Over much of the shelf, net cooling from the ocean surface during the winter months combined with high winter winds, results in a homogenous water-column where properties are uniform from the surface to depth. This winter homogeneity does not always occur in near-coastal environments, such as estuaries, where large buoyancy inputs from riverine outflow maintain vertical density (salinity) gradients throughout the year.

Further towards spring, as surface net heating increases whilst winter winds subside, positive buoyancy inputs may be sufficient to outcompete the mixing processes, resulting in seasonal stratification. Initially, stratification is very weak and easily eroded by sporadic inputs of wind energy (e.g. Sharples et al 2006). In shallow areas with strong tidal currents, tidal mixing can outcompete the buoyancy flux from solar heating, resulting in a well-mixed water column throughout the year. In deeper areas, or regions where the tidal currents are relatively low, buoyancy fluxes tend to dominate and so sustained stratification occurs.

As surface heating continues to increase, thermal stratification strengthens until there is a thermocline, forming defined surface and bottom mixed layers that are largely isolated from each other during warmer months. At the thermocline, mixing is enhanced by variations in the spring-neap tidal cycle (Sharples et al, 2007; Sharples et al, 2013; Zhao et al, 2019), near-inertia motions (Rippeth et al, 2005), wind stress (e.g. Williams et al, 2013; Palmer et al, 2013), and variable bathymetry (Moum and Nash, 2000; Palmer et al, 2013) that support localised patches of enhanced productivity (e.g. Palmer et al, 2013; Davidson et al 2013). Seasonal stratification remains until a combination of net cooling and wind stress towards autumn gradually erodes the seasonal thermocline (Pingree et al 1976; Townsend et al, 2015; Wihsgott et al, 2018), with wind effects largely dominating throughout the winter period (Wihsgott et al, 2018).

Tidal forcing is a significant source of mixing and ventilation in shelf seas (Simpson, 1998). Despite there being approximately 400 different tidal constituents (Simpson and Sharples,

2012), the semi-diurnal M2 tide accounts for over two-thirds of the global tidal dissipation (Egbert and Ray, 2001). Much of the tidal energy comes from the deep ocean, which ultimately crosses the shelf break and amplifies (Simpson, 1998). At the shelf break, the interaction between a stratified flow and changeable topography results in this internal tide to break, forming non-linear solitons that propagate onto the shelf (Inall et al, 2000; Rippeth and Inall, 2002; Sharples et al, 2007). It is this enhanced shelf break mixing, specifically during the spring and summer, that supports shelf-edge primary productivity (Pingree and Mardell, 1997; Sharples et al, 2013). Despite the strong mixing at the shelf break, energy from these breaking internal waves typically only propagate up to 30km on-shelf before dissipating (Green et al, 2008). Further on-shelf, internal waves can be generated by flow over variable topography (e.g. Baines, 1973; Chen et al, 2013; Palmer et al, 2013). Nevertheless, tidal energy dissipation in shelf seas accounts for 70% of the total oceanic energy dissipation (Egbert and Ray, 2000).

1.2 How does the physics impact biogeochemistry?

On an annual scale, the broad cycle of phytoplankton variability in temperate regimes is largely understood, being dominated by the spring bloom: a large-scale biological event that acts to resupply the marine ecosystem with organic matter (Sharples, 2008). The general paradigm for the onset of the spring bloom is based on the principle that phytoplankton need adequate light and nutrients to grow. In the winter months, as the water column is homogenised, turbulence rapidly transports phytoplankton in and out of the euphotic zone, limiting light and inhibiting growth despite replete nutrients (Sverdrup, 1953; Townsend et al, 1992; Townsend et al, 1994; Franks, 2014). Only when phytoplankton are retained in the euphotic zone for prolonged periods will exponential phytoplankton growth occur (Sverdrup, 1953; Townsend et al, 1992; Taylor and Ferrari, 2011). Other concepts to explain the spring bloom include the relaxation of turbulent mixing, particularly in less turbid regimes, which results in net phytoplankton growth rates in the upper water column exceeding vertical mixing rates (Huisman et al, 1999). Other hypotheses to explain net phytoplankton growth also include the recoupling-dilation hypothesis (Behrenfeld, 2010), whereby grazing pressure on phytoplankton is reduced when the mixed layer is deep. The shutdown of convective mixing (Taylor and Ferrari, 2011) and local decreases in wind stress (Chiswell, 2011; Chiswell et al, 2013) have also been postulated

to increase net phytoplankton growth by maintaining cells in the euphotic zone. In temperate shelf seas, net phytoplankton growth usually occurs at the spring onset of seasonal stratification, as phytoplankton are retained in the well-lit surface mixed layer.

The spring bloom is a vital component of shelf sea biogeochemical cycles. Firstly, it has been shown that both the timing and quality of the spring bloom is essential for fish recruitment (e.g. Cushing et al, 1974; Cushing et al, 1990; Platt and Sathyendranath, 1996; Platt et al, 2003). Secondly, the spring bloom is a key component of the biological carbon pump: the mechanism by which carbon is exported into the deep ocean. Continental shelf seas play an important part in this process, contributing to ~20% of the total anthropogenic carbon uptake (Thomas et al, 2004).

The spring bloom has a distinct phytoplankton succession, with the larger, fast-growing and more opportunistic species such as diatoms (Margalef, 1978; Smayda and Reynolds, 2001; Gilbert, 2016) dominating the start of the spring bloom period (Rees et al, 1999; Needham and Fuhrman, 2016). These are then succeeded by smaller species of phytoplankton, such as dinoflagellates, that thrive in the low nutrient, highly stratified regions typical of a summer shelf sea (Holligan, 1984; Hickman et al, 2009; Gilbert, 2016; McQuatters-Gollop et al, 2007). In terms of fisheries, the spring bloom is a vital part of the fish spawning cycle, with many species timing their spawning cycles to the onset of the spring bloom (Cushing, 1973; Cushing, 1990; Platt et al, 2003). The fact that diatoms encompass a significant portion of the spring bloom is beneficial to grazing species, as they are considered high-quality food items (Legendre, 1990; Jónasdóttir and Kiørboe, 1996) and form the base of the copepod-fish food web (Verity and Smetacek 1996). More so, the increased sinking velocity associated with large-celled diatoms makes them significant contributors to the biological pump (Ducklow et al, 2001; Tréguer et al, 2017).

Following the spring bloom, nutrients become depleted in the surface layer, with estimates representing a 98%, 85% and 75% reduction in nitrate, silicate and phosphate respectively (Pingree et al, 1976). As a consequence of this nutrient depletion, phytoplankton congregate at the base of the pycnocline in a subsurface chlorophyll maximum (SCM; Pingree et al, 1982) and utilise nutrients that are mixed from the bottom mixed layer due to turbulent dissipation (Palmer et al, 2013) or wind-driven nutrient pulses (Williams et al, 2013). The presence of this

thermocline effectively separates net production above from net respiration below and can act as a mechanism for carbon export off the shelf and into the deep ocean (e.g. Thomas et al, 2004). New production in the SCM is estimated to be half that of the spring bloom (Hickman et al, 2009), and is a direct control on the carbon fluxes in temperate shelf seas (Kitidis et al, 2012).

During the autumnal breakdown of stratification, there is a flux of nutrients into the surface layer. Phytoplankton populations are no longer limited by nutrients and there is another exponential increase of phytoplankton that can be of similar magnitude to the peak chlorophyll biomass recorded during the spring bloom (Wihsgott et al, 2018). Seasonal stratification is gradually eroded by a combination of high winds and convection, distributing phytoplankton over the entire water column. Despite the replenished nutrients, phytoplankton once again become light limited and their numbers continue to decrease. In areas inundated with riverine runoff, phytoplankton populations can still be maintained over the winter period, as cells are kept in the euphotic zone (Labry et al, 2001).

1.3 What are the meteorological controls on a shelf sea?

Given their shallow depth and subsequent low volume (0.5% of the world's oceans; Simpson and Sharples, 2012), shelf seas are rapidly affected by meteorological conditions. It has already been stated that wind stress acts as a control on the level of mixing and can directly impact both the physics and biogeochemistry of a shelf sea throughout the annual cycle.

As expected, the impact of meteorology on shelf seas is highly regional and depends on the location of the shelf sea. In this thesis, the area of focus is the Northwest (NW) European Shelf – a large expanse of continental shelf that sits directly beneath the North Atlantic Storm Track (Woollings et al, 2010). The NW European Shelf experiences storms year-round, resulting in high winds and rainfall that can directly influence the shelf sea physics and ecosystem. Although storms do occur in summer, fuelling new production through diapycnal nutrient flux (e.g. Williams et al, 2013; Davis et al, 2014), the majority of storms occur throughout the winter period.

In both shelf and open ocean regimes, winter storms can directly affect the timing of seasonal stratification and the subsequent timing and duration of the spring phytoplankton bloom (Waniek, 2003; Waniek and Holliday, 2006; Henson et al, 2006; Sharples et al, 2006). Storms further affect phytoplankton variability through changes in the light environment. Aside from higher winds resulting in more vigorous vertical mixing (Townsend et al, 1994; Henson et al, 2006), storms can act both to reduce and increase phytoplankton growth through increasing turbidity and halostratification from enhanced riverine runoff (Gohin et al, 2015).

Another cause of meteorological variability over the NW European Shelf are atmospheric rivers (Newell et al, 1982; Zhu and Newell, 1988): narrow corridors in the atmosphere that transport moisture from the tropics into extratropical regions (Zhu and Newell, 1998; Gimeno et al, 2014), so named due to volumetric flow rates comparable to the Amazon River (Newell et al, 1992). This has the potential to deliver large amounts of rainfall over NW Europe, with extreme UK flood events being linked to such occurrences (e.g. Lavers et al, 2012; Lavers and Viliarini, 2013). The influence of increased buoyancy from rainfall has been explored in subtropical (Price, 1979; Anderson et al, 1996) and monsoonal regions (Kromkamp et al, 1997), yet the influence of rain events on stratification has been largely discounted over the NW European shelf (e.g. Simpson and Hunter, 1974). Pingree et al (1976) postulated that buoyancy input from a rain event could trigger stratification during critical transition periods, while others speculated that rain-induced stratification could result in episodic phytoplankton growth (Franks, 2014). Despite this, rain is often considered negligible as a primary or important physical forcing mechanism (e.g. Simpson and Hunter, 1974; Rumyantseva et al, 2015).

1.3.1 The North Atlantic Oscillation

The North Atlantic Oscillation (NAO) is a highly variable mode of climatic variability that is often considered to be the dominant mode of meteorological variability across the North Atlantic (Hurrell 1995; Marshall *et al,* 2001; Hurell and Deser, 2009). Defined as the pressure difference between Iceland and the Azores, the transition from one NAO phase to another

directly impacts the North Atlantic wind speed and direction, heat and moisture transport and the storm track position and intensity (Pinto et al, 2009; Hurrell et al, 2003). Therefore, it could be argued that the NAO has large socio-economic impacts that include droughts (Vincente-Serrano et al, 2011), disruption from extreme snowfall (Seager et al, 2010), changes in sea level (Wakelin et al, 2003), flood events (Salguerio et al, 2013; Huntingford et al, 2014) and even wave power supply (Neill and Hashemi, 2013).

Although the impacts of the NAO are present throughout the year (e.g. Dong et al, 2013), the NAO is in its most prominent phase during the winter months (Hurrell et al, 2003). This has implications for shelf sea physics. For example, Sharples et al (2006) demonstrated that a delayed spring bloom onset date resulted from an increase in wind stress associated with positive phases of the NAO, and Sheehan et al (2017) identified negative correlation between the NAO and transport into the northern North Sea.

1.3.2 The Atlantic Multidecadal Oscillation

The Atlantic Multidecadal Oscillation (AMO; Kerr, 2000) represents the relative warming or cooling of the North Atlantic relative to long-term trends, with a periodicity of approximately 60-80 years and an amplitude of $\pm 0.4^{o}C$ (Knight et al, 2006; Alexander et al, 2014). The cycling from negative (cooler) to positive (warmer) phases has allowed intrinsic links to be made between the AMO and various meteorological properties across the oceanic basin. For example, during positive AMO phases, there is both increased rainfall over Northwest Europe (Sutton and Hodson, 2005) and increased hurricane activity over the whole of the North Atlantic (Goldenberg et al, 2001). The opposite is true during negative AMO phases, with favourable conditions for cyclogenesis also reported in the mid-latitude region of the North Atlantic (Gomara-Cardalliaguet et al, 2012).

In this study, Vellinga and Wu (2004) demonstrated that the AMO stemmed from variations in the thermohaline circulation (THC). Anomalously strong periods of the THC resulted in a northward shift in an intensified Intertropical Convergence Zone (ITCZ) and created a low salinity anomaly due to enhanced rainfall. Following a northward propagation period of ~55

years, this freshwater reached the THC, weakens it, and thus the AMO shifts to the opposite phase.

While climatological extremes have been linked to AMO phases across the North Atlantic (e.g. Goldenberg et al, 2001), our understanding of the influence the AMO has on shelf sea systems is limited. However, with the rate of warming averaging ~0.15^{o}C per decade (Folland et al, 2001), the current relatively warm (positive) phase of the AMO offers a valuable insight into how shelf seas might respond to future anthropogenic climate change.

1.4 Key questions

From this brief review, it is clear that shelf seas play a large role in the marine ecosystem and the biosphere. Of particular importance is the spring bloom, a precursor of which is the onset of seasonal stratification. The onset of both stratification and the spring bloom on the NW European Shelf is directly affected by meteorological variability, given its position beneath the North Atlantic Storm Track and the associated influence from large-scale climatological oscillations.

While the impact of enhanced wind stress has received considerable attention (e.g. Simpson and Hunter, 1974; Waniek, 2003; Sharples et al, 2006) the positive buoyancy input from rainfall has been overshadowed by the other sources of freshwater input, such as riverine runoff. The vast majority of the NW European shelf is, however, remote from the direct influence of riverine runoff and so the impact of rainfall at critical moments, such as the winter-spring transition, demand more investigation.

In this thesis, the key questions that will be addressed are:

1. What is the influence of local meteorological conditioning the onset of seasonal stratification on the NW European Shelf?
2. How do sporadic rainfall events throughout winter influence winter phytoplankton growth?

3. What is the climatological link between the onset of rain-induced seasonal stratification and the large-scale, long-term variability in the North Atlantic?
4. What are the biogeochemical implications for the onset, magnitude and composition of the spring phytoplankton bloom in different climatological phases?

1.5 Thesis Structure

An extensive collection of observational and model data were used throughout this thesis. **Chapter 2** provides a review of the instruments used to collect observational data, as well as a brief overview of the coupled hydrodynamic-biogeochemical models. The air-sea flux equations and a mathematical description of buoyancy controls are also described.

Using a combination of observational and model data, **Chapter 3** presents a new physical forcing mechanism for the onset of seasonal stratification in a temperate shelf sea. This chapter further looks at the climatological variability of stratification from 1982 to 2015.

Chapter 4 focusses on ephemeral rain-induced stratification events throughout the winter period, before the onset of seasonal stratification. Using observational data only, this chapter explores when such sporadic, short-term stratification events can promote phytoplankton growth and/or sustain phytoplankton populations over the winter period.

Using entirely model output, **Chapter 5** builds upon the results from Chapters 3 and 4 and investigates the biogeochemical response of four different phytoplankton functional groups between contrasting climatological modes.

Chapter 6 synthesises the results and conclusions presented throughout this thesis and recommendations for future work.

Appendix 1 reviews the routines used in the processing toolbox that corrected and calibrated the glider data.

Appendix 2 reviews the key routines and parameterisations in the CO5 configuration of the AMM7 NEMO-ERSEM model.

Appendix 3 is a first assessment of the nutrient behaviour in the model, validated with observed nutrient concentrations. Results from these analyses remained inconclusive, however it has been included at the end of this thesis for completion.

1.6 References

Alexander, M.A., Kilbourne, K.H. and Nye, J.A., 2014. Climate variability during warm and cold phases of the Atlantic Multidecadal Oscillation (AMO) 1871–2008. *Journal of Marine Systems*, *133*, pp.14-26.

Anderson, S.P., Weller, R.A. and Lukas, R.B., 1996. Surface buoyancy forcing and the mixed layer of the western Pacific warm pool: Observations and 1D model results. *Journal of Climate*, *9*(12), pp.3056-3085.

Baines, P.G., 1973, February. The generation of internal tides by flat-bump topography. In *Deep Sea Research and Oceanographic Abstracts* (Vol. 20, No. 2, pp. 179-205). Elsevier

Behrenfeld, M.J., 2010. Abandoning Sverdrup's critical depth hypothesis on phytoplankton blooms. *Ecology*, *91*(4), pp.977-989.

Béné, C., Barange, M., Subasinghe, R., Pinstrup-Andersen, P., Merino, G., Hemre, G.I. and Williams, M., 2015. Feeding 9 billion by 2050–Putting fish back on the menu. *Food Security*, *7*(2), pp.261-274.

Chiswell, S.M., 2011. Annual cycles and spring blooms in phytoplankton: don't abandon Sverdrup completely. *Marine ecology progress series*, *443*, pp.39-50.

Chiswell, S.M., Bradford-Grieve, J., Hadfield, M.G. and Kennan, S.C., 2013. Climatology of surface chlorophyll a, autumn-winter and spring blooms in the southwest Pacific Ocean. *Journal of Geophysical Research: Oceans*, *118*(2), pp.1003-1018.

Chen, Z.W., Xie, J., Xu, J., Zhan, J.M. and Cai, S., 2013. Energetics of nonlinear internal waves generated by tidal flow over topography. *Ocean Modelling*, *68*, pp.1-8.

Cushing, D.H., 1973. The natural regulation of fish populations. *Sea fisheries research*.

Cushing, D.H., 1990. Plankton production and year-class strength in fish populations: an update of the match/mismatch hypothesis. In *Advances in marine biology* (Vol. 26, pp. 249-293). Academic Press.

Davidson, K., Gilpin, L.C., Pete, R., Brennan, D., McNeill, S., Moschonas, G. and Sharples, J., 2013. Phytoplankton and bacterial distribution and productivity on and around Jones Bank in the Celtic Sea. *Progress in oceanography*, *117*, pp.48-63.

Davis, C.E., Mahaffey, C., Wolff, G.A. and Sharples, J., 2014. A storm in a shelf sea: Variation in phosphorus distribution and organic matter stoichiometry. *Geophysical Research Letters*, *41*(23), pp.8452-8459.

Dong, B., Sutton, R.T., Woollings, T. and Hodges, K., 2013. Variability of the North Atlantic summer storm track: mechanisms and impacts on European climate. *Environmental Research Letters*, *8*(3), p.034037.

Ducklow, H.W., Steinberg, D.K. and Buesseler, K.O., 2001. Upper ocean carbon export and the biological pump. *Oceanography*, *14*(4), pp.50-58.

Egbert, G.D. and Ray, R.D., 2000. Significant dissipation of tidal energy in the deep ocean inferred from satellite altimeter data. *Nature*, *405*(6788), p.775.

Egbert, G.D. and Ray, R.D., 2001. Estimates of M2 tidal energy dissipation from TOPEX/Poseidon altimeter data. *Journal of Geophysical Research: Oceans*, *106*(C10), pp.22475-22502.

FAO. 2018. *The State of World Fisheries and Aquaculture 2018 - Meeting the sustainable development goals.* Rome. Licence: CC BY-NC-SA 3.0 IGO.

Fenchel, T., 1988. Marine plankton food chains. *Annual Review of Ecology and Systematics*, *19*(1), pp.19-38.

Field, C.B., Behrenfeld, M.J., Randerson, J.T. and Falkowski, P., 1998. Primary production of the biosphere: integrating terrestrial and oceanic components. *science*, *281*(5374), pp.237-240.

Folland, C.K., Karl, T.R., Christy, J.R., Clarke, R.A., Gruza, G.V., Jouzel, J., Mann, M.E., Oerlemans, J., Salinger, M.J. and Wang, S.W., 2001. Observed climate variability and change. Climate change 2001: the scientific basis. Contribution of Working Group I to the Third Assessment Report of the Intergovernmental Panel on Climate Change. *HoughtonJ, DingY, GriggsetD (eds). Cambridge University Press: New York*.

Franks, P.J., 2014. Has Sverdrup's critical depth hypothesis been tested? Mixed layers vs. turbulent layers. *ICES Journal of Marine Science*, *72*(6), pp.1897-1907.

Frederiksen, M., Edwards, M., Richardson, A.J., Halliday, N.C. and Wanless, S., 2006. From plankton to top predators: bottom-up control of a marine food web across four trophic levels. *Journal of Animal Ecology*, *75*(6), pp.1259-1268.

Gimeno, L., Nieto, R., Vázquez, M. and Lavers, D.A., 2014. Atmospheric rivers: A mini-review. *Frontiers in Earth Science*, *2*, p.2.

Glibert, P.M., 2016. Margalef revisited: a new phytoplankton mandala incorporating twelve dimensions, including nutritional physiology. *Harmful Algae*, *55*, pp.25-30.

Gohin, F., Bryère, P. and Griffiths, J.W., 2015. The exceptional surface turbidity of the North-West European shelf seas during the stormy 2013–2014 winter: Consequences for the initiation of the phytoplankton blooms?. *Journal of Marine Systems*, *148*, pp.70-85.

Goldenberg, S.B., Landsea, C.W., Mestas-Nuñez, A.M. and Gray, W.M., 2001. The recent increase in Atlantic hurricane activity: Causes and implications. *Science*, *293*(5529), pp.474-479.

Gómara, Í., Rodríguez Fonseca, B. and Zurita Gotor, P., 2012. Explosive cyclones in the North Atlantic: NAO influence and multidecadal variability. *Publicaciones de la Asociación Española de Climatología. Serie A; 8*.

Green, J.M., Simpson, J.H., Legg, S. and Palmer, M.R., 2008. Internal waves, baroclinic energy fluxes and mixing at the European shelf edge. *Continental Shelf Research*, *28*(7), pp.937-950.

Henson, S.A., Robinson, I., Allen, J.T. and Waniek, J.J., 2006. Effect of meteorological conditions on interannual variability in timing and magnitude of the spring bloom in the Irminger Basin, North Atlantic. *Deep Sea Research Part I: Oceanographic Research Papers*, *53*(10), pp.1601-1615.

Hickman, A.E., Holligan, P.M., Moore, C.M., Sharples, J., Krivtsov, V. and Palmer, M.R., 2009. Distribution and chromatic adaptation of phytoplankton within a shelf sea thermocline. *Limnology and Oceanography*, *54*(2), pp.525-536.

Holligan, P.M., leB. Williams, P.J., Purdie, D. and Harris, R.P., 1984. Photosynthesis, respiration and nitrogen supply of plankton populations in stratified, frontal and tidally mixed shelf waters. *Marine Ecology Progress Series*, pp.201-213.

Huisman, J.E.F., van Oostveen, P. and Weissing, F.J., 1999. Critical depth and critical turbulence: two different mechanisms for the development of phytoplankton blooms. *Limnology and oceanography*, *44*(7), pp.1781-1787.

Huntingford, C., Marsh, T., Scaife, A.A., Kendon, E.J., Hannaford, J., Kay, A.L., Lockwood, M., Prudhomme, C., Reynard, N.S., Parry, S. and Lowe, J.A., 2014. Potential influences on the United Kingdom's floods of winter 2013/14. *Nature Climate Change*, *4*(9), p.769.

Huntingford, C., Marsh, T., Scaife, A.A., Kendon, E.J., Hannaford, J., Kay, A.L., Lockwood, M., Prudhomme, C., Reynard, N.S., Parry, S. and Lowe, J.A., 2014. Potential influences on the United Kingdom's floods of winter 2013/14. *Nature Climate Change*, *4*(9), p.769.

Hurrell, J.W. and Deser, C., 2010. North Atlantic climate variability: the role of the North Atlantic Oscillation. *Journal of Marine Systems*, *79*(3-4), pp.231-244.

Hurrell, J.W., 1995. Decadal trends in the North Atlantic Oscillation: regional temperatures and precipitation. *Science*, *269*(5224), pp.676-679.

Hurrell, J.W., Kushnir, Y., Ottersen, G. and Visbeck, M., 2003. An overview of the North Atlantic oscillation. *Geophysical Monograph-American Geophysical Union*, *134*, pp.1-36.

Huthnance, J.M., 1995. Circulation, exchange and water masses at the ocean margin: the role of physical processes at the shelf edge. *Progress in Oceanography*, *35*(4), pp.353-431.

Inall, M.E., Rippeth, T.P. and Sherwin, T.J., 2000. Impact of nonlinear waves on the dissipation of internal tidal energy at a shelf break. *Journal of Geophysical Research: Oceans*, *105*(C4), pp.8687-8705.

Jónasdóttir, S.H. and Kiørboe, T., 1996. Copepod recruitment and food composition: do diatoms affect hatching success?. *Marine Biology*, *125*(4), pp.743-750.

Kerr, R.A., 2000. A North Atlantic climate pacemaker for the centuries. *Science*, *288*(5473), pp.1984-1985.

Kitidis, V., Hardman-Mountford, N.J., Litt, E., Brown, I., Cummings, D., Hartman, S., Hydes, D., Fishwick, J.R., Harris, C., Martinez-Vicente, V. and Woodward, E.M.S., 2012. Seasonal dynamics of the carbonate system in the Western English Channel. *Continental Shelf Research*, *42*, pp.30-40.

Knight, J.R., Folland, C.K. and Scaife, A.A., 2006. Climate impacts of the Atlantic multidecadal oscillation. *Geophysical Research Letters*, *33*(17).

Kromkamp, J., De Bie, M., Goosen, N., Peene, J., Van Rijswijk, P., Sinke, J. and Duinevel, G.C., 1997. Primary production by phytoplankton along the Kenyan coast during the SE monsoon and November intermonsoon 1992, and the occurrence of Trichodesmium. *Deep Sea Research Part II: Topical Studies in Oceanography*, *44*(6-7), pp.1195-1212.

Labry, C., Herbland, A., Delmas, D., Laborde, P., Lazure, P., Froidefond, J.M., Jegou, A.M. and Sautour, B., 2001. Initiation of winter phytoplankton blooms within the Gironde plume waters in the Bay of Biscay. *Marine Ecology Progress Series*, *212*, pp.117-130.

Lavers, D.A. and Villarini, G., 2013. The nexus between atmospheric rivers and extreme precipitation across Europe. *Geophysical Research Letters*, *40*(12), pp.3259-3264.

Lavers, D.A., Villarini, G., Allan, R.P., Wood, E.F. and Wade, A.J., 2012. The detection of atmospheric rivers in atmospheric reanalyses and their links to British winter floods and the large-scale climatic circulation. *Journal of Geophysical Research: Atmospheres*, *117*(D20).

Legendre, L., 1990. The significance of microalgal blooms for fisheries and for the export of particulate organic carbon in oceans. *Journal of plankton research*, *12*(4), pp.681-699.

Liu, K.K., Tang, T.Y., Gong, G.C., Chen, L.Y. and Shiah, F.K., 2000. Cross-shelf and along-shelf nutrient fluxes derived from flow fields and chemical hydrography observed in the southern East China Sea off northern Taiwan. *Continental Shelf Research*, *20*(4-5), pp.493-523.

Margalef, R., 1978. Life-forms of phytoplankton as survival alternatives in an unstable environment. *Oceanol. Acta 1*, 493–509.

Marshall, J., Kushnir, Y., Battisti, D., Chang, P., Czaja, A., Dickson, R., Hurrell, J., McCartney, M., Saravanan, R. and Visbeck, M., 2001. North Atlantic climate variability: phenomena, impacts and mechanisms. *International Journal of Climatology: A Journal of the Royal Meteorological Society*, *21*(15), pp.1863-1898.

McQuatters-Gollop, A., Raitsos, D.E., Edwards, M. and Attrill, M.J., 2007. Spatial patterns of diatom and dinoflagellate seasonal cycles in the NE Atlantic Ocean. *Marine Ecology Progress Series*, *339*, pp.301-306.

Moum, J.N. and Nash, J.D., 2000. Topographically induced drag and mixing at a small bank on the continental shelf. *Journal of Physical Oceanography*, *30*(8), pp.2049-2054.

Neill, S.P. and Hashemi, M.R., 2013. Wave power variability over the northwest European shelf seas. *Applied energy*, *106*, pp.31-46.

Newell, R.E., Newell, N.E., Zhu, Y. and Scott, C., 1992. Tropospheric rivers?–A pilot study. *Geophysical Research Letters*, *19*(24), pp.2401-2404.

Palmer, M.R., Inall, M.E. and Sharples, J., 2013. The physical oceanography of Jones Bank: A mixing hotspot in the Celtic Sea. *Progress in oceanography*, *117*, pp.9-24.

Palmer, M.R., Rippeth, T.P. and Simpson, J.H., 2008. An investigation of internal mixing in a seasonally stratified shelf sea. *Journal of Geophysical Research: Oceans*, *113*(C12).

Pauly, D., Christensen, V., Guénette, S., Pitcher, T.J., Sumaila, U.R., Walters, C.J., Watson, R. and Zeller, D., 2002. Towards sustainability in world fisheries. *Nature*, *418*(6898), p.689.

Pingree, R.D. and Mardell, G.T., 1981. Slope turbulence, internal waves and phytoplankton growth at the Celtic Sea shelf-break. *Philosophical Transactions of the Royal Society of London. Series A, Mathematical and Physical Sciences*, *302*(1472), pp.663-682.

Pingree, R.D., Holligan, P.M., Mardell, G.T. and Head, R.N., 1976. The influence of physical stability on spring, summer and autumn phytoplankton blooms in the Celtic Sea. *Journal of the Marine Biological Association of the United Kingdom*, *56*(4), pp.845-873.

Pingree, R.D., Mardell, G.T., Holligan, P.M., Griffiths, D.K. and Smithers, J., 1982. Celtic Sea and Armorican current structure and the vertical distributions of temperature and chlorophyll. *Continental Shelf Research*, *1*(1), pp.99-116.

Pinto, J.G., Zacharias, S., Fink, A.H., Leckebusch, G.C. and Ulbrich, U., 2009. Factors contributing to the development of extreme North Atlantic cyclones and their relationship with the NAO. *Climate dynamics*, *32*(5), pp.711-737.

Platt, T., Fuentes-Yaco, C. and Frank, K.T., 2003. Marine ecology: spring algal bloom and larval fish survival. *Nature*, *423*(6938), p.398.

Platt, T., Sathyendranath, S., 1996. Biological oceanography and fisheries management. *Int. Counc. Explor. Sea*, *900*, p.3.

Price, J.F., 1979. Observations of a rain-formed mixed layer. *Journal of Physical Oceanography*, *9*(3), pp.643-649.

Rippeth, T.P. and Inall, M.E., 2002. Observations of the internal tide and associated mixing across the Malin Shelf. *Journal of Geophysical Research: Oceans*, *107*(C4), pp.3-1.

Rippeth, T.P., Palmer, M.R., Simpson, J.H., Fisher, N.R. and Sharples, J., 2005. Thermocline mixing in summer stratified continental shelf seas. *Geophysical Research Letters*, *32*(5).

Rippeth, T.P., Palmer, M.R., Simpson, J.H., Fisher, N.R. and Sharples, J., 2005. Thermocline mixing in summer stratified continental shelf seas. *Geophysical Research Letters*, *32*(5).

Rumyantseva, A., Lucas, N., Rippeth, T., Martin, A., Painter, S.C., Boyd, T.J. and Henson, S., 2015. Ocean nutrient pathways associated with the passage of a storm. *Global Biogeochemical Cycles*, *29*(8), pp.1179-1189.

Seager, R., Kushnir, Y., Nakamura, J., Ting, M. and Naik, N., 2010. Northern Hemisphere winter snow anomalies: ENSO, NAO and the winter of 2009/10. *Geophysical research letters*, *37*(14).

Sharples, J., 2007. Potential impacts of the spring-neap tidal cycle on shelf sea primary production. *Journal of Plankton Research*, *30*(2), pp.183-197.

Sharples, J., Ellis, J.R., Nolan, G. and Scott, B.E., 2013. Fishing and the oceanography of a stratified shelf sea. *Progress in oceanography*, *117*, pp.130-139.

Sharples, J., Moore, C.M., Hickman, A.E., Holligan, P.M., Tweddle, J.F., Palmer, M.R. and Simpson, J.H., 2009. Internal tidal mixing as a control on continental margin ecosystems. *Geophysical Research Letters*, *36*(23).

Sharples, J., Ross, O.N., Scott, B.E., Greenstreet, S.P. and Fraser, H., 2006. Inter-annual variability in the timing of stratification and the spring bloom in the North-western North Sea. *Continental Shelf Research*, *26*(6), pp.733-751.

Sharples, J., Tweddle, J.F., Mattias Green, J.A., Palmer, M.R., Kim, Y.N., Hickman, A.E., Holligan, P.M., Moore, C.M., Rippeth, T.P., Simpson, J.H. and Krivtsov, V., 2007. Spring-neap modulation of internal tide mixing and vertical nitrate fluxes at a shelf edge in summer. *Limnology and Oceanography*, *52*(5), pp.1735-1747

Sherr, E.B. and Sherr, B.F., 1991. Planktonic microbes: tiny cells at the base of the ocean's food webs. *Trends in Ecology & Evolution*, *6*(2), pp.50-54.

Simpson, J.H. and Bowers, D., 1981. Models of stratification and frontal movement in shelf seas. *Deep Sea Research Part A. Oceanographic Research Papers*, *28*(7), pp.727-738.

Simpson, J.H. and Hunter, J.R., 1974. Fronts in the Irish sea. *Nature*, *250*(5465), p.404-406

Simpson, J.H. and Sharples, J., 2012. *Introduction to the physical and biological oceanography of shelf seas*. Cambridge University Press.

Simpson, J.H., 1998. Tidal processes in shelf seas. *The sea*, *10*, pp.113-150.

Smayda, T.J. and Reynolds, C.S., 2001. Community assembly in marine phytoplankton: application of recent models to harmful dinoflagellate blooms. *Journal of Plankton Research*, *23*(5), pp.447-461.

Sutton, R.T. and Hodson, D.L., 2005. Atlantic Ocean forcing of North American and European summer climate. *science*, *309*(5731), pp.115-118.

Sverdrup, H.U., 1953. On conditions for the vernal blooming of phytoplankton. *J. Cons. Int. Explor. Mer*, *18*(3), pp.287-295.

Taylor, J.R. and Ferrari, R., 2011. Shutdown of turbulent convection as a new criterion for the onset of spring phytoplankton blooms. *Limnology and Oceanography*, *56*(6), pp.2293-2307.

Thomas, H., Bozec, Y., Elkalay, K. and De Baar, H.J., 2004. Enhanced open ocean storage of CO2 from shelf sea pumping. *Science*, *304*(5673), pp.1005-1008.

Townsend, D.W., Cammen, L.M., Holligan, P.M., Campbell, D.E. and Pettigrew, N.R., 1994. Causes and consequences of variability in the timing of spring phytoplankton blooms. *Deep Sea Research Part I: Oceanographic Research Papers*, *41*(5-6), pp.747-765.

Townsend, D.W., Keller, M.D., Sieracki, M.E. and Ackleson, S.G., 1992. Spring phytoplankton blooms in the absence of vertical water column stratification. *Nature*, *360*(6399), p.59.

Townsend, D.W., Pettigrew, N.R., Thomas, M.A., Neary, M.G., McGillicuddy, J., Dennis, J. and O'Donnell, J., 2015. Water masses and nutrient sources to the Gulf of Maine. *Journal of marine research*, *73*(3-4), pp.93-122.

Tréguer, P., Bowler, C., Moriceau, B., Dutkiewicz, S., Gehlen, M., Aumont, O., Bittner, L., Dugdale, R., Finkel, Z., Iudicone, D. and Jahn, O., 2018. Influence of diatom diversity on the ocean biological carbon pump. *Nature Geoscience*, *11*(1), p.27.

Tweddle, J.F., Sharples, J., Palmer, M.R., Davidson, K. and McNeill, S., 2013. Enhanced nutrient fluxes at the shelf sea seasonal thermocline caused by stratified flow over a bank. *Progress in oceanography*, *117*, pp.37-47

Vellinga, M. and Wu, P., 2004. Low-latitude freshwater influence on centennial variability of the Atlantic thermohaline circulation. *Journal of Climate*, *17*(23), pp.4498-4511.

Verity, P.G. and Smetacek, V., 1996. Organism life cycles, predation, and the structure of marine pelagic ecosystems. *Marine Ecology Progress Series*, *130*, pp.277-293.

Vicente-Serrano, S.M., López-Moreno, J.I., Lorenzo-Lacruz, J., El Kenawy, A., Azorin-Molina, C., Morán-Tejeda, E., Pasho, E., Zabalza, J., Beguería, S. and Angulo-Martínez, M., 2011. The NAO impact on droughts in the Mediterranean region. In *Hydrological, socioeconomic and ecological impacts of the north Atlantic oscillation in the mediterranean region* (pp. 23-40). Springer, Dordrecht.

Wakelin, S.L., Woodworth, P.L., Flather, R.A. and Williams, J.A., 2003. Sea-level dependence on the NAO over the NW European Continental Shelf. *Geophysical Research Letters*, *30*(7).

Waniek, J.J. and Holliday, N.P., 2006. Large-scale physical controls on phytoplankton growth in the Irminger Sea, Part II: Model study of the physical and meteorological preconditioning. *Journal of Marine Systems*, *59*(3-4), pp.219-237.

Waniek, J.J., 2003. The role of physical forcing in initiation of spring blooms in the northeast Atlantic. *Journal of Marine Systems*, *39*(1-2), pp.57-82.

Wihsgott, J.U., Sharples, J., Hopkins, J.E., Woodward, E.M.S., Hull, T., Greenwood, N. and Sivyer, D.B., 2019. Observations of vertical mixing in autumn and its effect on the autumn phytoplankton bloom. *Progress in Oceanography*.

Wollast, R., 1998. Evaluation and comparison of the global carbon cycle in the coastal zone and in the open ocean. *The sea*, *10*, pp.213-252

Zhao, C., Daewel, U. and Schrum, C., 2019. Tidal impacts on primary production in the North Sea. *Earth System Dynamics*, *10*(2), pp.287-317.

Zhu, Y. and Newell, R.E., 1998. A proposed algorithm for moisture fluxes from atmospheric rivers. *Monthly weather review*, *126*(3), pp.725-735.

2. Methodology

This chapter outlines instruments used for observational data collection, as well as a brief overview on the model data used, including model validations to observations. A preliminary overview of the data is also presented, as well as key calculations used throughout this thesis.

2.1 Introduction to autonomous underwater gliders

Autonomous underwater gliders are instruments used to measure key ocean bio-physical parameters, recorded at spatial and temporal resolutions that cannot easily be reached using ship-based observational instruments. Conceptually visualised by Henry Stommel in 1989, a number of gliders have been developed since 1995 (Ghani and Abdullah, 2012), with the majority of deployments being covered by the Spray Glider (Sherman et al, 2001), Sea Glider (Ericsen et al, 2001) and the Slocum Glider (Webb et al, 2001). Designed for long duration missions of several months (Osse et al, 2007), one of the main advantages of using gliders for oceanographic data collection is that a glider is able to cover wide areas with relatively little cost and power consumption, they can be remotely operated by one or two members of staff and with relatively little infrastructure, and crucially they can be operational in severe weather, rough seas and remote locations (e.g. Aragon et al, 2015).

2.1.1. Slocum Gliders

The Teledyne Slocum Electric Glider (Slocum glider) was chosen for this mission as they are specifically tuned to shelf sea operations, such as a greater ability to inflect in relatively short spaces (30 to 200m; Meyer et al, 2016). Manoeuvring through subtle changes in buoyancy, Slocum gliders alter their volume by actively displacing water through the inflation/deflation of an external oil bladder (for deep water operations) or using a retractable piston (for shallow water operations) that creates an upward/downwards motion that the glider's drag and internal

ballast adjustments then convert into forwards motion. This allows them to glide through water in a trajectory resembling a sawtooth pattern (Fig. 2.1b). Slocum gliders routinely surface

a)

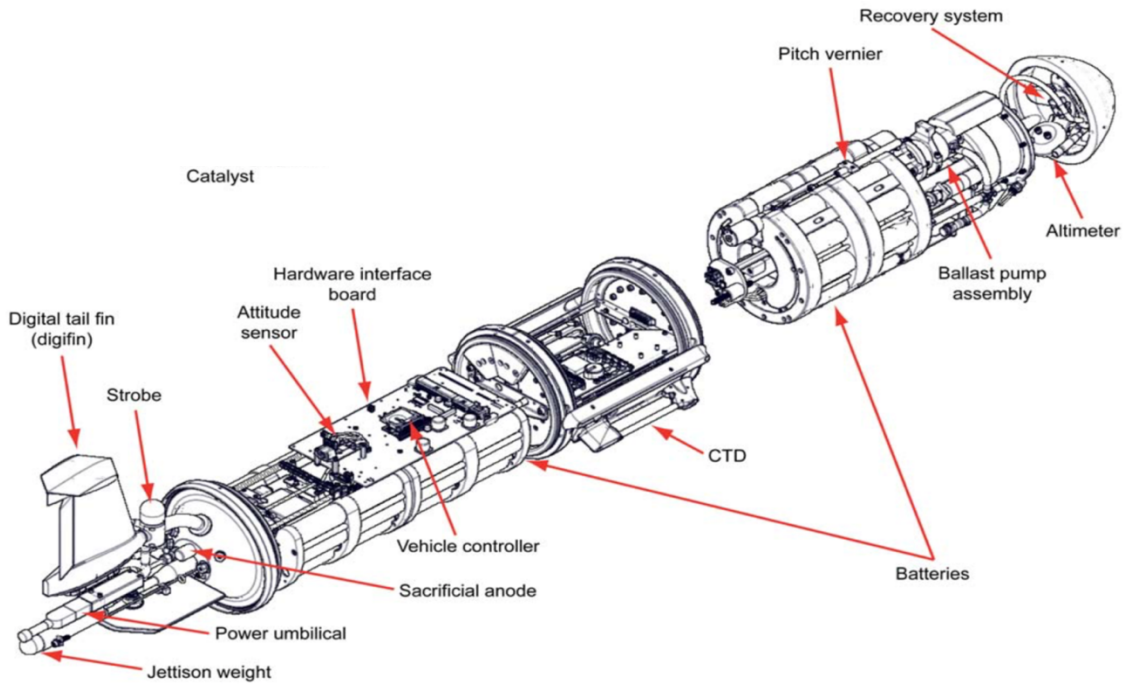

b)

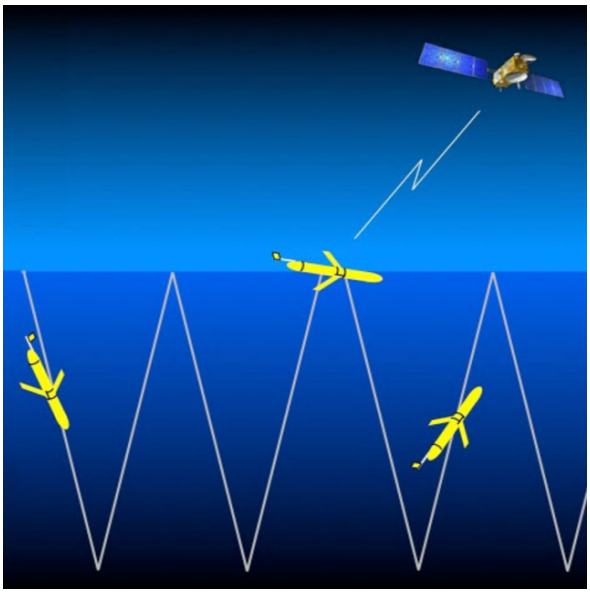

c)

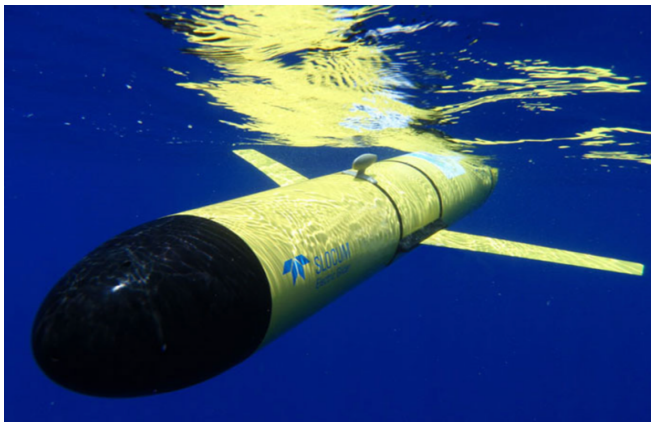

Fig. 2.1. a) Schematic of a Slocum glider, including the CTD sensor. Note that optional sensors, such as the Wetlabs triplet puck, which is used to measure chlorophyll fluorescence, and the oxygen optode are not included in the diagram. Schematic taken from the 2012 Slocum G2 Glider Operations Manual by Teledyne Webb Research; b) Schematic of a Slocum glider in flight (Credit: WHOI), and c) an underwater photo of a Slocum glider (Credit: Teledyne Webb)

for a GPS fix and to transfer data via iridium satellite. The glider transmits compressed files that provide a "snapshot" view of the data, as well as a report on the condition of the glider, including battery life and flight characteristics that can be used to identify problems (e.g. leaks). These small data packages are crucial for the glider mission, as pilots are able to make educated judgements about the state of the glider, allowing them to change the mission accordingly, or abort the mission entirely if deemed necessary.

Data collection from a glider is relatively straightforward, with data stored across two flash cards. Navigational and system data is stored on the mainboard flash card located on the forward bay, and science data is stored on the science bay. Raw data is recorded in binary format as a series of `*.*bd` files, which are then processed using a Glider Toolbox. More information about the routines in the Toolbox used for this data, as well as the necessary corrections and calibrations, can be found in Appendix I.

2.2 The Shelf Sea Biogeochemistry Project

2.2.1 Project Overview

The Shelf Sea Biogeochemistry project (SSB; www.uk-ssb.org) was a £10.5 million research programme that ran from 2011 to 2017 and was jointly funded by the Natural Environment Research Council (NERC) and the Department for Environmental, Food and Rural Affairs (DEFRA). Involving over 100 researchers from over 15 institutions, the aim of the SSB programme was to better understand the role of carbon storage, the global cycling of key nutrients (such as nitrate, silicate, phosphate and iron), oxygen cycling, and the subtle functioning and associated

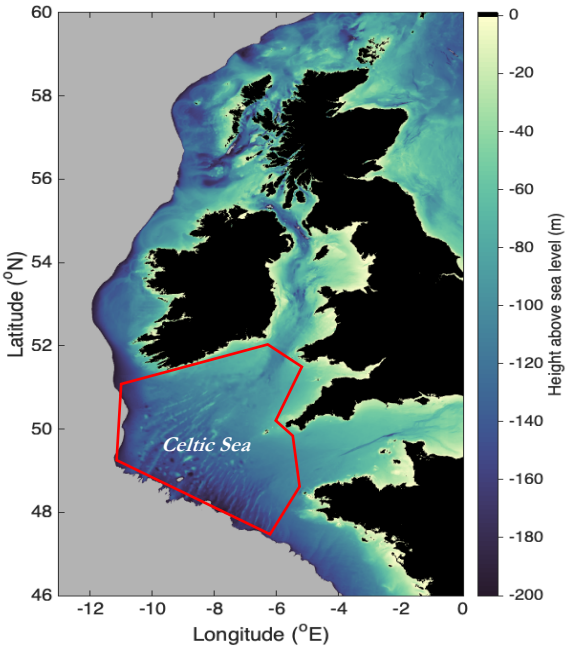

Fig. 2.2. Bathymetry map of the Western Approaches of the Northwest European Shelf, from 0 to -200m above sea level (Gebco 2014). The red box defines the limits of the Celtic Sea.

interactions of planktonic and microbial communities, both pelagic and benthic. SSB observations were mainly focussed in the Celtic Sea (Fig. 2.2) with a suite of observational platforms, including Slocum gliders, long-term moorings and process cruises, with fieldwork campaigns active throughout 2014 and 2015. In conjunction with the observations, advances in quantitative coupled marine physical-biogeochemical modelling allowed state-of-the-art model runs from 1982 to 2015. More details of these models can be found in Section 2.4 and Appendix II.

2.2.2 The Celtic Sea

Situated south of Ireland and west of the British Isles, the Celtic Sea is a ~500km wide (Huthnance et al, 2009) open-shelf region that sits at the western approaches of the North Atlantic Ocean (Fig. 2.2). Tidal currents range from 0.5 knots on the northern flank to 3 knots at the eastern edges (Pingree et al, 1976), and has low low-frequency circulation (Pingree and LeCann, 1989). Although riverine output from the Bristol Channel acts as a significant contribution to buoyancy in the northeast part of the Sea (Brown et al, 2003; Young et al, 2004), the influence of riverine input further towards the shelf break is likely to be limited (Ruiz-Castillo et al, 2018). Critically, this means that any freshwater input during the winter and early spring is primarily a result of precipitation, demonstrating that the Celtic Sea is a suitable location to investigate the short-term meteorological effects of storm systems.

2.2.3 Glider Deployments

As part of a larger glider campaign in the SSB programme, two Slocum gliders were deployed in the Celtic Sea, and were programmed to conduct repeat transects between the Central Celtic Sea (CCS) and the shelf break site (CS2). Spanning a time period of over four months between November 2014 and April 2015, the gliders cumulatively collected over 7500 profiles detailing essential bio-physical parameters across contrasting seasonal and spatial regimes. The gliders deployed are shown in Fig. 2.3. Results detailed in this thesis focus on the physical-biogeochemical processes occurring during the winter and winter-spring transition, measured by glider Unit 349 ("CABOT", 22nd November 2014 to 22nd March 2015), and Unit 419

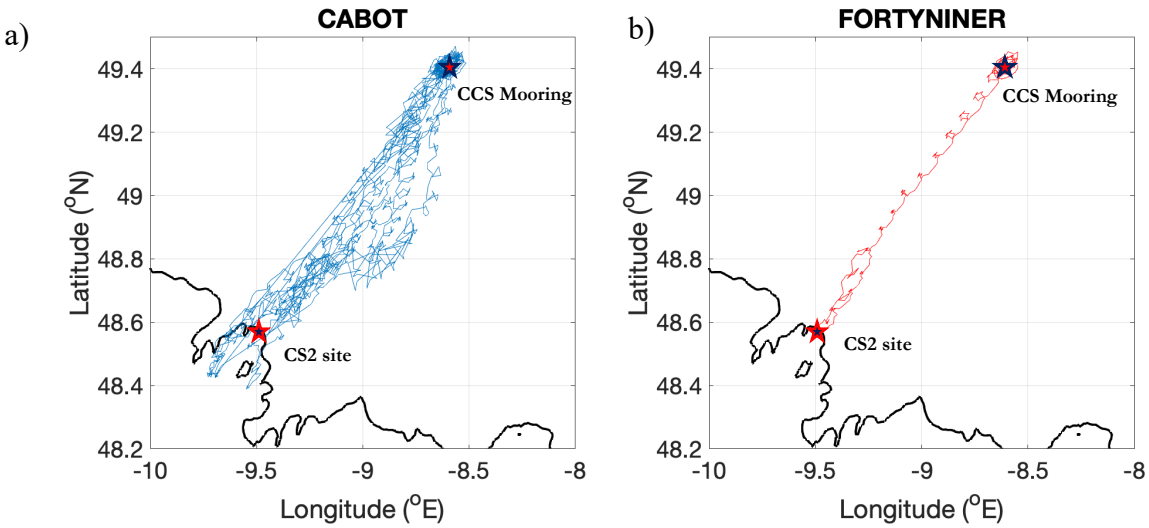

Fig. 2.3. Schematics showing the glider tracks for Unit 349 ("CABOT", 22nd November 2014 to the 22nd March 2015) and Unit 419 ("Fortyniner", 22nd March to the 2nd April 2015). The solid blank line is the 200m contour (GEBCO 2014), and the locations for the Central Celtic Sea (CCS) and CS2 sites are marked and labelled

("FORTYNINER", 22nd March to the 2nd April 2015). Also shown in Fig. 2.3 are the locations of the Central Celtic Sea Mooring and the CS2 site at the shelf break.

Both gliders were equipped with the following sensors:

- A pumped seabird CTD package to measure pressure, temperature and conductivity
- An Aanderaa oxygen optode
- A Wet Labs triplet puck to measure chlorophyll-a fluorescence, backscatter and coloured dissolved organic matter (CDOM)
- A photosynthetically active radiation (PAR) sensor. On recovery, it was noted that there were consistent issues with the PAR sensors on both gliders, resulting in no PAR data recorded for the entirety of the mission.

2.2.4 Thermal inertia in glider salinity data

In oceanography, temperature is the only parameter that can be easily measured directly, with others being inferred from proxy measurements. For example, salinity is calculated from conductivity and temperature measurements using the dynamic equations of state (UNESCO, 1981). On a glider, the CTD is positioned so that it measures temperature outside the cell and

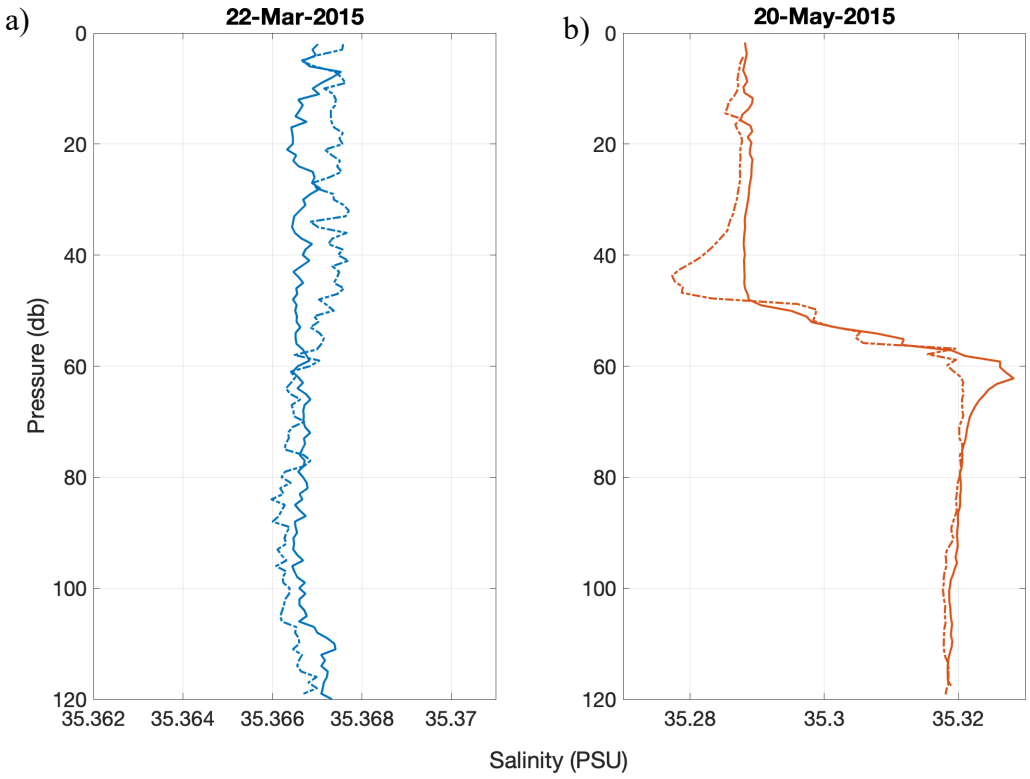

Fig. 2.4. Two consecutive up (solid) and down (dashed) profiles, illustrating the impact thermal inertia can have on the salinity in two separate periods: a) the winter-spring transition, on 22nd March 2015 and; b) the spring-summer transition, 22nd May 2015. The profiles from the winter-spring period show considerably less influence of thermal inertia, due to the lack of a defined temperature gradient such as what is observed further towards summer (note the different scales on the x-axis between the different periods). The profiles from May 2015 were recorded by glider Unit 397, which covered the spring-summer season, and were only included in this thesis as an example of thermal inertia.

conductivity through the cell. Lueck and Picklo (1990) predicted that Seabird conductivity cells retain heat in the walls of the device, resulting in erroneous salinity measurements.

Due to these thermal characteristics of the conductivity cell, when the sensor passes through a temperature gradient, the water temperature inside the cell is different to the temperature outside the cell. For example, if the glider is moving from warm to cold water, more heat is retained inside the cell and subsequently warms the water. Conversely, the conductivity cell acts to remove heat from the water inside the cell if moving from a cold to warm environment.

When calculating the salinity based on those temperature and conductivity values, the resulting salinity is erroneous as it is calculated using a different temperature value to what was observed. This is known as the thermal lag effect. According to Lueck and Picklo (1990), the response time of the conductivity cell is based on the initial flushing of the cell, the heat retained on

boundary layer wall and heat stored within the wall itself. It is this retained heat, especially within the wall of the cell, that causes the majority of the thermal lag error (Lueck and Picklo, 1990). The severity of the error is thus proportional to the strength of the temperature gradient, with a stronger thermal lag effect occurring during summer than in winter.

Thermal lag is an unavoidable problem when using glider data, which the Glider Toolbox corrects accordingly (see Appendix I). The effect of thermal lag is further reduced when considering data recorded during winter and winter-spring transition; as stratification is weak during this time, any residual thermal lag effect is minimal (Fig. 2.4).

2.2.5 Non-photochemical quenching

Phytoplankton are oxygenic photoautotrophic organisms (Müller et al, 2001), and as such need light for photosynthesis. However, too much light can damage, if not kill the cell by means of photooxidation (Müller et al, 2001). Counterintuitively, it was noticed that levels of fluorescence emitted from phytoplankton cells were lower at high irradiance than at night

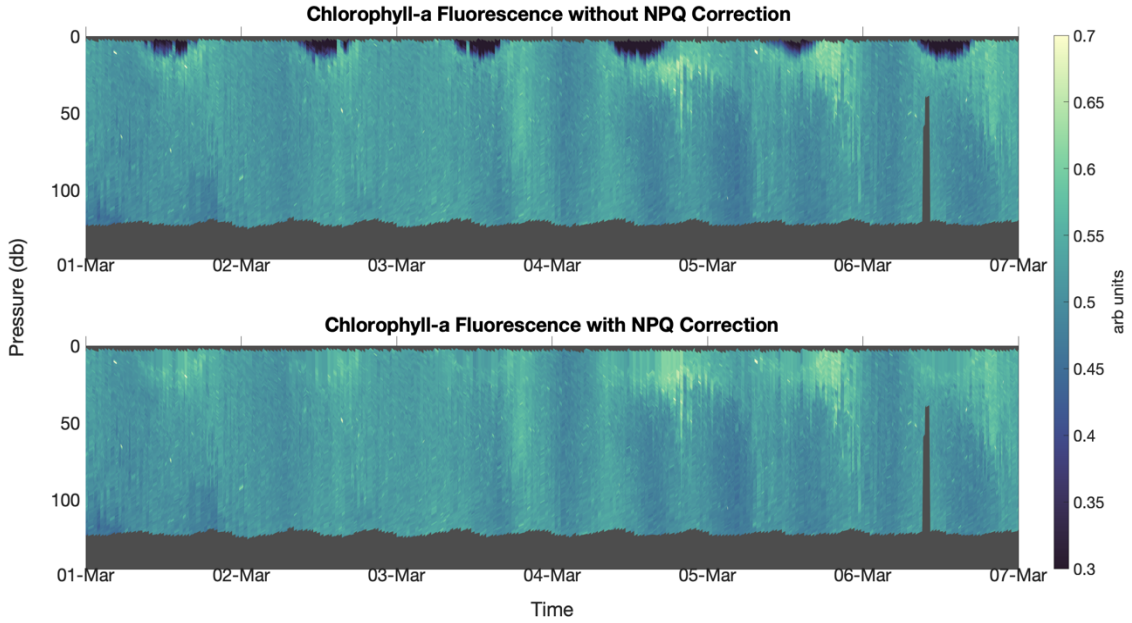

Fig. 2.5: Glider transects from the 1st to the 7th March 2015, emphasising the unavoidable problem with measured chlorophyll-a fluorescence. Non-photochemical quenching can clearly be observed in the upper plot, as erroneously low values for surface chlorophyll-a fluorescence during daylight hours. This has been corrected for in the lower plot, following the methods of Xing et al (2012)

(Sackmann et al, 2008). Referred to as non-photochemical-quenching (NPQ), this phenomenon is composed of two components: photoinhibitory quenching, and energy-dependent quenching (Sackmann et al, 2008), both of which lead to decreases in fluorescence with increased irradiance.

NPQ is an unavoidable problem in observational oceanography and needs to be addressed before any robust analyses can take place. NPQ is extensively observed in the glider transects, exhibiting as erroneously low dips in the chlorophyll-a fluorescence during daytime periods, even during the winter (Fig. 2.5). In order to sufficiently correct for NPQ, I implemented the method used by Xing et al (2012), who assumed that when the mixed layer depth is shallower than the active turbulent layer depth, such as in winter when the water column is homogenised, phytoplankton cells are evenly distributed within that layer. As such, chlorophyll-a fluorescence at the base of the NPQ zone can be extended to the surface (Xing et al, 2012). A fixed daytime period of 5.30am to 8.30pm was chosen as the quenching period, based on the first and last times the chlorophyll profiles showed evidence of NPQ in the surface. Although this fixed criteria is likely to change across the year, this was the time scale implemented across the winter and winter-spring transition. NPQ during the early winter is minimal but has still been corrected for.

2.2.6 Preliminary glider data

Combining the glider transects reveals a highly dynamic system where the glider observes the relatively quiescent shelf (CCS) and the energetic shelf break (Fig 2.6a). There is a well-defined salinity gradient on shelf equivalent to approximately 0.003 PSU km^{-1} during the winter-spring transition (Fig. 2.6c), with more saline water being present at the shelf break, due to the presence of Atlantic water. This gradient is intensified during summer, when riverine influence reaches the CCS site (Ruiz-Castillo et al, 2018). It is important to note that riverine runoff does not reach the CCS site before this time and so does not influence winter or spring physical conditioning.

The physical structure of the water column, characteristic of the winter and winter-spring periods, can clearly be seen in the glider temperature and potential density (Fig 2.6a and 2.6c). Water column homogenisation occurred by the 16th December 2014, following the breakdown

of seasonal stratification in the autumn. Once homogenised, the water-column temperature continued to decrease before reaching a minimum of 9.9°C on the 22nd March 2015. This is 66 days after the minimum air temperature (5.2°C on the 15th January 2015; not shown), as seawater is able to retain more heat than air due to its higher heat capacity. Other than sporadic stratification events that lasted up to two days (see Chapter 4), the water column remained homogenised until the 25th March 2015, when seasonal stratification was initiated (see Chapter 3).

Internal waves can clearly be seen during the autumnal breakdown of stratification, exhibiting as large oscillations in the pycnocline that can reach a vertical displacement of 65m during November; over one-third of the total depth of the water column. The transition from the on-shelf zone and into the shelf break regime is also clear, characterised by relatively cooler

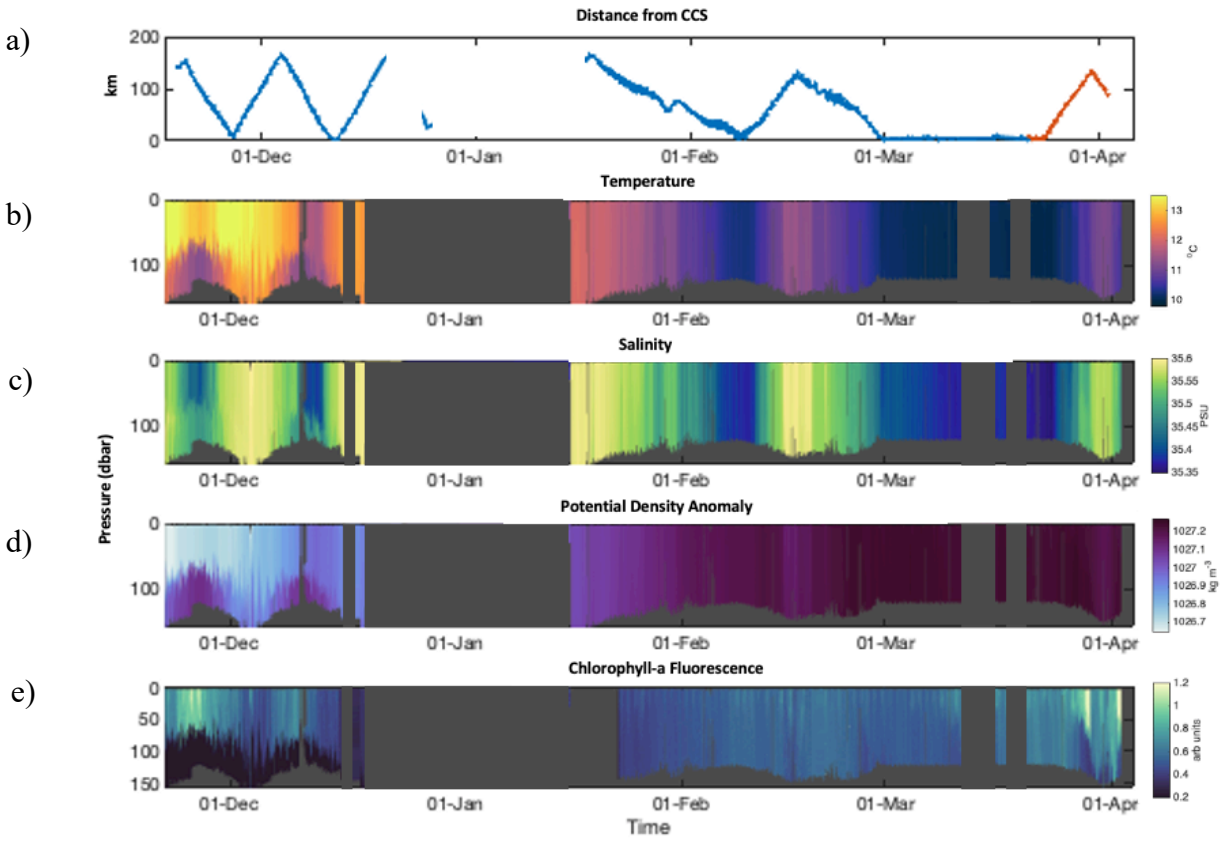

Fig. 2.6 Glider transects for Unit 354 (CABOT) and Unit 419 (FORTYNINER), from the 22nd November 2014 to the 4th April 2015, showing the breakdown of stratification in the late autumn, winter homogenisation and the start of the winter-spring transition. The different subplots are a) distance (in km) from the CCS mooring, where the blue line is representative of CABOT and red is representative of FORTYNINER, b) temperature (°C), c) salinity (PSU), d) potential density (kg m^{-3}, calculated from Gibbs Seawater Toolbox) and e) chlorophyll-a fluorescence.

temperatures compared to on-shelf during the autumnal breakdown, followed by relatively warmer temperatures from January to April 2015. The switch from cooler to warmer temperatures at the shelf break, relative to the shelf (Fig. 2.6b), is a result of open ocean water retaining more heat than the shelf, which has a lower volume and thus equilibrates quicker with atmospheric conditions.

There are clear vertical and seasonal gradients in the chlorophyll-a fluorescence measured by the glider (Fig. 2.6e), which is a proxy for phytoplankton biomass. The glider only measured chlorophyll-a fluorescence, and so other pigments (such as chlorophyll-b and chlorophyll-c) have been excluded. Enhanced chlorophyll fluorescence traces the depth of the pycnocline during the autumnal breakdown, before being distributed across the entire depth of the water column during January, with winter homogenisation. There are sporadic increases in surface chlorophyll fluorescence, which is quickly mixed to depth, before a more gradual increase from the 25th March 2015, reaching a maximum on the 29th March 2015. This is a direct result of the initiation of seasonal stratification and will be discussed more in Chapter 3.

1.3 Other observational data

2.3.1 Observational Mooring and Meteorological Data

In conjunction with glider data, other observational moorings were deployed as part of the SSB programme. A mooring, supporting temperature and salinity sensors, was stationed at the CCS site (see Fig. 2.3) and recorded data continuously across 17 months from the 26th March 2014 to 25th July 2015 (Wihsgott et al, 2018a). Temperature and salinity were measured at a higher vertical resolution of 2.5m at the pycnocline, and a lower resolution of up to 20m in the surface and bottom mixed layers (Wihsgott et al, 2018a). A series of sensors were fixed on the mooring, ranging from 13m to 143m depth. In this thesis, data from the CCS Mooring has been used to compare the magnitude of stratification (through the potential energy anomaly) at a single location, providing a contrasting view to the glider, which is constantly transitioning on (CCS) and off (CS2) the shelf.

Additional parameters of PAR and chlorophyll-a fluorescence were measured by the nearby Smartbuoy, deployed by the Centre for Environment, Fisheries and Aquaculture Science (CEFAS), with data processed and supplied by Tom Hull (CEFAS). The mooring consisted of a Seapoint Chlorophyll Fluorometer (in $\mu g\ l^{-1}$) and a PAR ($\mu E\ m^2\ s^{-1}$) sensor that measured incident PAR at the sea surface. To omit the impact of NPQ on chlorophyll-a fluorescence, CEFAS chlorophyll data was only used when PAR was less than 10 $\mu E\ m^2\ s^{-1}$ (i.e. during hours of darkness).

Observational meteorological data was recorded by the MetOffice Ocean Data Acquisition Sensor (ODAS) Buoy moored at the CCS site over the study period (UK Met Office). This provided critical meteorological data including wind speed (ms^{-1}), air density (kgm^{-3}), mean surface sea level pressure (hPA) and relative humidity (%), that would later feed into the calculations for the 2015 surface heat flux calculations (Wihsgott et al, 2018b).

2.3.2 Satellite-derived products

Only two satellite-derived observational products have been used throughout this thesis: satellite-derived precipitation and the light attenuation coefficient (Kd_{PAR}).

Satellite values of Kd_{PAR} at 490nm were mapped seasonal and monthly climatologies (2002 to 2017), taken from the MODIS-Aqua satellite. This data is freely available at https://oceancolor.gsfc.nasa.gov/l3/

It is important to note that the satellite-derived precipitation only serves as a visual representation as to the spatial scale of the 2015 March rain event. While satellite data is often used for better spatial resolution of parameters, specific values for the March 2015 precipitation has been reanalysis data sourced from ERA-Interim (Dee et al, 2011; see Section 2.5.1). This decision was based on personal correspondence with colleagues at the Met Office (John Siddorn, Elizabeth Sykes), as calibration algorithms for the satellite-derived precipitation often result in a data point that is significantly removed (physically) from the radar measurements informing them. Nevertheless, a map of derived satellite precipitation data has been used simply to visualise the spatial extent of the 2015 rain event discussed in Chapter 3 (see Section 3.7.2).

2.4 An introduction to NEMO-ERSEM

Analysis of hydrodynamic-biogeochemical models was crucial for determining the long-term and historical implications of storminess in shelf seas. This also gave valuable insight into how realistic oceanic processes were parameterised and replicated within the model framework. In order to analyse both the physical and biogeochemical implications, we used the coupled physics-biogeochemical model NEMO-ERSEM.

The Nucleus for European Modelling of the Ocean (NEMO) is a model framework that incorporates both ocean dynamics and thermodynamics (Madec et al, 2015), and was developed from the Océan PArallélisé (OPA) model described by Madec et al (1997). This was then adapted for use in a shelf sea environment (O'Dea et al, 2012) and on the 7km Atlantic Margin Model (AMM7; O'Dea et al, 2017) domain before being coupled to the biogeochemical European Regional Sea Ecosystem Model (ERSEM; Baretta et al, 1995; Blackford et al 2004). ERSEM is able to parameterise the complex physiological processes of planktonic and microbial communities within different size classes and functional groups, based on the local stoichiometry and nutrient load of the system (Butenschön et al, 2016; Edwards et al, 2012). A list of parameters extracted from the NEMO-ERSEM model can be found in Table 2.1.

NEMO Parameters	ERSEM Parameters
Temperature (°C)	Chlorophyll concentration (P1, P2, P3, P4)
Salinity (PSU)	Nitrate (mmol m^{-3})
	Silicate (mmol m^{-3})
	Phosphate (mmol m^{-3})

Table 2.1: List of parameters extracted from the NEMO-ERSEM model repository. For 2015, high-resolution (hourly) daily is used, and for the 1982 to 2015 reanalysis, the data is in daily resolution. The subscripts in the ERSEM parameters are as follows: P1 = diatoms, P2 = microphytoplankton (> 20 μm), P3 = nanophytoplankton (2-20 μm) and P4 = picoplankton (< 2 μm).

2.4.1 Evaluation of model data

It was necessary to validate the model against observations, to ensure the subtly of atmospheric-ocean coupling was being adequately captured in both the hourly (2015) and daily (1982-2015) model runs (Fig. 2.7). One caveat of the AMM7 model domain is that it is unable to fully resolve the internal Rossby Radius on shelf (O'Dea et al, 2017). Coincidentally, this means that the model

is unable to resolve the fine-scale physics on the shelf, such as internal waves, and would thus influence physics-biogeochemical coupling (Edwards et al, 2012).

The model data is recorded at single points on a 7km resolution grid. This is a direct contrast to the glider, which is constantly moving through the water column at a sampling rate of 1Hz, covering a range of up to 150km between the CCS and CS2 sites. In order to correct for the discrepancies between the glider and model locations, the data plotted in Fig. 2.7 are the model profiles at the closest location to the glider at each time step.

The surface variations in both temperature and salinity are small, with anomalies of up to ±0.08°C and ±0.15 PSU respectively (Fig. 2.7). An added complexity is the on-shelf salinity gradient, as well as the occurrence of salinity fronts, as seen in the observations (Fig. 2.6). To reduce the impact of these background physical variations, the temperature and salinity anomalies for both the model and the glider were examined.

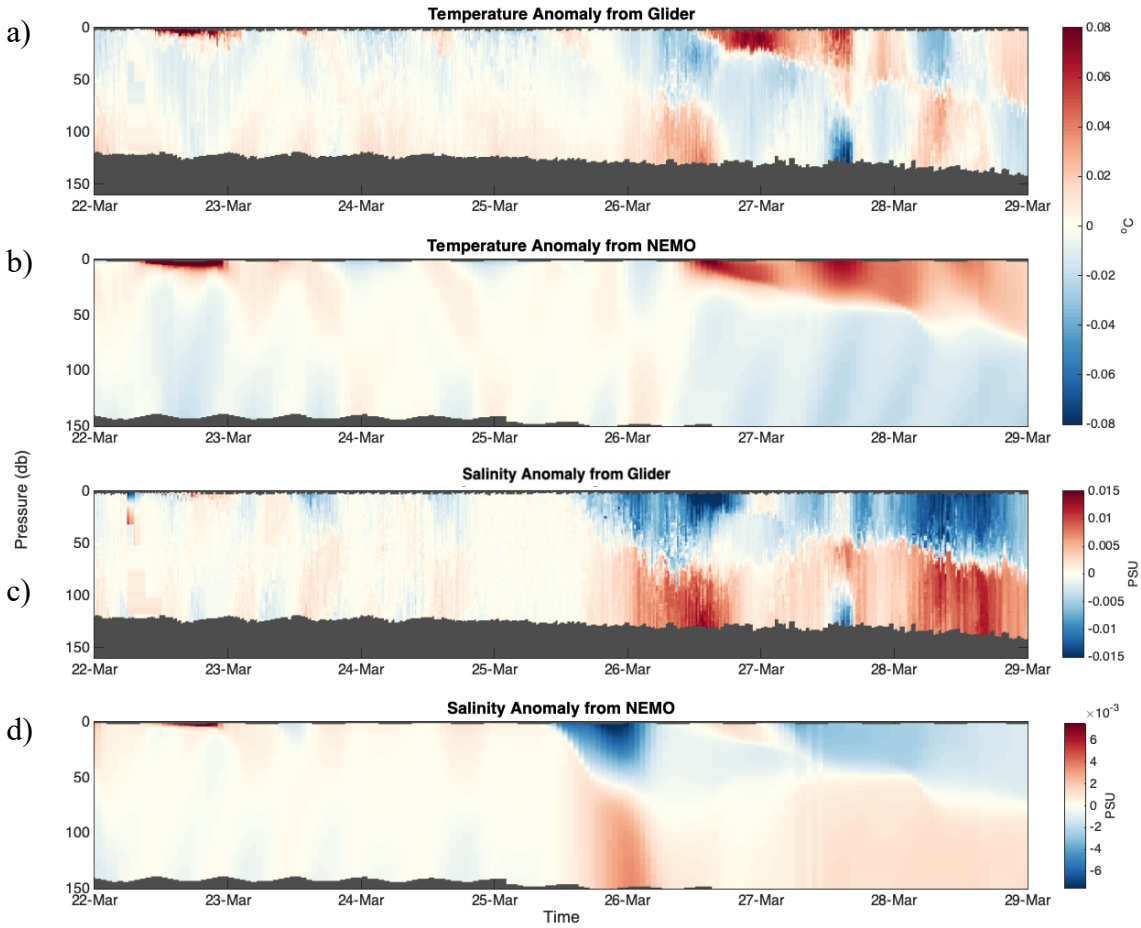

Fig. 2.7: Comparisons of the NEMO temperature and salinity anomalies to those recorded by the glider, from the 22nd to the 29th March 2015 (covering the initial onset of seasonal stratification). Note the differences in scale between the temperature and salinity plots, as due to discrepancies between the data, it was necessary to plot the salinity anomaly for the model and glider data on slightly different colour axes.

The model adequately replicated the small-scale variations in both the temperature and salinity anomalies, with only a 3-hour offset between the initial decrease in surface salinity on the 25th March 2015, likely resulting from discrepancies between the modelled and observed precipitation timing, or the spatial resolution of the model grid. Temperature anomalies were represented well in the model, with consistent maximum and minimum values, yet some of the more subtle switches in positive and negative surface temperature anomalies are not captured. For salinity, the model captures the initial surface decrease in salinity anomalies, accurately mixing it to the depth recorded in the glider data (approximately 65m). The temporal variation of temperature and salinity is represented in the model, in terms of the depth of the thermocline and halocline. Despite that the modelled salinity is approximately an order of magnitude lower than what is observed by the glider, alternating positive and negative salinity anomalies are well represented throughout the time period. We can therefore be confident that small scale variations in the surface, resulting from episodic meteorological events, are adequately represented in the model data.

2.5 Additional model data

2.5.1 ERA-Interim

Reanalysis precipitation and evaporation data for 2015 was obtained from European Reanalysis (ERA)-Interim (Dee et al, 2011) at 00:00 and 12:00 and at 3 hourly time steps. Reanalysis metrological data for analysis between 1982 and 2015 was only available at a slightly lower resolution, at 00:00 and 12:00 at 12 hourly time steps. Spatial resolution of the model data is at 80km, with parameters averaged across the glider track (equating to two grid boxes). Parameters downloaded from ERA-Interim include:

i. 10m vertical windspeed component (ms^{-1})
ii. 10m horizontal windspeed component (ms^{-1})
iii. Total precipitation (m of water equivalent)
iv. Total evaporation (m of water equivalent)
v. Sea surface temperature (K)
vi. Surface pressure (Pa)
vii. PAR at the surface (Jm^{-3})
viii. Incoming shortwave solar radiation (Wm^{-2})

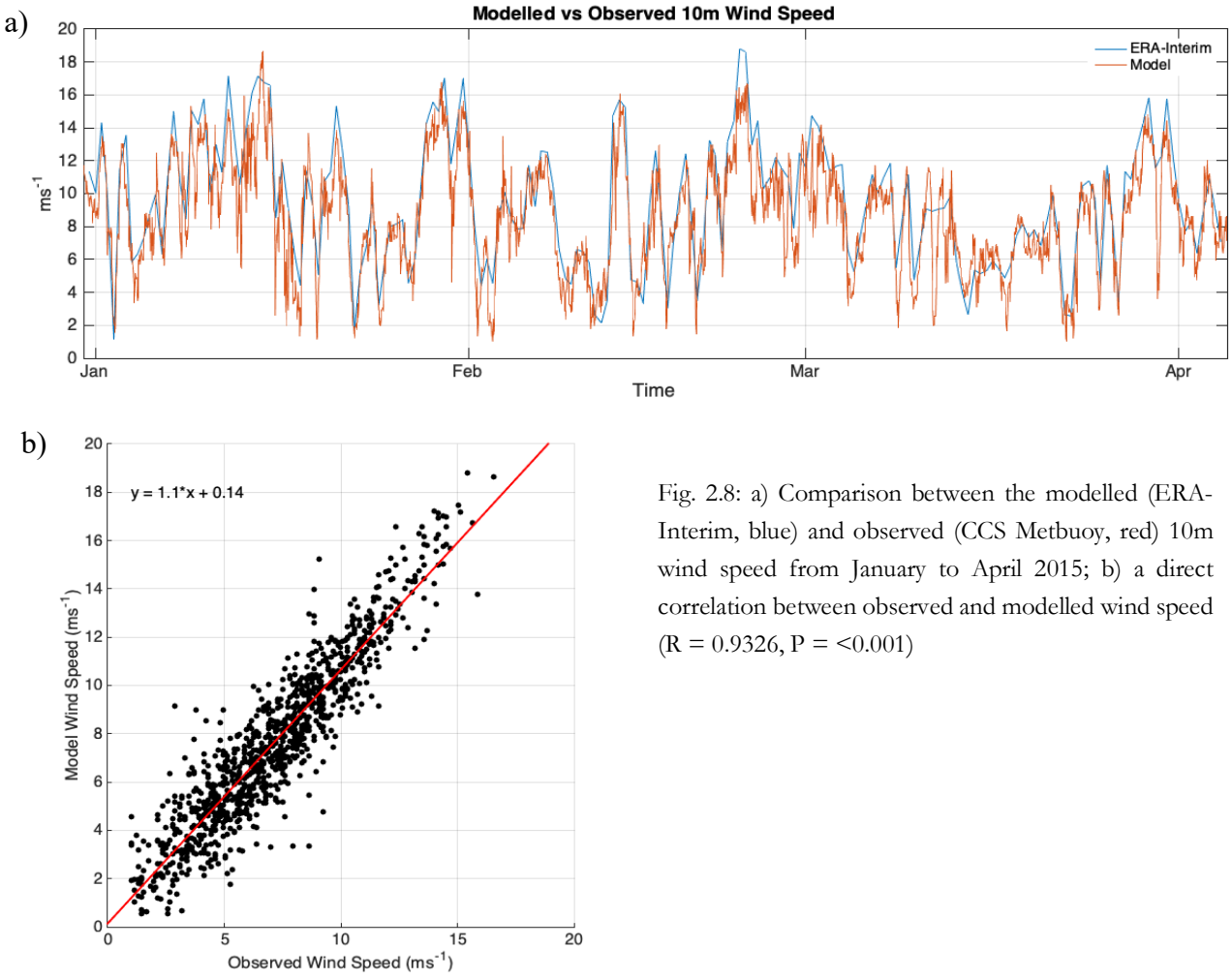

Fig. 2.8: a) Comparison between the modelled (ERA-Interim, blue) and observed (CCS Metbuoy, red) 10m wind speed from January to April 2015; b) a direct correlation between observed and modelled wind speed (R = 0.9326, P = <0.001)

Other components of the total surface heat flux, including longwave, surface sensible heat and latent heat of evaporation were derived using observed parameters and are described in Section 2.6. Example comparisons between modelled and observed windspeed (from the ODAS Buoy) agree well (R= 0.9326, P = < 0.001) providing confidence that these modelled meteorological parameters are representative of observed conditions (Fig. 2.8).

2.5.2 POLPRED

The Proudman Oceanographic Laboratory Prediction (POLPRED) software is a tidal modelling package designed for offshore tidal prediction (National Oceanography Centre, 2014). By incorporating tidal elevation and currents from the hydrodynamic models at the National Oceanography Centre, POLPRED is able to compute the tides at a singular location.

POLPRED calculates tides moving in a northward and eastward direction in and out of a 10km grid cell. Tides from POLPRED were computed using the glider's exact location, within the bounds of the 10km model grid. For comparison, tides were computed at the CCS Mooring site from 2014 to 2015, over the same time stamp as the observed tidal velocities. Whilst comparing the tidal ellipses from the CCS Mooring to the POLPRED output, differences in the tidal ellipses were noted (Wihsgott et al, 2018b). On further analysis, it was found that the internal compass of the Acoustic Doppler Current Profiler (ACDP), which is used to measure currents, was offset by local variations in the magnetic field (e.g. batteries and metal frames), thus causing deviations in the tidal ellipse and therefore slightly incorrect tidal amplitudes (Wihsgott et al, 2018b).

As such, output from the POLPRED tidal software has been used for the entirety of the study period, as it was considered to be the most consistent and least erroneous option.

2.6 Buoyancy vs. Mixing

Stratification in shelf seas is controlled by a delicate balance of buoyancy inputs, from thermal heating and rain/evaporation, versus mixing from convection, and wind and tidal stresses (Simpson and Bowers, 1981; Simpson et al, 1990). Only when the positive buoyancy inputs from heating and rain outcompete the mixing terms will sustained stratification occur. The relative importance of each of these constituents will now be described, summarised from Gill (1982), Sharples et al (2006) and Simpson and Sharples (2012).

2.6.1 Buoyancy from heating/cooling

The primary forcing mechanism for shelf sea physics is the seasonal cycle of heating and cooling, resulting from energy exchanges at the air-sea interface. The primary driver is the incoming solar radiation (Q_{sr}) that acts to heat up the ocean. Most of this heat is retained, although certain proportions are expelled as long-wave radiation (Q_{lw}), as well latent heat from evaporation (Q_{lh}) and sensible heat due to conduction (Q_{sr}).

The total heat flux (Q_{net}, Wm^{-2}), modified by albedo (a), of the incoming and outgoing radiation terms is defined as:

$$Q_{net} = Q_{sr}(1 - a) - Q_{lw} - Q_{sh} - Q_{lh} \quad (2.1)$$

Incoming solar radiation (Q_{sr}, Wm^{-2}) is shortwave radiation reaching the Earth's surface, which has an average energy input over an area of ~340 Wm^{-2} at the top of the atmosphere (Simpson and Sharples, 2012). Due to the ellipticity of the earth's orbit, incoming radiation received by the Earth varies by ±3.5% (Kondratyev, 1969). The amount of heat being absorbed into the ocean from solar radiation varies considerably by location, time of day and seasonality. Gaseous concentrations in the atmosphere, local meteorological conditions (e.g. cloud cover), and the solar elevation all act to scatter and/or absorb the incoming radiation, with the latter producing more reflectance if the solar angle is low. This scattered or reflected energy (*albedo)* is usually small (< 20%) so it can be inferred that most of the incoming solar radiation energy goes directly into the ocean and is distributed exponentially with depth.

Longwave radiation (Q_{lw} Wm^{-2}), the radiation emitted by the ocean, can be calculated by:

(2.2) $$Q_{lw} = e_m \sigma_s \ (T_s + 273.15)^4 (0.39 - 0.05 e_a^{0.5})(1.0 - 0.6c^2)$$

Where e_m is the emissivity (0.985), σ_s is Stephan's Constant (5.67 x 10^{-8} W m^{-2} K^{-4}), T_s is the sea surface temperature (°C), c is cloud cover (%) and e_a is the vapour pressure of water:

(2.3) $$e_a = 0.01 r_h e_w$$

In equation [2.3], r_h is the relative humidity (%) and e_w (mbar) is the saturated vapour pressure of water, which is related to the air temperature (T_a) by:

(2.4) $$\log 10 e_w = \frac{0.7859 + 0.03477\, T_a}{1 + 0.00412\, T_a}$$

Like Q_{sr}, this is also dependent on location meteorological conditions. For example, high cloud cover can act to redistribute heat back to the sea surface, whereas clear skies allow a higher proportion of Q_{lw} to be released into space. As per equation [2.2], Q_{lw} also dependent on the sea surface temperature (T_s).

The latent heat transfer flux (Q_{lh}, Wm^{-2}) is the loss of heat from the sea surface as a result of evaporation or condensation, defined by:

(2.5) $$Q_{lh} = 1.5 \text{ x } 10^{-3} \rho_a W (q_s - q_a) L_H$$

where ρ_a is the density of air (kg m^{-3}), W is the 10m wind speed, q_s and q_a is the relative humidity of the sea surface and air respectively, and L_H is the latent heat transfer amount (~2.5 x 10^6 J kg^{-1}).

The sensible heat flux (Q_{sh} Wm^{-2}) is defined as the transfer of heat through conduction, as a result of differences in air-sea temperatures, defined by:

(2.6) $$Q_{sh} = 1.45 \times 10^{-3} C_a \rho_a W (T_s - T_a)$$

where T_s and T_a are the temperatures of the sea surface and air, respectively, and C_a is the specific heat capacity of air (1004 J kg^{-1} $^oC^{-1}$).

Q_{net} follows a predicable seasonal progression and is dominated by Q_{sr}. In general, Q_{sr} is at its maximum and minimum values during the summer and winter solstices respectively, mirrored by weaker values of Q_{lw} due to the relatively smaller change in sea surface temperature. Q_{lh} and Q_{sh} also exhibit seasonal variability, where fluxes are highest during the winter due to an increase in winter winds. Q_{lw} is maximum during summer due to the generally lower cloud cover and higher sea surface temperatures experienced during the summer months. Together, the solar radiation and loss terms create a Q_{net} that is strongly positive during summer (net heat gain) and strongly negative (neat heat loss) during winter.

2.6.2 Buoyancy flux

A positive heat input of Q_{net} has a direct result on the temperature (T, ^oC) by:

(2.7) $$\Delta T = \frac{\Delta Q_{net}}{C_p \rho}$$

Where C_p is the specific heat capacity of seawater (taken to be 3985 J kg^{-1} $^oC^{-1}$), and ρ is the density of the water column (kg m^{-3}).

The input of rain also has a direct effect on the buoyancy. Rainwater is less dense than seawater, promoting a layer of freshwater on the surface ocean. The buoyancy flux (m^2 s^{-3}) is a measure of a stable (stratified) vs unstable (convective) regime and can be calculated with (b_{f1}; Gill, 1982) and without (b_{f2}; Rumyantseva *et al,* 2015) the effects of precipitation and evaporation.

(2.8) $$b_{f1} = \frac{g\alpha Q_{net} + g\beta\,(E-P)s}{\rho_0\, C_p}$$

(2.9) $$b_{f2} = \frac{g\alpha Q_{net}}{\rho_0\, C_p}$$

where E and P are the evaporation and precipitation rates in kg m^{-2}, g is the gravitational acceleration (9.81 ms^{-2}), ρ_0 is the reference density (kg m^{-3}) and s is the salinity (PSU). The expansion coefficients due to temperature (α, $^{O}C^{-1}$) and salinity (β, PSU^{-1}) are defined as:

(2.10) $$\alpha = -\frac{1}{\rho_0}\frac{\delta\rho}{\partial T}$$

(2.11) $$\beta = \frac{1}{\rho_0}\frac{\delta\rho}{\partial S}$$

2.6.3 The potential energy anomaly

A measure of stratification in shelf seas is the potential energy anomaly, ϕ (Jm^{-3}, Simpson and Bowers, 1981), defined as the amount of mechanical energy needed to mix the water column. As such, the strength of stratification is proportional to ϕ, with the water column being homogenous when ϕ is equal to zero:

(2.12) $$\phi = \frac{1}{h}\int_h^0 (\hat{\rho} - \rho) g z\, dz \qquad\qquad \hat{\rho} = \frac{1}{h}\int_h^0 \rho\, dz$$

where ρ (z) is the density profile (kg m^{-3}) over a water column of depth h (m), and $\hat{\rho}$ is the water column mean density (kg m^{-3}).

The change in potential energy anomaly with time *(t)* can be subdivided into its separate components, including heating/cooling, rain/evaporation, wind mixing and tidal mixing (Simpson et al, 1990).

(2.13) $$\frac{d\phi}{dt} = \frac{d\phi^{heat}}{dt} + \frac{d\phi^{rain/evap}}{dt} - \frac{d\phi^{wind}}{dt} - \frac{d\phi^{tides}}{dt} \qquad [W\ m^{-3}]$$

Heating and cooling (ϕ^{heat}) influences buoyancy by:

(2.14) $$\frac{d\phi^{heat}}{dt} = \frac{agQ_{net}}{2C_p} \qquad [W\ m^{-3}]$$

However, freshwater input from rain also has a positive buoyancy effect. By combining the buoyancy effects from both thermal heating and freshwater from rain events, then:

(2.15) $$\frac{d\phi^{heat}}{dt} + \frac{d\phi^{rain/evap}}{dt} = \frac{d\phi^{b}}{dt} = \frac{g}{2}\left(\frac{aQ_{net}}{C_p} + \dot{P}\Delta\rho\right) \quad [\text{W m}^{-3}]$$

where $\dot{P}$ is precipitation rate (ms^{-1}) and $\Delta\rho$ is the density difference between seawater and freshwater.

The mixing terms, from wind (ϕ^{wind}) and tidal mixing (ϕ^{tides}), can be calculated by equations [2.16] and [2.17]:

(2.16) $$\frac{d\phi^{wind}}{dt} = \epsilon_1 k_s \rho_s \frac{W^3}{h} \quad [\text{W m}^{-3}]$$

(2.17) $$\frac{d\phi^{tides}}{dt} = \frac{4}{3\pi}\,\epsilon_2 k_b \rho\,\frac{u_1^3}{h} \quad [\text{W m}^{-3}]$$

where ϵ_1 and ϵ_2 are the mixing efficiencies for winds (0.023) and tides (0.004) respectively, u_1 is the tidal stream amplitude (taken from POLPRED tidal output), ρ and ρ_s are the densities of seawater and air, and k_b is the bottom drag coefficient (0.0025). The term k_s is taken to be $C_D\gamma_s$, where C_D is the drag coefficient (0.0012) and γ_s is the slippage factor (0.02).

2.7 References

Aragon, D., Glenn, S., Miles, T. and Curry, R., 2015, October. Glider performance during Hurricane Gonzalo. In *OCEANS 2015-MTS/IEEE Washington* (pp. 1-5). IEEE.

Baretta, J.W., Ebenhöh, W. and Ruardij, P., 1995. The European regional seas ecosystem model, a complex marine ecosystem model. *Netherlands Journal of Sea Research*, *33*(3-4), pp.233-246.

Blackford, J.C., Allen, J.I. and Gilbert, F.J., 2004. Ecosystem dynamics at six contrasting sites: a generic modelling study. *Journal of Marine Systems*, *52*(1-4), pp.191-215.

Brown, J., Carrillo, L., Fernand, L., Horsburgh, K.J., Hill, A.E., Young, E.F. and Medler, K.J., 2003. Observations of the physical structure and seasonal jet-like circulation of the Celtic Sea and St. George's Channel of the Irish Sea. *Continental Shelf Research*, *23*(6), pp.533-561.

Butenschön, M., Clark, J., Aldridge, J.N., Allen, J.I., Artioli, Y., Blackford, J., Bruggeman, J., Cazenave, P., Ciavatta, S., Kay, S. and Lessin, G., 2016. ERSEM 15.06: a generic model for marine biogeochemistry and the ecosystem dynamics of the lower trophic levels. *Geoscientific Model Development*, *9*(4), pp.1293-1339.

Dee, D.P., Uppala, S.M., Simmons, A.J., Berrisford, P., Poli, P., Kobayashi, S., Andrae, U., Balmaseda, M.A., Balsamo, G., Bauer, D.P. and Bechtold, P., 2011. The ERA-Interim reanalysis: Configuration and performance of the data assimilation system. *Quarterly Journal of the royal meteorological society*, *137*(656), pp.553-597.

Edwards, K.P., Barciela, R. and Butenschön, M., 2012. Validation of the NEMO-ERSEM operational ecosystem model for the North West European Continental Shelf. *Ocean Science*, *8*(6), pp.983-1000.

Eriksen, C.C., Osse, T.J., Light, R.D., Wen, T., Lehman, T.W., Sabin, P.L., Ballard, J.W. and Chiodi, A.M., 2001. Seaglider: A long-range autonomous underwater vehicle for oceanographic research. *IEEE Journal of oceanic Engineering*, *26*(4), pp.424-436.

Gill, A. E. (1982). Atmosphere-Ocean Dynamics. International Geophysics Series, 30. *Academic Press, New York*.

Huthnance, J.M., Holt, J.T. and Wakelin, S.L., 2009. Deep ocean exchange with west-European shelf seas. *Ocean Science*, *5*(4), pp.621-634.

Lueck, R.G. and Picklo, J.J., 1990. Thermal inertia of conductivity cells: Observations with a Sea-Bird cell. *Journal of Atmospheric and Oceanic Technology*, *7*(5), pp.756-768.

Madec, G., 2015. NEMO ocean engine.

Madec, G., Delecluse, P., Imbard, M. and Levy, C., 1997. Ocean general circulation model reference manual. *Note du Pôle de modélisation*.

Meyer, D., 2016. Glider technology for ocean observations: a review. *Ocean Sci. Discuss*, *2016*, pp.1-26.

Müller, P., Li, X.P. and Niyogi, K.K., 2001. Non-photochemical quenching. A response to excess light energy. *Plant physiology*, *125*(4), pp.1558-1566.

O'Dea, E., Furner, R., Wakelin, S., Siddorn, J., While, J., Sykes, P., King, R., Holt, J. and Hewitt, H., 2017. The CO5 configuration of the 7 km Atlantic Margin Model: large-scale biases and sensitivity to forcing, physics options and vertical resolution. *Geoscientific Model Development*, *10*(8), p.2947.

O'Dea, E.J., Arnold, A.K., Edwards, K.P., Furner, R., Hyder, P., Martin, M.J., Siddorn, J.R., Storkey, D., While, J., Holt, J.T. and Liu, H., 2012. An operational ocean forecast system incorporating NEMO and SST data assimilation for the tidally driven European North-West shelf. *Journal of Operational Oceanography*, *5*(1), pp.3-17.

Osse, T.J. and Lee, T.J., 2007. Composite pressure hulls for autonomous underwater vehicles. In *OCEANS 2007* (pp. 1-14). IEEE.

Pingree, R.D. and Le Cann, B., 1989. Celtic and Armorican slope and shelf residual currents. *Progress in Oceanography*, *23*(4), pp.303-338.

Pingree, R.D., Holligan, P.M., Mardell, G.T. and Head, R.N., 1976. The influence of physical stability on spring, summer and autumn phytoplankton blooms in the Celtic Sea. *Journal of the Marine Biological Association of the United Kingdom*, *56*(4), pp.845-873.

Ruiz-Castillo, E., Sharples, J., Hopkins, J. and Woodward, M., 2019. Seasonality in the cross-shelf physical structure of a temperate shelf sea and the implications for nitrate supply. *Progress in Oceanography*, *177*, p.101985.

Rumyantseva, A., Lucas, N., Rippeth, T., Martin, A., Painter, S.C., Boyd, T.J. and Henson, S., 2015. Ocean nutrient pathways associated with the passage of a storm. *Global Biogeochemical Cycles*, *29*(8), pp.1179-1189.

Sackmann, B.S., Perry, M.J. and Eriksen, C.C., 2008. Seaglider observations of variability in daytime fluorescence quenching of chlorophyll-a in Northeastern Pacific coastal waters. *Biogeosciences Discussions*, *5*(4), pp.2839-2865.

Sharples, J., Ross, O.N., Scott, B.E., Greenstreet, S.P. and Fraser, H., 2006. Inter-annual variability in the timing of stratification and the spring bloom in the North-western North Sea. *Continental Shelf Research*, *26*(6), pp.733-751.

Sherman, J., Davis, R.E., Owens, W.B. and Valdes, J., 2001. The autonomous underwater glider" Spray". *IEEE Journal of Oceanic Engineering*, *26*(4), pp.437-446

Simpson, J.H. and Bowers, D., 1981. Models of stratification and frontal movement in shelf seas. *Deep Sea Research Part A. Oceanographic Research Papers*, *28*(7), pp.727-738.

Simpson, J.H. and Sharples, J., 2012. *Introduction to the physical and biological oceanography of shelf seas*. Cambridge University Press.

Simpson, J.H., Brown, J., Matthews, J. and Allen, G., 1990. Tidal straining, density currents, and stirring in the control of estuarine stratification. *Estuaries*, *13*(2), pp.125-132.

UNESCO. 1981, The Practical Salinity Scale 1978 and the International Equation of State of Seawater 1980. *UNESCO Technical Papers in Marine Science* 36, 25 pp.

Webb, D.C., Simonetti, P.J. and Jones, C.P., 2001. SLOCUM: An underwater glider propelled by environmental energy. *IEEE Journal of oceanic engineering*, *26*(4), pp.447-452.

Wihsgott, J., Hopkins, J., Sharples, J., Balfour, C.A. and Jones, E., 2018a. Long-term, Full Depth Observations of Horizontal Velocities Spanning 17 Months, Collected in a Temperate Shelf Sea (Celtic Sea) on the NW European Shelf. *British Oceanographic Data Centre–Natural Environment Research Council, UK doi*, *10*.

Wihsgott, J.U., 2018b. *A Tale of Four Seasons: Investigating the seasonality of physical structure and its biogeochemical responses in a temperate continental shelf sea* (Doctoral dissertation, University of Liverpool).

Xing, X., Claustre, H., Blain, S., d'Ortenzio, F., Antoine, D., Ras, J. and Guinet, C., 2012. Quenching correction for in vivo chlorophyll fluorescence acquired by autonomous platforms: A case study with instrumented elephant seals in the Kerguelen region (Southern Ocean). *Limnology and Oceanography: Methods*, *10*(7), pp.483-495.

Ya Kondratyev, K., 1969. Radiation in the Atmosphere.

Young, E.F., Brown, J., Aldridge, J.N., Horsburgh, K.J. and Fernand, L., 2004. Development and application of a three-dimensional baroclinic model to the study of the seasonal circulation in the Celtic Sea. *Continental Shelf Research*, *24*(1), pp.13-36.

3. Storms trigger seasonal stratification in a temperate continental shelf sea

Jennifer Jardine[1], Matthew Palmer[2], Claire Mahaffey[1], Jason Holt[2], Sarah Wakelin[2], André Düsterhus[1] & Juliane Wihsgott[2]

Prepared for submission to Nature Communications

[1.] University of Liverpool, Liverpool, L69 3BX

[2.] National Oceanography Centre Liverpool, Liverpool, L3 5DA

[3.] University of Hamburg, Institute of Oceanography, 20146 Hamburg

The North Atlantic Storm Track acts as a conveyor belt for extratropical cyclones that can deliver high winds and intense rainfall to northwest Europe. The impact of these storms on land is well documented, but little is known about the influence of rain on seasonal stratification in continental shelf seas. The current paradigm is that away from the coasts, vertical density stratification on the Northwest European Shelf is controlled via a balance between thermal exchange with the atmosphere and mixing by wind, waves and tides. In temperate latitudes, the onset of stratification is key to the initiation of the spring bloom: a key biological event in shelf sea ecosystems. Here we show rainfall, combined with wind-driven transport from a storm event during spring 2015 was sufficient to trigger seasonal stratification, which challenges the assumption that thermal conditioning is the dominant buoyancy control during spring stratification. Analysis of a multi-decadal hydrodynamic model confirms that storm related rainfall events contributed to triggering seasonal stratification in 30 out of the 34 years analysed between 1982 and 2015. These storm-induced events are shown to be modulated by the Atlantic Multidecadal Oscillation (AMO): stratification onset dates during positive AMO phases displayed a two-fold increase in variability compared to negative AMO phases, driven by an increase in storm intensity. This work highlights how storms, modulated by climate variability, have important implications for the timing of continental shelf sea seasonal cycles. Increased storm activity, as has been predicted in a warmer climate, is likely to impact physical and chemical functioning of shelf seas with potentially significant implications for productivity and ecosystem function.

3.1 Controls on stratification on the Northwest European Shelf

Positioned directly beneath the North Atlantic Storm Track (NAST), the western approaches of Northwest (NW) Europe experience extratropical cyclones year-round (Woollings, 2010), with the strongest storms usually occurring during the winter months (Matthews et al, 2016). The intensity and frequency of these storms has immense economic and societal impacts, with

the winters of 2013-14 and 2015-16 highlighted as being particularly destructive storm seasons that caused widespread damage to coastal defences and infrastructure (Kendon and McCarthy, 2015; Muchan et al, 2015; McCarthy et al 2016).

While the impact of storms on terrestrial environments and at the coast is well reported, their effects on the wider marine environment is less well studied. In temperate continental shelf seas, the seasonal transition from well-mixed waters during winter to summer stratified conditions acts as a precursor to the rapid growth of phytoplankton known as the spring bloom (Sverdrup, 1953; Pingree et al 1976; Ruardij et al, 1997, Sharples et al 2006). This phytoplankton growth event accounts for up to one third of the total primary productivity (Townsend et al, 1994), thus helping to underpin the estimated US$143 billion of the global fishing industry (FAO, 2018). As 4.5 billion people rely on fish for an estimated 15% of their protein intake (Béné et al, 2015), a better understanding of how climate influences both the timing of stratification and the development of the spring bloom is essential to understand how marine ecosystems will change in future climate change scenarios, for sustainable management of the 'Blue Economy' (Smith-Godfrey, 2016).

Due to their relatively shallow depth and low volume, continental shelf seas are typically characterised by a vertically homogenised water column during the winter months. A combination of net cooling, tidal mixing and winter winds act to mix the water column entirely to the seabed, resulting in an even distribution of high nutrient availability across the entire water column. This homogeneity also distributes phytoplankton cells from the surface to the seabed, resulting in low light availability and limited growth (Sverdrup, 1953). Nevertheless, ephemeral winter patches of phytoplankton have been observed, associated with brief periods of stratification resulting from transient eddies (Lacour et al, 2017), Langmuir circulation (Brereton et al, 2018) and shoaling of the turbulent surface layer (Taylor and Ferrari, 2011). The effect of increased buoyancy from rain has been explored in subtropical (Price, 1979; Anderson et al, 1996) and monsoonal regions (Kromkamp et al, 2007). On the NW European shelf, although rain has been postulated to contribute to shelf sea stratification (Pingree et al, 1976) and could act to support episodic phytoplankton growth (Franks 2014), it has largely been discounted as a critical mechanism controlling seasonal stratification (e.g. Simpson and Hunter, 1974).

The triggering of seasonal stratification by rainfall is not just a local process but important on a global scale. Several continental shelf seas experience heavy rain or storm activity, particularly those beneath atmospheric rivers (Newell et al, 1982; Zhu and Newell, 1988). Occurring in the warm conveyor belt of extratropical cyclones (Lavers et al, 2012; Gimeno et al, 2014), atmospheric rivers are so named due to the extreme volume of water they transport in the atmosphere, equivalent to the world's largest rivers (Zhu and Newell, 1998; Gimeno et al, 2014). Globally, there are eight such "rivers" distributed across both northern and southern hemispheres, including NW Europe, the Western United States, and Southeast America (Zhu and Newell, 1998; Waliser et al, 2012; Gimeno et al, 2014). These atmospheric rivers have the potential to deliver unusually large quantities of rainfall to the continental shelf sea regions. The Celtic Sea is one such continental shelf region, positioned beneath the North Atlantic atmospheric river that has been linked to extreme flooding events in the UK (e.g. Lavers et al, 2012; Lavers and Villiarini, 2013).

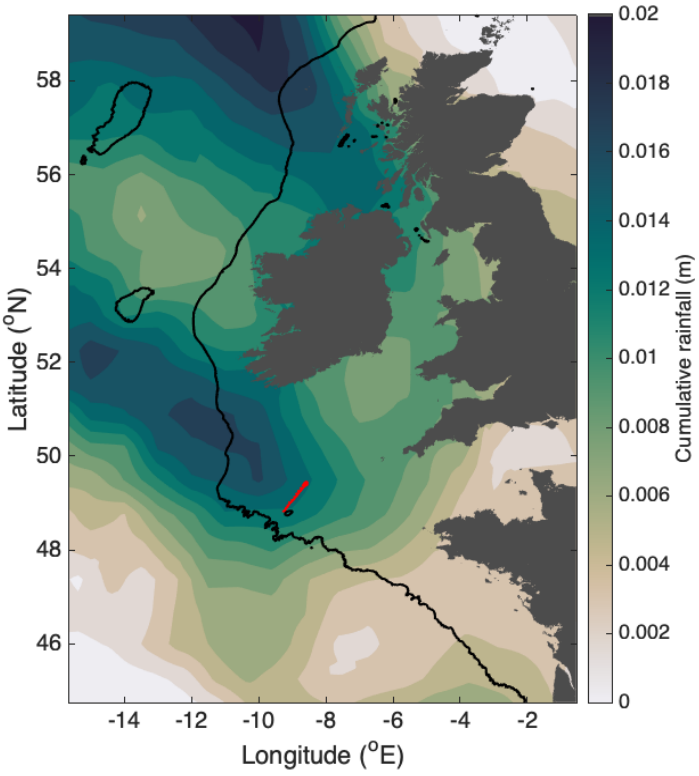

Figure 3.1: Location of the glider track in red from the 22nd to the 29th March 2015 in relation to the North West European Shelf. The black line is the 200m contour, while the colours show the accumulated rainfall over 24 hours on the 25th to 26th March 2015 (ERA-Interim, Dee et al, 2011).

A lack of observations at high spatial and temporal resolution during winter, and throughout storm events, are an inevitable barrier to increased understanding of winter ocean conditioning. Autonomous ocean gliders provide a valuable contribution to ocean observing that has the potential to fill this knowledge gap; they can sample several months through adverse weather conditions and can resolve near surface processes away from the potential contamination of large research vessels or traditional fixed ocean platforms. A series of gliders, deployed in the Celtic Sea as part of the Shelf Sea Biogeochemistry Project (www.uk-ssb.org, see Chapter 2.2) were able to capture the subtle ocean-atmosphere coupling from passing

storm events, enabling a full investigation into the meteorological conditioning of the water column at the winter-spring transition.

3.2 The onset of stratification in a temperate continental shelf sea

An ocean glider following a repeat transect in the Celtic Sea captured the onset of seasonal stratification that was triggered by a large rain event (Fig. 3.1). The daily heating and cooling cycle was clearly identifiable between the 22nd and 25th March, resulting in daytime thermal stratification that was convectively overturned during the night (Phase 1 in Fig. 3.2). Following a rain event on the evening of the 25th March, density decreases in surface waters by 0.006 kg m^{-3} over a 12-hour period. This relatively small addition of positive buoyancy is sufficient to form sustained stratification that lasts throughout the remainder of these glider observations (Phase 2 in Fig. 3.2). We can confidently conclude that this stratification caused by a reduction in the surface potential density was due to the addition of freshwater, and not due to thermal conditioning, as night-time (21:00 to 03:00) changes in the potential density gradient, $\partial\sigma\rho/\partial z$ (Supp. Material 3.7.1), are strongly correlated to changes in the salinity gradient, $\partial S/\partial z$ (r = 0.9; p = 0) and poorly correlated with the temperature gradient, $\partial T/\partial z$ (r = 0.1; p = <0.001). The positive correlation for $\partial T/\partial z$ also indicates a cold-water cap that has the effect of reducing buoyancy and so would help promote overturning if it were not for the stabilising effect of freshwater introduced by rain. Satellite-derived estimates for precipitation show that the rain event between the 25th and 26th March covered the majority of the Celtic Sea region (Supp. Material 3.7.2)

The resulting layer of freshened water becomes separated from turbulence below and retained phytoplankton close to the surface (Franks, 2014). Subsequently, there was an increase in chlorophyll fluorescence immediately following the initial onset of rain-induced stratification and peaked four days after the rain event on the 28th March (Fig. 3.2c). Coincident measurements of enhanced optical backscatter (not shown) in the surface layer provides confidence that this increase in chlorophyll fluorescence was due to increased phytoplankton biomass and not a result of photoacclimation (Supp. Material 3.7.3; Sackmann et al, 2008;

Perry et al, 2008; Huot et al, 2007). Work undertaken after the recovery of this glider confirmed that elevated chlorophyll fluorescence was maintained beyond the 2nd April and throughout

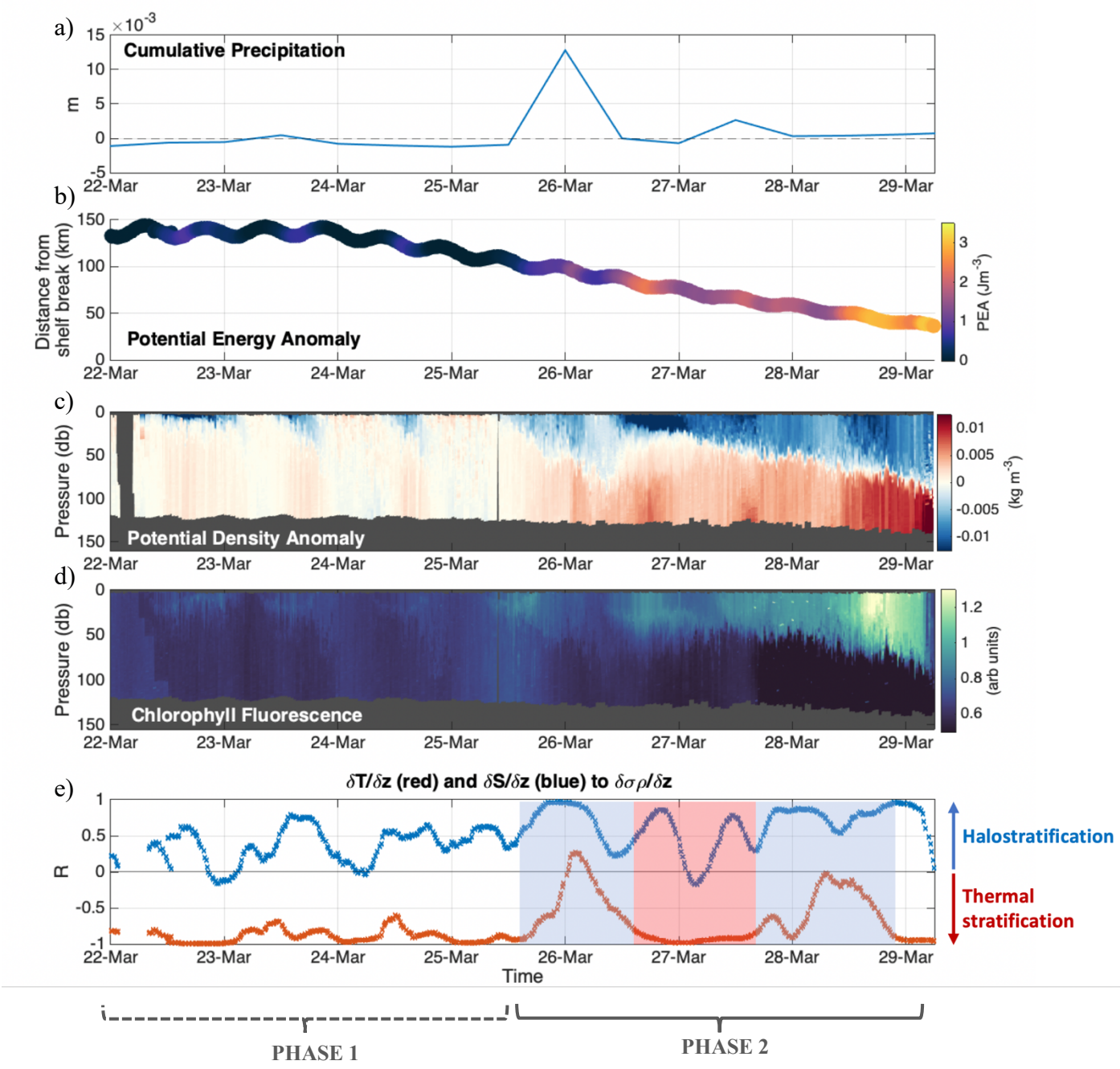

Figure 3.2: a) Total cumulative precipitation (m) over 12 hours (ERA-Interim, Dee et al, 2011) with positive values equating that precipitation > evaporation; **b)** The distance (in km) the glider was from the shelf break, with the colours indicating the potential energy anomaly (Jm^{-3}); **c)** The potential density anomaly ($\sigma\rho$) observed by the glider; **d)** Observed chlorophyll fluorescence; **e)** Correlative analysis to determine if the change in potential density with depth is more correlated with changes in salinity ($\partial S/\partial z$, blue) or temperature ($\partial T/\partial z$, red) gradient. The shaded areas are to highlight which part of the stratification observed in Phase 2 is controlled by salinity and temperature. It is important to note that glider moved into the shelf break on the 29th March and returned on shelf on the 2nd April. For clarity this has been removed from the figure, but an on-shelf mooring confirmed that stratification was sustained over this time.

the spring period (Poulton et al, 2017, García-Martín et al, 2018). Further work undertaken by Wihsgott et al (2018) identified that the timing of seasonal stratification observed in this study reached deep into the Celtic Sea interior, suggesting that these results are representative at regional scales.

3.3 Quantifying the importance of rainfall as a trigger for stratification

The strength of vertical stratification can be represented by the potential energy anomaly (ϕ, Jm^{-3}), defined as the amount of mechanical energy required to homogenise a column of water (Simpson, 1981; Simpson and Bowers, 1981). Analysing the different contributions to the temporal variability of ϕ permits a quantitative assessment of the importance of positive and negative buoyancy inputs, such as heating/cooling and rain/evaporation, relative to the mixing effects of wind and tidal stresses (Simpson and Bowers, 1981; Simpson et al, 1990).

[3.1]
$$\frac{d\phi}{dt} = \underbrace{\frac{d\phi^{heat}}{dt} + \frac{d\phi^{rain/evap}}{dt}}_{\text{Contributions to buoyancy (can be positive or negative)}} - \underbrace{\frac{d\phi^{wind}}{dt} - \frac{d\phi^{tides}}{dt}}_{\text{Contributions to mixing}}$$

Sustained stratification will only occur when the net positive buoyancy contribution manages to sufficiently outcompete the combined mixing effects of wind and tides, to counteract consecutive night-time convective periods. Storm activity has previously been shown to delay the onset of stratification on the NW European shelf due to increased wind mixing (Sharples et al, 2006). The relative phase of the spring-neap cycle also adds a substantial contribution to the timing of stratification through local variability in tidal mixing (Pingree et al, 1978; Sharples et al, 2006; Sharples et al, 2007).

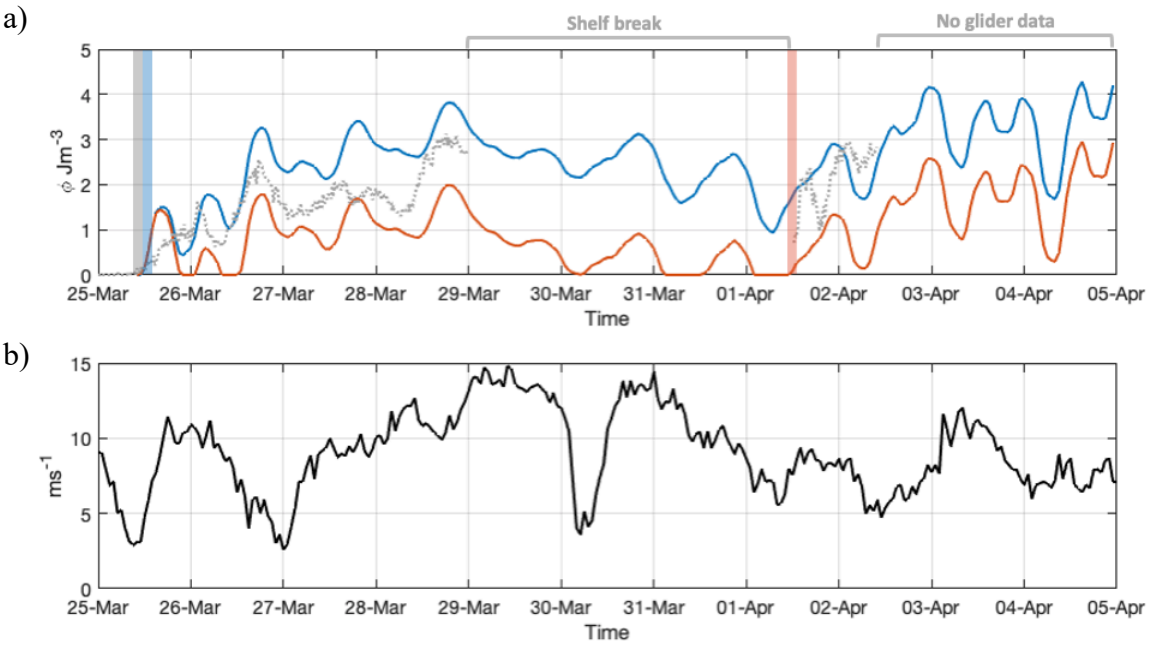

Figure 3.3: a) The potential energy anomaly calculated with (blue) and without (red) the added (removed) buoyancy from rain and evaporation, compared to the observed potential energy anomaly (dotted grey line) from the glider. Note that, unlike the glider, the modelled ϕ assumes a fixed point and is thus independent of processes observed by the glider as it moved towards the shelf break. As such, all data recorded when the glider moved into the shelf break regime has been omitted, and there is no glider data after the 2nd April. The coloured bars are indicative of when sustained seasonal stratification began; **b)** The observed 10m wind speed recorded from the ODAS Met Buoy (in ms^{-1})

Analysing the different components that contribute to stratification, represented by ϕ (Equation 3.1), allows a quantitative assessment of the importance of rainfall in triggering stratification.

To compare the relative magnitude of the different contributors to buoyancy, ϕ was calculated with and without the influence of rain and evaporation (Fig. 3.3a). Results show that without the additional input of rain, any daytime thermal stratification events would have been quickly eroded during the night, with sustained stratification only occurring a weak later than observations. To explain this discrepancy, the surface buoyancy flux was also formulated with (Gill et al, 1982) and without (Rumyantseva et al, 2015) rain and evaporation (Supp. Material 3.7.4). The buoyancy flux demonstrates that without the positive contribution provided by rain, the net negative buoyancy flux (indicating heat leaving the ocean) during the night-time period of 25 to 26th March was sufficient to promote convection and stratification would not have occurred (Supp. Material 3.7.4). The increased buoyancy introduced by rain during the night of the 25th March 2015 was sufficient to cause sustained stratification to form a week

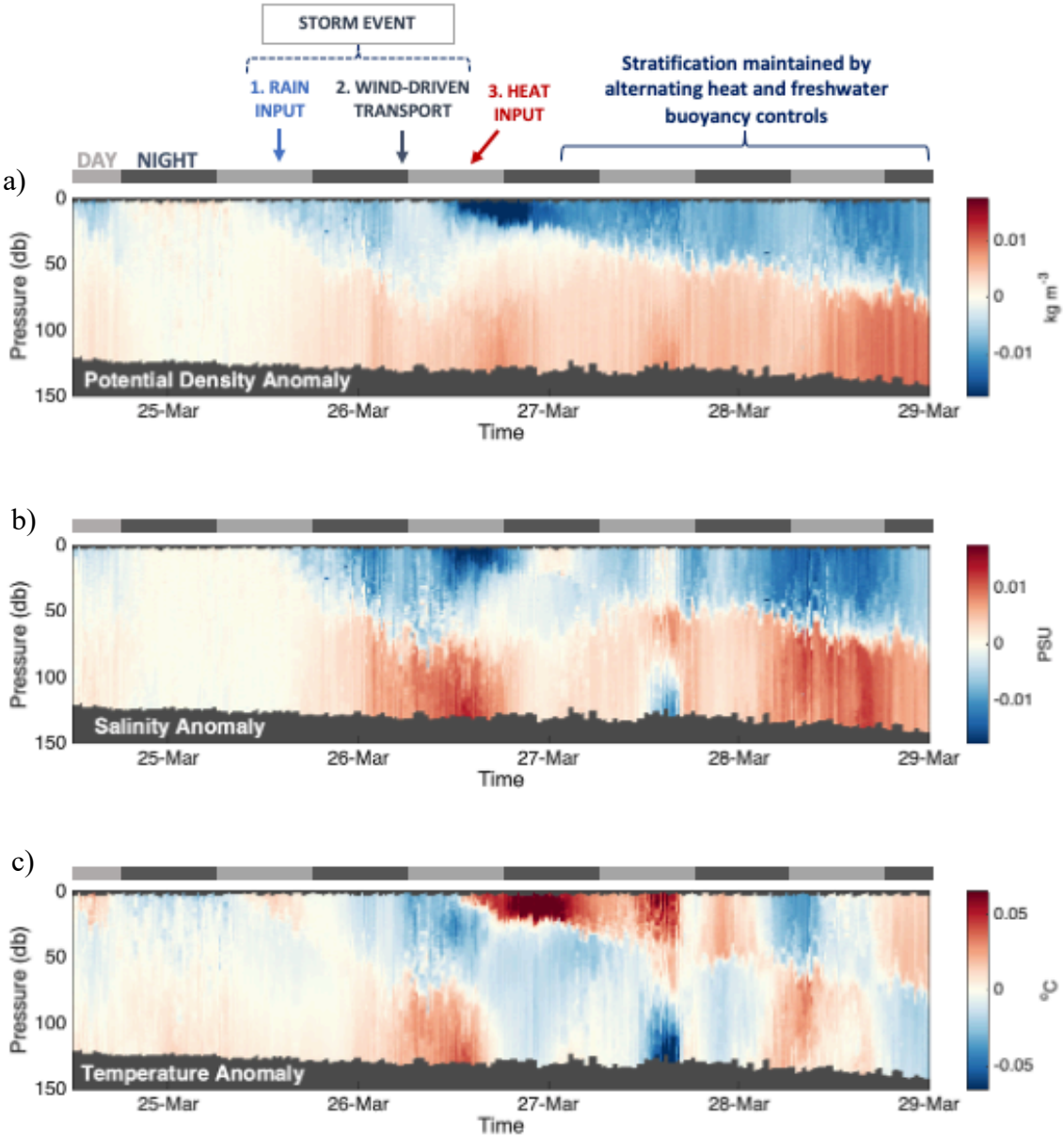

Figure 3.4: Glider transects between the 24th and 25th March that show **a)** potential density anomaly (kgm^{-3}), **b)** salinity anomaly (PSU) and **c)** temperature anomaly (^{o}C). A scale has been included to indicate night and day cycles, as well as the labels to indicate the rain event, wind-driven transport and heat input. Numbers on the labels denote the Phase number of the series of events, as described in the text.

earlier than predicted by [3.1] when only considering thermal inputs. While weak stratification would likely have developed on the 26th March by thermal inputs alone, the water column would have become fully mixed again on the 30th March, due to insufficient net buoyancy to outcompete mixing by wind. Subsequently, seasonal stratification due to thermal inputs alone were predicted to occur after the 1st April, 7 days later than what was observed.

In addition to the freshwater buoyancy effects of rainfall, there was also an associated positive thermal buoyancy input of up to 0.35 Wm^{-2} (Supp. Material, 3.7.5), which represents the sensible heat transferred into the ocean by rainfall (Gosnell et al, 1995; Fairall et al, 1996). Yet, as this only accounted for <1% of the maximum daytime heat flux into the ocean, it is not considered to be a controlling factor. To fully disseminate whether the rain event did fully contribute to the observed surface freshening, we can estimate the salinity change in the surface mixed layer (ΔS) using the equation:

[3.2] $$\Delta S = S_o \left(1 - \frac{Z_{SML}}{Z_{SML}+P}\right)$$

Where So is the initial salinity in the surface mixed layer, Z_{SML} is the depth of the surface mixed layer (m), and P is the amount of rain (m).

From 18:00 on the 25th March to 06:00 on the 26th March, 13.1mm of rainfall coincided with a surface freshening of 0.0124 PSU. Taking an average Z_{SML} of 44m over the same 12-hour time period, the estimated salinity change in the surface mixed layer was calculated at 0.0104 PSU and suggests that up to 84% of the surface freshening was due to rainfall.

While the remaining 16% of the freshwater could be due to errors in the ERA-Interim precipitation data, the sustained winds of approximately 10.3 ms^{-1} during the same time period indicate advection of fresher water in the surface due to wind-driven transport. Using observations the Central Celtic Sea site, Ruiz-Castillo et al (2019) observed that sustained westerly winds produced a weak wind-driven flow in the surface layer that caused a surface freshening of 0.05 g kg^{-1} from the 29th March to the 4th April 2015. While the maximum wind-driven transport occurred on the 29th March, calculations by Ruiz-Castillo et al (2019) support a weak wind-driven transport of fresher water from the northern Celtic Sea that occurred on the 26th March.

As such, it was the increase in buoyancy from rain (Phase 1 in Fig 3.4), combined with the subsequent weak wind-driven flow (Phase 2 in Fig 3.4), that produced the freshening in the surface mixed layer and maintained stratification overnight. Following the storm, wind speeds dropped throughout the 26th March to a minimum of 2.5 ms^{-1} and allowed positive thermal buoyancy contributions, from solar heating, to be distributed over a subsequently reduced mixed layer depth (Phase 3 in Fig. 3.4). This final contribution from thermal inputs is

considered a critical feedback mechanism to maintain storm-triggered stratification in the subsequent night-time periods, when convection is otherwise likely.

This series of events is repeated during a second, smaller rain event that occurred on the 27th March 2015 (Fig. 3.2). Although this rain event was significantly smaller (2.8 mm), it still accounted for 69% of the observed freshening. The remaining 31% of freshwater was likely advected into the region due to wind-driven transport, which dominated the stratification control up until the relaxation of westerly winds from the 5th April (Ruiz-Castillo et al, 2019), by which point thermal heating began to dominate.

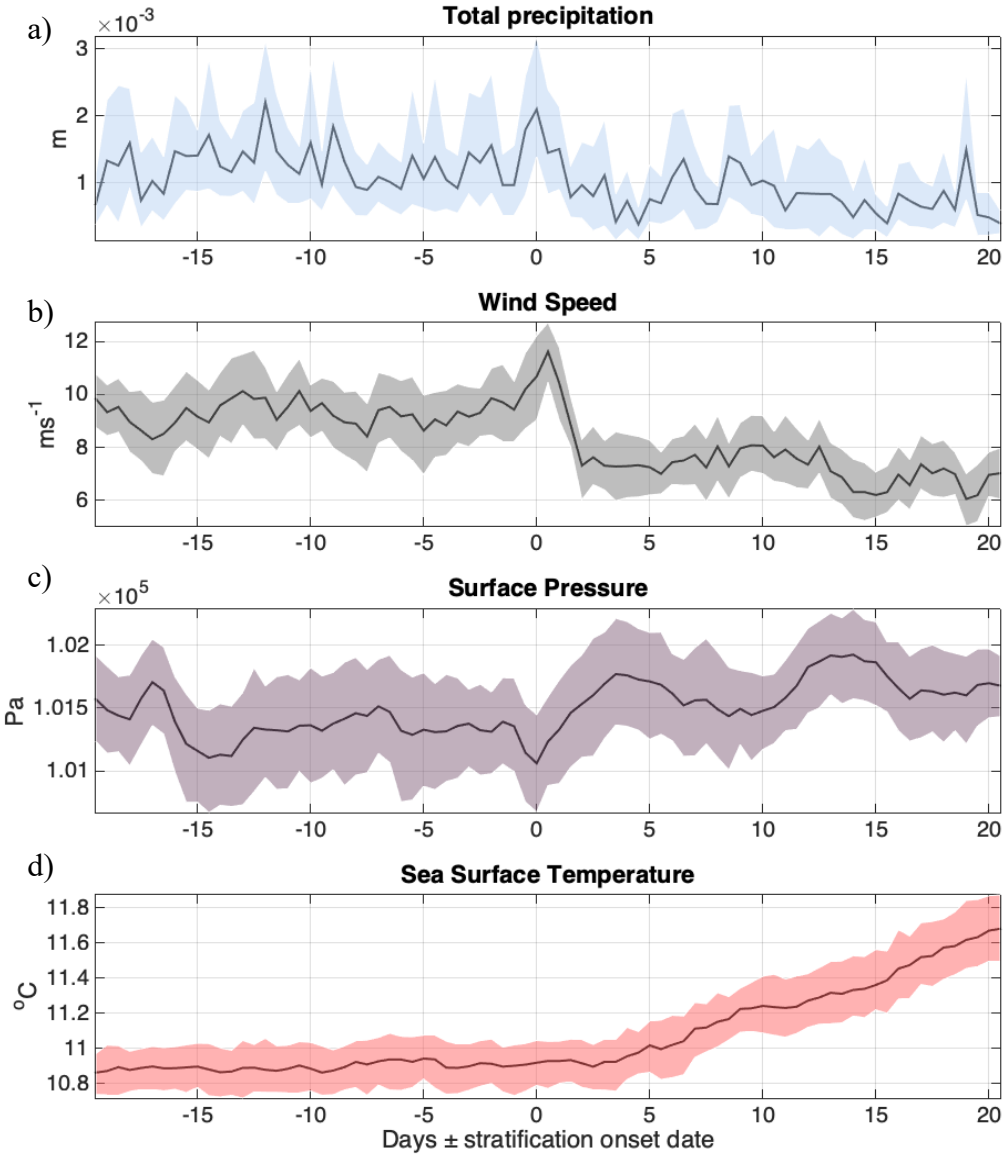

Figure 3.5: Climatology of meteorological parameters (ERA-Interim; Dee *et al*, 2011) from 1982 to 2015; **a)** total precipitation (m), **b)** sea surface pressure (Pa); **c)** wind speed at 10m (ms^{-1}) and **d)** sea surface temperature (^{o}C) relative to the stratification onset date. The shaded areas are the 95% confidence limits.

To test the repeatability of these physical processes on the formation of seasonal stratification, results from a multi-decadal hydrodynamic model, NEMO AMM7 3D (Madec, 2015; O'Dea et al, 2017), were analysed. Using climatological means of rainfall, wind speed, atmospheric pressure and sea surface temperature (ERA-Interim; Dee et al, 2011; Fig 3.5), results indicated that winter-spring storm events were capable of triggering seasonal stratification on the NW European Shelf in 30 out of 34 years from 1982 to 2015.

Climatological means of rainfall are high at the model predicted onset of sustained seasonal stratification (Fig. 3.5a) which, combined with decreased atmospheric pressure (Fig 3.5c), suggests that rain from storm activity is a frequent occurrence at the initial stratification onset (Phase 1). Windspeeds peak approximately 12 hours after the rain event (Fig. 3.5b), which supports wind-driven transport of freshwater that would further strengthen the existing halo-stratification (Phase 2). Sea surface temperatures only increases 2 days after the initial stratification onset (Fig. 3.5d), which coincides with the period of meteorological quiescence after the storm has passed (Phase 3). This highlights that the initial onset of stratification is not thermally induced, challenging the current paradigm of stratification in temperate shelf seas.

3.4 Impacts of large-scale variability

The influence of climate change on seasonal stratification is still under debate (Holt et al, 2010). While regional warming may result in an earlier onset of stratification (Coma et al, 2008), more energetic winds may also act to delay it (Sharples et al, 2006). To test climate conditions on seasonal stratification, the timing of stratification from 1982 to 2015 was analysed using model results from NEMO AMM7 (Madec, 2015; O'Dea et al, 2017)

To fully understand the variability of storms systems on stratification onset, the large-scale climate cycles related to storm variability across NW Europe must first be understood. These are the Atlantic Multidecadal Oscillation (AMO) and the North Atlantic Oscillation (NAO). The AMO is defined as the long-term temperature anomaly in the North Atlantic. The AMO has generally been in a negative phase (relatively cool) from 1960 before transitioning into a generally positive phase (relatively warm) in the mid-1990s, which remains until today. This

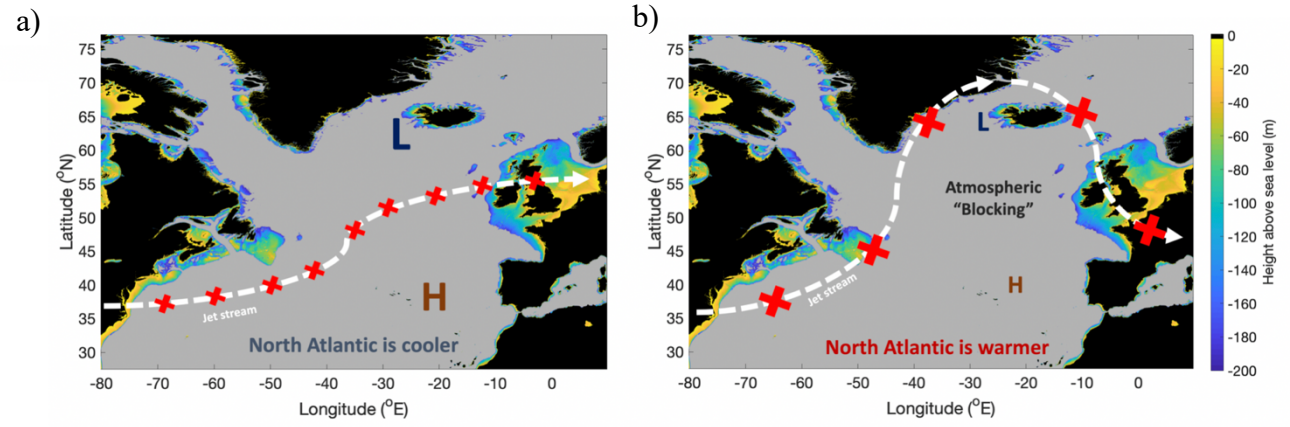

Negative AMO / Positive NAO 1982 to 1996
Energetic storm track
Higher frequency of intense cyclones
Straighter jet steam

Positive AMO / Negative NAO 1998 to 2015
Lethargic storm track
Intense cyclones are less frequent
Wavy jet stream allows increased atmospheric blocking over NW Europe

Figure 3.6: Schematics detailing the changes of the North Atlantic Storm track with **a)** a negative (positive) AMO (NAO) from 1982-1996, and **b)** a positive (negative) AMO (NAO) from 1998 to 2015. The table in the lower plots summarises the key changes in storm track characteristic over Northern Europe. The coloured sections represent the bathymetry of the continental shelf seas, defined as <200m deep. Red crosses on the jet stream are indicative of storms; larger crosses are more energetic storms.

phase shift in the AMO roughly coincides with that of the NAO, which is defined as the relative strength of the Azores-Icelandic sea level pressure (Hurell et al, 2003; Peings and Magnusdottir, 2014). The NAO was considered to be more frequently positive from 1965 to 1995 (Marshall et al, 2001), resulting in a straight jet stream across the North Atlantic (Fig. 3.6a). From the mid-1990s, the NAO has been in a predominantly negative phase (Li et al, 2013; Cohen et al, 2014) with a consequently wavy jet stream (Fig. 3.6b).

Comparing the onset dates of stratification to the AMO phase (Fig. 3.7) reveals a distinct shift in the year-to-year variability of stratification: positive AMO phases exhibit an almost two-fold increase in variability to that of negative AMO phases; 13 days compared to 20 days. This suggests the AMO provides a potential controlling mechanism on the timing of stratification on the NW European shelf. The NAO is often considered to be the dominant winter control of meteorological variability in the North Atlantic (Hurrell 1995; Marshall et al, 2001; Hurell

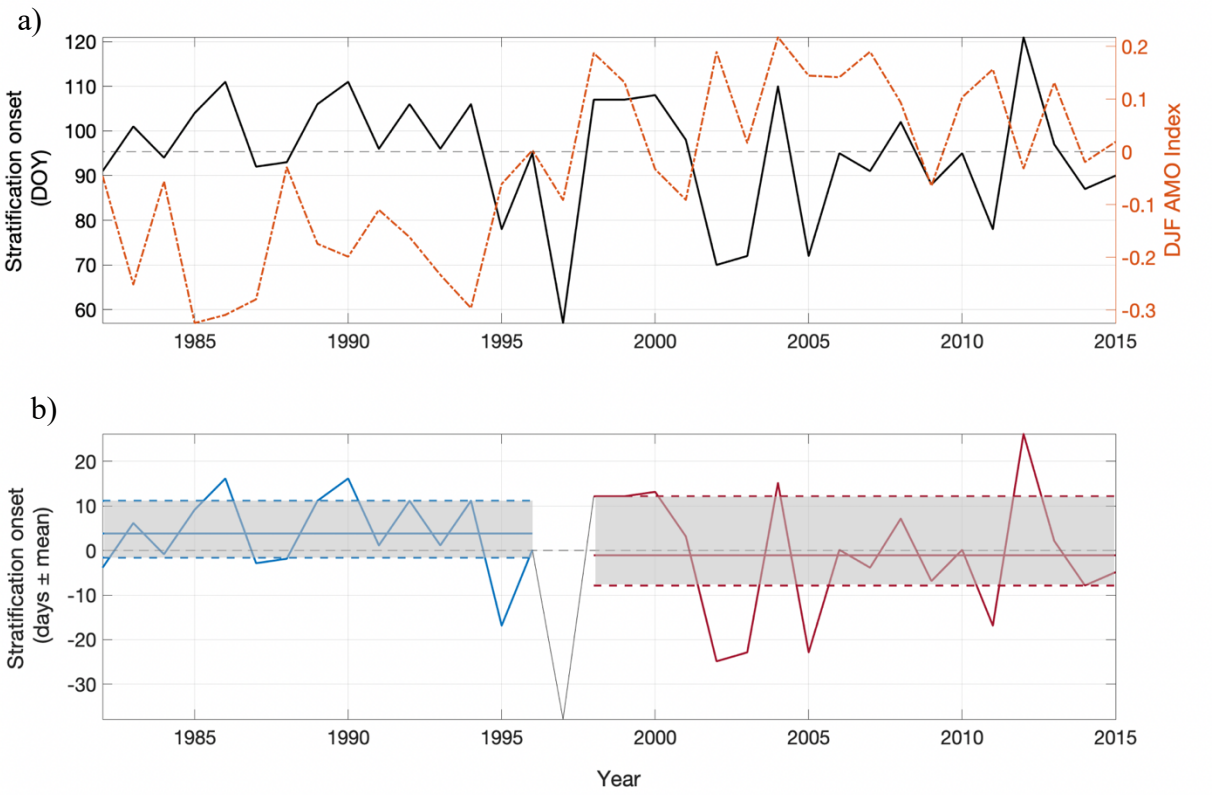

Figure 3.7: a) Comparison of the stratification onset dates (black) to the DJF AMO Index (red) from 1982-2015; **b)** The stratification onset dates in days ± from the mean of the full period, from a negative (blue) to positive (red) AMO phase; the mean (solid straight lines), as well as the 25th and 75th percentiles (dotted coloured lines), are also marked. Note that 1997 is an anomalous point direct on the transition period between AMO phases and has such been omitted from the phase statistics.

and Deser, 2009) and previous studies have shown a positive correlation between the NAO and the timing of stratification on the NW European shelf during positive phases (1974 to the early 1990s; Sharples et al, 2006). Our multi-decadal analysis of both positive and negative phases, however, suggests this relationship to be somewhat ambiguous (Supp. Material 3.7.6). Nevertheless, as the NAO acts as a controlling influence on the position of the jet stream (Fig. 3.6) and thus influences the frequency of storms experienced by NW Europe, it cannot be discounted as a control on stratification variability on the NW European Shelf.

From 1982 to 1997, when the AMO was in a negative phase, there was a more energetic storm track with stronger westerly winds (Peings and Magnusdottir, 2014) and a higher frequency of intense cyclones (Pinto et al, 2009; Hurrell et al, 2013; Yamamoto et al 2015). More frequent storms in negative AMO phases, combined with a straighter jet stream from a predominantly positive NAO, promotes more regular and prolonged periods of high wind stress. The constant bombardment of storms would bring consistently high winds that would continually

homogenise the water column before sustained stratification had time to develop, delaying the onset of seasonal stratification. This is reflected in the relatively stable period of stratification onset dates that occur from 1982 to 1996.

Conversely, the combined effects of a warmer North Atlantic and a wavy jet stream are likely to result in a lower frequency of intense storms being delivered to NW Europe. Conditions for cyclogenesis are unfavourable during positive AMO periods (Gomara-Cardalliaguet et al, 2012), and combined with a negative NAO, results in a wavy jet stream that causes increased atmospheric blocking over NW Europe (Woollings et al, 2008; Hakkinen et al, 2011) that deflects migratory cyclones, promoting periods of relatively low storm activity (Fig. 3.6).

Once initial stratification has been triggered by a storm event, the relatively quiescent conditions between these less frequent storm systems allow stratification to be continually strengthened. Homogenisation of the water column is only then likely to occur during extreme conditions, such as from an explosive cyclone (Pinto et al, 2009; Gomara-Cardalliaguet et al, 2012). Our model suggests this occurred in 2012, when an initial period of sustained stratification formed on the 19th March, producing a peak in ϕ of 23.3 Jm^{-3} on the 31st March (Supp. Material 3.7.7). A week-long period of high winds subsequently eroded stratification sufficiently to fully homogenise the water column. Sustained stratification was again re-established on the 30th April, following a week-long period of heavy rain and sustained high windspeeds. This was the latest predicted seasonal stratification onset date in this 34-year period.

The onset of stratification is therefore shown to have some dependence on the intensity of the storm, which may act to trigger or destroy stratification depending on the underlying condition of the water column, i.e. the magnitude of ϕ. If storms that follows initial stratification are not as energetic, then stratification is maintained and continues to strengthen. An extreme example of this is 1997 (defined as an anomalous point in Fig. 3.7b), where relatively calm conditions following a period of high wind and rain resulted in sustained stratification forming on the 26th February (Supp. Material 3.7.8).

3.5 Global implications

Although this study focussed on the Celtic Sea, these results are relevant to other continental shelf sea environments, particularly those positioned in close proximity to storm tracks and atmospheric rivers. One such example is the "Pineapple Express", an atmospheric river that delivers large amounts of rainfall to the continental shelf off the west coast of the Unites States (Dettiger, 2004; Dettinger et al, 2018). As intense storms and rain events associated with the Pineapple Express are most common from October to March (Dettinger et al, 2004), it can be inferred that large amounts of rainfall are delivered to the shelf during winter-spring transitional periods, which combined with sustained westerlies, would potentially influence the onset of seasonal stratification in this region.

Similar to the NW European Shelf, the variability of stratification onset on the Western US continental shelf could further be influenced by the Pacific Decadal Oscillation (PDO; Mantua et al, 1997). Similar to the AMO, the PDO is the detection of warm or cool ocean temperatures north of 20^{O}N, characteristic of an El Niño-like pattern (Mantua et al, 1997; Zhang, 1996; Mantua and Hare, 2002). Violent storms associated with the Pineapple Express are most common when the PDO is in a positive phase and neutral El Niño Southern Oscillation (ENSO) conditions (Dettinger, 2004), thus adding to the potential of climatic oscillations influencing multi-decadal variability of stratification onset dates on the Western US continental shelf.

3.6 Implications for a changing climate

The influence of intense rainfall on shelf sea stratification in the future is highly uncertain. There is a '*broad consensus that the frequency and intensity of storms, cyclones and high-impact wind speeds will increase over central and western Europe'* towards the end of the century (Mölter et al 2016). However, it is uncertain whether this leads to a less variable stratification onset due to the high wind stress associated with frequent storm activity (as seen in negative AMO periods) or whether increased intense rainfall associated with an accelerated hydrological cycle (Held and Soden 2006) under future climate conditions will lead to a more variable stratification onset.

Some regional ocean model studies have shown stratification occurring earlier under future climate conditions (Holt et al 2010), and this may mean an increased importance of rainfall events in the driving the onset of seasonal stratification, as it coincides more with winter storms.

Across Europe, the frequency of atmospheric rivers is expected to increase from ~2.5 $year^{-1}$ to as much as 10 $year^{-1}$ (Ramos et al 2016). Combined with an increase in the number of extratropical cyclones translating across NW Europe, irrespective of the NAO phase (Pinto et al, 2009), it is essential that meteorological impacts on stratification are adequately represented in models. In this study, high resolution spatial and temporal data collected from autonomous underwater gliders allowed new insights into the controlling physical drivers of seasonal stratification in the Celtic Sea. Furthermore, the 3D hydrodynamical model NEMO adequately replicated the small-scale variations in surface salinity from rain events, linking the decadal variability of shelf sea stratification on the NW European Shelf to large-scale climatic oscillations. Future work needs to investigate the implications of passing storm systems on productivity and ecosystem function, particularly as a result of climatic oscillations. We emphasise that rainfall from passing storm systems cannot be ignored as an initial trigger for seasonal stratification in temperate regions.

3.7 Supplementary Material

3.7.1 Temperature/Salinity correlation to potential density

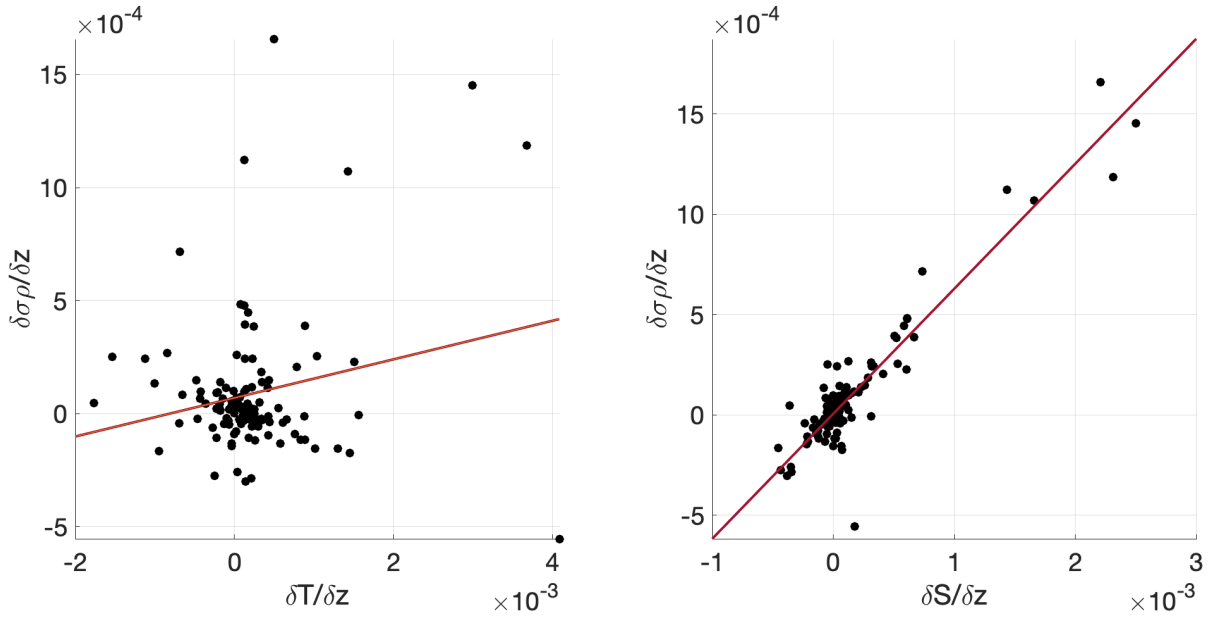

Figure 3.8: Comparisons between the changes in temperature (left) and salinity (right) with depth to the changes in the potential density anomaly with depth, between 21:00 and 03:00 on the 25th-26th March 2015

3.7.2 Satellite-derived precipitation

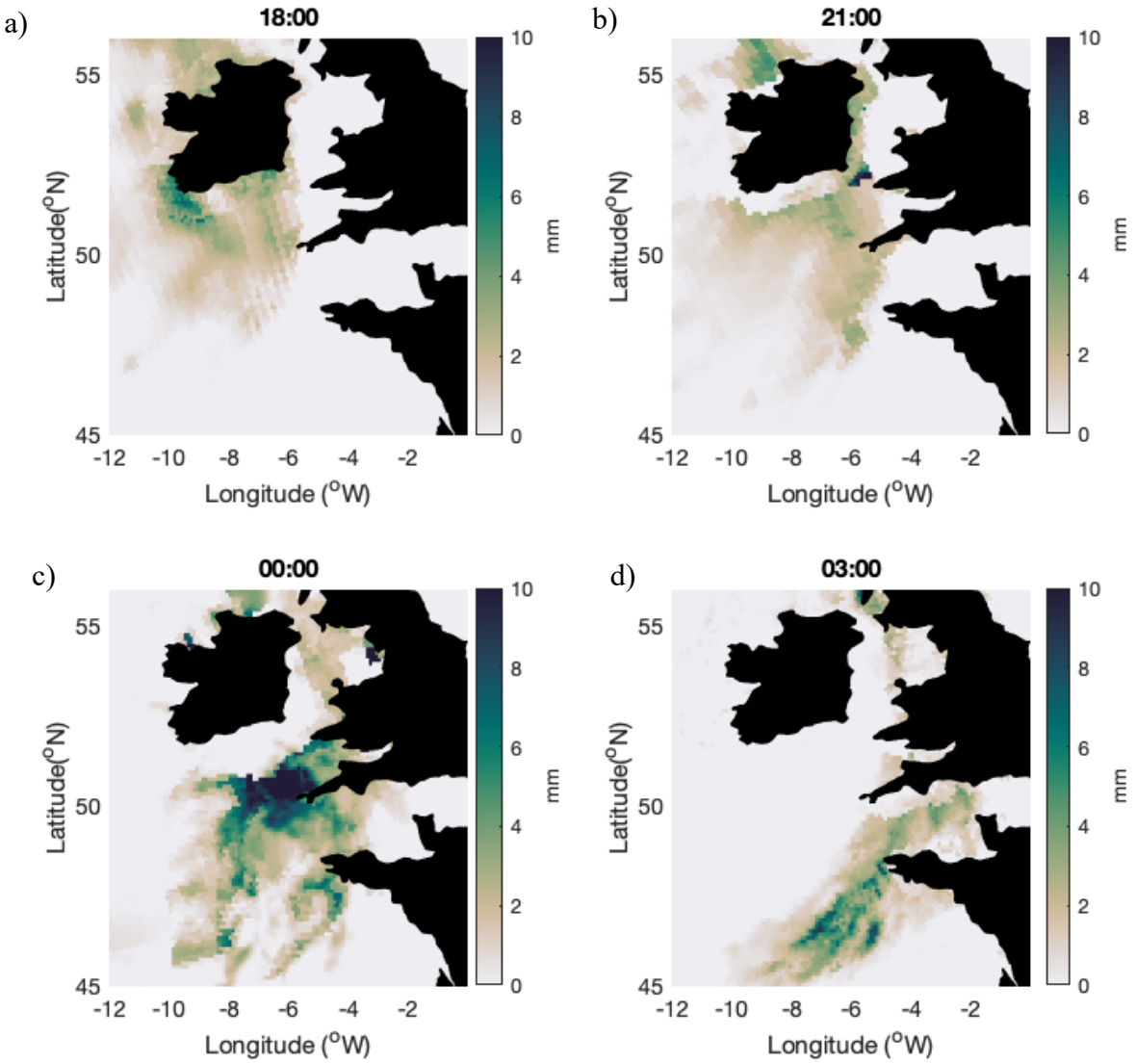

Figure 3.9: Satellite-derived precipitation (IMERG) for a) 18:00; b) 21:00; c) 00:00 and d) 03:00 from the 25th to the 26th March 2015, to show the spatial distribution of the precipitation over the Celtic Sea. Data downloaded from https://gpm.nasa.gov

3.7.3 Chlorophyll-a fluorescence vs optical backscatter

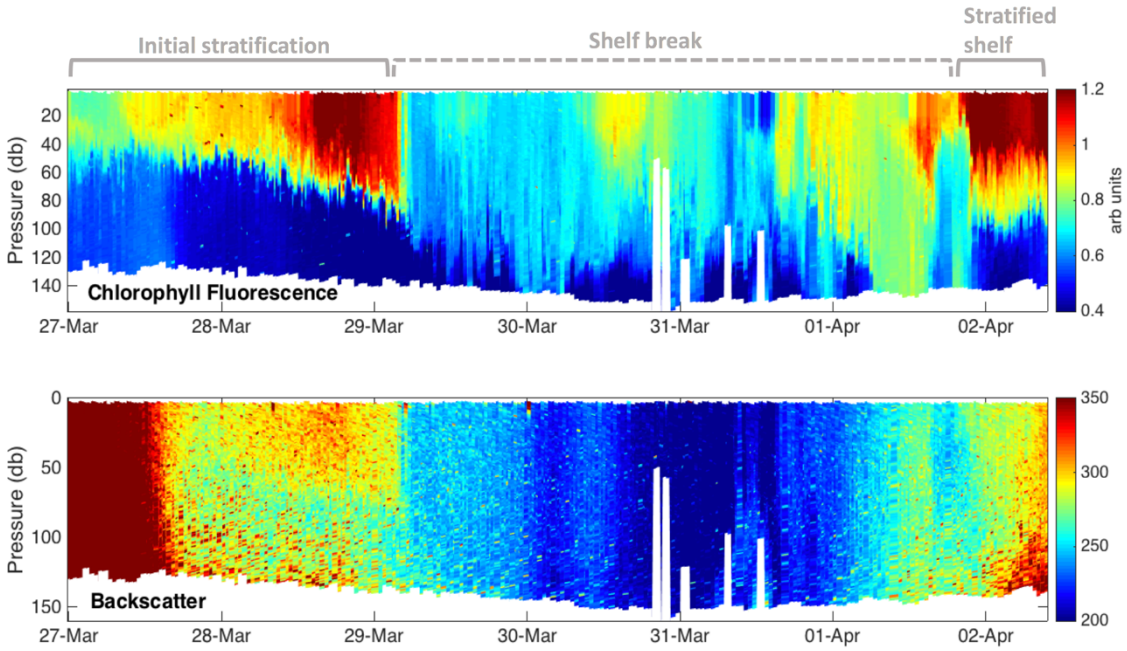

Figure 3.10: Comparison between chlorophyll fluorescence (upper) and backscatter (lower) following the rainfall event on the 25th March 2015. The transect has been cut to just show the period of high backscatter in the surface, coinciding with high chlorophyll-a fluorescence and thus inferring an increase in phytoplankton biomass.

3.7.4 Buoyancy flux with and without stratification

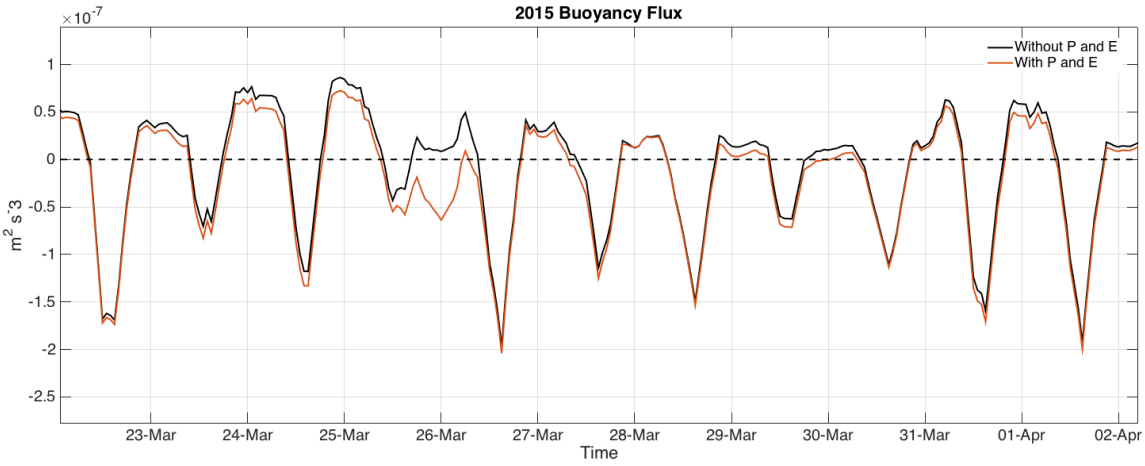

Figure 3.11: Buoyancy flux calculated with (red) and without (black) the effects of precipitation and evaporation. Positive numbers denote convection.

The timing of the rainfall events is crucial to initiating stratification, as shown by the buoyancy flux in Figure 4. To gauge the importance of the timing of these rainfall events, the buoyancy flux was calculated with (equation 1; Gill, 1982) and without (equation 2, Rumyantseva et al, 2015) the effects of precipitation and evaporation. Note the input of extra buoyancy is most noticeable during the night.

(3.3)
$$b_{f1} = \frac{g\alpha Q_{net} + g\beta\,(E - P)s}{\rho_0 C_p}$$

(3.4)
$$b_{f2} = \frac{g\alpha Q_{net}}{\rho_0\, C_p}$$

In equations [3.3] and [3.4] above, b_f is the buoyancy flux, E is the evaporation rate, P is the precipitation rate, C_p is the specific heat of water, Q_{net} is the surface heat flux, β is the salinity coefficient of seawater and α is the thermal coefficient of seawater (see Chapter 2.6.2), s is the surface salinity and g is the gravitational acceleration.

3.7.5 Sensible heat flux into the ocean due to rain

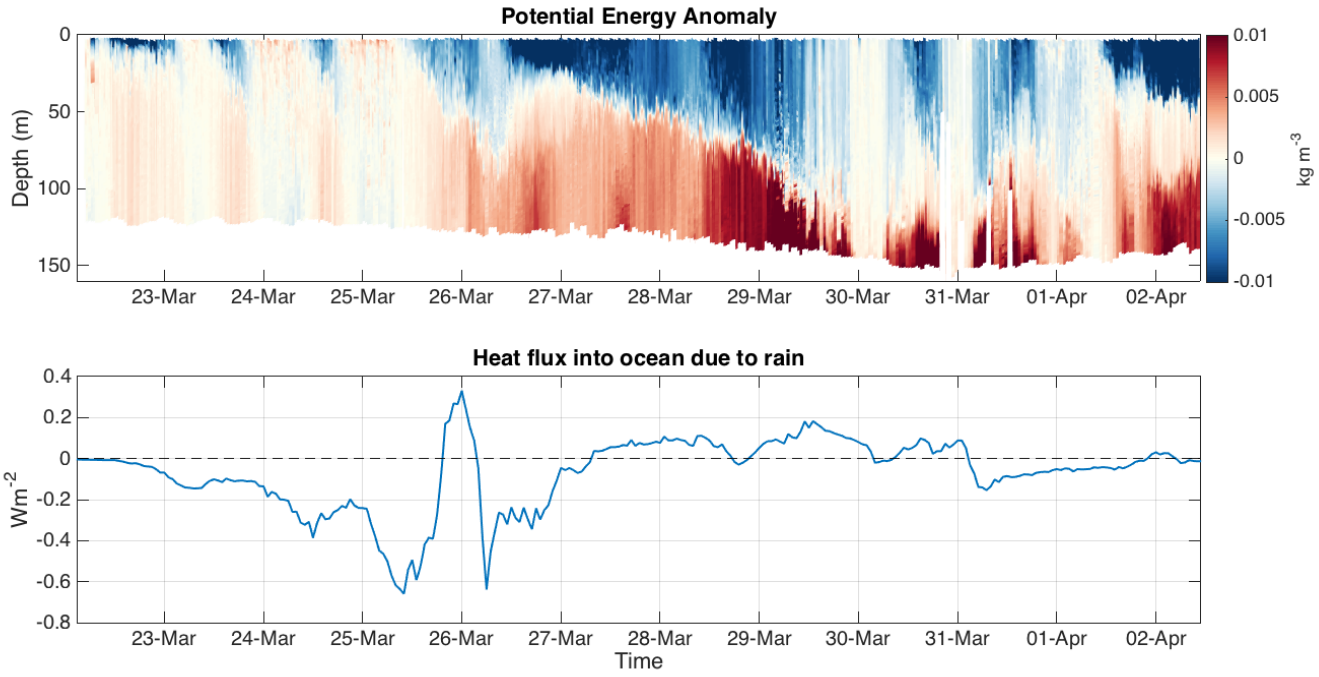

Figure 3.12: Potential density anomaly (kgm^{-3}; top) and the sensible heat flux due to rain (bottom), whereby positive numbers denote heat being fluxed into the ocean, calculated using the Air-Sea Toolbox and based on the Fortran code by Fairall et al (1996).

3.7.6 NAO and stratification onset variability

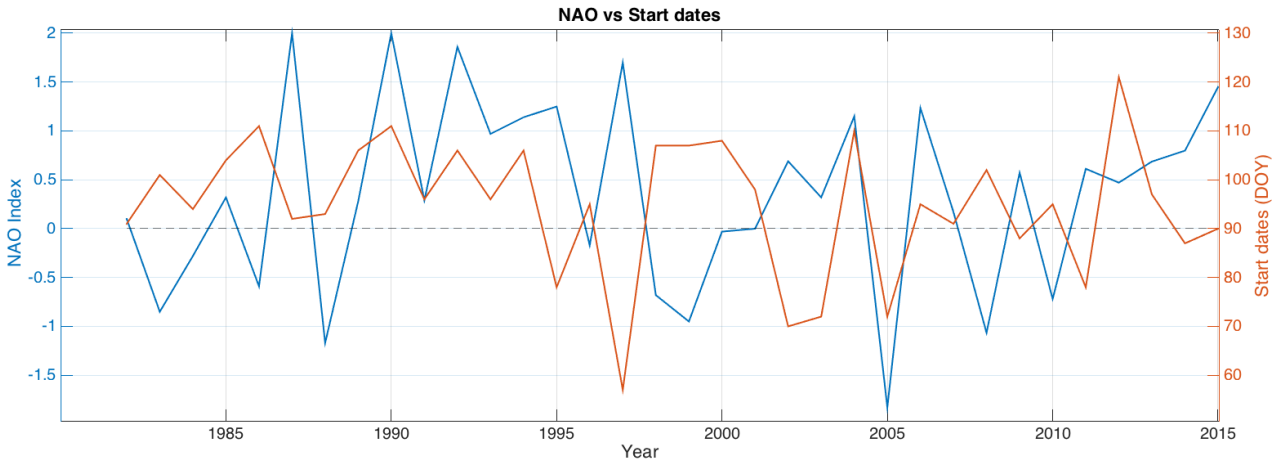

Figure 3.13: Comparison between the NAO (blue), averaged across the month of stratification onset to account for the high variability, compared to the onset date of seasonal stratification (red). While there is some evidence of negative correlation from 1996 to 2002, this is not consistent throughout the entire 1982-2015 time period

3.7.7 Stratification and meteorological variability in 2012

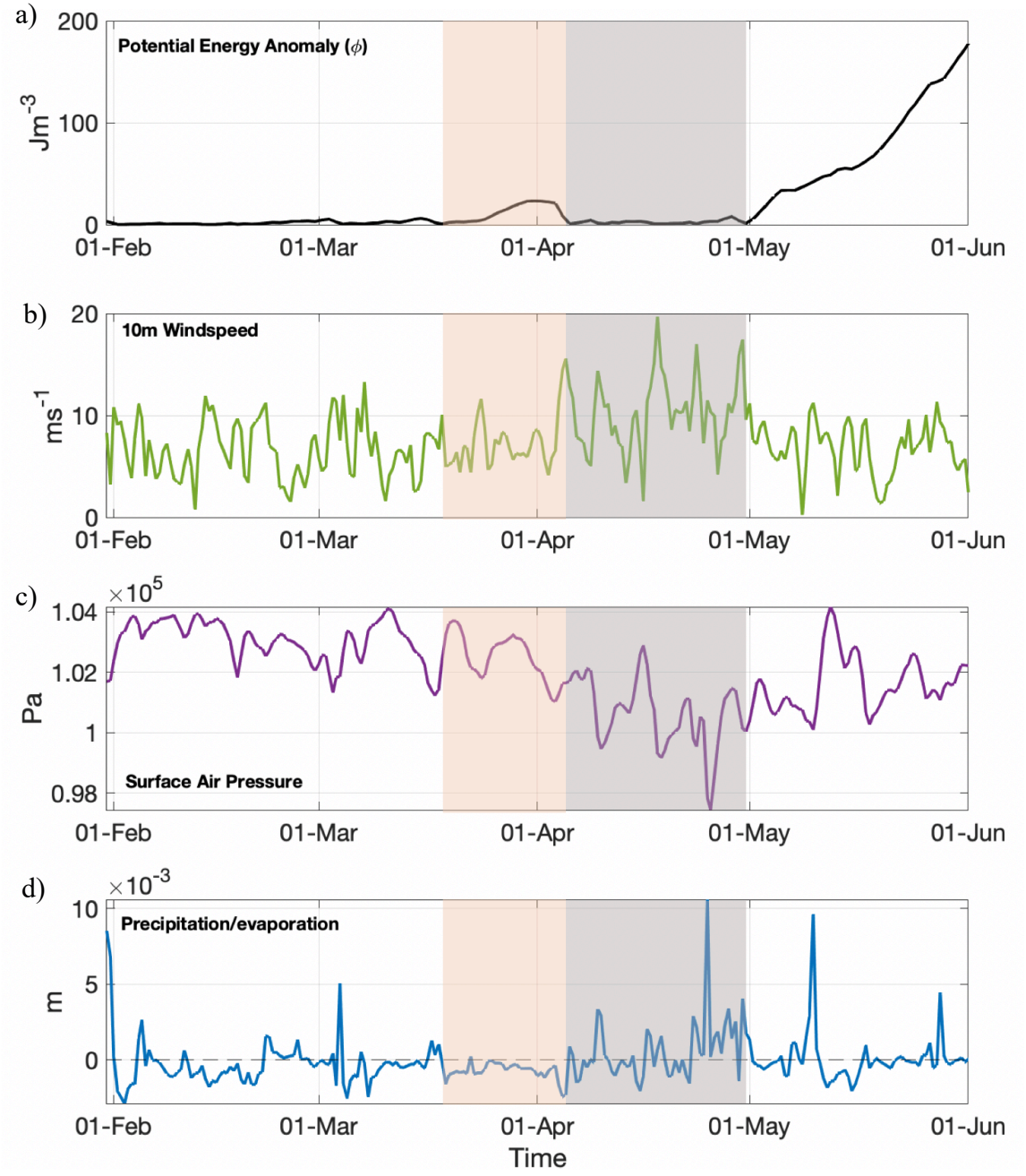

Figure 3.14: a) Potential Energy Anomaly (φ; Jm^{-3}), b) 10m windspeed (ms^{-1}), c) surface air pressure (Pa) and d) the amount of water gained (m) from 12hr cumulative precipitation plus evaporation between the 1st February and the 1st June 2012. The orange box indicates the ephemeral stratification event from the 19th March to the 2nd April 2012, that was later homogenised by a series of storms, indicated by the grey box. Seasonal stratification ultimately formed on the 30th April. The potential energy anomaly was calculated from NEMO-ERSEM model data, while meteorological data was sourced from ERA-Interim (Dee et al, 2011)

3.7.8 Stratification and meteorological variability in 1997

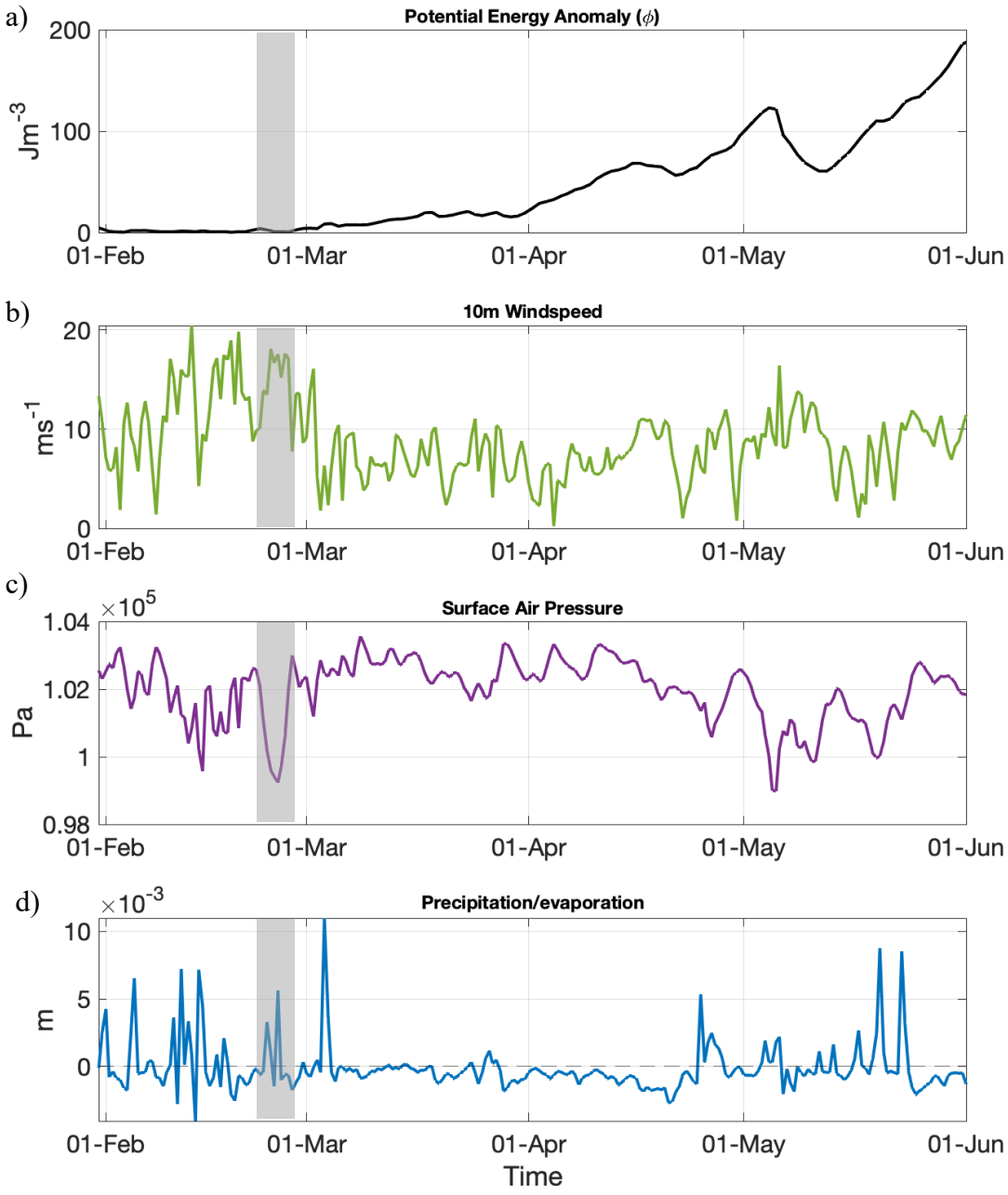

Figure 3.15: a) Potential Energy Anomaly (φ; Jm^{-3}), b) 10m windspeed (ms^{-1}), c) surface air pressure (Pa) and d) the amount of water gained (m) from 12hr cumulative precipitation plus evaporation between the 1st February and the 1st June 1997. Seasonal stratification was initiated on the 26th February 1997, at the end of a low-pressure event that occurred on the 21st February for five days (as indicated by the grey box). This was followed by a long period of relatively quiescent conditions that lasted almost two months. The potential energy anomaly was calculated from NEMO-ERSEM model data, while meteorological data was sourced from ERA-Interim (Dee et al, 2011)

3.8 References

Anderson, S.P., Weller, R.A. and Lukas, R.B., 1996. Surface buoyancy forcing and the mixed layer of the western Pacific warm pool: Observations and 1D model results. *Journal of Climate*, *9*(12), pp.3056-3085.

Béné, C., Barange, M., Subasinghe, R., Pinstrup-Andersen, P., Merino, G., Hemre, G.I. and Williams, M., 2015. Feeding 9 billion by 2050–Putting fish back on the menu. *Food Security*, *7*(2), pp.261-274.

Brereton, A., Siddons, J. and Lewis, D.M., 2018. Large-eddy simulation of subsurface phytoplankton dynamics: an optimum condition for chlorophyll patchiness induced by Langmuir circulations. *Marine Ecology Progress Series*, *593*, pp.15-27.

Cohen, J., Screen, J.A., Furtado, J.C., Barlow, M., Whittleston, D., Coumou, D., Francis, J., Dethloff, K., Entekhabi, D., Overland, J. and Jones, J., 2014. Recent Arctic amplification and extreme mid-latitude weather. *Nature geoscience*, *7*(9), p.627.

Coma, R., Ribes, M., Serrano, E., Jiménez, E., Salat, J. and Pascual, J., 2009. Global warming-enhanced stratification and mass mortality events in the Mediterranean. *Proceedings of the National Academy of Sciences*, *106*(15), pp.6176-6181.

Dee, D.P., Uppala, S.M., Simmons, A.J., Berrisford, P., Poli, P., Kobayashi, S., Andrae, U., Balmaseda, M.A., Balsamo, G., Bauer, D.P. and Bechtold, P., 2011. The ERA-Interim reanalysis: Configuration and performance of the data assimilation system. *Quarterly Journal of the royal meteorological society*, *137*(656), pp.553-597.

Dettinger, M.D., 2004. Fifty-two years of "pineapple-express" storms across the West Coast of North America. *US Geological Survey, Scripps Institution of Oceanography for the California Energy Commission, PIER Project Rep. CEC-500-2005-004*, *20*.

Dettinger, M.D., Ralph, F.M. and Rutz, J.J., 2018. Empirical return periods of the most intense vapor transports during historical atmospheric river landfalls on the US West Coast. *Journal of Hydrometeorology*, *19*(8), pp.1363-1377.

FAO. 2018. *The State of World Fisheries and Aquaculture 2018 - Meeting the sustainable development goals.* Rome. Licence: CC BY-NC-SA 3.0 IGO.

Fairall, C.W., Bradley, E.F., Rogers, D.P., Edson, J.B. and Young, G.S., 1996. Bulk parameterization of air-sea fluxes for tropical ocean-global atmosphere coupled-ocean atmosphere response experiment. *Journal of Geophysical Research: Oceans*, *101*(C2), pp.3747-3764.

Franks, P.J., 2014. Has Sverdrup's critical depth hypothesis been tested? Mixed layers vs. turbulent layers. *ICES Journal of Marine Science*, *72*(6), pp.1897-1907.

García-Martín, E.E., Daniels, C.J., Davidson, K., Lozano, J., Mayers, K.M., McNeill, S., Mitchell, E., Poulton, A.J., Purdie, D.A., Tarran, G.A. and Whyte, C., 2017. Plankton community respiration and bacterial metabolism in a North Atlantic Shelf Sea during spring bloom development (April 2015). *Progress in Oceanography*.

Gill, A. E. (1982). Atmosphere-Ocean Dynamics. International Geophysics Series, 30. *Academic Press, New York*.

Gimeno, L., Nieto, R., Vázquez, M. and Lavers, D.A., 2014. Atmospheric rivers: A mini-review. *Frontiers in Earth Science*, *2*, p.2.

Gómara, Í., Rodríguez Fonseca, B. and Zurita Gotor, P., 2012. Explosive cyclones in the North Atlantic: NAO influence and multidecadal variability. *Publicaciones de la Asociación Española de Climatología. Serie A; 8*.

Gosnell, R., Fairall, C.W. and Webster, P.J., 1995. The sensible heat of rainfall in the tropical ocean. *Journal of Geophysical Research: Oceans*, *100*(C9), pp.18437-18442.

Held, I.M. and Soden, B.J., 2006. Robust responses of the hydrological cycle to global warming. *Journal of climate*, *19*(21), pp.5686-5699.

Holt, J., Wakelin, S., Lowe, J. and Tinker, J., 2010. The potential impacts of climate change on the hydrography of the northwest European continental shelf. *Progress in Oceanography*, *86*(3-4), pp.361-379.

Huot, Y., Morel, A., Twardowski, M.S., Stramski, D. and Reynolds, R.A., 2007. Particle optical backscattering along a chlorophyll gradient in the upper layer of the eastern South Pacific Ocean. *Biogeosciences Discussions*, *4*(6), pp.4571-4604.

Hurrell, J.W. and Deser, C., 2010. North Atlantic climate variability: the role of the North Atlantic Oscillation. *Journal of Marine Systems*, *79*(3-4), pp.231-244.

Hurrell, J.W., 1995. Decadal trends in the North Atlantic Oscillation: regional temperatures and precipitation. *Science*, *269*(5224), pp.676-679.

Hurrell, J.W., Kushnir, Y., Ottersen, G. and Visbeck, M., 2003. An overview of the North Atlantic oscillation. *Geophysical Monograph-American Geophysical Union*, *134*, pp.1-36.

Kendon, M. and McCarthy, M., 2015. The UK's wet and stormy winter of 2013/2014. *Weather*, *70*(2), pp.40-47.

Kromkamp, J., De Bie, M., Goosen, N., Peene, J., Van Rijswijk, P., Sinke, J. and Duinevel, G.C., 1997. Primary production by phytoplankton along the Kenyan coast during the SE monsoon and November intermonsoon 1992, and the occurrence of Trichodesmium. *Deep Sea Research Part II: Topical Studies in Oceanography*, *44*(6-7), pp.1195-1212.

Lacour, L., Ardyna, M., Stec, K.F., Claustre, H., Prieur, L., Poteau, A., D'Alcala, M.R. and Iudicone, D., 2017. Unexpected winter phytoplankton blooms in the North Atlantic subpolar gyre. *Nature Geoscience*, *10*(11), p.836.

Lavers, D.A. and Villarini, G., 2013. The nexus between atmospheric rivers and extreme precipitation across Europe. *Geophysical Research Letters*, *40*(12), pp.3259-3264.

Lavers, D.A., Villarini, G., Allan, R.P., Wood, E.F. and Wade, A.J., 2012. The detection of atmospheric rivers in atmospheric reanalyses and their links to British winter floods and the large-scale climatic circulation. *Journal of Geophysical Research: Atmospheres*, *117*(D20).

Li, J., Sun, C. and Jin, F.F., 2013. NAO implicated as a predictor of Northern Hemisphere mean temperature multidecadal variability. *Geophysical research letters*, *40*(20), pp.5497-5502.

Madec, G., 2015. NEMO ocean engine.

Mantua, N.J. and Hare, S., 2002. Pacific-Decadal Oscillation (PDO). *Encyclopedia of global environmental change*, *1*, pp.592-594.

Mantua, N.J., Hare, S.R., Zhang, Y., Wallace, J.M. and Francis, R.C., 1997. A Pacific interdecadal climate oscillation with impacts on salmon production. *Bulletin of the American Meteorological Society*, *78*(6), pp.1069-1080.

Marshall, J., Kushnir, Y., Battisti, D., Chang, P., Czaja, A., Dickson, R., Hurrell, J., McCartney, M., Saravanan, R. and Visbeck, M., 2001. North Atlantic climate variability: phenomena, impacts and mechanisms. *International Journal of Climatology: A Journal of the Royal Meteorological Society*, *21*(15), pp.1863-1898.

Matthews, T., Murphy, C., Wilby, R.L. and Harrigan, S., 2016. A cyclone climatology of the British-Irish Isles 1871–2012. *International Journal of Climatology*, *36*(3), pp.1299-1312.

McCarthy, M., Spillane, S., Walsh, S. and Kendon, M., 2016. The meteorology of the exceptional winter of 2015/2016 across the UK and Ireland. *Weather*, *71*(12), pp.305-313.

Mölter, T., Schindler, D., Albrecht, A. and Kohnle, U., 2016. Review on the projections of future storminess over the North Atlantic European region. *Atmosphere*, *7*(4), p.60.

Muchan, K., Lewis, M., Hannaford, J. and Parry, S., 2015. The winter storms of 2013/2014 in the UK: hydrological responses and impacts. *Weather*, *70*(2), pp.55-61.

Newell, R.E., Newell, N.E., Zhu, Y. and Scott, C., 1992. Tropospheric rivers?–A pilot study. *Geophysical Research Letters*, *19*(24), pp.2401-2404.

O'Dea, E., Furner, R., Wakelin, S., Siddorn, J., While, J., Sykes, P., King, R., Holt, J. and Hewitt, H., 2017. The CO5 configuration of the 7 km Atlantic Margin Model: large-scale biases and sensitivity to forcing, physics options and vertical resolution. *Geoscientific Model Development*, *10*(8), p.2947.

Omrani, N.E., Keenlyside, N.S., Bader, J. and Manzini, E., 2014. Stratosphere key for wintertime atmospheric response to warm Atlantic decadal conditions. *Climate Dynamics*, *42*(3-4), pp.649-663.

Peings, Y. and Magnusdottir, G., 2014. Forcing of the wintertime atmospheric circulation by the multidecadal fluctuations of the North Atlantic ocean. *Environmental Research Letters*, *9*(3), p.034018.

Perry, M.J., Sackmann, B.S., Eriksen, C.C. and Lee, C.M., 2008. Seaglider observations of blooms and subsurface chlorophyll maxima off the Washington coast. *Limnology and Oceanography*, *53*(5part2), pp.2169-2179.

Pingree, R.D., Holligan, P.M., Mardell, G.T. and Head, R.N., 1976. The influence of physical stability on spring, summer and autumn phytoplankton blooms in the Celtic Sea. *Journal of the Marine Biological Association of the United Kingdom*, *56*(4), pp.845-873.

Pingree, R.D., Holligan, P.M., Mardell, G.T. and Head, R.N., 1976. The influence of physical stability on spring, summer and autumn phytoplankton blooms in the Celtic Sea. *Journal of the Marine Biological Association of the United Kingdom*, *56*(4), pp.845-873.

Pingree, R.D., Mardell, G.T., Holligan, P.M., Griffiths, D.K. and Smithers, J., 1982. Celtic Sea and Armorican current structure and the vertical distributions of temperature and chlorophyll. *Continental Shelf Research*, *1*(1), pp.99-116.

Pinto, J.G., Zacharias, S., Fink, A.H., Leckebusch, G.C. and Ulbrich, U., 2009. Factors contributing to the development of extreme North Atlantic cyclones and their relationship with the NAO. *Climate dynamics*, *32*(5), pp.711-737.

Poulton, A.J., Davis, C.E., Daniels, C.J., Mayers, K.M., Harris, C., Tarran, G.A., Widdicombe, C.E. and Woodward, E.M.S., 2017. Seasonal phosphorus and carbon dynamics in a temperate shelf sea (Celtic Sea). *Progress in Oceanography*.

Price, J.F., 1979. Observations of a rain-formed mixed layer. *Journal of Physical Oceanography*, *9*(3), pp.643-649.

Ramos, A.M., Tomé, R., Trigo, R.M., Liberato, M.L. and Pinto, J.G., 2016. Projected changes in atmospheric rivers affecting Europe in CMIP5 models. *Geophysical Research Letters*, *43*(17), pp.9315-9323.

Ruardij, P., Van Haren, H. and Ridderinkhof, H., 1997. The impact of thermal stratification on phytoplankton and nutrient dynamics in shelf seas: a model study. *Journal of Sea Research*, *38*(3-4), pp.311-331.

Ruiz-Castillo, E., Sharples, J. and Hopkins, J., 2019. Wind-driven strain extends seasonal stratification. *Geophysical Research Letters*, *46*(22), pp.13244-13252.

Rumyantseva, A., Lucas, N., Rippeth, T., Martin, A., Painter, S.C., Boyd, T.J. and Henson, S., 2015. Ocean nutrient pathways associated with the passage of a storm. *Global Biogeochemical Cycles*, *29*(8), pp.1179-1189.

Sackmann, B.S., Perry, M.J. and Eriksen, C.C., 2008. Seaglider observations of variability in daytime fluorescence quenching of chlorophyll-a in Northeastern Pacific coastal waters. *Biogeosciences Discussions*, *5*(4), pp.2839-2865.

Sharples, J., 2007. Potential impacts of the spring-neap tidal cycle on shelf sea primary production. *Journal of Plankton Research*, *30*(2), pp.183-197.

Sharples, J., Ross, O.N., Scott, B.E., Greenstreet, S.P. and Fraser, H., 2006. Inter-annual variability in the timing of stratification and the spring bloom in the North-western North Sea. *Continental Shelf Research*, *26*(6), pp.733-751.

Simpson, J.H. and Bowers, D., 1981. Models of stratification and frontal movement in shelf seas. *Deep Sea Research Part A. Oceanographic Research Papers*, *28*(7), pp.727-738.

Simpson, J.H., Brown, J., Matthews, J. and Allen, G., 1990. Tidal straining, density currents, and stirring in the control of estuarine stratification. *Estuaries*, *13*(2), pp.125-132.

Simpson, J.H. and Hunter, J.R., 1974. Fronts in the Irish sea. *Nature*, *250*(5465), p.404-406

Simpson, J.H., 1981. The shelf-sea fronts: implications of their existence and behaviour. *Philosophical Transactions of the Royal Society of London. Series A, Mathematical and Physical Sciences*, *302*(1472), pp.531-546.

Smith-Godfrey, S., 2016. Defining the blue economy. *Maritime affairs: Journal of the national maritime foundation of India*, *12*(1), pp.58-64.

Sverdrup, H.U., 1953. On conditions for the vernal blooming of phytoplankton. *J. Cons. Int. Explor. Mer*, *18*(3), pp.287-295.

Taylor, J.R. and Ferrari, R., 2011. Shutdown of turbulent convection as a new criterion for the onset of spring phytoplankton blooms. *Limnology and Oceanography*, *56*(6), pp.2293-2307.

Townsend, D.W., Cammen, L.M., Holligan, P.M., Campbell, D.E. and Pettigrew, N.R., 1994. Causes and consequences of variability in the timing of spring phytoplankton blooms. *Deep Sea Research Part I: Oceanographic Research Papers*, *41*(5-6), pp.747-765.

Waliser, D.E., Moncrieff, M.W., Burridge, D., Fink, A.H., Gochis, D., Goswami, B.N., Guan, B., Harr, P., Heming, J., Hsu, H.H. and Jakob, C., 2012. The "year" of tropical convection (May 2008–April 2010): Climate variability and weather highlights. *Bulletin of the American Meteorological Society*, *93*(8), pp.1189-1218.

Wihsgott, J.U., Sharples, J., Hopkins, J.E., Woodward, E.M.S., Hull, T., Greenwood, N. and Sivyer, D.B., 2019. Observations of vertical mixing in autumn and its effect on the autumn phytoplankton bloom. *Progress in Oceanography*.

Woollings, T., Hannachi, A. and Hoskins, B., 2010. Variability of the North Atlantic eddy-driven jet stream. *Quarterly Journal of the Royal Meteorological Society*, *136*(649), pp.856-868.

Woollings, T., Hoskins, B., Blackburn, M. and Berrisford, P., 2008. A new Rossby wave–breaking interpretation of the North Atlantic Oscillation. *Journal of the Atmospheric Sciences*, *65*(2), pp.609-626.

Yamamoto, A., Palter, J.B., Lozier, M.S., Bourqui, M.S. and Leadbetter, S.J., 2015. Ocean versus atmosphere control on western European wintertime temperature variability. *Climate dynamics*, *45*(11-12), pp.3593-3607.

Zhu, Y. and Newell, R.E., 1998. A proposed algorithm for moisture fluxes from atmospheric rivers. *Monthly weather review*, *126*(3), pp.725-735.

4. Stratification triggered by winter storm events: is there enough light for phytoplankton growth?

Jennifer Jardine[1], Matthew Palmer[2], Claire Mahaffey[1], Jason Holt[2]

Prepared as a paper submission

[1.] University of Liverpool, Liverpool, L69 3BX

[2.] National Oceanography Centre Liverpool, Liverpool, L3 5DA

Light is the primary limiting factor for winter phytoplankton growth at temperate latitudes, and is therefore a control on spring bloom seeder populations and subsequent succession. In continental shelf seas, a combination of net cooling and high winter winds result in turbulent mixing that distributes phytoplankton cells over the entire depth of the water column, resulting in light limitation. Here we present observations from winter 2015 that show sporadic rain events help to initiate ephemeral periods of stratification that may persist up to 2 days, coinciding with increased chlorophyll florescence. Ephemeral stratification is more likely to occur during late winter, when a combination of positive buoyancy from increased heating, freshwater input and a decrease in winter winds is more likely to outcompete the mixing effects of wind, waves and convection. The time that phytoplankton cells spend in the euphotic zone is derived from the turbulent eddy diffusivity under varying euphotic depth conditions (between 16m and 51m). We investigate phytoplankton dynamics under two mixed layer depth (z_{sml}) conditions: a highly dynamic z_{sml} that is representative of sporadic rain events, and a fixed z_{sml}, derived from observed daily averages. The classification of the z_{sml} is shown to be critical when determining mixing timescales during short-lived stratification events. A highly dynamic, time-varying estimate for the z_{sml} results in phytoplankton cells spending up to 1.5 hours longer in the euphotic zone than a fixed z_{sml}. Crucially, sporadic rain events allow phytoplankton cells to remain for 5 hours longer in the euphotic zone during periods of high turbidity. Using a simplified model, we demonstrate that ephemeral winter stratification are critical in helping to maintain winter phytoplankton populations by improving light conditions.

4.1 Introduction

In mid and high-latitude regions, light is a first order control on phytoplankton growth and carbon fixation (Riley, 1957; Sverdrup, 1953; Smetacek and Passow, 1990; Siegal et al, 2002). Light is seasonal, with maximum and minimum light levels occurring during the summer and winter solstices respectively. The amount of light available for phytoplankton cells is further modulated by meteorological conditions, such as cloud cover (Hickman et al, 2012), and vertical mixing due to wind (Townsend et al, 1994; Waniek 2003; Sharples et al 2006; Henson

et al 2006) and spring-neap tidal modulations (Sharples et al, 2007; Sharples et al, 2009). Observations suggest that exponential phytoplankton growth can only occur once the average light level within a mixed layer exceeds a threshold of 20.9 Wm^{-2} (Riley, 1957; Townsend et al 1994), or when the mixed layer shoals above a critical depth where net growth through photosynthesis exceeds net losses through respiration (Sverdrup, 1953; Chiswell et al 2011).

In temperate regions, light typically limits phytoplankton growth in winter due to low incoming solar irradiance accentuated by vertical mixing driven by wind stress (Townsend et al, 1992; Henson et al 2006; Sharples et al 2006). This is particularly relevant in continental shelf sea regimes, where phytoplankton cells are rapidly transported throughout a homogenised water column. Nevertheless, phytoplankton growth is still observed during these winter months (Townsend et al, 1994; Taylor and Ferrari, 2011), and is common in coastal areas inundated with riverine outflow, where the formation of a halocline can trap phytoplankton within a shallow euphotic zone (Labry et al 2001).

In continental shelf seas, the onset of seasonal stratification is often considered a precursor for phytoplankton growth, yet observations from the open ocean suggest that enhanced phytoplankton productivity can occur in the absence of vertical stratification (Townsend et al, 1992; Huisman et al, 1999; Durbin et al 2003; Taylor and Ferrari, 2011). For example, Taylor and Ferrari (2011) demonstrated that net phytoplankton growth can occur following the shutdown of turbulent convection, suspending phytoplankton cells within the euphotic zone. There are other instances when winter phytoplankton growth has occurred due to ephemeral stratification, for example, from transient eddies in the North Atlantic (Lacour et al, 2017). It has been postulated that rainfall could potentially promote phytoplankton growth in winter, due to the initiation of short-term, transient stratification events that would trap phytoplankton cells near to the surface (Franks, 2014). However, the influence of freshwater input on vertical stability has been primarily attributed to riverine outflow, particularly on continental shelves (e.g. Labry et al, 2001; Gohin et al, 2015).

The Northwest (NW) European Continental Shelf is positioned directly beneath the North Atlantic Storm Track (Woollings et al, 2012), which acts as a conveyor belt for storms that bring strong winds and rainfall across the entire continental shelf. Extreme rainfall may also occur as a result of atmospheric rivers, which occur in the warm belt of cyclones as they translate across the Atlantic (Newell et al, 1992; Zhu and Newell, 1998). These phenomenon

transport large volumes of atmospheric water (Newell et al, 1992; Zhu and Newell, 1998; Gimeno et al, 2014), and have been linked to extreme flooding events in the UK (Lavers and Viliarini, 2013; Lavers et al, 2012).

In this thesis, Chapter 3 demonstrated that rain from storm events can provide sufficient buoyancy to directly trigger the onset of seasonal stratification on the NW European Shelf. In this Chapter, we explore the biological response of phytoplankton to short-term rain events that occur throughout the winter period. We disentangle the photo-adaptive response of chlorophyll to changing light fields, to identify how ephemeral stratification events maintain phytoplankton growth during a traditionally unproductive season.

4.2 Methodology

4.2.1 Study Site

Located on the western approaches of the North Atlantic, the Celtic Sea is a 500km (Huthnance et al, 2009) open-shelf region that was the main study region for the Shelf Sea Biogeochemistry Project (SSB, www.uk-ssb.org). As part of SSB, two gliders were deployed between February and March 2015 (Fig. 4.1), programmed to conduct repeat 150km transects from the Central Celtic Sea (CCS) mooring, to the shelf break site (CS2). Due to the high-resolution temporal and spatial sampling, the glider captured near-surface buoyancy at sufficiently high resolutions that subtle ocean-atmosphere coupling could be captured, such as from rain events.

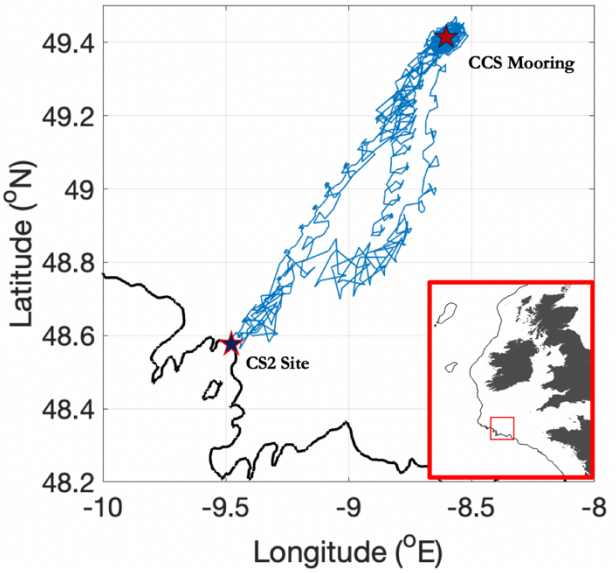

Fig. 4.1: Location of the glider track (blue), in relation to the Northwest European Shelf, from the 1st February 2015 to the 1st April 2015. The locations of the Central Celtic Sea (CCS) Mooring site and the shelf break (CS2) site are also labelled, along with the 200m isobath (black line)

The Celtic Sea is an ideal location to investigate the short-term meteorological variations in surface buoyancy, as riverine outflow is constrained to the coastal currents that only weakly impact the open shelf regions (Pingree and Le Cann, 1989; Brown et al, 2003; Fernand et al 2006). Although riverine water from Bristol Channel could have a significant influence on surface buoyancy in the northern region of the Celtic Sea (Brown we al, 2003; Young et al, 2004), the direct influence of riverine inputs towards the CCS site is limited (Ruiz-Castillo et al, 2019a).

The dynamic geology of the Celtic Sea results in isolated regions of intense mixing, such as over banks (Palmer et al, 2013), that can promote elevated summer phytoplankton growth through the flux of new nutrients into the nutrient-depleted surface layer (Davidson et al, 2013; Tweddle et al, 2013). During winter, when light is the primary limiting factor for phytoplankton growth, such localised mixing events could result in any weak stratification being rapidly eroded, consequently inhibiting phytoplankton growth. However, as the gliders are isolated from the large banks (e.g. Jones' Bank is 71 km from the CCS mooring), the influence of such enhanced mixing should be limited.

Supplementary data used in this Chapter was collected by a nearby CEFAS Smartbuoy (data provided by Tom Hull, CEFAS) that measured photosynthetically active radiation (PAR; μE m^2 s^{-1}) and chlorophyll concentrations (μg l^{-1}). Meteorological data was recorded by the UK MetOffice ODAS Buoy, moored at the CCS site over the study period, that provided observed windspeed and net surface heat flux (Q_{net}; Wihsgott et al, 2018). Observed meteorological data was complimented by modelled evaporation and precipitation, downloaded from ERA-Interim (Dee et al, 2011). Further details of data methodology and acquisition are described in Chapter 2.

4.2.2 Assessing the light environment with varying mixed layer depths

The euphotic zone depth is defined as the depth where light is at 1% the incident light intensity at the surface and is thus independent of vertical water column density structure. Net phytoplankton growth occurs above the euphotic depth, yet for a phytoplankton cell to spend suitably long periods of time within this euphotic zone, their position within it must be maintained. This is largely governed by the rate of vertical mixing and/or the depth of the

surface mixed layer, z_{sml} (Sverdrup, 1953; Taylor and Ferrari, 2011; Chiswell et al, 2011; Brody and Lozier, 2015).

Rain-induced stratification events will directly affect upper ocean stability through the input of buoyancy. The formation of a freshwater surface layer will modulate the amount of light available for phytoplankton growth throughout the course of the day. The amount of time phytoplankton would spend in the euphotic zone as a result of such short-term stratification events will be investigated through dimensional analysis, where representative mixing timescale (t_{mix}) for individual cells (Denman and Gargett, 1983; Moore et al 2003) can be defined by:

(4.1) $$t_{mix} = L^{2/3}. \varepsilon^{-1/3}$$

In equation [4.1], L represents the scale of the largest turbulent eddies, which in the upper ocean is defined by z_{sml} (m), and ε is the turbulent kinetic eddy dissipation rate (m^2s^{-3}).

In previous literature, phytoplankton mixing timescales have been averaged over an entire day (e.g. Moore et al, 2003). While this gives the average amount of light the phytoplankton will receive over the course of a day, rain-induced stratification events are highly dynamic, often persisting on time scales of less than 1 day. Consequently, the amount of light phytoplankton will receive as a result of such meteorological events will vary throughout the day itself, and thus a daily averaged t_{mix} may not fully capture the effect of ephemeral rain events on the surface ocean.

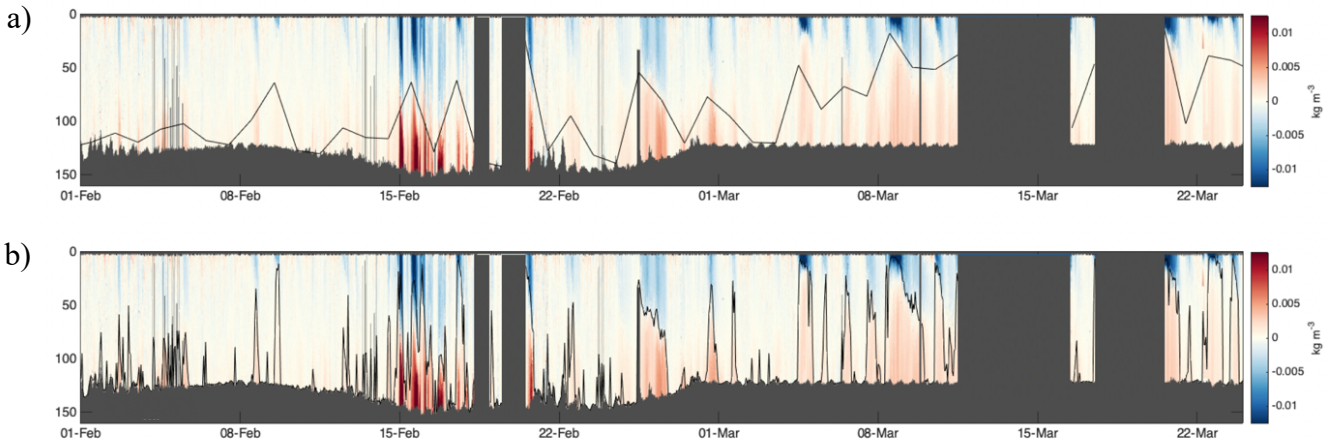

Fig. 4.2: Potential energy anomaly (kg m^{-3}) with the black lines defining two different estimates for the surface mixed layer depth, z_{sml}: a) the z_{sml}: averaged over the entirety of the photoperiod (ML_{ph}), and b) the 1-hourly z_{sml}: (ML_{1hr})

To quantify the importance of using a highly dynamic z_{sml} compared to a more stable regime, two estimates for z_{sml} were used (Fig 4.2). Using a bespoke criterion to fully capture the subtly of ephemeral stratification events, the depth of this time-varying z_{sml} was defined as the depth where the difference in surface potential density ($\sigma\rho_0$) and potential density at depth z ($\sigma\rho_z$) was equal to 0.004 kg m^{-3}. This z_{sml} was then interpolated onto a 1-hourly temporal grid and defined as the 1-hourly Mixed Layer Depth (ML_{1hr}; Fig 4.2b). A more stable Mixed Layer Depth (ML_{ph}; Fig 2a) was also estimated by averaging ML_{1hr} across the entirety of the photoperiod, which is estimated from nearby Smartbuoy PAR data to be from 06:00 to 19:00.

Realistic, time-varying estimates for ε within an exponentially decaying surface mixed layer can be calculated using (Haskell et al, 2016):

$$\varepsilon = \left(\frac{\rho_a C_D W_{10}^2}{\rho_w}\right)^{\frac{3}{2}} (k_* z)^{-1} \quad (4.2)$$

In equation [4.3], ρ_a is the density of air (kg m^{-3}), C_D is the drag coefficient, z is the thickness of the SML (m) and k_* is the von Karman constant, taken to be 0.41 (Thorpe, 2007). The initial surface forcing is based on the wind speed at 10m above the surface (W_{10}).

A time varying estimate for C_D at 10m can be estimated using the equation from Amorocho and Devries (1980):

$$C_D = 0.0015 \left[1 + exp\left(\frac{w_{10} - 12.5}{1.56}\right)\right]^{-1} + 0.00104 \quad (4.3)$$

4.3 Results and Discussion

4.3.1 Short-term stratification events from glider measurements

Between February and March 2015, the gliders sampled through a number of winter rain events, defined as where the rate of precipitation exceeded the rate of evaporation (Fig. 4.3a), that correspond to the periods of ephemeral stratification observed in the potential density anomaly (Fig. 4.3b). These stratification events persisted for 1 and 2 days, at a time when the water column would otherwise have been considered characteristically homogenous. The

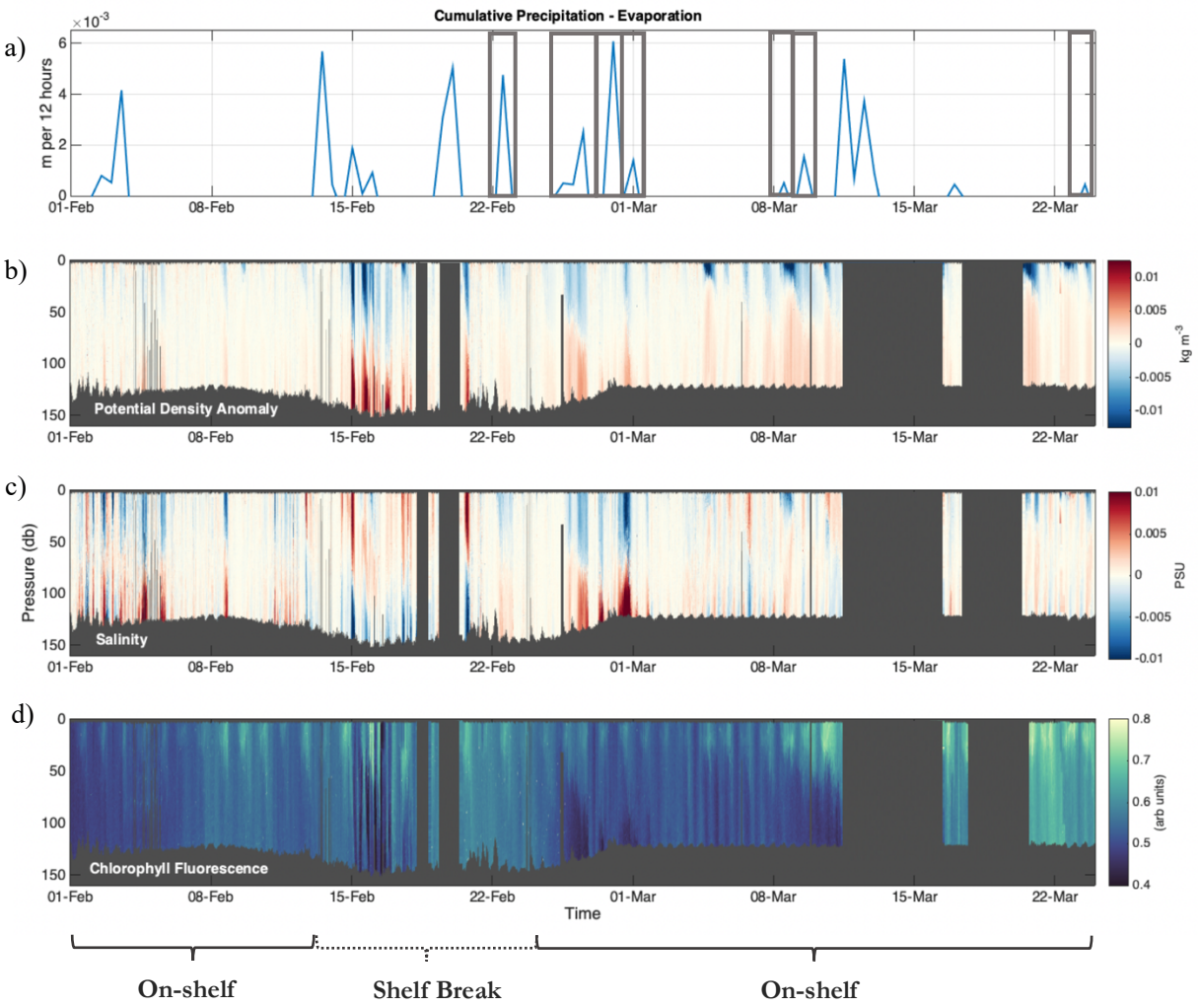

Fig. 4.3: a) Cumulative precipitation minus evaporation over 12 hours from ERA-Interim (Dee et al, 2011), b) potential density anomaly (kg m-3), c) salinity anomaly (PSU), and d) chlorophyll fluorescence (arb units). The grey boxes indicate the rain events that cause ephemeral stratification events, as seen in the salinity anomaly.

salinity anomaly displayed a surface freshwater layer in 7 out of 15 rain events, indicative of a halocline. The biological response to these stratification events, as seen in Fig. 4.3d, will be further discussed in Section 4.3.2.

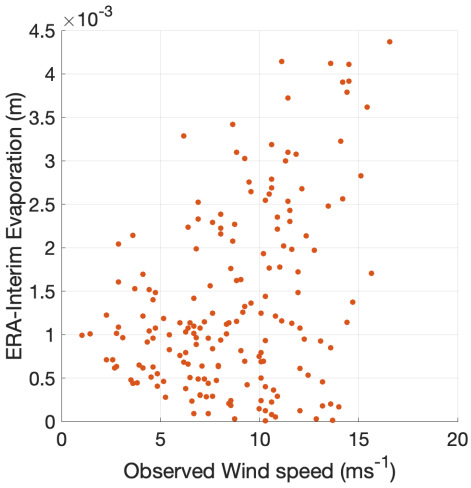

Fig. 4.4: Observed 12-hour wind speed (ms^{-1}) to the 12-hour cumulative evaporation (m) from ERA-Interim (Dee et al, 2011).

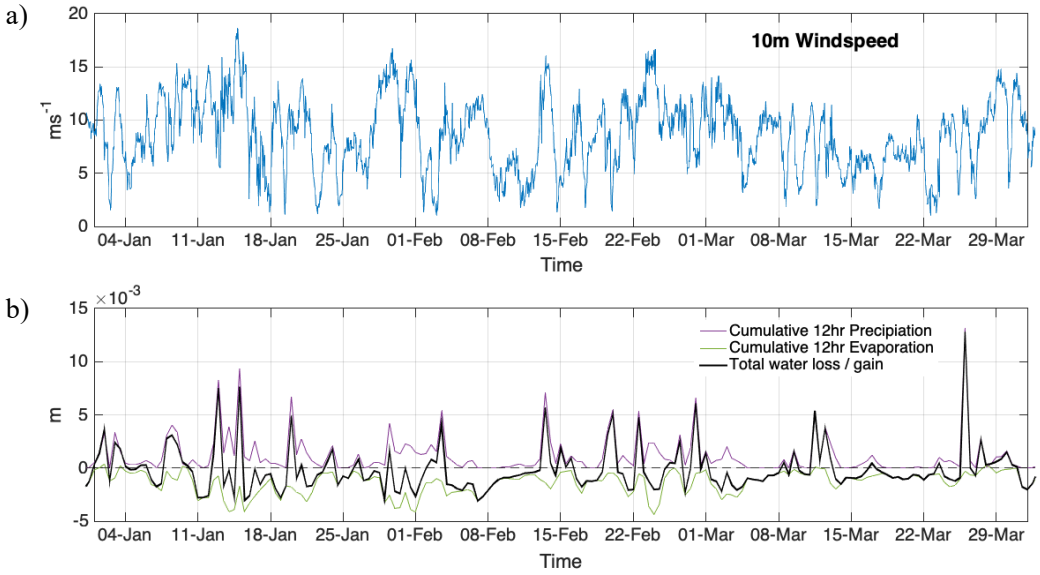

Fig. 4.5: a) Observed 10m windspeed, as measured by the OSAS Metbuoy and b) comparisons of the precipitation (purple), evaporation (green) and the total freshwater loss (negative) or gain (positive) from the sea surface (black). Both the precipitation and evaporation are cumulative sums across 12 hours (source: ERA-Interim. Dee et al 2011).

As earlier stated, 8 of the observed rain events did not cause surface freshening (Fig 4.3a). One example is the rain event that occurred on the 13th February 2015, where the cumulative 12-hour precipitation reached 5.6×10^{-3} m, and yet there was no observed change in the surface salinity. An explanation for this can be found when comparing the 10m windspeed to the evaporation (Fig. 4.4), as the highest evaporation rates were only present during periods of high windspeed. The maximum evaporation of 4.4×10^{-3} m occurred on the 24th February 2015, when observed wind speeds reached a maximum of 16.7 ms^{-1}. Evaporation is proportional to wind speeds, due to the physical removal of water molecules from the sea surface whilst also maintaining the humidity gradient (Yu, 2007). As such, the bulk evaporation (Brown and Kummerow, 2014) is directly related to windspeed by:

$$E = \rho_a C_q W_{10}(q_0 - q_a) \tag{4.4}$$

where ρ_a is the density of air, C_q is the transfer coefficient, W_{10} is the 10m windspeed and q_0 and q_a are the specific humidity at the surface and 10m respectively. Therefore, a higher evaporation rate will directly reduce the stability of a water column, as described by the buoyancy flux, b_f (in $m^2\ s^{-3}$; modified from Gill, 1982):

(4.4) $$b_f = \frac{g\alpha Q_{net} + g\beta\,(E-P)s}{\rho_0\, C_p}$$

where E and P are the evaporation and precipitation rates (kg m^{-2}), α and β are the expansion coefficients due to temperature and salinity respectively, Q_{net} is the surface heat flux, ρ_o is the surface density, C_p is the specific capacity of seawater and g is the gravitational constant. As such, the rate of precipitation needs to exceed the rate of evaporation, which is proportional to wind stress, to result in a positive buoyancy effect from rainfall (Fig. 4.5). Yet, only when the combined positive buoyancy effects from freshwater and surface heating outcompete mixing from convection, wind and tidal stresses will stratification occur.

During early winter 2015, this criterion is rarely met. The mean wind speed observed from January to April 2015 was 8.6 ms^{-1}, with a maximum wind speed of 18.6 ms^{-1} recorded on the 14th January 2015 (Fig. 4.5). This, combined with a predominantly negative Q_{net} (Fig. 4.6),

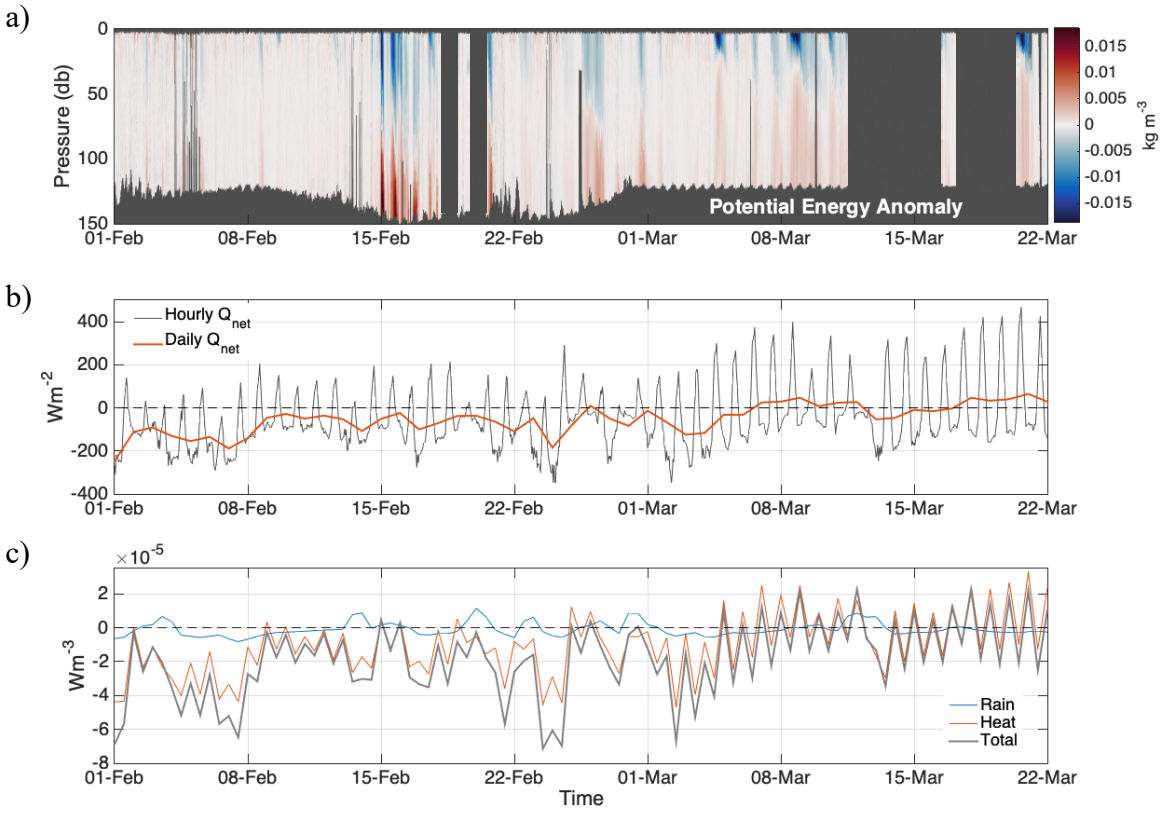

Fig 4.6: a) Potential density anomaly, for reference (kg m^{-3}), b) Net surface heat flux into the ocean (Q_{net}) both at an hourly resolution (black) and daily-averaged (red) and; c) contributions to the potential energy anomaly ($\delta\phi$ / δt) from rain and evaporation (blue), heating and cooling (red) and the total contributions (grey) from rain/evaporation, heating/cooling, tides and wind. Note that for clarity, the individual contributions from wind and tides have been neglected from c, but they have been included when calculating the total contributions.

resulted in a system where freshwater input was the only positive contributor to buoyancy. Mixing processes still completely dominated and acted to rapidly homogenise the water column. Stratification only occurred when the positive buoyancy effects of heating and freshwater input combined to outcompete mixing terms. Such occurrences were more frequent towards the winter-spring transition, throughout late February and March, when the seasonal increase in Q_{net} allowed stratification to be more readily formed. Note that throughout the time series, heating and cooling were the most dominant contributors to stratification formation and destruction (Fig. 4.6c).

In contrast to the surface freshening, more saline waters were observed from the surface to 100m depth between the 15th and 19th February 2015, despite the high rainfall. This is likely a consequence of cross-shelf exchange of oceanic water onto the shelf, as the glider was an average of 37.4 km away from the shelf break during this time.

Although direct riverine inputs to this region of the Celtic Sea interior are limited during the winter (Ruiz-Castillo et al 2019a), the persistent on-shelf salinity gradient could result in wind-driven transport of freshwater into the glider path from the more northerly regions (Ruiz-Castillo et al, 2019b). As wind and rain events often co-exist, a proportion of the halostratification observed in Fig 4.3 is then likely to be a combination of freshwater input through rain, and wind-driven transport (as described by Ruiz-Castillo et al, 2019b). For example, by calculating the estimated salinity change in the SML based on the amount of rain that fell, the contribution of the rainfall events to the stratification observed on the 22nd, 25th and 28th February was 77%, 5% and 15% respectively. The remainder of the surface freshening could be a result of errors within the ERA-Interim dataset, or a due to wind-driven transport of freshwater into the area (see Ruiz-Castillo et al, 2019b and Chapter 3). As such, it is possible that a combination of these two meteorological processes resulted in the ephemeral halostratification events observed throughout the winter period. Nevertheless, the biological response to such ephemeral halostratification, as a result of sporadic meteorological conditions, can still be explored (see Section 4.3.2).

4.3.2 The biogeochemical response to ephemeral stratification events

There is an increase in chlorophyll from short-term winter stratification events, displayed as an increase in chlorophyll fluorescence (Fig. 3d). It is unclear if the increase in chlorophyll fluorescence measured at the shelf break from the 15th to the 19th February 2015 reflects net phytoplankton growth due to ephemeral stratification, or advection of oceanic phytoplankton onto the shelf. Nevertheless, locations on-shelf also displayed a clear increase in chlorophyll fluorescence that we hypothesise is due to an increase in phytoplankton biomass and not a photo-adaptive response of phytoplankton cells to varying light environments (Moore et al, 2006).

To test this hypothesis, data from a nearby Smartbuoy was used to investigate changes in night-time chlorophyll concentrations. As the photo-adaptive response of phytoplankton are limited, night-time values of chlorophyll give a more representative view of changes in phytoplankton biomass. Night-time Smartbuoy chlorophyll concentrations displayed a gradual increase in chlorophyll concentrations from 0.5 to 1.1 $\mu g\ l^{-1}$ over 45 days (2nd February to the 21st March), corresponding with a near-linear PAR increase from 199 to 423 $\mu Em^{-2}s^{-1}$ over the same time period (Fig. 4.7). As the accuracy of the SmartBuoy is within 0.01$\mu g\ l^{-1}$, we can be confident

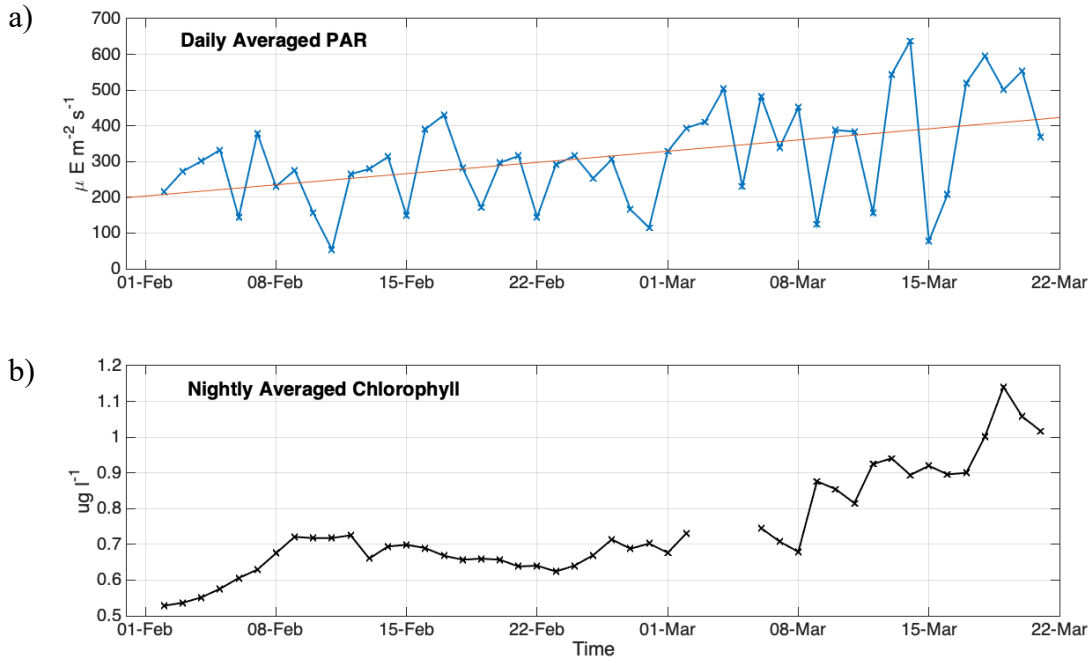

Fig. 4.7: a) Daily averaged photosynthetically active radiation (PAR, blue) at the sea surface, measured by the CEFAS Smartbuoy, including a linear regression (red); b) Nightly averaged chlorophyll-a concentrations from the Smartbuoy

that this is a robust increase and suggests strong evidence of phytoplankton growth, as opposed to the photoacclimation of cells in a low-light environment (Moore et al, 2006).

Smartbuoy data further supports this result as the rate of chlorophyll increase accelerated by a factor of two, from 0.002 $\mu g\ l^{-1}\ d^{-1}$ during February to 0.2 $\mu g\ l^{-1}\ d^{-1}$ in March (Fig. 4.7), coinciding with the more frequent occurrences of ephemeral stratification events (Fig 4.6b). A similar slow response of winter phytoplankton growth was found by Mignot et al (2018) in the North Atlantic Ocean and was speculated to be a direct result of a deepening mixed layer that diluted the ratio of zooplankton to phytoplankton (Evans and Parslow, 1985; Behrenfeld, 2010; Mignot et al 2018). As the maximum depth of the mixed layer here is constrained by the maximum depth of the water column, this is unlikely to be the cause in this case or in shelf sea environments generally.

4.3.3 Assessing the light environment under variable mixing

Following equations [4.1-4.3], an estimate for the mixing timescales of phytoplankton under realistic estimates for mixing (ε), observed wind forcing (Fig. 4.8a) and the two estimates for z_{sml} (ML_{hr} or ML_{ph}) were calculated. Estimated values for C_D (Fig. 4.8b), based upon the approximation by Amorocho and Devries (1980), displayed periods of high variability, particularly from 22nd to the 23rd February 2015. Background estimates of $2.7x10^{-3}$ were consistent with the upper limit recorded by Yelland and Taylor (1996). Estimated values for ε during the winter in the Celtic Sea (Fig 4.8c) were typically 2-3 orders of magnitude higher than the $1x10^{-6}$ to $1x10^{-7}\ m^2s^{-3}$ estimates observed by Moore et al (2003) over a homogenised 100m water-column in the Irish Sea. While this difference seems large, the z_{sml} in this study was highly variable and could be as shallow as 10m depth. This, combined with high winds of up to $17ms^{-1}$ (Fig. 4.6a), would result in a turbulent surface mixed layer where values for ε could readily exceed $1x10^{-6}\ m^2s^{-3}$.

By incorporating the time-varying estimates for ε, with ML_{1hr} and ML_{ph}, into equation [4.1], the phytoplankton mixing timescales under a range of scenarios can be explored.

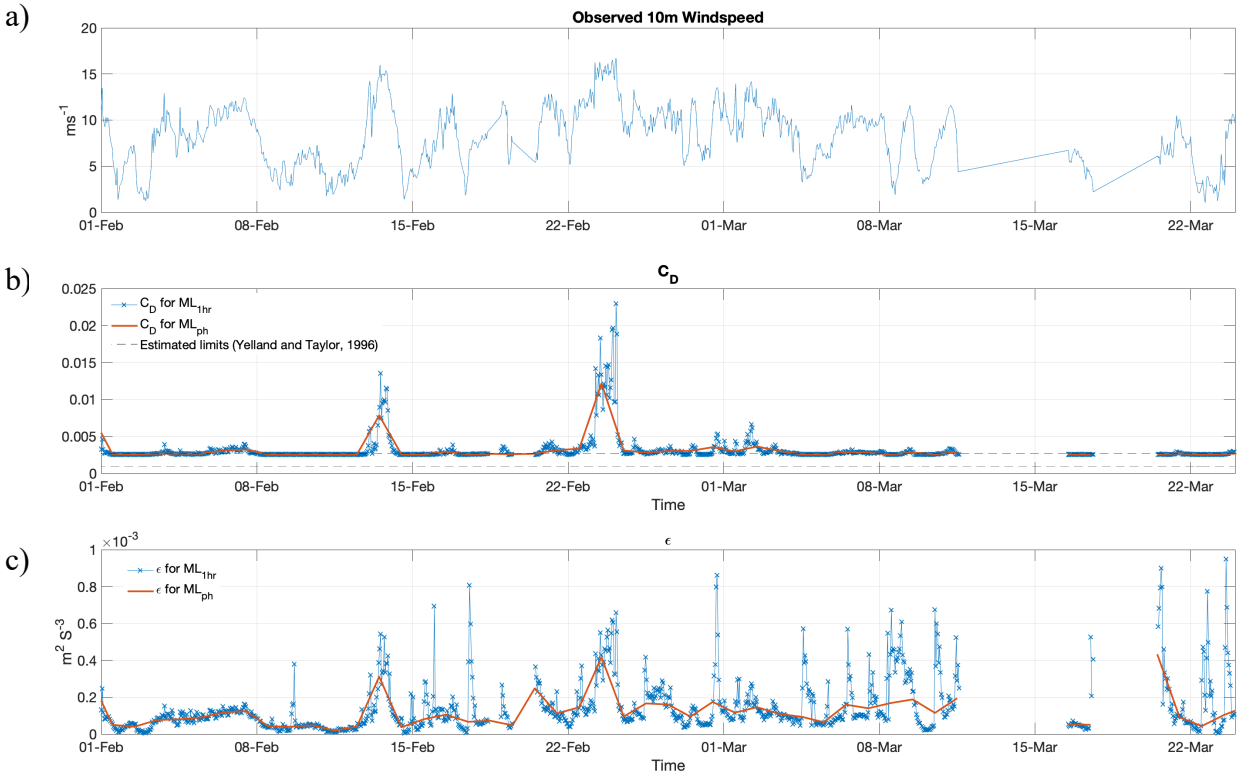

Fig. 4.8: a) Measured 10m windspeed from the ODAS Metbuoy, b) Estimates for the drag coefficient (C_D) using the approximation by Amorocho and Devries (1980) for the ML_{1hr} (blue) and the ML_{ph} (red) mixed layers, where the dashed lines are the upper and lower limits of C_D estimates from Yelland and Taylor (1996); c) estimates of the vertical turbulent eddy dissipation for ML_{1hr} (blue) and ML_{ph} (red)

a) No mixed layer

Despite the formation of short-lived stratification events throughout late February and March 2015, the water column from the 1st to the 15th February was relatively homogenised. Under these conditions, ML_{1hr} and ML_{ph} were equal and displayed equivalent mixing over the maximum water depth. In this homogenised water column, the length of time phytoplankton remained in the euphotic zone was relatively constant (Fig. 4.9 and Fig. 4.10), despite varying ε. An explanation for this can be considered by the ratio of time spent in and out of the euphotic zone with varying mixing. For example, over an 8-hour photoperiod, a phytoplankton cell in a very low ε environment may spend 4 continuous hours in the euphotic zone, and then 4 hours at depth. In contrast, a phytoplankton cell that experiences a high ε environment may alternate between 1 hour in the euphotic zone and then 1 hour at depth, but this still equates to a cumulative 4 hours spent in the euphotic zone over the course of the photoperiod.

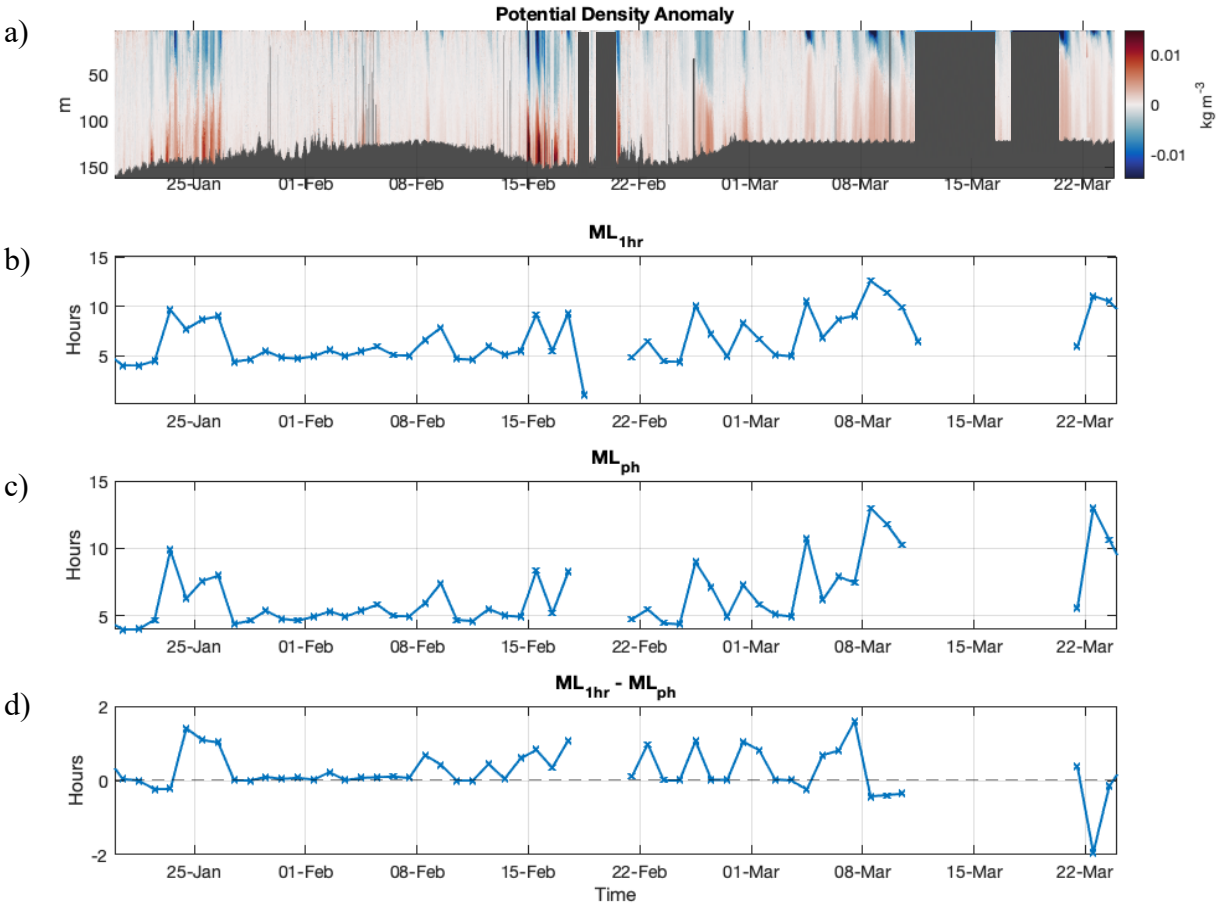

Fig. 4.9: a) the potential density anomaly (kg m^{-3}), for reference; b-d) the number of hours phytoplankton cells remain in the euphotic zone in ML_{1hr} (b) and ML_{ph} (c) and the number of hours difference between ML_{1hr} and ML_{ph} (d), with a realistic euphotic depth of 46m (using satellite-derived Kd_{PAR}) and realistic, time-varying values for ε

The comparison between a constant light and a variable light environment in homogenised environments makes it difficult to interpret whether the continual change in light would promote active phytoplankton growth, or result in photoacclimation. However, night-time chlorophyll increased from 0.52 µg l^{-1} on the 1st February to 0.72 µg l^{-1} on the 9th February (Fig. 4.7). As the water column was homogenised during this time, it can be construed that phytoplankton growth is still possible during these homogenised periods, provided there is sufficient light for growth. Such an environment would benefit certain species of phytoplankton more than others. While there is no observational evidence for the composition of phytoplankton species during February, it can be assumed that species adapted to highly

turbulent, low light conditions (such as diatoms; Margalef 1978; Gilbert et al, 2016), will benefit the most from these highly energetic periods.

b) ML_{1hr} and ML_{ph} at the 46m euphotic depth.

The vertical light attenuation coefficient (Kd_{PAR}) in shelf seas typically ranges from ~0.1m^{-1} in a summer stratified shelf sea, to ~0.3m^{-1} in a shallow, vertically mixed environment (Simpson and Sharples, 2012). Using a winter seasonal climatology (2002-2017) from the MODIS-Aqua satellite, average values of Kd_{PAR} across the glider track was 0.05 m^{-1}. This, combined with observed Smartbuoy PAR, suggests a euphotic depth estimate of 46m. Direct comparisons between the ML_{1hr} and ML_{ph} with this euphotic depth revealed up to a 1.6 hour increase in the amount of time phytoplankton cells spent in the euphotic zone (Fig. 4.9), such as at 12:00 on the 7th March where t_{mix} for ML_{1hr} and ML_{ph} were 9.1 hours (z_{sml} = 26m) and 7.4 hours (z_{sml} = 80m) respectively. This is not the case for all stratification events, as the 26th February 2015 displayed no difference between the ML_{1hr} and ML_{ph} estimates, likely due to similarities between the two z_{sml} estimates, which had a difference of 3m. There are also some instances where phytoplankton cells are retained longer in the euphotic zone when using the ML_{ph} estimate, as opposed to the higher resolution Ml_{1hr}, e.g. the 22nd March, where t_{mix} for phytoplankton is 2 hours longer for ML_{ph}, as opposed to ML_{1hr}. This was due to the rapid shoaling of ML_{1hr} from 121m to 7m during the course of a single photoperiod, whereas ML_{ph} remained at a stable 43m throughout the day.

c) Varying euphotic depths

Annual climatologies of satellite-derived Kd_{PAR} indicate the average depth of the euphotic zone along the glider track can vary by 35m over the course of the year. To fully gauge the importance of ephemeral stratification events in environments with different light attenuations, t_{mix} was calculated using ML_{1hr} and ML_{ph} in a) a highly turbid regime, where the euphotic depth is taken to be 16m and b) a less turbid regime, where the euphotic zone is taken to be 51m depth (Fig. 4.10). While these values for the euphotic depth were based upon the maximum/minimum Kd_{PAR} observed along the glider track in the Celtic Sea, these results are representative of all coastal regimes with high and/or low light attenuation.

Intuitively, phytoplankton cells were retained for longer in the euphotic zone when the euphotic depth was deeper. When the water column was vertically homogenised (e.g. early

February), phytoplankton remained in the euphotic zone for up to 2 and 5.5 hours when the euphotic zone depth was 16m and 51 m, respectively, over the course of the photoperiod. During periods of ephemeral stratification, such as that observed on the 8th March 2015, phytoplankton remained in the euphotic zone for a maximum of 13 hours, or the entire length of the photoperiod. As phytoplankton adapt to high light conditions during the winter period (Moore et al, 2006), this implies that cells are unlikely to be quenched whilst remaining in the euphotic zone for such long periods, further intensifying the potential for productivity.

The mixing time scales between ML_{1hr} and ML_{ph} under different euphotic scenarios were most striking during the short-lived ephemeral stratification periods, such as the 4th March. In turbid environments (euphotic depth = 16m), phytoplankton cells remained up to 5 hours longer in

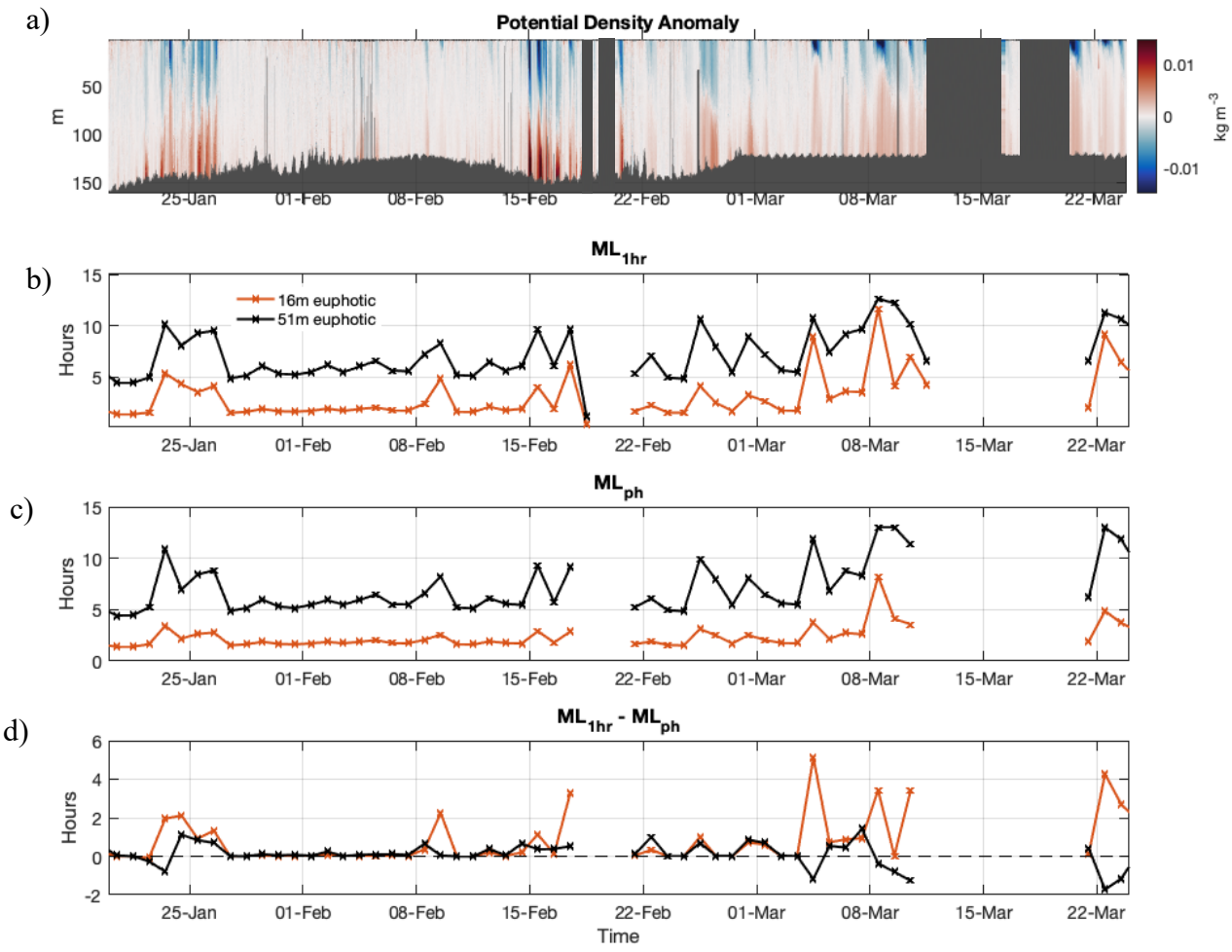

Fig. 4.10: a) the potential density anomaly (kg m^{-3}), for reference; b-d) the number of hours phytoplankton cells remain in the euphotic zone in ML_{1hr} (b) and ML_{ph} (c) and the number of hours difference between ML_{1hr} and ML_{ph} (d), with a euphotic depth of 16m and 51m (based on the monthly maximum and minimum climatology of Kd_{PAR} along the glider track) and realistic, time-varying values for ε

the euphotic zone with a highly-variable z_{sml} (ML_{1hr}), as opposed to the daily z_{sml} (ML_{ph}). Thus, during periods of high turbidity, the development of these ephemeral stratification periods are vital for improving the light environment and reducing light limitation.

An indication of water-column turbidity can be taken from the glider's optical backscatter measurements, with higher backscatter equating to higher turbidity. In the Celtic Sea, on-shelf regions exhibited higher backscatter, with clearer waters further towards the shelf (Fig. 4.11). Highest backscatter measurements occur during March 2015, coincident with the highest frequency of ephemeral stratification events (as seen by Fig 4.6). Fig. 4.11 also suggests a spatial control on when ephemeral stratification events are most beneficial to phytoplankton, with shallower regions further inshore having higher light attenuation. As the highest backscatter is seen nearest the seabed, this is likely due to the tidal resuspension of sediments.

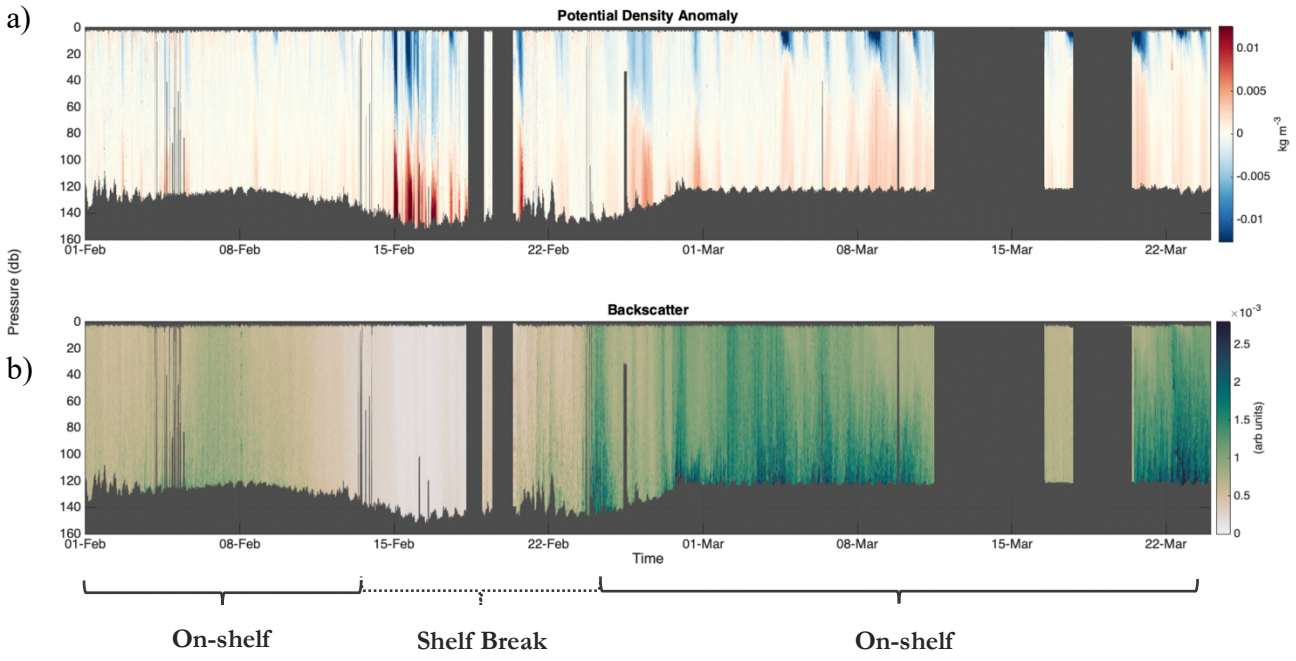

Fig. 4.11: a) Potential density anomaly, for reference (kg m^{-3}), b) optical backscatter as measured by the glider (arb units)

4.3.4 Modelling the effect of stratification on phytoplankton growth

To fully gauge the response of phytoplankton growth to ephemeral winter stratification events, a simplified model (based on Sharples, 2008, and references therein) was used to investigate

the change in phytoplankton carbon, P_C (in mg C) in the SML when the Z_{SML} was ML_{1hr}, ML_{ph} and with no mixed layer (i.e. Z_{SML} was equal to the maximum water column depth, taken to be 150m). The maximum growth rate, μ_m (s^{-1}) was modelled by:

(4.5) $$\mu_m = 1.16 \times 10^{-5} \left(\frac{Q - Q_{sub}}{Q_m - Q_{sub}}\right) 0.59e^{0.0633T}$$

Where the Q_{sub} is the subsidence cell quota (in [mmol N (mg C)$^{-1}$]), taken as 0.008, Q_m is the maximum cell quota (in [mmol N (mg C)$^{-1}$]), taken as 0.04, and T is the mean temperature within the SML (^{o}C). The cell nitrogen quota, Q (in [mmol N (mg C)$^{-1}$]) is modelled by P_N/P_C, where P_N is the cell nitrogen quota (in [mmol N (mg C)$^{-1}$]) and is assumed to follow the 106:16 Redfield Ratio (Redfield, 1934).

By incorporating PAR, the phytoplankton growth rate (μ) is further determined by:

(4.6) $$\mu = \mu_m \left(1 - e^{-(\alpha I_{PAR}\, \theta / \mu_m)}\right) - r^B$$

Where α (in [mg C (mg Chl)$^{-1}$ (Wm^{-2})$^{-1}$ s^{-1}]) is the maximum light utilisation coefficient and θ is a fixed phytoplankton Chl:C ratio (in [mg Chl (mg C)$^{-1}$]), which are taken to be 4.63 x 10^{-5} and 0.04 respectively. The term r^B (in s^{-1}) represents losses through respiration, as is assumed to be a constant value of 1.39 x 10^{-6}. The PAR utilised for phytoplankton growth, I_{PAR} (in Wm^{-2}), is averaged throughout the SML using a Kd_{PAR} value of 0.05 ms^{-1}. The exponential decay of surface PAR throughout the water column was calculated by:

(4.7) $$I_{PAR} = I_0\, e^{Kd_{PAR} z}$$

Where I_0 is the surface PAR, taken from the Smartbuoy (Wm^{-2}), and z is the vertical co-ordinate.

The change in phytoplankton carbon, P_C, with time, t, can therefore by calculated by:

(4.8) $$\frac{\partial P_C}{\partial t} = \mu P_C$$

Photoinhibition through non-photochemical quenching has been ignored and losses by grazing are assumed to be negligible. As the model is focussing on the winter period, where both surface irradiance and grazing rates are both likely to be reduced compared to spring and summer rates, the omission of these terms is likely to have minimal impacts. Furthermore,

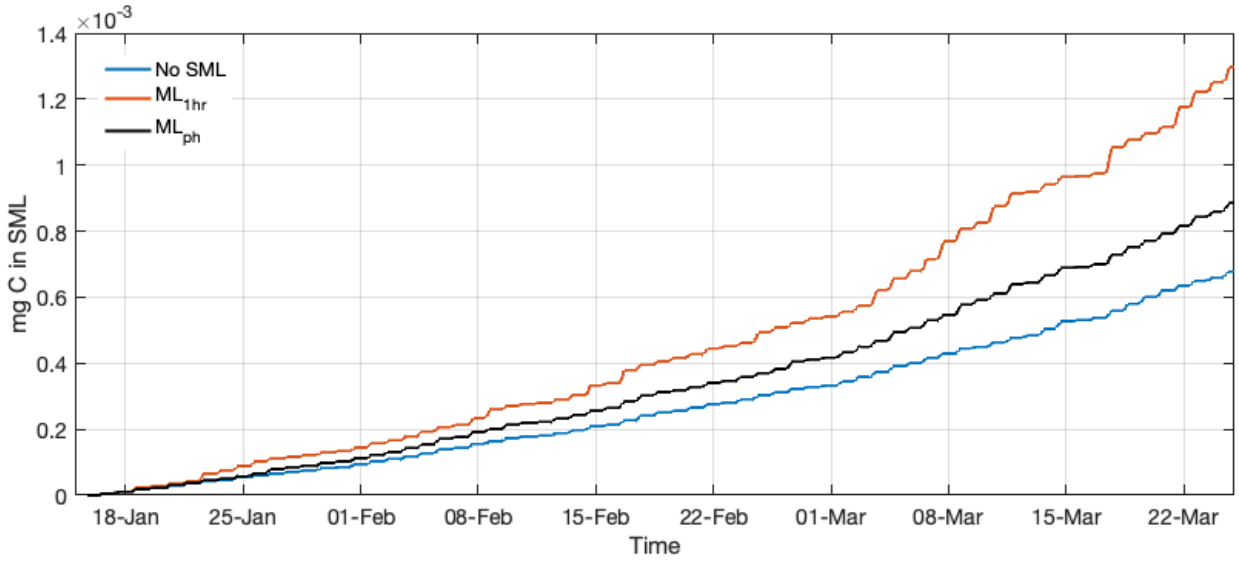

Fig. 4.12: Cumulative changes in phytoplankton carbon, P_C (mg C) within the SML, where the Z_{SML} is defined as ML_{1hr} (red line), ML_{ph} (black line) or the maximum depth of the water column (taken as 150m, blue line)

vertical mixing rates have also been ignored. Instead, phytoplankton growth is assumed to be constrained within the SML, with phytoplankton cells uniformly distributed throughout.

This simplified model (Fig. 4.12) suggests that is there a significant increase in phytoplankton growth during ephemeral stratification events (ML_{1hr}), as phytoplankton are trapped within a more favourable light environment. Assuming no losses from grazing, these boosted phytoplankton populations are subsequently maintained during periods of high mixing (i.e. where Z_{SML} = maximum depth), before another boost in growth occurs in the next stratification event. As such, it can be assumed that as the frequency of stratification events increases, so does the phytoplankton growth. This is consistent with the accelerated chlorophyll increase from February to March observed in the Smartbuoy data (as described in section 4.3.2).

This is replicated well in the ML_{1hr} model, which displayed over double the rate of P_C increase in March compared to February (a rise from $1.4x10^{-5}$ mg C d^{-1} to $3.1x10^{-5}$ mg C d^{-1}). Conversely, P_C in the ML_{ph} model only increases from $1.0x10^{-5}$ mg C d^{-1} during February to only $1.8x10^{-5}$ mg C m^{-1} d^{-1} during March, which is almost half the March rate modelled when using ML_{1hr}. For comparison, the rate of increase in P_C with no SML remains relatively constant at $8.7x10^{-6}$ mg C d^{-1} throughout both February and March, consistent with the gradual increase in PAR towards the summer solstice. Results from this simplified model suggest that

ephemeral stratification events, as shown by ML_{1hr}, are significant in boosting phytoplankton growth across the winter period.

4.4 The importance of ephemeral stratification events to phytoplankton populations

This Chapter has identified a gradual increase in phytoplankton biomass throughout the winter period. Previous studies in the open ocean have reported that the diurnal heating and cooling cycle could result in an increase of phytoplankton standing stock, as the absence of daytime convection could retain phytoplankton in the euphotic zone (Woods and Onken, 1982; Taylor and Stephens, 1993). While some daytime periods of thermal stratification occurred in this study, such as between 4th to the 8th March 2015 (Fig. 4.2), and directly before the onset of seasonal stratification on the 25th March 2015 (see Chapter 3.2), it is likely that these daily thermal stratification events were only partially responsible for maintaining phytoplankton populations, as they were limited to restricted daytime heating periods.

In comparison, this Chapter has demonstrated that 2-day periods of ephemeral halostratification form during late winter, resulting from sporadic meteorological events. These are further shown to boosting phytoplankton growth, maintaining winter phytoplankton populations at a scale not considered by daytime stratification events alone. A key result from this study is that ephemeral stratification events, initiated by meteorological forcing, are most important for maintaining phytoplankton populations in the euphotic zone during periods of high turbidity.

Light attenuation in shelf seas is highly dynamic. Particles comprising of phytoplankton, detritus and suspended particular matter (SPM) along with coloured dissolved organic matter will scatter and absorb light (IOCCG 2000). There is a linear relationship between the amount of SPM and Kd_{PAR} (Delvin et al 2009), with inshore and near-coastal regions highlighted as environments where primary productivity is directly limited by water clarity (Bowers et al, 2002; Painting et al, 2007). Although the Celtic Sea is a considerable distance from direct coastal influence, the effects of higher turbidity on phytoplankton cannot be discounted.

Sediment resuspension is particularly high in regions where there is high trawling activity, such as the northern Celtic Sea and the North Sea (Eigaard et al, 2017). Globally, trawling disturbs over 9.74 million km^2 of continental shelves and suspends approximately 21.87 Gt yr^{-1} of sediments (Oberle et al, 2016). For a number of centuries, the NW European Shelf has been known to support high abundances of bottom-dwelling fish species (Horwood, 1993; Kerby et al, 2012), with trawling activity in the Celtic Sea alone impacting over 80% of the total seabed area (Eigaard et al 2017). As such, in regions of high trawling activity, large rainfall events may act as a mechanism to maintain winter phytoplankton growth in regions, by providing a suitable light environment despite the high SPM concentrations.

As phytoplankton also act to attenuate light (Townsend et al, 1994; IUCCG, 2000), it can be speculated that high aggregations of phytoplankton would further reduce the clarity of the water column. Observations from both glider and Smartbuoy in March 2015 indicated a gradual increase in chlorophyll concentrations, suggesting that late winter phytoplankton populations may act to decrease Kd_{PAR}. This creates an environment of gradually intensified self-shading, suggesting phytoplankton may become increasingly dependent on ephemeral stratification events to be retained in non-limiting light conditions.

Storm activity and changes in wind speed increase water column turbidity through sediment resuspension (Greenwood et al, 2010; Capuzzo et al, 2013) as well as sediment transport (Vitorino et al, 2002a, 2002b). On the Iberian Shelf, it has been estimated that moderate storms are sufficient to suspend sediment in water depths of 120m (Oberle et al 2014). Although storm induced resuspension of sediments is rare when water is deeper than 150 m (Oberle et al 2016), they do occur. For example, satellite-derived surface SPM concentrations in the Celtic Sea were high following the exceptionally stormy winter of 2013-2014 (Gohin et al, 2015).

Nearer the coast, this increased turbidity was counterbalanced by increased riverine runoff, resulting in halostratification that promoted a late winter phytoplankton bloom (Gohin et al, 2015). The study by Gohin et al (2015) not only proves that exceptional storm activity can increase the entire water-column turbidity in the open-shelf regions of the Celtic Sea, but also that freshwater inputs can counterbalance such decreases in light-attenuation. Further offshore, away from regions of riverine influence, the addition of freshwater following the storms promotes a shallow z_{sml} whereby phytoplankton are able to grow in non-limiting light conditions. As both storm frequency and intensity are predicted to increase in the future (Pinto

et al, 2009; Mölter et al, 2016), such events may become increasingly more important for maintaining phytoplankton population during stormy seasons.

4.5 Conclusions and key findings

This Chapter emphasises that ephemeral stratification events likely contributes to the maintenance of phytoplankton populations over the winter period, by reducing the surface mixed depth and increase light availability in surface waters. Increased chlorophyll concentrations observed from two independent platforms indicated a gradual increase in chlorophyll in February and March 2015, coinciding with identifiable surface freshening from transient meteorological events. Analysis of the mixing time scales for phytoplankton cells implied that increasing PAR, alongside more frequent ephemeral stratification events, acted to sustain phytoplankton populations in the otherwise low-growth winter period.

The length of time phytoplankton spend in the euphotic zone was calculated with different values for z_{sml}, realistic values for ε and varying turbidity, as implied by euphotic depth estimates of 16m and 51m. The occurrence of ephemeral stratification is most important during a period of high turbidity, as phytoplankton cells were maintained several hours longer in the euphotic zone than those in a deeper, more stable mixed layer. This study highlights the need for high-resolution representation of the $z_{sml,}$ as daily estimates are likely to under- or overestimate the amount of time phytoplankton cells are maintained in the euphotic zone. This is further emphasised using a simplified model, which demonstrated that phytoplankton growth is significantly increased when incorporating a SML that captures short-lived stratification events. Crucially, however, this Chapter demonstrates that even sporadic stratification events that are maintained for 2 days cannot be discounted in maintaining phytoplankton populations throughout the winter period, particularly in turbid environments.

4.6 References

Amorocho, J. and DeVries, J.J., 1980. A new evaluation of the wind stress coefficient over water surfaces. *Journal of Geophysical Research: Oceans*, *85*(C1), pp.433-442.

Behrenfeld, M.J., 2010. Abandoning Sverdrup's critical depth hypothesis on phytoplankton blooms. *Ecology*, *91*(4), pp.977-989.

Bowers, D.G., Gaffney, S., White, M. and Bowyer, P., 2002. Turbidity in the southern Irish Sea. *Continental Shelf Research*, *22*(15), pp.2115-2126.

Brody, S.R. and Lozier, M.S., 2015. Characterizing upper-ocean mixing and its effect on the spring phytoplankton bloom with in situ data. *ICES Journal of Marine Science*, *72*(6), pp.1961-1970.

Brown, J., Carrillo, L., Fernand, L., Horsburgh, K.J., Hill, A.E., Young, E.F. and Medler, K.J., 2003. Observations of the physical structure and seasonal jet-like circulation of the Celtic Sea and St. George's Channel of the Irish Sea. *Continental Shelf Research*, *23*(6), pp.533-561.

Brown, P.J. and Kummerow, C.D., 2014. An assessment of atmospheric water budget components over tropical oceans. *Journal of Climate*, *27*(5), pp.2054-2071.

Capuzzo, E., Painting, S.J., Forster, R.M., Greenwood, N., Stephens, D.T. and Mikkelsen, O.A., 2013. Variability in the sub-surface light climate at ecohydrodynamically distinct sites in the North Sea. *Biogeochemistry*, *113*(1-3), pp.85-103.

Chiswell, S.M., 2011. Annual cycles and spring blooms in phytoplankton: don't abandon Sverdrup completely. *Marine ecology progress series*, *443*, pp.39-50.

Davidson, K., Gilpin, L.C., Pete, R., Brennan, D., McNeill, S., Moschonas, G. and Sharples, J., 2013. Phytoplankton and bacterial distribution and productivity on and around Jones Bank in the Celtic Sea. *Progress in oceanography*, *117*, pp.48-63.

Dee, D.P., Uppala, S.M., Simmons, A.J., Berrisford, P., Poli, P., Kobayashi, S., Andrae, U., Balmaseda, M.A., Balsamo, G., Bauer, D.P. and Bechtold, P., 2011. The ERA-Interim reanalysis: Configuration and performance of the data assimilation system. *Quarterly Journal of the royal meteorological society*, *137*(656), pp.553-597.

Denman, K.L. and Gargett, A.E., 1983. Time and space scales of vertical mixing and advection of phytoplankton in the upper ocean. *Limnology and oceanography*, *28*(5), pp.801-815.

Devlin, M., Barry, J., Painting, S. and Best, M., 2009. Extending the phytoplankton tool kit for the UK Water Framework Directive: indicators of phytoplankton community structure. *Hydrobiologia*, *633*(1), pp.151-168.

Durbin, E.G., Campbell, R.G., Casas, M.C., Ohman, M.D., Niehoff, B., Runge, J. and Wagner, M., 2003. Interannual variation in phytoplankton blooms and zooplankton productivity and abundance in the Gulf of Maine during winter. *Marine Ecology Progress Series*, *254*, pp.81-100.

Eigaard, O.R., Bastardie, F., Hintzen, N.T., Buhl-Mortensen, L., Buhl-Mortensen, P., Catarino, R., Dinesen, G.E., Egekvist, J., Fock, H.O., Geitner, K. and Gerritsen, H.D., 2017. The footprint of bottom trawling in European waters: distribution, intensity, and seabed integrity. *ICES Journal of Marine Science*, *74*(3), pp.847-865.

Evans, G.T. and Parslow, J.S., 1985. A model of annual plankton cycles. *Biological oceanography*, *3*(3), pp.327-347.

Fernand, L., Nolan, G.D., Raine, R., Chambers, C.E., Dye, S.R., White, M. and Brown, J., 2006. The Irish coastal current: A seasonal jet-like circulation. *Continental Shelf Research*, *26*(15), pp.1775-1793.

Franks, P.J., 2014. Has Sverdrup's critical depth hypothesis been tested? Mixed layers vs. turbulent layers. *ICES Journal of Marine Science*, *72*(6), pp.1897-1907.

Gill, A. E. (1982). Atmosphere-Ocean Dynamics. International Geophysics Series, 30. *Academic Press, New York*.

Gimeno, L., Nieto, R., Vázquez, M. and Lavers, D.A., 2014. Atmospheric rivers: A mini-review. *Frontiers in Earth Science*, *2*, p.2.

Glibert, P.M., 2016. Margalef revisited: a new phytoplankton mandala incorporating twelve dimensions, including nutritional physiology. *Harmful Algae*, *55*, pp.25-30.

Gohin, F., Bryère, P. and Griffiths, J.W., 2015. The exceptional surface turbidity of the North-West European shelf seas during the stormy 2013–2014 winter: Consequences for the initiation of the phytoplankton blooms?. *Journal of Marine Systems*, *148*, pp.70-85.

Greenwood, N., Parker, E.R., Fernand, L., Sivyer, D.B., Weston, K., Painting, S.J., Kröger, S., Forster, R.M., Lees, H.E., Mills, D.K. and Laane, R.W.P.M., 2010. Detection of low bottom water oxygen concentrations in the North Sea; implications for monitoring and assessment of ecosystem health. *Biogeosciences*, *7*(4), pp.1357-1373.

Haskell, W.Z., Prokopenko, M.G., Stanley, R.H.R. and Knapp, A.N., 2016. Estimates of vertical turbulent mixing used to determine a vertical gradient in net and gross oxygen production in the oligotrophic South Pacific Gyre. *Geophysical Research Letters*, *43*(14), pp.7590-7599.

Henson, S.A., Robinson, I., Allen, J.T. and Waniek, J.J., 2006. Effect of meteorological conditions on interannual variability in timing and magnitude of the spring bloom in the Irminger Basin, North Atlantic. *Deep Sea Research Part I: Oceanographic Research Papers*, *53*(10), pp.1601-1615.

Hickman, A.E., Moore, C.M., Sharples, J., Lucas, M.I., Tilstone, G.H., Krivtsov, V. and Holligan, P.M., 2012. Primary production and nitrate uptake within the seasonal thermocline of a stratified shelf sea. *Marine Ecology Progress Series*, *463*, pp.39-57.

Holligan, P.M., 2006. Phytoplankton photoacclimation and photoadaptation in response to environmental gradients in a shelf sea. *Limnology and Oceanography*, *51*(2), pp.936-949.

Holt, J., Wakelin, S., Lowe, J. and Tinker, J., 2010. The potential impacts of climate change on the hydrography of the northwest European continental shelf. *Progress in Oceanography*, *86*(3-4), pp.361-379.
Horwood, J., 1993. The Bristol Channel sole (Solea solea (L.)): a fisheries case study. In *Advances in Marine Biology*(Vol. 29, pp. 215-367). Academic Press.

Huisman, J.E.F., van Oostveen, P. and Weissing, F.J., 1999. Critical depth and critical turbulence: two different mechanisms for the development of phytoplankton blooms. *Limnology and oceanography*, *44*(7), pp.1781-1787.

Huthnance, J.M., Holt, J.T. and Wakelin, S.L., 2009. Deep ocean exchange with west-European shelf seas. *Ocean Science*, *5*(4), pp.621-634.

IOCCG 2000. Remote sensing of ocean colour in coastal and other optically complex waters. In: Sathyendrannath, S. (Ed.), Reports of the International Ocean Colour Coordinating Group. No. 3, IOCCG, Dartmouth, Canada, 140 pp

Kerby, T.K., Cheung, W.W. and Engelhard, G.H., 2012. The United Kingdom's role in North Sea demersal fisheries: a hundred year perspective. *Reviews in Fish Biology and Fisheries*, *22*(3), pp.621-634.

Labry, C., Herbland, A., Delmas, D., Laborde, P., Lazure, P., Froidefond, J.M., Jegou, A.M. and Sautour, B., 2001. Initiation of winter phytoplankton blooms within the Gironde plume waters in the Bay of Biscay. *Marine Ecology Progress Series*, *212*, pp.117-130.

Lacour, L., Ardyna, M., Stec, K.F., Claustre, H., Prieur, L., Poteau, A., D'Alcala, M.R. and Iudicone, D., 2017. Unexpected winter phytoplankton blooms in the North Atlantic subpolar gyre. *Nature Geoscience*, *10*(11), p.836.

Lavers, D.A. and Villarini, G., 2013. The nexus between atmospheric rivers and extreme precipitation across Europe. *Geophysical Research Letters*, *40*(12), pp.3259-3264.

Lavers, D.A., Villarini, G., Allan, R.P., Wood, E.F. and Wade, A.J., 2012. The detection of atmospheric rivers in atmospheric reanalyses and their links to British winter floods and the large-scale climatic circulation. *Journal of Geophysical Research: Atmospheres*, *117*(D20).

Margalef, R., 1978. Life-forms of phytoplankton as survival alternatives in an unstable environment. *Oceanol. Acta*, *1*(4).

Mignot, A., Ferrari, R. and Claustre, H., 2018. Floats with bio-optical sensors reveal what processes trigger the North Atlantic bloom. *Nature communications*, *9*(1), p.190.

Mölter, T., Schindler, D., Albrecht, A. and Kohnle, U., 2016. Review on the projections of future storminess over the North Atlantic European region. *Atmosphere*, *7*(4), p.60.

Moore, C.M., Suggett, D., Holligan, P.M., Sharples, J., Abraham, E.R., Lucas, M.I., Rippeth, T.P., Fisher, N.R., Simpson, J.H. and Hydes, D.J., 2003. Physical controls on phytoplankton physiology and production at a shelf sea front: a fast repetition-rate fluorometer based field study. *Marine Ecology Progress Series*, *259*, pp.29-45.

Moore, C.M., Suggett, D.J., Hickman, A.E., Kim, Y.N., Tweddle, J.F., Sharples, J., Geider, R.J. and Newell, R.E., Newell, N.E., Zhu, Y. and Scott, C., 1992. Tropospheric rivers?–A pilot study. *Geophysical Research Letters*, *19*(24), pp.2401-2404.

Oberle, F.K., Storlazzi, C.D. and Hanebuth, T.J., 2014. Wave-driven sediment mobilization on a storm-controlled continental shelf (Northwest Iberia). *Journal of Marine Systems*, *139*, pp.362-372.

Oberle, F.K., Storlazzi, C.D. and Hanebuth, T.J., 2016. What a drag: Quantifying the global impact of chronic bottom trawling on continental shelf sediment. *Journal of Marine Systems*, *159*, pp.109-119.

Painting, S.J., Devlin, M.J., Malcolm, S.J., Parker, E.R., Mills, D.K., Mills, C., Tett, P., Wither, A., Burt, J., Jones, R. and Winpenny, K., 2007. Assessing the impact of nutrient enrichment in estuaries: susceptibility to eutrophication. *Marine pollution bulletin*, *55*(1-6), pp.74-90.

Palmer, M.R., Inall, M.E. and Sharples, J., 2013. The physical oceanography of Jones Bank: A mixing hotspot in the Celtic Sea. *Progress in oceanography*, *117*, pp.9-24.

Redfield, A.C., 1934. On the proportions of organic derivatives in sea water and their relation to the composition of plankton. *James Johnstone memorial volume*, pp.176-192.

Pingree, R.D. and Le Cann, B., 1989. Celtic and Armorican slope and shelf residual currents. *Progress in Oceanography*, *23*(4), pp.303-338.

Pinto, J.G., Zacharias, S., Fink, A.H., Leckebusch, G.C. and Ulbrich, U., 2009. Factors contributing to the development of extreme North Atlantic cyclones and their relationship with the NAO. *Climate dynamics*, *32*(5), pp.711-737.

Riley, G.A., 1957. Phytoplankton of the North Central Sargasso Sea, 1950–52 1. *Limnology and Oceanography*, *2*(3), pp.252-270.

Ruiz-Castillo, E., Sharples, J., Hopkins, J. and Woodward, M., 2019a. Seasonality in the cross-shelf physical structure of a temperate shelf sea and the implications for nitrate supply. *Progress in Oceanography*, *177*, p.101985.

Ruiz-Castillo, E., Sharples, J. and Hopkins, J., 2019b. Wind-driven strain extends seasonal stratification. *Geophysical Research Letters*, *46*(22), pp.13244-13252.

Sharples, J., 2007. Potential impacts of the spring-neap tidal cycle on shelf sea primary production. *Journal of Plankton Research*, *30*(2), pp.183-197.

Sharples, J., Moore, C.M., Hickman, A.E., Holligan, P.M., Tweddle, J.F., Palmer, M.R. and Simpson, J.H., 2009. Internal tidal mixing as a control on continental margin ecosystems. *Geophysical Research Letters*, *36*(23).

Sharples, J., Ross, O.N., Scott, B.E., Greenstreet, S.P. and Fraser, H., 2006. Inter-annual variability in the timing of stratification and the spring bloom in the North-western North Sea. *Continental Shelf Research*, *26*(6), pp.733-751.

Siegel, D.A., Doney, S.C. and Yoder, J.A., 2002. The North Atlantic spring phytoplankton bloom and Sverdrup's critical depth hypothesis. *science*, *296*(5568), pp.730-733.

Simpson, J.H. and Sharples, J., 2012. *Introduction to the physical and biological oceanography of shelf seas*. Cambridge University Press.

Smetacek, V. and Passow, U., 1990. Spring bloom initiation and Sverdrup's critical-depth model. *Limnology and oceanography*, *35*(1), pp.228-234.

Sverdrup, H.U., 1953. On conditions for the vernal blooming of phytoplankton. *J. Cons. Int. Explor. Mer*, *18*(3), pp.287-295.

Taylor, A.H. and Stephens, J.A., 1993. Diurnal variations of convective mixing and the spring bloom of phytoplankton. *Deep Sea Research Part II: Topical Studies in Oceanography*, *40*(1-2), pp.389-408.

Taylor, J.R. and Ferrari, R., 2011. Shutdown of turbulent convection as a new criterion for the onset of spring phytoplankton blooms. *Limnology and Oceanography*, *56*(6), pp.2293-2307.

Thorpe, S.A., 2007. *An introduction to ocean turbulence*. Cambridge University Press.

Townsend, D.W., Cammen, L.M., Holligan, P.M., Campbell, D.E. and Pettigrew, N.R., 1994. Causes and consequences of variability in the timing of spring phytoplankton blooms. *Deep Sea Research Part I: Oceanographic Research Papers*, *41*(5-6), pp.747-765.

Townsend, D.W., Keller, M.D., Sieracki, M.E. and Ackleson, S.G., 1992. Spring phytoplankton blooms in the absence of vertical water column stratification. *Nature*, *360*(6399), p.59.

Tweddle, J.F., Sharples, J., Palmer, M.R., Davidson, K. and McNeill, S., 2013. Enhanced nutrient fluxes at the shelf sea seasonal thermocline caused by stratified flow over a bank. *Progress in oceanography*, *117*, pp.37-47

Vitorino, J., Oliveira, A., Jouanneau, J.M. and Drago, T., 2002a. Winter dynamics on the northern Portuguese shelf. Part 1: physical processes. *Progress in Oceanography*, *52*(2-4), pp.129-153.

Vitorino, J., Oliveira, A., Jouanneau, J.M. and Drago, T., 2002b. Winter dynamics on the northern Portuguese shelf. Part 2: bottom boundary layers and sediment dispersal. *Progress in Oceanography*, *52*(2-4), pp.155-170.

Waniek, J.J., 2003. The role of physical forcing in initiation of spring blooms in the northeast Atlantic. *Journal of Marine Systems*, *39*(1-2), pp.57-82.

Wihsgott, J.U., 2018. *A Tale of Four Seasons: Investigating the seasonality of physical structure and its biogeochemical responses in a temperate continental shelf sea* (Doctoral dissertation, University of Liverpool).

Woods, J.D. and Onken, R., 1982. Diurnal variation and primary production in the ocean preliminary results of a Lagrangian ensemble model. *Journal of Plankton Research*, *4*(3), pp.735-756.

Woollings, T., Gregory, J.M., Pinto, J.G., Reyers, M. and Brayshaw, D.J., 2012. Response of the North Atlantic storm track to climate change shaped by ocean–atmosphere coupling. *Nature Geoscience*, *5*(5), p.313.

Yelland, M. and Taylor, P.K., 1996. Wind stress measurements from the open ocean. *Journal of Physical Oceanography*, *26*(4), pp.541-558.

Young, E.F., Brown, J., Aldridge, J.N., Horsburgh, K.J. and Fernand, L., 2004. Development and application of a three-dimensional baroclinic model to the study of the seasonal circulation in the Celtic Sea. *Continental Shelf Research*, *24*(1), pp.13-36.

Yu, L., 2007. Global variations in oceanic evaporation (1958–2005): The role of the changing wind speed. *Journal of climate*, *20*(21), pp.5376-5390.

Zhu, Y. and Newell, R.E., 1998. A proposed algorithm for moisture fluxes from atmospheric rivers. *Monthly weather review*, *126*(3), pp.725-735.

5. Climatological controls on the spring phytoplankton growing season

---

Jennifer Jardine[1], Matthew Palmer[2], Claire Mahaffey[1], Jason Holt[2] and Sarah Wakelin[2]

Prepared for paper submission

[1.] University of Liverpool, Liverpool, L69 3BX

[2.] National Oceanography Centre Liverpool, Liverpool, L3 5DA

The onset of seasonal stratification in a temperate continental shelf sea is considered a precursor for the spring bloom: a vital biological event in shelf sea ecosystems. Previous work has demonstrated that the onset of seasonal stratification is modulated by storm events, which act to create or destroy established stratification, yet the biological response to this meteorological variability remains unknown. Here we show the influence of storms on phytoplankton variability throughout the winter period. We define two separate spring phytoplankton growth events: the spring bloom, defined as the exponential phytoplankton growth following seasonal stratification, and the prebloom, which occurs before the onset of seasonal stratification and can be as much as 22% of total spring phytoplankton growth. Our results support the paradigm that light is a first order control on spring phytoplankton growth, with the spring bloom initiating up to 22 days following the onset of seasonal stratification should light levels be insufficient. The prebloom is heavily influenced by the phase of the Atlantic Multidecadal Oscillation (AMO), with normalised prebloom chlorophyll concentrations (± 90% confidence limit) increasing from 7.6 ± 2.8 mg m^{-2} d^{-1} to 13.1 ±4.3 mg m^{-2} d^{-1} across all phytoplankton functional groups in positive AMO phases. Case study years support the hypothesis that this increase in phytoplankton growth is due to rain-induced periods of ephemeral stratification, initiated and sustained by changes in storm track activity associated with climatological oscillations. Phytoplankton growth in prebloom events could help buffer the mismatch between phytoplankton supply and larval recruitment, particularly during years where the spring bloom is delayed. We further suggest prebloom phytoplankton growth could directly act as seed populations for the spring bloom, with implications for carbon fixation.

5.1 Introduction

In temperate regions, the onset of the spring phytoplankton bloom is considered light limited, hypothesised to only occur once the mixed layer depth shoals above a critical depth whereby net phytoplankton growth from photosynthesis exceeds net losses from respiration (Sverdrup, 1953). This criterion is often met following the onset of seasonal stratification, which is thus considered a precursor for the initiation of the spring phytoplankton bloom.

While some studies still support the Critical Depth Hypothesis (Siegal et al, 2002; Chiswell, 2011), phytoplankton growth observed during the winter months (Behrenfeld 2010; Boss and Behrenfeld, 2010; Taylor and Ferrari, 2011) cast doubt on the theory's validity. Observations further show that the spring bloom can be initiated before the mixed layer has shoaled above the critical depth (Townsend et al, 1992; Körtzinger et al, 2008; Behrenfeld, 2010). Other hypotheses to explain this net phytoplankton growth have been explored, including the recoupling-dilation hypothesis (Behrenfeld, 2010), the shutdown of convective mixing (Taylor and Ferrari, 2011) and local decreases in wind stress (Chiswell, 2011; Chiswell et al, 2013).

On the Northwest (NW) European Shelf, the current paradigm is that the onset of thermal stratification is exclusively dominated by the balance of thermal inputs to wind and tidal stresses (Pingree et al 1976; Simpson and Hunter, 1974). However, earlier work in this thesis has challenged this paradigm and demonstrated that storm events also act to trigger seasonal stratification through positive buoyancy input of freshwater to the surface (see Chapter 3).

The frequency and intensity of these storms are modulated by large-scale climate oscillations, such as the Atlantic Multidecadal Oscillation (AMO). With an estimated frequency of ~60-80 years (Alexander et al, 2014; Delworth and Zhang, 2007; Schlesinger and Ramankutty, 1994), the AMO is defined as the temperature anomaly in the North Atlantic and was primarily in a negative (colder) phase from the 1960s until transitioning to the current positive (warmer) phase from the mid-1990s. Another climatological mode is the North Atlantic Oscillation (NAO): a highly variable mode of meteorological variability, defined as the difference between the Azores and Icelandic pressure systems (Li et al, 2013; Cohen et al, 2014). The NAO is largely out of phase with the AMO and was more frequently positive from 1965 to 1995 (Marshall et al, 2001), and in predominantly negative phase since the mid-1990s (Li et al, 2013; Cohen et al, 2014).

Through a combination of observational and hindcast hydrodynamic-biogeochemical model data, Chapter 3 demonstrated that the timing of the onset of seasonal stratification varied by a factor of two between negative and positive AMO periods. During positive AMO phases, the increased likelihood of explosive cyclones (Gómara Cardalliaguet *et al*, 2010), interspersed with periods of meteorological quiescence due to atmospheric blocking (Häkkinen *et al*, 2011), has the potential to increase the interannual variability of stratification onset through the formation and sporadic destruction of stratification events (see Chapter 3). Only when the

successive storms are insufficient to outcompete the positive buoyancy effects from freshwater and thermal inputs, will vertical stratification be maintained and seasonal stratification be initiated.

The effect of this climatic control on the timing of the spring bloom remains uncertain. It has been postulated that an increase in storminess might induce a delayed spring bloom response, as increased wind mixing would rapidly transport phytoplankton out of euphotic zone and limit light availability (Collins *et al*, 2009; Henson et al 2006; Townsend et al, 1994; Sharples et al, 2006). However, previous work in this thesis (Chapter 3) demonstrated the stabilising effect of freshwater input during storm events to have a counteracting influence on upper ocean stability. It was identified that a distinct freshwater layer formed during a storm event, that coincided with a gradual increase in chlorophyll fluorescence (Chapter 3), which was confirmed by subsequent in situ observations to be the initiation of the spring bloom (e.g. Poulton et al, 2017). Chapter 4 further demonstrated that short periods of phytoplankton growth can occur before the onset of seasonal stratification. These prebloom growth events occurred due to short-lived ephemeral stratification events, that trapped phytoplankton cells in the surface and thus provided a series of temporary favourable light conditions.

In this Chapter, we quantify the importance of meteorological events on the timing, magnitude and composition of phytoplankton in the Celtic Sea (Fig. 5.1). Using the AMM7 configuration of the coupled hydrodynamic-biogeochemical model, NEMO-ERSEM (Madec, 2015; Butenshön et al, 2016; see Chapter 2.4 and Appendix II), we extend the work of Chapters 3 and 4 to explore the variability and magnitude of key biogeochemical properties across a multi-decadal period, to determine the effect of these storm systems on the spring phytoplankton growing season.

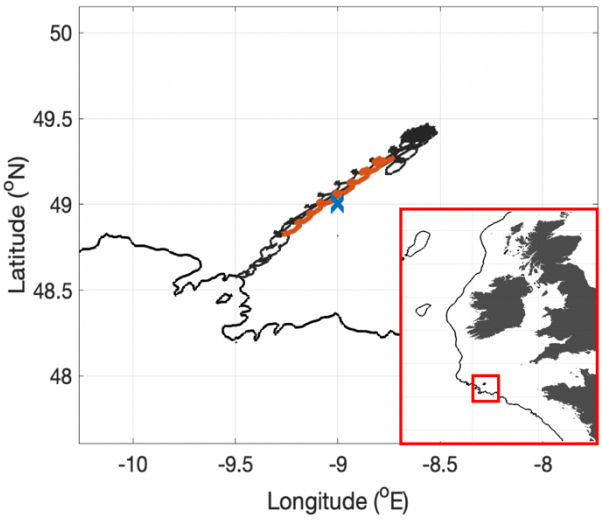

Fig. 5.1: Location of the glider track, in relation to the Northwest European Shelf, from the 1st March 2015 to the 2nd April 2015. The red section of the track is indicative of where the initial rain-induced stratification was observed in Chapter 3. The blue cross indicates the location of the virtual mooring for the modelled data. Also included is the 200m isobath (GEBCO, 2014).

5.2 Methods

5.2.1 Model validation

To assess the influence of storms and large-scale climate variability on phytoplankton populations, it was first necessary to ensure the model adequately replicated observed conditions. Observational data, collected from ocean glider deployments in the Celtic Sea during March 2015 (see Chapter 2.2.3), allowed a qualitative comparison between the observed chlorophyll fluorescence and modelled chlorophyll concentrations from the model (Fig. 5.1). Physical properties, such as temperature and salinity, were found to be adequately captured in the model and are discussed in Chapter 2.4.1.

Model data was taken 78 km in-shore from the shelf break, at 49.0005°N, -9.0001°E, and acted as a virtual mooring that was consistent with an area identified to experience rain-induced stratification (see Chapter 3). This observed stratification occurred on the 25th March 2015 that resulted in a gradual increase in depth-integrated chlorophyll from 78 mg m^{-2} on the 25th March to a maximum of 112 mg m^{-2} on the 29th March 2015 (Fig. 5.2a). This increase is replicated well in the model, which captures the vertical distribution of chlorophyll concentrations from the surface to a depth of 100m on the 28th March 2015 (Fig. 5.2b).

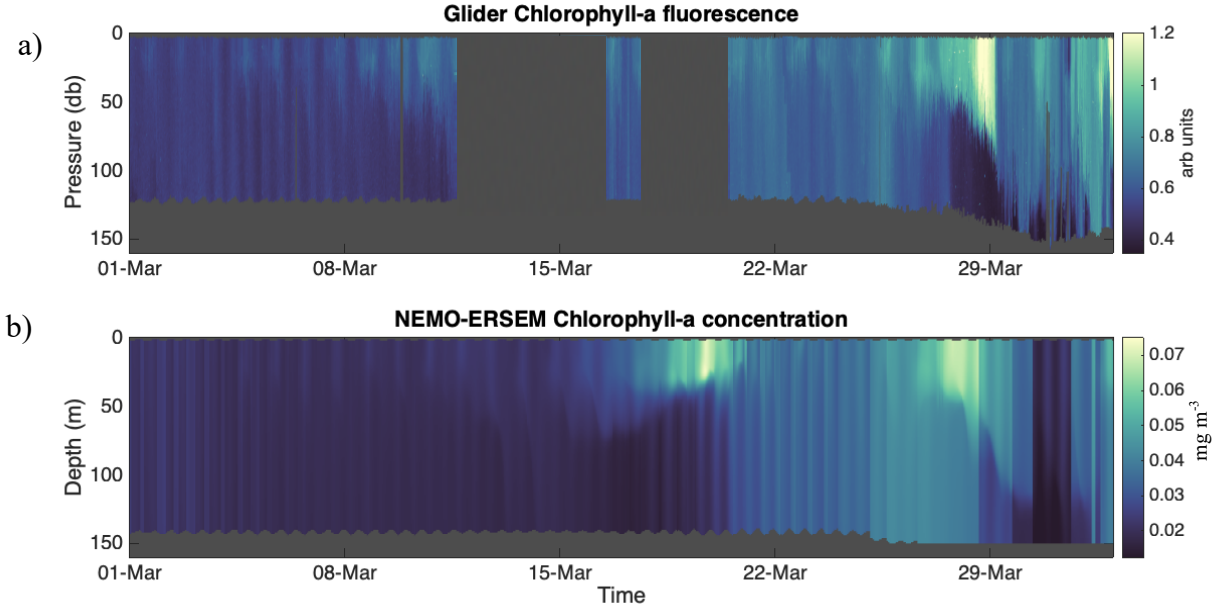

Fig. 5.2: a) Chlorophyll-a fluorescence measured from the glider; b) chlorophyll-a concentration from the AMM7 NEMO-ERSEM model, at the closest location to the glider (within 7km bounds)

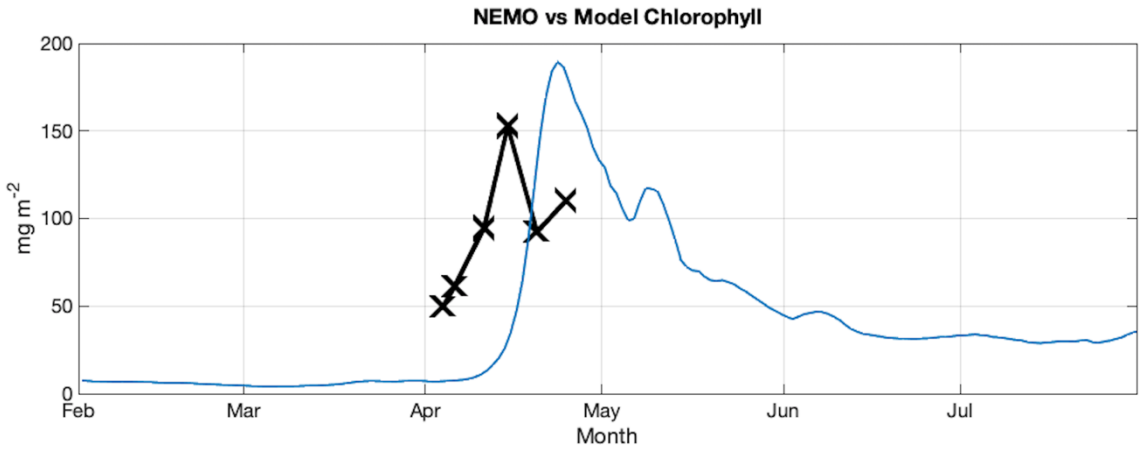

Fig. 5.3: Comparison of the depth-integrated total chlorophyll concentration from the AMM7 NEMO-ERSEM model at the CCS site (blue line) to observed depth integrated chlorophyll-a concentrations, measured at CCS throughout 2014 and 2015 (Poulton et al, 2017)

Before the onset of stratification, observations are limited with gaps between the 11th and the 20th March 2015 due to technical failures. Increased depth-integrated chlorophyll from our model was, however, consistent with glider observations, insofar that a relative increase in chlorophyll concentrations at depth, from 10th to the 22nd March, is captured in both observations and model data. Despite the lack of data during this time, it can be speculated that enhanced surface chlorophyll was redistributed throughout the water-column, following the erosion of ephemeral rain-induced stratification events that formed between the 8th and 13th of March 2015 (as seen in Chapter 4.3.1).

During April and May 2015 (which includes the peak of the spring bloom), the magnitude of depth-integrated modelled chlorophyll concentrations was comparable to bottled samples taken on nearby process cruises (Poulton et al, 2017). While the peak magnitudes of the observed (189 mg m^{-2}) and modelled (152 mg m^{-2}) spring blooms differed by 37 mg m^{-2}, the shape of the spring bloom is consistent, insofar that the local minima in chlorophyll observed from the 15th to the 25th April is well captured in the model. However, the timing of the spring bloom is 8 days later than what was observed (Poulton et al, 2017; Fig 5.3). The discrepancy between the observed and modelled spring bloom initiations and magnitudes may be explained by considering the horizontal variability of phytoplankton, i.e. phytoplankton patchiness (e.g. Martin, 2003).

Phytoplankton patchiness is also observed in the model, as seen by Fig. 5.4, which shows the daily averaged chlorophyll concentrations from the shelf break, the inner shelf (CCS) and two mid-point locations, named X_1 and X_2 and located 52km and 66km from the shelf break respectively. While the shelf break and CCS model points have the maximum distance of 125km, they show little variations in the timing of the spring bloom. It is, in fact, the X_1 and X_2 locations that show the most deviation from the CCS spring bloom initiation, with an offset of 4.5 days. Furthermore, while timing of X_1 and X_2 differ by only 7 hours, they possess large differences in the shape of their respective spring blooms. Both X_1 and X_2 have similar magnitudes on the 21st April, yet soon diverge to a maximum difference of 47 mg m^{-2} by the 3rd May, despite a relatively short separation distance of 14 km. Chlorophyll concentrations converge and stabilise from the 23rd May 2015, suggesting a spatial homogenisation of phytoplankton across the region.

This analysis highlights the complex spatial variability of phytoplankton and could explain the discrepancy observed between the timing of the model and observed spring blooms. In an effort to mitigate the spatial complexity of phytoplankton within the model, analysis of the spring bloom will only serve to describe decadal trends in the timing of its initiation. The use

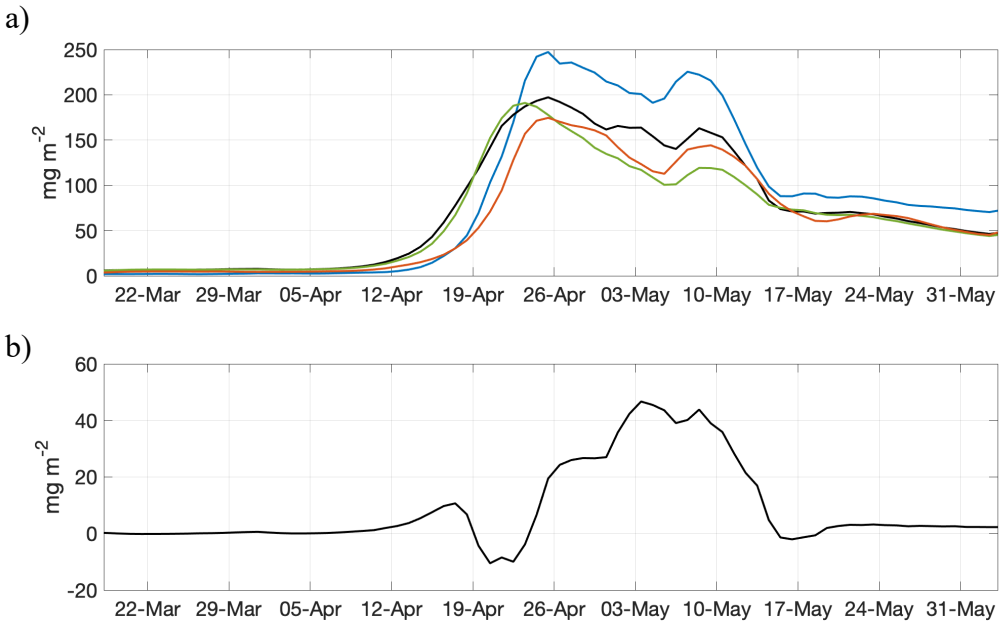

Fig. 5.4: a) Total depth-integrated chlorophyll concentrations from the AMM7 NEMO-ERSEM model, at four different locations: the shelf break (blue), the inner shelf (CCS; red) and two mid-point locations located 52km (X_1; green) and 66km (X_2; black) from the shelf break; b) The difference in chlorophyll concentrations between X_1 and X_2

of a single point location (49.0005°N, -9.0001°E) from 1982 to 2015 also adds spatial consistency with which to determine mean multidecadal changes across contrasting climatological modes.

5.2.2 Defining the prebloom and spring bloom

Following the methods described in Chapter 3.4, the phases of the AMO from 1982 to 2015 are split into the negative (or cooler) AMO phases, occurring from 1982 to 1996, and the positive (or warmer) AMO phase from 1998 to 2015. The year 1997 was a transition year between negative and positive AMO phases and experienced an anomalously early stratification onset of the 26th February. As such, it has not been included in either the negative or positive AMO phase and remains an isolated point between the two, as shown by Fig. 5.5. Nevertheless, 1997 is an important case study year for investigating the timing of the spring bloom in relation to an anomalously early stratification onset, and will be discussed in more detail in Section 5.3.2.

Modelled chlorophyll concentrations (mg m^{-3}) were analysed according to the onset of the prebloom and spring bloom. Phytoplankton prebloom periods were defined as when the rate of increase in surface (0-10m) chlorophyll concentrations first exceeded 0.01 mg m^{-2} d^{-1}, and was used to identify the start of gradual phytoplankton growth following the unproductive winter period. In contrast, the spring bloom was defined as the date where the rate of increase in surface (0-10m) chlorophyll concentrations exceeded 0.15 mg m^{-2} d^{-1} consistently for 5 days, and was used to identify the exponential increase in phytoplankton biomass that is characteristic of the spring bloom.

5.3. Results and Discussion

5.3.1. The spring bloom

Throughout the 1982 to 2015 model study period, there was a downward linear trend in spring bloom initiation dates of 8 hours yr^{-1}. Considering AMO phases independently, with negative periods defined as 1982 to 1996 and positive periods from 1998 to 2015, analysis demonstrated a shift towards an earlier spring bloom during positive AMO phases, with the mean spring bloom initiation occurring 7 days earlier in positive AMO periods than in negative AMO periods. In shelf sea environments, seasonal stratification is considered to be a precursor for spring bloom initiation, due to phytoplankton cells being suspended in a more favourable light environment (e.g. Sverdrup, 1953). As such, an earlier spring bloom during positive AMO phases is consistent with previous work in this thesis that states the onset of seasonal stratification occurs 5 days earlier from negative to positive AMO periods (see Chapter 3).

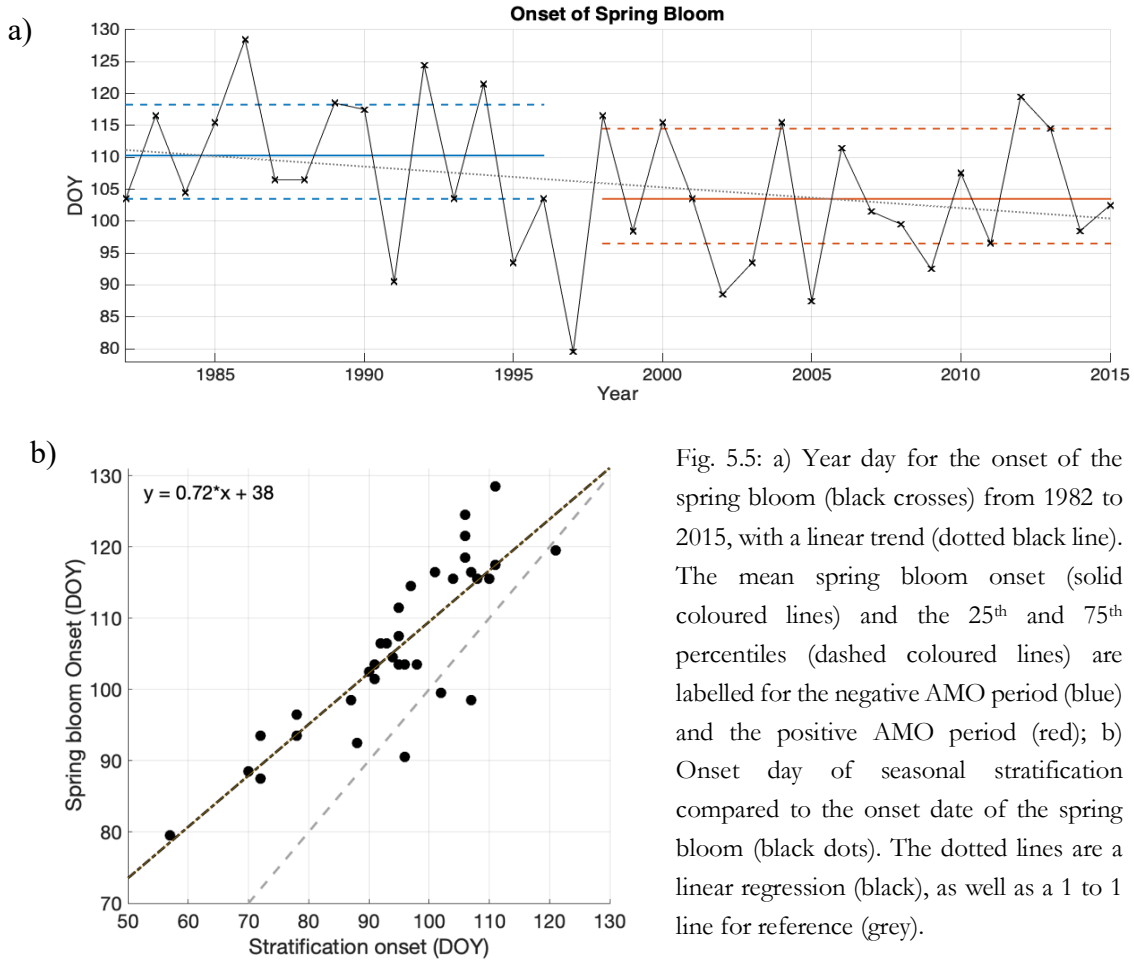

Fig. 5.5: a) Year day for the onset of the spring bloom (black crosses) from 1982 to 2015, with a linear trend (dotted black line). The mean spring bloom onset (solid coloured lines) and the 25th and 75th percentiles (dashed coloured lines) are labelled for the negative AMO period (blue) and the positive AMO period (red); b) Onset day of seasonal stratification compared to the onset date of the spring bloom (black dots). The dotted lines are a linear regression (black), as well as a 1 to 1 line for reference (grey).

This is reinforced by the strong positive correlation between the onset of seasonal stratification and the initiation of the spring bloom ($R = 0.85$ and $P = <0.0001$), and at first glance, implies a coupling between the two.

However, a linear regression further revealed a variable lag time between the onset of seasonal stratification and the initiation of the spring bloom (Fig 5.5b). If the onset of stratification occurred on the 1 January, the spring bloom would not occur until 38 days later. This is in direct contrast to an immediate spring bloom initiation following a much later seasonal stratification onset date of the 10th May, and implies a decoupling between the onset of seasonal stratification and spring bloom initiation. To explain this offset, an example of an anomalously early stratification onset will be discussed below.

5.3.2. Case study: 1997

Seasonal stratification occurred on the 26th February 1997, following a low-pressure system that lasted 5 days. This was accompanied by strong winds of between 13.9 and 18.1 ms^{-1} that would have promoted mixing of the upper water column, inhibiting the formation of stratification. Following the onset of stratification on the 26th February, meteorological conditions were relatively calm and stable, with air pressures and wind speeds averaging 1024 hPa and 7.2 ms^{-1} respectively. However, as seen by Fig. 5.6, a clear lag is observed between the onset of stratification (as seen by potential energy anomaly, ϕ; Simpson and Bowers, 1981; Simpson et al, 1990) and the initiation of the spring bloom. Initial phytoplankton growth does not occur until the 10th March 1997, with the spring bloom only occurring 22 days after seasonal stratification onset, on the 20th March 1997.

Total integrated winter PAR levels for 1997 were the lowest throughout the 34-year study period and exceeded two standard deviations from the mean (Fig 5.7a). This variation in light is due to meteorological conditions, specifically cloud coverage. Average cloud cover for February 1997 was 74%, which then fell to an average March coverage of 70% (Fig. 5.7c). While this is not the largest cloud coverage recorded out of the 34-year study period, 1997 did experience an anomalously early stratification onset that the other years did not. The cloudy conditions that occurred in February 1997 would have produced an unfavourable light

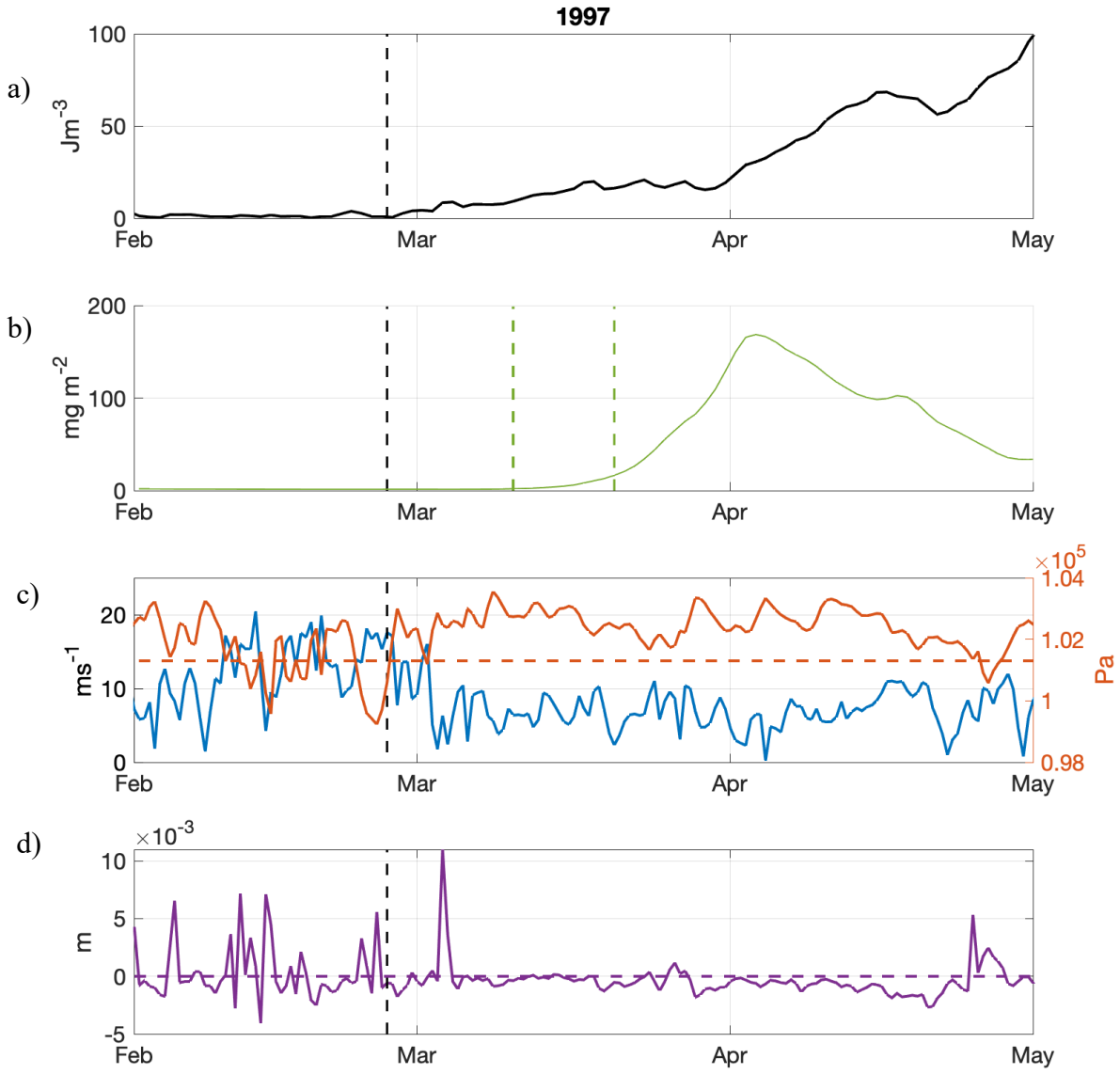

Fig. 5.6: a) The 1997 potential energy anomaly (ϕ, Jm^{-3}) from February to May; b) the depth-integrated chlorophyll concentration (mg m^{-2}) with the initial and exponential phytoplankton growth indicated by the vertical green dashed lines; c) the 10m wind speed (ms^{-1}, blue) and surface air pressure (Pa, red), with the red dashed line indicating standard sea level pressure (Met Office); d) the difference between the 12-hr cumulative precipitation and evaporation, including a zero line (purple dashed line). The onset of stratification (vertical black lines) are also added. Source of meteorological data: ERA-Interim (Dee et al, 2011).

environment that would be directly limiting to phytoplankton growth. In contrast, 1986 and 2012 both received higher amounts of February cloud cover than 1997, averaging 91% and 86% respectively. Yet, unlike 1997, stratification in these years ultimately occurred two months later, on the 21st April 1986 and the 30th April 2012, when the seasonal increase in light and reduced cloud cover would have likely produced more favourable conditions for phytoplankton growth.

The onset of seasonal stratification is hypothesised to become earlier in the future (Sharples et al, 2013), and thus it is also conceivable that the spring bloom will also be initiated earlier. However, as shown by this multidecadal analysis, this is not the case and emphasises the potential decoupling between the onset of seasonal stratification and the spring bloom initiation. Despite the earlier onset seasonal stratification in future warming scenarios (Sharples et al, 2013), the spring bloom will not be initiated until favourable light levels are reached. These results are consistent with mesocosm experiments by Sommer and Lengfellner (2008), who found that light was more critical than temperature for spring bloom initiation.

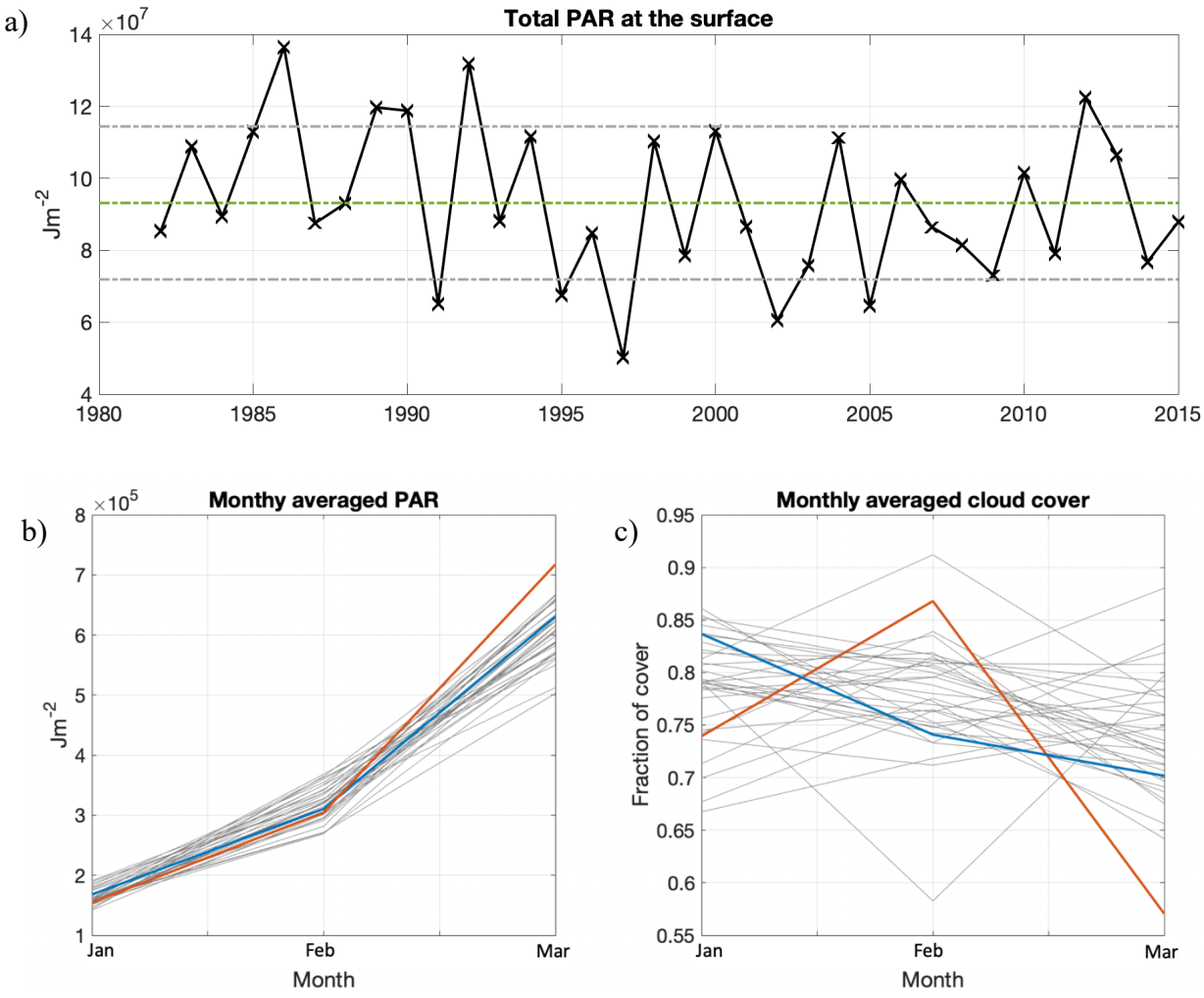

Fig. 5.7: a) Total photosynthetically active radiation (PAR; Jm^{-2}) at the surface from 1982 to 2015 from January to March. The green dotted line is the mean, and the grey lines are the standard deviations from the mean; b) Monthly averaged PAR from January to March from 1982 to 2015; and c) the average cloud cover from January to March 1982 to 2015. In b) and c) 1997 and 2012 are labelled as the blue and red lines respectively. Data downloaded from ERA-Interim (Dee et al, 2011).

5.3.3 The Prebloom

Previous work in this thesis has demonstrated that storms act to both trigger and erode stratification. In Chapter 3, it was demonstrated that established stratification can be homogenised if subsequent storms are sufficiently energetic, with sustained seasonal stratification only reforming once the combined positive buoyancy inputs from rain and heat outcompete the homogenising effect of wind and tidal stresses. Chapter 3 detailed 2012 as an example, where a stratification event of up 23.3 Jm^{-3} was homogenised and sustained seasonal stratification did not occur until 30 days later. In this section, we further this analysis to demonstrate that substantial phytoplankton growth can occur between such ephemeral stratification events and before the onset of seasonal stratification.

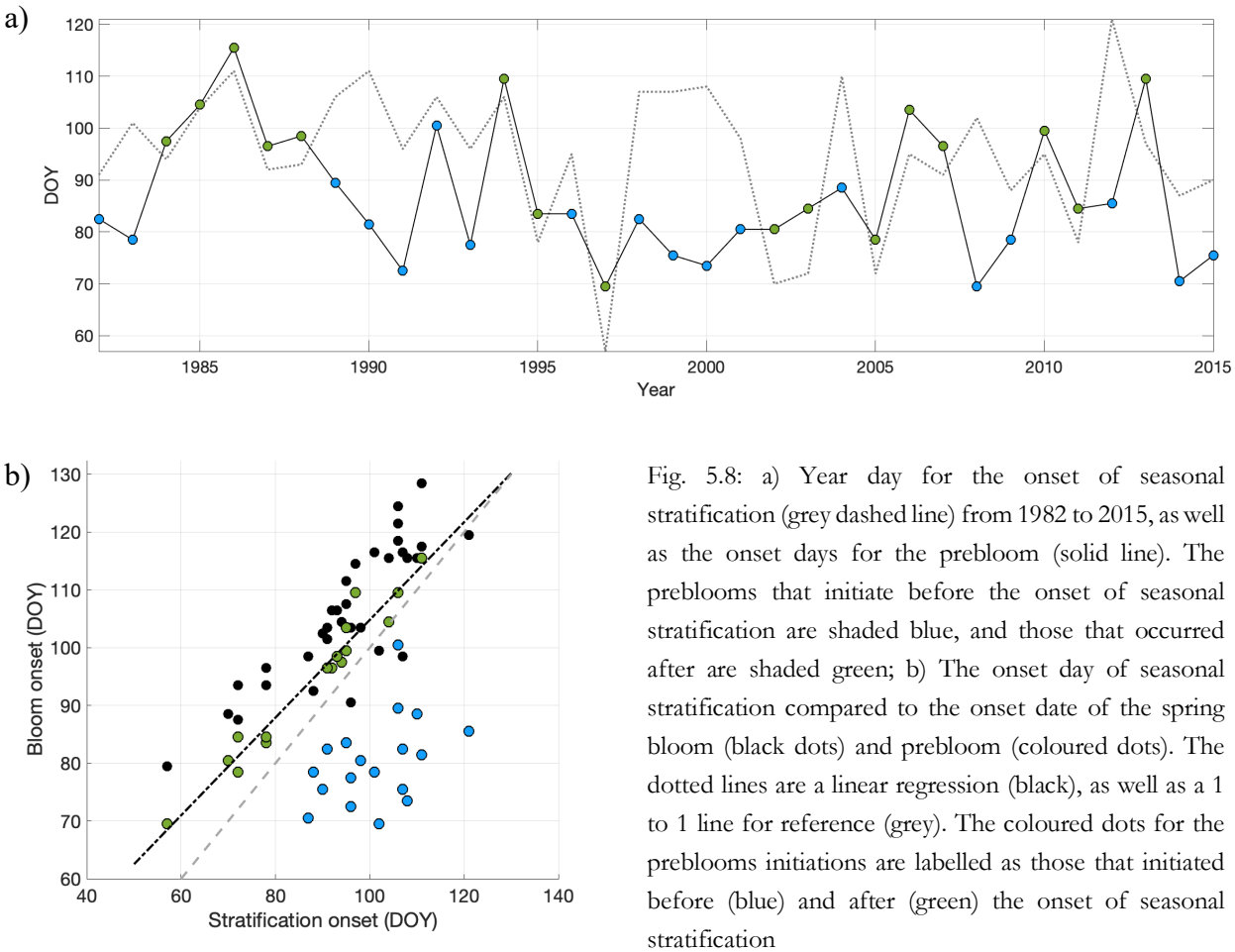

Fig. 5.8: a) Year day for the onset of seasonal stratification (grey dashed line) from 1982 to 2015, as well as the onset days for the prebloom (solid line). The preblooms that initiate before the onset of seasonal stratification are shaded blue, and those that occurred after are shaded green; b) The onset day of seasonal stratification compared to the onset date of the spring bloom (black dots) and prebloom (coloured dots). The dotted lines are a linear regression (black), as well as a 1 to 1 line for reference (grey). The coloured dots for the preblooms initiations are labelled as those that initiated before (blue) and after (green) the onset of seasonal stratification

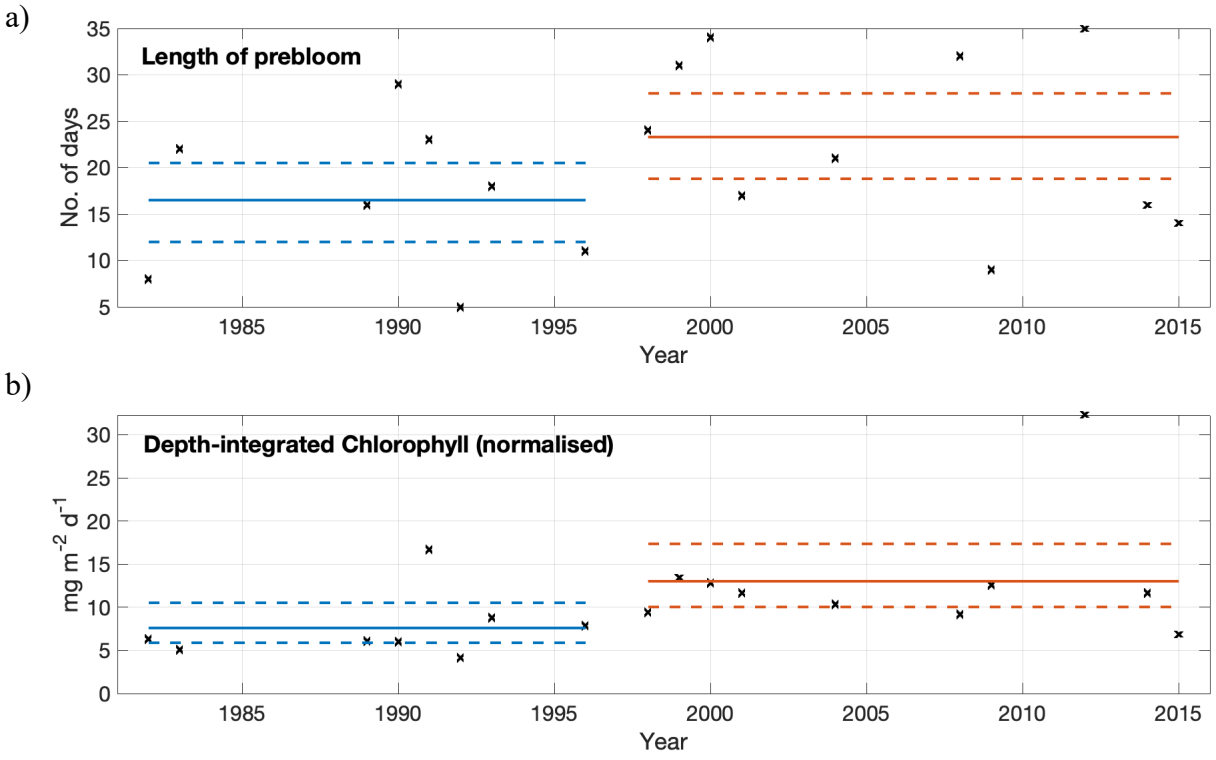

Fig. 5.9: a) The length of the prebloom period, for the years where the prebloom occurred before the onset of seasonal stratification (black crosses), and b) the total depth-integrated chlorophyll concentration from NEMO-ERSEM, normalised to the length of the prebloom (in days). In both a) and b), the mean (solid lines) and the 90% confidence limits (dashed lines) have been included for the negative (blue) and positive (red) AMO phases.

A comparison between the onset dates of the prebloom and the onset of seasonal stratification can be seen in Fig. 5.8. Out of the 34 years, 16 of the prebloom periods occurred after the onset of seasonal stratification, as shown by the green dots in Fig. 5.8a. These are simply slow initiations of the spring bloom, and further displayed a strong correlation to the onset of seasonal stratification ($R = 0.97$; $P = < 0.0001$). However, the remaining 18 preblooms occurred before the onset of seasonal stratification (blue dots in Fig. 5.8a). These prebloom initiation dates are connected to other mechanisms and are thus decorrelated to the onset of seasonal stratification ($R = 0.41$; $P = 0.09$), as highlighted in Fig. 5.8b. As such, only these 18 prebloom periods will be included in further analysis.

Analysis of the preblooms in the associated negative and positive AMO periods indicated a 6.8 day increase in mean prebloom duration (Fig. 5.9a). This agrees with the hypothesis that during positive AMO phases, the presence of atmospheric blocking interspersed with intense

cyclones results in periods of prolonged stratification that are subsequently homogenised by strong storms.

The total depth-integrated chlorophyll concentrations within the prebloom period, normalised relative to the length of the prebloom (in days), exhibited an almost twofold (1.7) increase in chlorophyll concentrations identified from negative and positive AMO phases (Fig. 5.9).

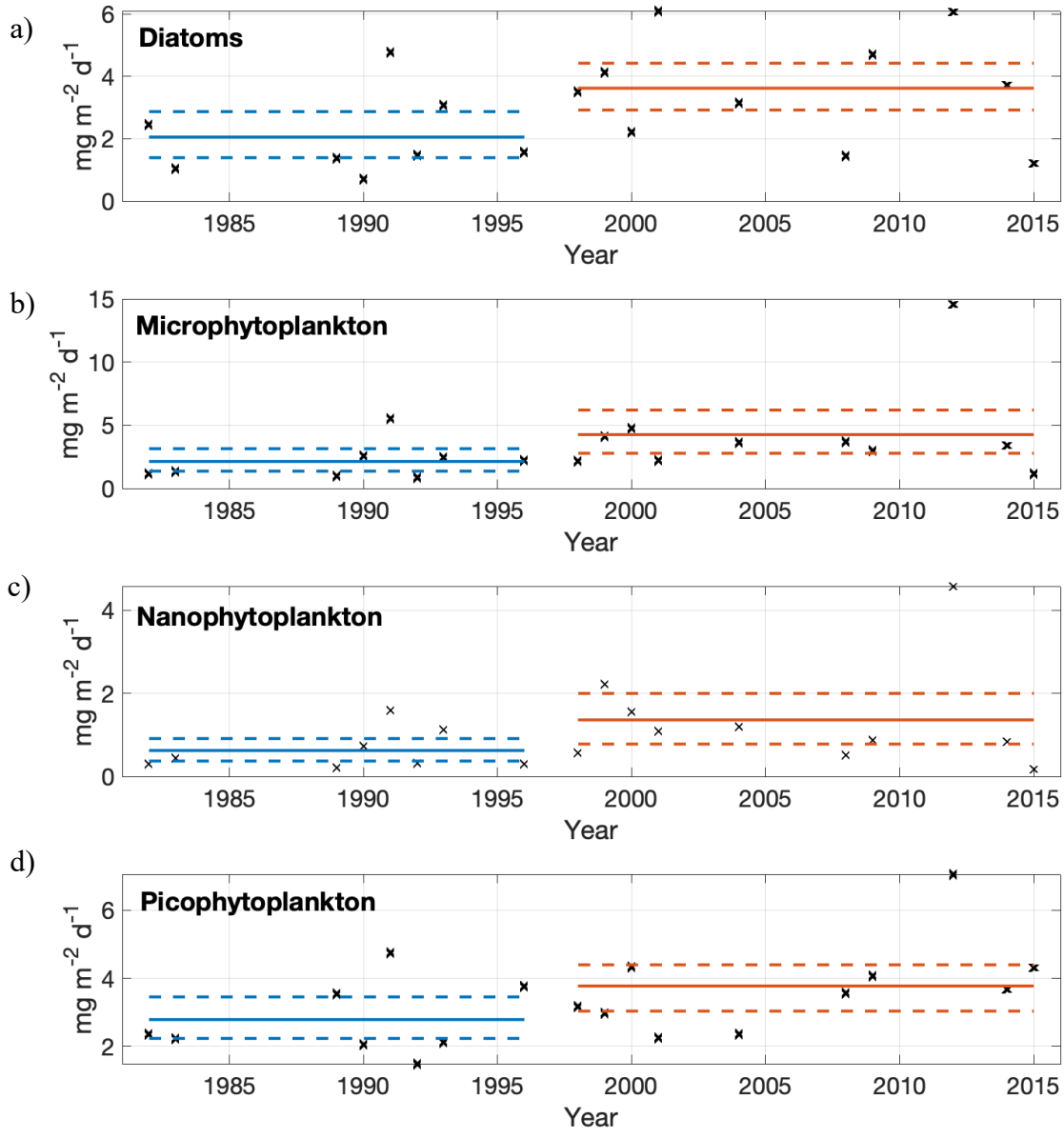

Fig. 5.10: a) The total depth-integrated concentrations for a) diatoms, b) microphytoplankton, c) nanophytoplankton and d) picophytoplankton in the prebloom periods, normalised by the length of the prebloom (in days). In all subplots, the mean (solid lines) and the 90% confidence limits (dashed lines) have been included for the negative (blue) and positive (red) AMO phases.

Further analysis indicated this increase was consistent across all phytoplankton functional groups incorporated in the model (Fig. 5.10). Normalised total depth-integrated concentrations (with a ± 90% confident interval) during the prebloom periods displayed increases of 1.7±1.3 mg m^{-2} d^{-1} (diatoms), 2.1 ± 2.6 mg m^{-2} d^{-1} (microphytoplankton), 0.73 ± 0.78 mg m^{-2} d^{-1} (nanophytoplankton) and 0.98 ± 0.98 mg m^{-2} d^{-1} (picophytoplankton). Although subtle, this equates to an increase in normalised chlorophyll concentrations from 7.6 ± 2.8 mg m^{-2} d^{-1} to 13.1 ±4.3 mg m^{-2} d^{-1} across all phytoplankton functional groups in positive AMO phases.

5.3.4. Case study: 2012

The physical drivers of these prebloom events can be further explored by considering 2012 as a case study (Fig. 5.11). In direct contrast to 1997, 2012 experienced the latest stratification onset out of the 34-year study period. Furthermore, a period of ephemeral stratification occurred between the 19th March and the 5th April that coincided with a prebloom phytoplankton growth event. This stratification was later homogenised by a series of storms that brought winds of up to 20 ms^{-1} on the 18th April. Seasonal stratification ultimately occurred on the 30th April 2012 as wind dropped to 8.6ms^{-1}, resulting in an apparent immediate exponential phytoplankton growth characteristic of the spring bloom.

The 2012 prebloom event was the largest out of the 34-year study period, accounting for 17% of the total prebloom chlorophyll concentrations from 1982 to 2015. The 2012 prebloom was initiated on the 25th March and coincided with an increase in stratification (ϕ) from 3.5 to 23.3 Jm^{-3} over 8 days, with increased phytoplankton growth initiated by a more favourable light environment. Phytoplankton growth continued to occur after water column homogenisation on the 5th April, increasing from 24 mg m^{-2} to 84 mg m^{-2} over the 30 days before the onset of seasonal stratification.

In direct contrast to 1997, 2012 received high light, with PAR levels in excess of the standard deviation from the mean (Fig. 5.7). Furthermore, average cloud coverage dramatically reduced from 86% in February to 56% March, the lowest March cloud coverage recorded in this study. This resulted in increased PAR at the surface, creating a highly favourable light environment for phytoplankton growth. This, combined with stratification events occurring relatively later

in the year where incident light was higher, provided a suitable environment for phytoplankton growth. Furthermore, a series of rain events occurring from the 5th to the 30th April 2012 eludes to periods of short-lived halostratification that would have acted to sustain phytoplankton growth. This is, again, consistent with results from Chapter 4 which identifies

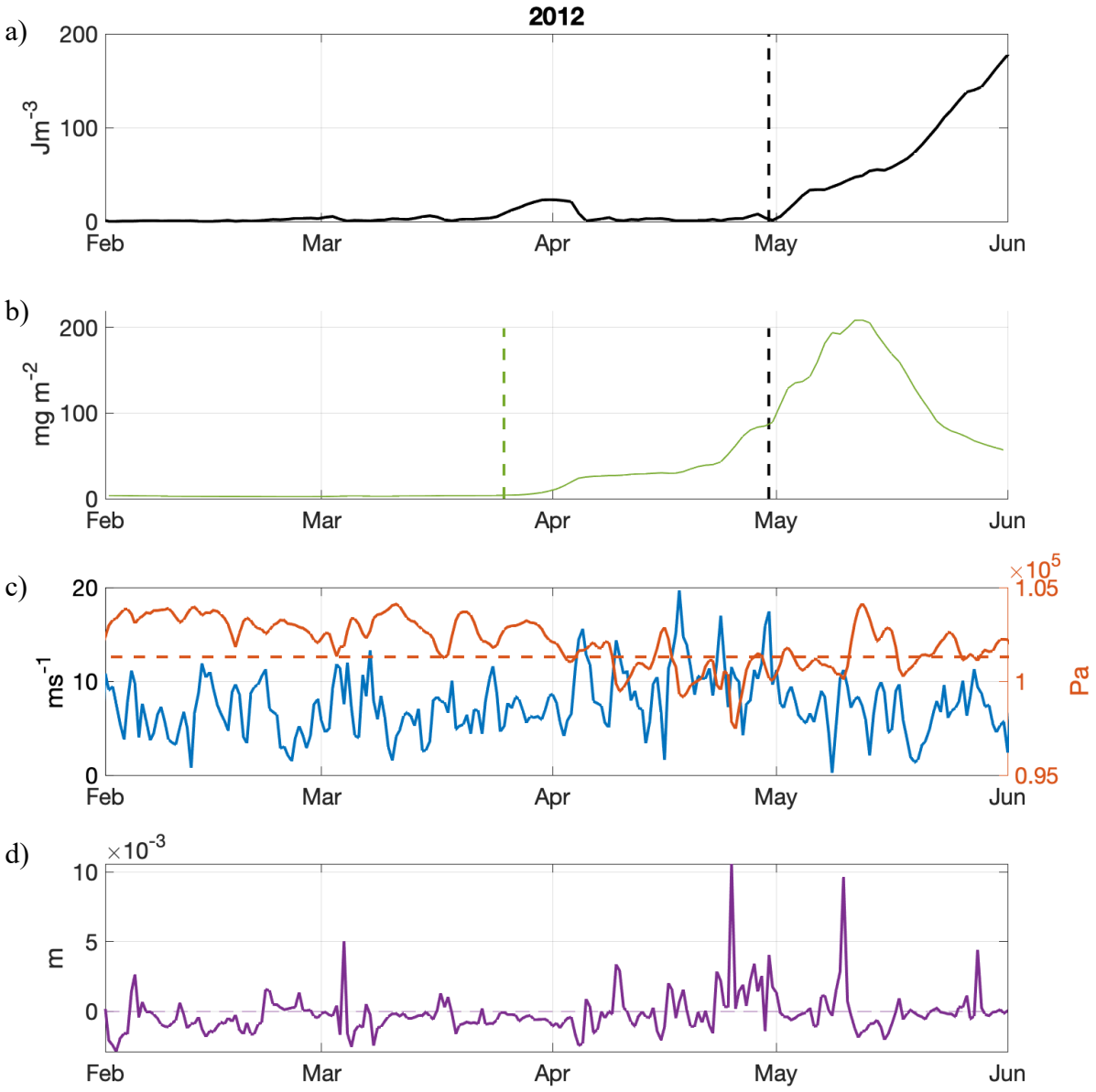

Fig. 5.11: a) The 2012 potential energy anomaly (ϕ, Jm^{-3}) from February to May; b) the depth-integrated chlorophyll concentration ($mg\ m^{-2}$) with the onset of the prebloom indicated by the vertical green dashed line; c) the 10m wind speed (ms^{-1}, blue) and surface air pressure (Pa, red), with the red dashed line indicating standard sea level pressure (Met Office); d) the difference between the 12-hr cumulative precipitation and evaporation, including a zero line (purple dashed line). The onset of stratification (vertical black lines) are also added. Source of meteorological data: ERA-Interim (Dee et al, 2011).

that rainfall occurring in February and March 2015 acted to sustained phytoplankton growth through the formation of temporary favourable light environments.

5.4 Implications for the wider ecosystem

From 1982 to 1996, the high frequency of storms associated with the predominantly negative AMO phase resulted in a completely homogenised water column, characteristic of winter shelf sea environments. By contrast, during positive AMO phases, the occurrence of extratropical cyclones was followed by relatively calm conditions, resulting in periods of ephemeral stratification that promoted phytoplankton growth. These stratification events were ultimately homogenised, yet elevated phytoplankton populations were still sustained through sporadic rain events that created a series of favourable light environments (see Chapter 3 and 4). If incident light levels were particularly high, such as in 2012, these conditions promoted gradual phytoplankton growth. Following the onset of seasonal stratification, prebloom phytoplankton populations form the initial spring bloom, and are likely to act as seeder populations.

Early winter phytoplankton blooms have been shown to consist primarily of diatoms (e.g. Lacour et al, 2017). Diatoms are often considered to thrive at the start of spring bloom succession (Margalef 1978, Gilbert 2016), before being outcompeted by the smaller dinoflagellates that thrive in the highly stratified, low nutrient conditions associated with a summer shelf sea (Holligan, 1984; Hickman et al, 2009; Gilbert, 2016; McQuatters-Gollop et al, 2007). Many winter phytoplankton blooms often consist mostly of diatoms (Glé et al, 2007; Lacour et al, 2017). It was found that in highly turbulent environments, heavier species such as diatoms that were adapted to low light conditions thrived (Huisman *et al*, 2004), and diatoms dominated in the tidally well-mixed regimes analogous to winter or spring periods (Pingree *et al*, 1976; Holligan *et al*, 1984; Ross and Sharples, 2007). Diatoms are then outcompeted by smaller phytoplankton species, such as dinoflagellates, that thrive in the low nutrient, highly stratified regions typical of a summer shelf sea (Holligan, 1984; Hickman et al, 2009; Gilbert, 2016; McQuatters-Gollop et al, 2007).

This is reflected in the coupled model used in this study, within which diatoms are parameterised to reach maximum growth at relatively lower levels of PAR (Butenschön et al, 2016) and are thus well adapted to prebloom conditions that are analogous with highly turbulent, low-light regimes. However, all phytoplankton functional groups represented in the model showed an increase in growth between contrasting AMO phases and implies the prebloom conditions are not advantageous to one particular phytoplankton group.

This has important implications for marine food-web dynamics. Many marine organisms synchronise their spawning cycles with the occurrence of the spring bloom (Cushing, 1973; Platt et al, 2003), ensuring larvae have an ample food source. As stratification is considered a precursor for the development of the spring bloom, any increase in spring bloom variability, such as observed during positive AMO periods, will likely exacerbate the mismatch between phytoplankton abundance and larval production (Cushing, 1973; Cushing, 1990; Durant et al, 2007). Longer, more productive prebloom periods may act to buffer this mismatch, by promoting sustained phytoplankton growth before the spring bloom has been initiated. An increase in diatoms in positive AMO periods will particularly benefit grazers, as they are considered high-quality food for zooplankton (Legendre, 1990; Jonasdottir and Kiørboe, 1996), particularly copepods (Verity and Smetacek, 1996).

The role of shelf seas in carbon fixation can also not be ignored. Lacour et al (2017) postulated that the cumulative amount of carbon fixation from several short-lived winter stratification events in the North Atlantic could result in a significant contribution to annual carbon export. However, the influence of this is likely to be reduced in shelf sea environments, given that the water column is ultimately homogenised following the ephemeral stratification periods, thus preventing carbon being stored away from the atmosphere. Nevertheless, a gradual increase in phytoplankton standing stock directly before the onset of stratification might be sufficient to increase carbon flux to the sediments, contributing towards the estimated 20% of anthropogenic carbon uptake that has been suggested in shelf seas (Thomas et al, 2004).

5.5 Conclusions and key findings

In this Chapter, a significant biogeochemical response to changing storm activity between different climatological phases is shown, with the spring bloom occurring an average of 7 days earlier in positive AMO phases. Despite this, the spring bloom initiation was primarily light limited, and may still occur up to 22 days after the onset of seasonal stratification should incident PAR be insufficient for growth.

Ephemeral winter stratification events were formed by transient storms, interspersed with periods of calm conditions, provided a non-limiting light environment for phytoplankton growth before the spring bloom. These prebloom periods occurred before the initiation of seasonal stratification and accounted up to 22% of the total phytoplankton growth across the spring phytoplankton growing period. This has important implications for food-web dynamics, with the longer prebloom periods associated with positive AMO phases acting to buffer the mismatch between spring bloom phytoplankton growth and larval production. Furthermore, increased phytoplankton growth directly before the onset of stratification could increase the efficiency of shelf sea carbon fixation.

Through the use of coupled hydrodynamic models, this Chapter has demonstrated that large-scale climatic oscillations in the North Atlantic directly impact the productivity of a winter shelf sea. Warmer conditions could result in significantly longer and more productive phytoplankton growth events that occur before the onset of seasonal stratification. Such elevated prebloom periods would directly feed into the higher tropic levels, through the availability of food for zooplankton larval recruitment, as well as preconditioning the spring bloom community succession and enhancing winter-spring carbon fixation. With marine air temperatures around the UK increasing at a rate of 0.2 to 0.4^{o}C decade^{-1} (Dye et al, 2013), the positive phase of the AMO studied here may be considered analogous to future climate conditions. This work emphasises that the intrinsic links between ocean-atmosphere coupling are crucial for predicting how ecosystem functioning will respond to anthropogenic warming.

5.6 References

Alexander, M.A., Kilbourne, K.H. and Nye, J.A., 2014. Climate variability during warm and cold phases of the Atlantic Multidecadal Oscillation (AMO) 1871–2008. *Journal of Marine Systems*, *133*, pp.14-26.

Behrenfeld, M.J., 2010. Abandoning Sverdrup's critical depth hypothesis on phytoplankton blooms. *Ecology*, *91*(4), pp.977-989.

Boss, E. and Behrenfeld, M., 2010. In situ evaluation of the initiation of the North Atlantic phytoplankton bloom. *Geophysical Research Letters*, *37*(18).

Butenschön, M., Clark, J., Aldridge, J.N., Allen, J.I., Artioli, Y., Blackford, J., Bruggeman, J., Cazenave, P., Ciavatta, S., Kay, S. and Lessin, G., 2016. ERSEM 15.06: a generic model for marine biogeochemistry and the ecosystem dynamics of the lower trophic levels. *Geoscientific Model Development*, *9*(4), pp.1293-1339.

Chiswell, S.M., 2011. Annual cycles and spring blooms in phytoplankton: don't abandon Sverdrup completely. *Marine ecology progress series*, *443*, pp.39-50.

Cohen, J., Screen, J.A., Furtado, J.C., Barlow, M., Whittleston, D., Coumou, D., Francis, J., Dethloff, K., Entekhabi, D., Overland, J. and Jones, J., 2014. Recent Arctic amplification and extreme mid-latitude weather. *Nature geoscience*, *7*(9), pp.627-637.

Collins, A.K., Allen, S.E. and Pawlowicz, R., 2009. The role of wind in determining the timing of the spring bloom in the Strait of Georgia. *Canadian Journal of Fisheries and Aquatic Sciences*, *66*(9), pp.1597-1616.

Cushing, D.H., 1973. The natural regulation of fish populations. *Sea fisheries research*.

Cushing, D.H., 1990. Plankton production and year-class strength in fish populations: an update of the match/mismatch hypothesis. In *Advances in marine biology* (Vol. 26, pp. 249-293). Academic Press.

Dee, D.P., Uppala, S.M., Simmons, A.J., Berrisford, P., Poli, P., Kobayashi, S., Andrae, U., Balmaseda, M.A., Balsamo, G., Bauer, D.P. and Bechtold, P., 2011. The ERA-Interim reanalysis: Configuration and performance of the data assimilation system. *Quarterly Journal of the royal meteorological society*, *137*(656), pp.553-597.

Delworth, T.L., Zhang, R. and Mann, M.E., 2007. Decadal to centennial variability of the Atlantic from observations and models. *Geophysical Monograph-American Geophysical Union*, *173*, p.131.

Durant, J.M., Hjermann, D.Ø., Ottersen, G. and Stenseth, N.C., 2007. Climate and the match or mismatch between predator requirements and resource availability. *Climate research*, *33*(3), pp.271-283.

Dye, S.R., Holliday, N.P., Hughes, S.L., Inall, M., Kennington, K., Smyth, T., Tinker, J., Andres, O. and Beszczynska-Möller, A., 2013. Climate change impacts on the waters around the UK and Ireland: Salinity. *MCCIP Science Review*, *2013*, pp.60-66.

Glé, C., Del Amo, Y., Bec, B., Sautour, B., Froidefond, J.M., Gohin, F., Maurer, D., Plus, M., Laborde, P. and Chardy, P., 2007. Typology of environmental conditions at the onset of winter phytoplankton blooms in a shallow macrotidal coastal ecosystem, Arcachon Bay (France). *Journal of plankton research*, *29*(11), pp.999-1014.

Glibert, P.M., 2016. Margalef revisited: a new phytoplankton mandala incorporating twelve dimensions, including nutritional physiology. *Harmful Algae*, *55*, pp.25-30.

Gómara, Í., Rodríguez Fonseca, B. and Zurita Gotor, P., 2012. Explosive cyclones in the North Atlantic: NAO influence and multidecadal variability. *Publicaciones de la Asociación Española de Climatología. Serie A; 8*.

Häkkinen, S., Rhines, P.B. and Worthen, D.L., 2011. Atmospheric blocking and Atlantic multidecadal ocean variability. *Science*, *334*(6056), pp.655-659.

Henson, S.A., Robinson, I., Allen, J.T. and Waniek, J.J., 2006. Effect of meteorological conditions on interannual variability in timing and magnitude of the spring bloom in the Irminger Basin, North Atlantic. *Deep Sea Research Part I: Oceanographic Research Papers*, *53*(10), pp.1601-1615.

Hickman, A.E., Holligan, P.M., Moore, C.M., Sharples, J., Krivtsov, V. and Palmer, M.R., 2009. Distribution and chromatic adaptation of phytoplankton within a shelf sea thermocline. *Limnology and Oceanography*, *54*(2), pp.525-536.

Holligan, P.M., leB. Williams, P.J., Purdie, D. and Harris, R.P., 1984. Photosynthesis, respiration and nitrogen supply of plankton populations in stratified, frontal and tidally mixed shelf waters. *Marine Ecology Progress Series*, pp.201-213.

Huisman, J., Sharples, J., Stroom, J.M., Visser, P.M., Kardinaal, W.E.A., Verspagen, J.M. and Sommeijer, B., 2004. Changes in turbulent mixing shift competition for light between phytoplankton species. *Ecology*, *85*(11), pp.2960-2970.

Jónasdóttir, S.H. and Kiørboe, T., 1996. Copepod recruitment and food composition: do diatoms affect hatching success?. *Marine Biology*, *125*(4), pp.743-750.

Körtzinger, A., Send, U., Lampitt, R.S., Hartman, S., Wallace, D.W., Karstensen, J., Villagarcia, M.G., Llinás, O. and DeGrandpre, M.D., 2008. The seasonal pCO2 cycle at 49 N/16.5 W in the northeastern Atlantic Ocean and what it tells us about biological productivity. *Journal of Geophysical Research: Oceans*, *113*(C4).

Lacour, L., Ardyna, M., Stec, K.F., Claustre, H., Prieur, L., Poteau, A., D'Alcala, M.R. and Iudicone, D., 2017. Unexpected winter phytoplankton blooms in the North Atlantic subpolar gyre. *Nature Geoscience*, *10*(11), p.836.

Legendre, L., 1990. The significance of microalgal blooms for fisheries and for the export of particulate organic carbon in oceans. *Journal of plankton research*, *12*(4), pp.681-699.

Li, J., Sun, C. and Jin, F.F., 2013. NAO implicated as a predictor of Northern Hemisphere mean temperature multidecadal variability. *Geophysical research letters*, *40*(20), pp.5497-5502.

Madec, G., 2015. NEMO ocean engine.

Margalef, R., 1978. Life-forms of phytoplankton as survival alternatives in an unstable environment. *Oceanol. Acta 1*, 493–509.

Marshall, J., Kushnir, Y., Battisti, D., Chang, P., Czaja, A., Dickson, R., Hurrell, J., McCartney, M.., Saravanan, R. and Visbeck, M., 2001. North Atlantic climate variability: phenomena, impacts and mechanisms. *International Journal of Climatology: A Journal of the Royal Meteorological Society*, *21*(15), pp.1863-1898.

Martin, A.P., 2003. Phytoplankton patchiness: the role of lateral stirring and mixing. *Progress in oceanography*, *57*(2), pp.125-174.

McQuatters-Gollop, A., Raitsos, D.E., Edwards, M. and Attrill, M.J., 2007. Spatial patterns of diatom and dinoflagellate seasonal cycles in the NE Atlantic Ocean. *Marine Ecology Progress Series*, *339*, pp.301-306.

Pingree, R.D., Holligan, P.M., Mardell, G.T. and Head, R.N., 1976. The influence of physical stability on spring, summer and autumn phytoplankton blooms in the Celtic Sea. *Journal of the Marine Biological Association of the United Kingdom*, *56*(4), pp.845-873.

Platt, T., Fuentes-Yaco, C. and Frank, K.T., 2003. Marine ecology: spring algal bloom and larval fish survival. *Nature*, *423*(6938), p.398.

Poulton, A.J., Davis, C.E., Daniels, C.J., Mayers, K.M., Harris, C., Tarran, G.A., Widdicombe, C.E. and Woodward, E.M.S., 2017. Seasonal phosphorus and carbon dynamics in a temperate shelf sea (Celtic Sea). *Progress in Oceanography*.

Ross, O.N. and Sharples, J., 2007. Phytoplankton motility and the competition for nutrients in the thermocline. *Marine Ecology Progress Series*, *347*, pp.21-38.

Schlesinger, M.E. and Ramankutty, N., 1994. An oscillation in the global climate system of period 65–70 years. *Nature*, *367*(6465), p.723.

Sharples, J., Holt, J. and Dye, S.R., 2013. Impacts of climate change on shelf sea stratification. *MCCIP Science Review*, *2013*, pp.67-70.

Sharples, J., Ross, O.N., Scott, B.E., Greenstreet, S.P. and Fraser, H., 2006. Inter-annual variability in the timing of stratification and the spring bloom in the North-western North Sea. *Continental Shelf Research*, *26*(6), pp.733-751.

Siegel, D.A., Doney, S.C. and Yoder, J.A., 2002. The North Atlantic spring phytoplankton bloom and

Simpson, J.H. and Bowers, D., 1981. Models of stratification and frontal movement in shelf seas. *Deep Sea Research Part A. Oceanographic Research Papers*, *28*(7), pp.727-738.

Simpson, J.H. and Hunter, J.R., 1974. Fronts in the Irish sea. *Nature*, *250*(5465), p.404-406

Simpson, J.H., Brown, J., Matthews, J. and Allen, G., 1990. Tidal straining, density currents, and stirring in the control of estuarine stratification. *Estuaries*, *13*(2), pp.125-132.

Sommer, U. and Lengfellner, K., 2008. Climate change and the timing, magnitude, and composition of the phytoplankton spring bloom. *Global Change Biology*, *14*(6), pp.1199-1208.

Sverdrup, H.U., 1953. On conditions for the vernal blooming of phytoplankton. *J. Cons. Int. Explor. Mer*, *18*(3), pp.287-295.

Taylor, J.R. and Ferrari, R., 2011. Shutdown of turbulent convection as a new criterion for the onset of spring phytoplankton blooms. *Limnology and Oceanography*, *56*(6), pp.2293-2307.

Thomas, H., Bozec, Y., Elkalay, K. and De Baar, H.J., 2004. Enhanced open ocean storage of CO2 from shelf sea pumping. *Science*, *304*(5673), pp.1005-1008.

Townsend, D.W., Cammen, L.M., Holligan, P.M., Campbell, D.E. and Pettigrew, N.R., 1994. Causes and consequences of variability in the timing of spring phytoplankton blooms. *Deep Sea Research Part I: Oceanographic Research Papers*, *41*(5-6), pp.747-765.

Townsend, D.W., Keller, M.D., Sieracki, M.E. and Ackleson, S.G., 1992. Spring phytoplankton blooms in the absence of vertical water column stratification. *Nature*, *360*(6399), p.59.

Verity, P.G. and Smetacek, V., 1996. Organism life cycles, predation, and the structure of marine pelagic ecosystems. *Marine Ecology Progress Series*, *130*, pp.277-293.

6. Summary and Conclusions

This thesis has presented new physical controls on the onset of shelf sea seasonal stratification across contrasting climatological modes. Using a combination of observed and model datasets, data analysed across 34 years revealed that rainfall is a crucial control on shelf sea stratification across the winter-spring period, with significant biogeochemical implications.

A series of autonomous underwater gliders, deployed as part of the Shelf Sea Biogeochemistry project, provided a high temporal and spatial resolution dataset of the winter-spring transition in the Celtic Sea region of the NW European Shelf. With negligible riverine input in open-shelf regions during the winter and early spring (Brown et al, 2003; Fernand et al, 2006; Ruiz-Castillo et al, 2019a), the Celtic Sea provided the ideal location to monitor the near-surface influence of passing storm systems in a temperate, continental shelf sea.

Observational data across February and March 2015 revealed the formation of ephemeral halostratification events that promoted isolated patches of phytoplankton growth. An increase in depth-integrated chlorophyll concentrations eluded to gradual phytoplankton growth across the winter period that is likely to be an increase in biomass, and not photoacclimation. Following the methods of Moore et al (2003) and Denman and Gargett (1983), the mixing time scales for phytoplankton cells were calculated with realistic turbulent eddy diffusivities, varying euphotic depths and two estimates for the mixed layer depth (z_{sml}), each derived from local conditions. The classification of the z_{sml} was shown to be critical when determining mixing timescales during short-lived stratification events, as phytoplankton cells spend up to 6 hours longer in the euphotic zone under a highly variable, realistic z_{sml} than a daily z_{sml} estimate. Sporadic stratification events also proved to be crucial for phytoplankton cells in periods of high turbidity, as they remained in the euphotic zone for several hours longer.

The onset of seasonal stratification was observed on the 25th March 2015, coinciding with a storm event that formed a freshwater surface layer from both rain and wind-driven transport (as described Ruiz-Castillo et al, 2019b). Despite high windspeeds, the combined effect of

increased buoyancy from both freshwater and thermal heating allowed sustained, seasonal stratification to form. A quantitative assessment of the contributions to the potential energy anomaly (ϕ, Simpson and Bowers, 1981; Simpson et al, 1990) revealed that without the added buoyancy from rainfall, stratification would have occurred over a week later than what was observed, highlighting that rainfall events are the initial trigger for seasonal stratification.

The CO5 configuration of the AMM7 model allowed the importance of this new stratification control to be quantified across decadal timescales. From 1982 to 2015, seasonal stratification in 30 out of the 34 years was triggered following a storm event that brought high rainfall and windspeeds. The main modes of meteorological variability across the North Atlantic, the AMO and the NAO, were compared with the stratification onset dates to reveal a twofold increase in stratification onset variability from negative (1982 to 1996) to positive (1998 to 2015) AMO phases. In positive AMO phases, increased atmospheric blocking resulted in strong storms interspersed with periods of relative quiescence, where sustained stratification formed. In some cases, these stratification periods were eroded by subsequent storms. As such, storms both triggered and eroded stratification. The onset of stratification was therefore dependent on the strength of the passing storm and the underlying physical condition of the water column (i.e. the magnitude of ϕ), resulting in highly variable stratification onset dates from 1998 to 2015. In contrast, negative AMO periods were characterised by a continual bombardment of storms that quickly eroded any stratification before it could become established. Thermal controls thus dominated the onset of seasonal stratification from 1982 to 1996, reducing interannual variability.

Despite the twofold variability increase in stratification onset between positive and negative AMO phases, the onset of the spring bloom remained relatively consistent. This was found to be a result of light limitation for phytoplankton growth, displayed as a delayed spring bloom response if the stratification onset occurred earlier in the year. An example year is 1997, where stratification occurred on the 26th February, yet the spring bloom did not initiate until 3 weeks later due to poor light conditions. In 18 out of 34 years, up to 22% of spring phytoplankton growth occurred before the onset of seasonal stratification, defined as prebloom events. Total chlorophyll concentrations within such preblooms displayed an almost twofold increase between negative and positive AMO phases. This was found to be a result of ephemeral stratification events that formed in positive AMO phases, that provided a favourable light

environment for phytoplankton growth. Although these stratification events were ultimately homogenised by subsequent strong storms, the presence of such short-lived stratification maintained winter phytoplankton populations until sustained seasonal stratification was initiated.

This thesis has demonstrated that storm events are a significant control on physical and ecosystem functioning in shelf sea environments. Storms act to both trigger and erode stratification and questions the current paradigm that stratification on the NW European Shelf is primarily driven by thermal inputs (e.g. Simpson and Hunter, 1974; Sharples et al, 2013). This meteorological control on stratification onset dates is reflected in contrasting AMO phases, with a twofold increase in stratification onset variability contradicting the prediction that a warmer climate will result in earlier stratification (Sharples et al, 2013).

From a biogeochemical perspective, sustained phytoplankton growth throughout the winter period challenges perceptions about shelf sea winters being unproductive seasons. Light is emphasised to be a first order control on spring bloom initiation, as shown by the decoupling between early stratification onset dates and the spring bloom initiation. Furthermore, it can be postulated that in warmer climates, which are analogous to temperate latitude conditions in positive AMO phases, a significant proportion of spring phytoplankton growth will occur before the onset of seasonal stratification. This will influence not only the annual primary productivity estimates, but also have crucial ramifications for larval recruitment, and thus fish stocks.

The combination of observed and modelled data has allowed an extensive multidecadal investigation into the physical and biogeochemical coupling during the winter-spring transition on the NW European Shelf. Results in this thesis demonstrate that rainfall is not a negligible contribution to the onset of seasonal stratification in the Celtic Sea, and can even help sustain winter phytoplankton growth. Future work will aim to expand the methods presented in this thesis to other continental shelf seas, particularly those that are positioned beneath storm tracks, to assess the global response of winter storms on water-column structure and ecosystem functioning.

7. Appendix I

This supplementary material briefly reviews the glider processing methods and calibrations used Matlab software primarily developed by Dr Gerd Krahmann at GEOMAR that has been modified for shelf sea applications at the NOC, hereafter referred to as the Glider Toolbox. All glider data was processed using this toolbox (Williams et al, in prep).

7.1 Data processing and calibration

As stated in Chapter 2.1.1, navigational and system data recorded by the glider is stored on the mainboard flash card located on the forward bay. Science data are stored on the science bay. Raw data are stored as binary ***.* bd** files which are then merged into a single datafile.

The files stored by the glider are in one continuous data stream, which is then concatenated into the respective upcast and downcast profiles. Very shallow dives (e.g. < 2m), such as the test dives occurring at the very beginning of the deployment, are discarded during this stage.

Slocum gliders record pressure via two independent pressure sensors: the navigational pressure sensor, and the CTD pressure sensor. The navigational pressure sensor is always on, is always reset to 0 bar at the beginning of a dive and can be calibrated in the lab. In comparison, the pressure measured by the CTD is only recording when the CTD is in use, is not reset to 0 dbar and can only be calibrated by the manufacturers. These two pressure sensors have different functions and thus record pressure at slightly varying spatial and temporal resolutions. Crucially, the CTD pressure sensor delivers a much higher resolution and with less of the operational erroneities associated with the navigational pressure sensors, including surface pressure jumps and scaling offsets. A hybrid of these two pressure estimates is thus used.

Slocum gliders contain multiple processors that all record data at slightly different temporal resolutions. All data recorded by the independent processors are linearly interpolated onto full

seconds of the main glider processing clock, which runs on a 4 second interval. Although this may result in small oversampling errors for some of the sensors and a marginal increase in additional noise, this significantly improves the further processing steps and is thus seen as a suitable compromise.

To minimise the effect of thermal inertia, the Glider Toolbox utilises the work from Garau et al (2011) and Leuck and Picklo (1990) to calculate a modified temperature from a non-linear optimisation method. To do this, Garau et al (2011) minimised the space between density curves in Temperature-Salinity-Space between consecutive glider profiles. The Glider Toolbox expanded on this idea, instead integrating the area in Density-Spiciness-Space and is optimised to the least possible density inversions.

The flight model in the Glider Toolbox is based on work by Merckelbach et al (2010) which outlined a way to determine the glider speed when acceleration is at a steady state. The Toolbox calculates the glider's speed whilst not in a steady state, simply by integrating the equations of motion. This is then applied to estimate the speed of the flow through the conductivity cell and results with a second optimisation for deriving the salinity. The two salinity optimisation methods are then compared and only the best one is kept.

The gliders use the Aanderaa 4330 oxygen optode to measure oxygen concentrations. A key issue with this type of optode is that it does suffer from lag issues, arising from the optode's response time to temperature, which is in the region of 20 seconds. To correct for this, oxygen concentrations are recalculated using the glider's CTD temperature. Further to this, another lag occurs from the optode's response time to changes in oxygen, which is approximately 25 seconds. Considering the glider moves at an average speed of $0.2ms^{-1}$, when travelling through large oxygen gradients (i.e. the oxycline) the ambient oxygen concentrations will have changed significantly before the optode has time to equilibrate. To correct for this, the methods employed by Bittig et al (2014) are employed.

Data is then vertically linearly interpolated onto a 1dbar resolution spatial grid.

Finally, the data is compared to nearby CTD casts, with the routines calculating an offset value. Applying this offset to the data and rerunning will deliver another offset. Repeating this

process will eventually result in no offsets, and the data is therefore sufficiently calibrated against the CTD data.

7.2 Quality control and data caveats

As the glider measures temperature and conductivity with a CTD, the same cautions apply as when using standard ship-based CTD platforms, particularly at the near surface (0-5m).

When the glider undergoes necessary satellite communication, there is a lag time for the CTD to re-equilibrate with the water temperature after influences from atmospheric conditions and incoming solar radiation. Bubbles occasionally become trapped in the conductivity cell and result in noise, particularly common in near surface data as there is increased likelihood of bubbles from wave and wind mixing, or during deployment or recovery when there is interference from ships. As a result, care should be taken when looking at the near surface values in temperature and conductivity, and all derived parameters.

Although the Toolbox mitigated the influence of thermal inertia and salinity spiking, some spiking still remained despite the optimal correction. This is an unavoidable and common consequence of glider CTD data, likely resulting from low frequency sampling. However, the problem is most apparent in periods of strong temperature gradients, such as summer. As the majority of the results in this thesis stem from the winter and winter-spring transition, any remaining thermal inertia is minimal (see Chapter 2.2.4).

Biofouling was a significant issue for late spring and summer glider deployments and resulted in many of the profiles being flagged by the Toolbox's routines as bad data and discarded. The remainder of the glider deployments, particularly during the winter and early spring, did not experience biofouling at a level that was detrimental to data retrieval.

The Glider Toolbox does not calibrate the optical properties measured by the Wet Labs triplet puck, such as chlorophyll-a fluorescence and optical backscatter. Upon analysis, it was decided that the chlorophyll fluorescence glider profiles were not sufficiently close to the chlorophyll-a fluorescence measured by ship-based CTD measurements, likely due to the highly patchy

nature of phytoplankton aggregations (e.g. Martin, 2003). In order to keep the chlorophyll-a fluorescence data consistent between gliders, the decision was made to leave all optical properties *uncalibrated*. Although the factory calibration has been applied to the chlorophyll-a fluorescence and optical backscatter, the units are arbitrary and merely serve to indicate relative changes in properties.

The salinity variations during the winter-spring transition are incredibly small. One of the main advantages of the glider is that the same sensors are used throughout, reducing the error of small salinity variations between different sensors. Comparison of the salinity to the potential density results in no prolonged unstable regimes, and so we are confident that the observed small-scale salinity changes are real.

7.3 References

Bittig, H.C., Fiedler, B., Scholz, R., Krahmann, G. and Körtzinger, A., 2014. Time response of oxygen optodes on profiling platforms and its dependence on flow speed and temperature. *Limnology and Oceanography: Methods*, *12*(8), pp.617-636.

Garau, B., Ruiz, S., Zhang, W.G., Pascual, A., Heslop, E., Kerfoot, J. and Tintoré, J., 2011. Thermal lag correction on Slocum CTD glider data. *Journal of Atmospheric and Oceanic Technology*, *28*(9), pp.1065-1071.

Lueck, R.G. and Picklo, J.J., 1990. Thermal inertia of conductivity cells: Observations with a Sea-Bird cell. *Journal of Atmospheric and Oceanic Technology*, *7*(5), pp.756-768.

Martin, A.P., 2003. Phytoplankton patchiness: the role of lateral stirring and mixing. *Progress in oceanography*, *57*(2), pp.125-174

Merckelbach, L., Smeed, D. and Griffiths, G., 2010. Vertical water velocities from underwater gliders. *Journal of Atmospheric and Oceanic Technology*, *27*(3), pp.547-563.

8. Appendix II

This supplementary material details the important parametrisations and caveats used in NEMO-ERSEM that are relevant to this thesis.

8.1 NEMO v3.6

NEMO is an open ocean model that incorporates ocean dynamics and thermodynamics (Madec et al 2015). Of particular interest for this thesis are boundary conditions used, in terms of air-sea and freshwater fluxes, summarised from Madec, 2015.

8.1.1 Surface heat fluxes

Two components make up the surface heat budget in NEMO v.3.6. The first is the outgoing / non-solar (Q_{ns}) part of the surface heat flux, which is the sum of the longwave, sensible and latent heat fluxes. This is applied as a surface boundary condition in the first level of the time-varying temperature (T) equation:

(8.1)
$$\frac{\partial T}{\partial t} \equiv \cdots + \left. \frac{Q_{ns}}{\rho_o \, C_p \, e_{3t}} \right|_{k=1}$$

Where ρ_o is the reference density, C_p is the specific heat capacity and e_3 is $\partial z/\partial k$, where z is the vertical coordinate, and k is the upward vector coordinate.

The second is the incoming / solar component (Q_{ns}) of the surface heat flux (i.e. the shortwave flux) and is applied as part of the temperature equation as follows:

(8.2)
$$\frac{\partial T}{\partial t} \equiv \cdots + \frac{Q_{sr}}{\rho_o C_p \, e_{3t}} \delta_k \left[I_w \right]$$

I_w is a non-dimensional function that describes how light penetrates the water column. It is assumed that the fraction of non-penetrative radiation within Q_{sr} is specified at 58%, which is absorbed by the ocean in the first few centimetres. The remaining 42% is assumed to penetrate the water column under a red-blue-green (RBG) regime (Legaigne et al, 2007), where light is split into separate wavelengths. For each band, the chlorophyll-dependent attenuation is fitted to coefficients derived from a model containing 61 wavebands (Morel, 1988; Morel and Maritorena, 2011). Normally, this full-spectral model would be too computationally expensive, yet by incorporating the more efficient RBG regime, light penetration profiles are close approximations.

This light penetration scheme feeds into the time-varying temperature equation. Where the ocean depth is less than 200m, such as on the shelf, it is not impossible for the light profile to reach the seabed. In this scenario, the remaining heat is absorbed in the last level.

8.1.2 Precipitation vs. evaporation

The surface freshwater budget (precipitation – evaporation; kg m^{-2} s^{-1}) both change the volume of the ocean (i.e. volume fluxes in the sea surface height parameterisations) and the surface concentration of salt (i.e. time-varying salinity evolution). Despite that precipitation often has a different temperature to the sea surface temperature (SST), precipitation in the model does not have a temperature associated with it and therefore has no direct effect on the SST. Instead, precipitation acts as a volume flux, and thus any addition of freshwater through precipitation changes the volume of the ocean and subsequently changes the ocean heat content. While this does provide a heat flux, this is likely to be small.

Only precipitation and evaporation modify the ocean volume, and not freshwater addition from freezing/melting. Also note that the salinity of both precipitation and evaporation is assumed to be zero (0).

8.2 AMM7 Domain and Configuration

Below is a summary of key model configurations applicable to results in this thesis, summarised from O'Dea et al (2012) and O'Dea et al (2017):

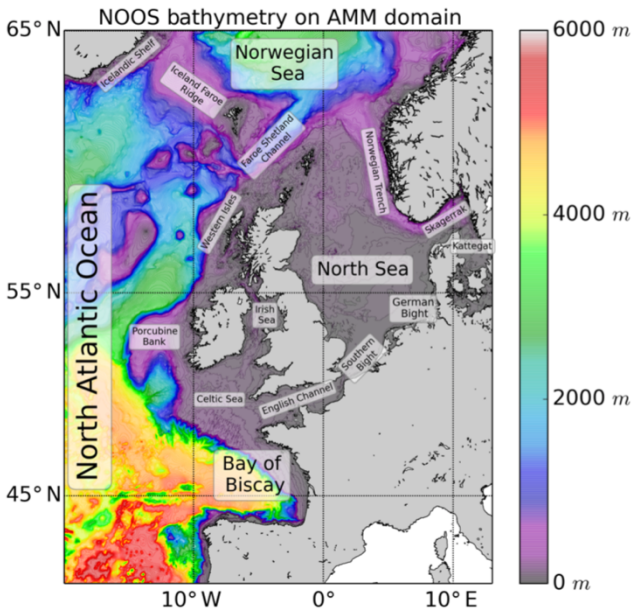

Fig. 8.1: Bathymetry (NOOS) from the AMM7 Model Domain. Taken from O'Dea et al (2017)

The model domain of AMM7 covers the entirety of the Northwest European Shelf and the Eastern Atlantic (20°W, 40°N to 13°E, 65°N). The model resolution varies from 9.4km to 5.2km, resulting in a mean resolution of 7.4km at 52.5°N (Fig. 8.1). It is important to note that this resolution is unable to capture the internal Rossby Radius (4km; Holt and Proctor, 2008), yet this is a justifiable compromise when considering the large computer resources needed to fully resolve it in the 34-year hindcast simulations.

Bathymetry is a combination of GEBCO 1 arcmin data and local data sourced from other partners of the Northwest European Shelf Operational Oceanographic System (NOOS). Following the vertical stretching routines of Siddorn and Furner (2013), there are 51 vertical levels (except in regions of steep topography). Crucially, vertical levels are uniform near the surface across the whole model domain, allowing for more consistent ocean-air exchanges.

Riverine data is sourced from the HYdrological Predictions for the Environment (HYPE) model (Lindström et al, 2010; Donnelly et al, 2015).

Meteorological and atmospheric forcing data is sourced from ERA-Interim (Dee et al, 2011), and is used in the 34-year hindcast model runs.

Although the modelled time period used in this thesis was from 1982 to 2015, the model is first spun up in 1981. Initial conditions and boundary forcing are from the 1/4° ORCA025 hindcast of GO5.0 (Megann et al, 2014). More details of GO5.0's initialisation can be found in Ingleby and Huddleson (2007).

A full review of the sensitivity tests and validations with observations and previous models (e.g. POLCOMS) can be found in O'Dea et al (2017).

8.3 ERSEM

Configurations for the ERSEM (Baretta et al, 1995; Baretta 1997) are discussed in Butenschön et al (2016), summarised below:

Organisms in the model are characterised by primary producers, consumers, bacterial decomposers in the pelagic system along with consumers and bacterial decomposers in the benthos. These are further subdivided into different groups and size-classes, in order to better represent the plasticity of the system.

Dissolved and particulate organic matter is included for both the pelagic and benthos components. For aspects of the model associated with this thesis, ERSEM uses a fully dynamic stoichiometry. Each organism in the model uptakes nutrients, assimilates carbon, and has generic loss term that include respiration, excretion, predation and mortality (e.g. lysis), as seen in Fig 8.2. ERSEM does not model specific cell physiology, and thus distributions of biomass and organic/inorganic constituents serve as smoothed approximations. In order to close the budget, ERSEM calculates the air-sea gas transfer rates of carbon and oxygen and benthic fluxes. More information of how to close the budgets, as well as the advection-diffusion terms, are described in Butenschön et al (2012)

Metabolic processes are temperature dependent, as are air-sea fluxes which also depend on the wind speed at the sea surface. A buffer, based on a carbon concentration of 0.01 mg m^{-3} , is used that is not accessible to biogeochemical loss terms. While it is applied to reduce negative

concentrations or numerical noise, it also acts to mimic the overwintering strategies observed in nature (Fennel 1995).

Chlorophyll-a is derived from the assimilation of carbon and decomposition of organic compounds. Phytoplankton gain and loss processes are modelled for each phytoplankton functional group (Varela et al 1995), which include diatoms, microphytoplankton (>20µm), nanophytoplankton (2-20µm) and picophytoplankton (<2µm). Photosynthesis is based on the balance of carbon assimilation, excretion and respiration (Baretta-Bekker et al, 1997) and the light model described by Jassby and Platt (1976), Platt et al (1982) and Geider et al (1997). It is assumed to be independent of nutrient limitation from nitrogen and phosphorous (e.g.

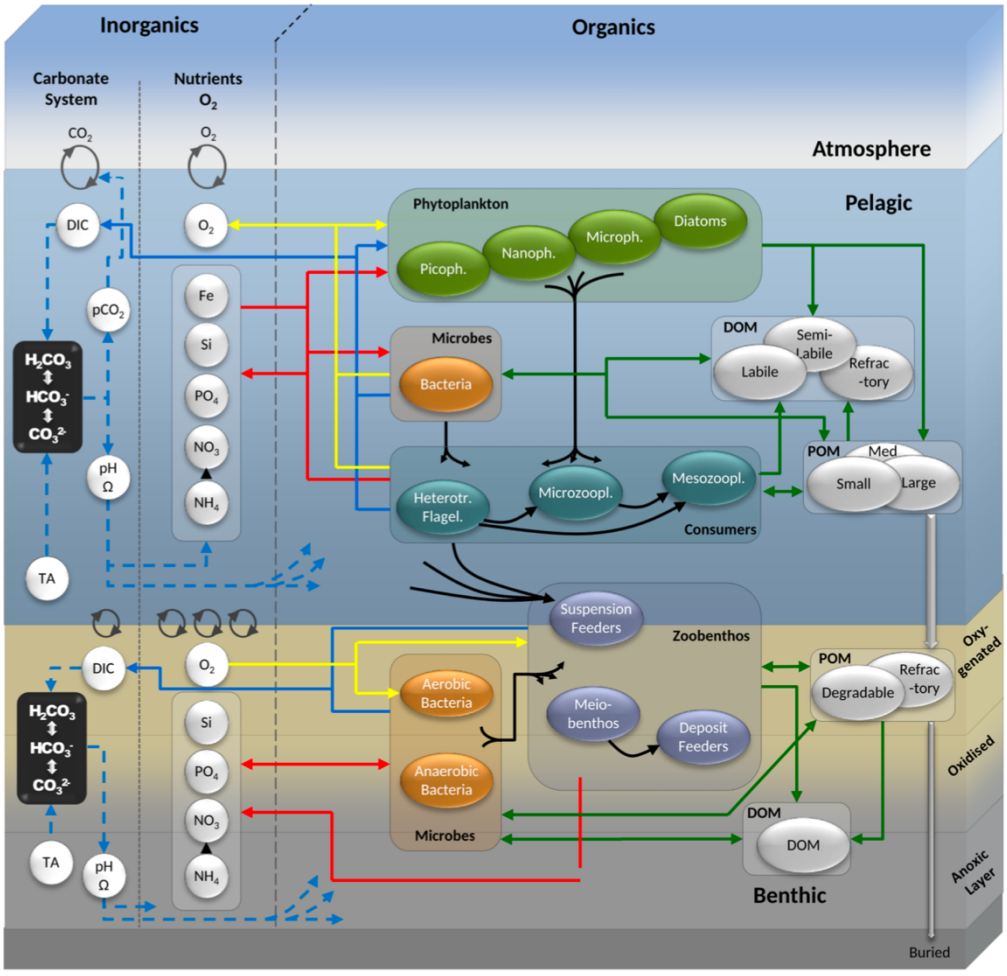

Fig. 8.2: Schematic taken from Butenschön et al (2016) detailing the interaction of pelagic and benthic components within the model. As per Butenschön et al (2016), the colours of the connectors are as follows: blue) inorganic carbon fluxes; red) nutrient fluxes; black) predator-prey relations; yellow) flow of oxygen ; and green) fluxes of non-living organisms

Falkowski and Raven, 2007). The photosynthesis term also incorporates photoinhibition, as described by Blackford et al (2004). Nutrient demands are specific to each phytoplankton group and dependant on external availability, with nitrate utilised exclusively by phytoplankton functional groups and regenerated by nitrification. In the absence of nitrifiers, nitrification is modelled based on temperature, oxygen and available ammonium. Phosphorous dynamics are similar to nitrogen dynamics, with the exception that only a single chemical species is considered. Phytoplankton themselves are in direct competition with bacteria if they are exposed to nitrogen or phosphorous deprivation, but if substrates are sufficiently good quality, bacteria release surplus nutrients into the environment.

For simplicity, the silicate is converted directly into detritus, and is not remineralised in the pelagic system. This is justified by observations that show that the majority of remineralisation is confined to the seabed, due to high sinking velocities (Broecker and Peng, 1982; Dugdale et al., 1995). Silicate uptake is exclusively by diatoms.

Pelagic predators (zooplankton) are split into three functional groups: mesozooplankton, microzooplankton and heterotrophic flagellates. They feed on phytoplankton according to size, including cannibalism. Predators display a form of grazing selection in the sense that patches of prey below a certain size are less likely to be grazed.

Vertical light attenuation through the water column is based on the Beer-Lambert formulation. Values for Kd_{PAR}, that takes into account both the living and non-living parts of the optically-active constituents in the water column, is based on a model used by Blackford et al (2004).

A key caveat in this model is the representation of phytoplankton groups according to size and/or their reliance on silica (e.g. diatoms). Butenschön et al (2016) highlights diatoms in particular, given the range of physiological and morphological diversity that is constrained within a single group. With a phytoplankton community, different species of diatoms can have varying photosynthetic quotas, and could thus potentially under- and/or overestimate key biogeochemical processes, such as carbon fixation and nutrient assimilation. However, Butenschön et al (2016) argues that phytoplankton size group is considered to be a representation of the community as a whole, with size being a crucial physiological trait

(Litchman et al., 2007, Lichtman et al 2010), impacting nutrient assimilation and affinity, predator-prey dynamics and photosynthetic rates (e.g. Finkel et al., 2010).

More information about ERSEM's configurations, including a full mathematical description of the pelagic and benthic components, can be found in Butenschön et al (2016). Validations for the ERSEM components of the AMM7 NEMO configuration can be found in Edwards et al (2012).

8.4. References

Baretta-Bekker, J.G., Baretta, J.W. and Ebenhöh, W., 1997. Microbial dynamics in the marine ecosystem model ERSEM II with decoupled carbon assimilation and nutrient uptake. *Journal of Sea Research*, *38*(3-4), pp.195-211.
Baretta, J. W., 1997, Preface, Journal of Sea Research, 38, 169–171, doi:10.1016/S1385-1101(97)00054-3

Baretta, J.W., Ebenhöh, W. and Ruardij, P., 1995. The European regional seas ecosystem model, a complex marine ecosystem model. *Netherlands Journal of Sea Research*, *33*(3-4), pp.233-246.

Blackford, J.C., Allen, J.I. and Gilbert, F.J., 2004. Ecosystem dynamics at six contrasting sites: a generic modelling study. *Journal of Marine Systems*, *52*(1-4), pp.191-215.

Broeker, W. and Peng, T., 1982. Tracers in the Sea, *Lamont-Doherty Geological Observatory, Columbia Univeristy, New York*.

Butenschön, M., Clark, J., Aldridge, J.N., Allen, J.I., Artioli, Y., Blackford, J., Bruggeman, J., Cazenave, P., Ciavatta, S., Kay, S. and Lessin, G., 2016. ERSEM 15.06: a generic model for marine biogeochemistry and the ecosystem dynamics of the lower trophic levels. *Geoscientific Model Development*, *9*(4), pp.1293-1339

Dee, D.P., Uppala, S.M., Simmons, A.J., Berrisford, P., Poli, P., Kobayashi, S., Andrae, U., Balmaseda, M.A., Balsamo, G., Bauer, D.P. and Bechtold, P., 2011. The ERA-Interim reanalysis: Configuration and performance of the data assimilation system. *Quarterly Journal of the royal meteorological society*, *137*(656), pp.553-597.

Donnelly, C., Andersson, J.C. and Arheimer, B., 2016. Using flow signatures and catchment similarities to evaluate the E-HYPE multi-basin model across Europe. *Hydrological Sciences Journal*, *61*(2), pp.255-273.

Dugdale, R.C., Wilkerson, F.P. and Minas, H.J., 1995. The role of a silicate pump in driving new production. *Deep Sea Research Part I: Oceanographic Research Papers*, *42*(5), pp.697-719.

Edwards, K. P., R. Barciela, and M. Butenschon (2012), Validation of the NEMO-ERSEM operational ecosystem model for the North West European Continental Shelf, Ocean Sci., 8(6), 983-1000.

Falkowski, P.G. and Raven, J.A., 2013. *Aquatic photosynthesis*. Princeton University Press.

Fennel, W., 1995. A model of the yearly cycle of nutrients and plankton in the Baltic Sea. *Journal of marine systems*, *6*(4), pp.313-329.

Finkel, Z.V., Beardall, J., Flynn, K.J., Quigg, A., Rees, T.A.V. and Raven, J.A., 2009. Phytoplankton in a changing world: cell size and elemental stoichiometry. *Journal of plankton research*, *32*(1), pp.119-137

Geider, R.J., MacIntyre, H.L. and Kana, T.M., 1997. Dynamic model of phytoplankton growth and acclimation: responses of the balanced growth rate and the chlorophyll a: carbon ratio to light, nutrient-limitation and temperature. *Marine Ecology Progress Series*, *148*, pp.187-200.

Holt, J. and Proctor, R., 2008. The seasonal circulation and volume transport on the northwest European continental shelf: A fine-resolution model study. *Journal of Geophysical Research: Oceans*, *113*(C6).

Ingleby, B. and Huddleston, M., 2007. Quality control of ocean temperature and salinity profiles—Historical and real-time data. *Journal of Marine Systems*, *65*(1-4), pp.158-175

Jassby, A.D. and Platt, T., 1976. Mathematical formulation of the relationship between photosynthesis and light for phytoplankton. *Limnology and oceanography*, *21*(4), pp.540-547.

Lengaigne, M., Menkes, C., Aumont, O., Gorgues, T., Bopp, L., André, J.M. and Madec, G., 2007. Influence of the oceanic biology on the tropical Pacific climate in a coupled general circulation model. *Climate Dynamics*, *28*(5), pp.503-516.

Lindström, G., Pers, C., Rosberg, J., Strömqvist, J. and Arheimer, B., 2010. Development and testing of the HYPE (Hydrological Predictions for the Environment) water quality model for different spatial scales. *Hydrology research*, *41*(3-4), pp.295-319.

Litchman, E., de Tezanos Pinto, P., Klausmeier, C.A., Thomas, M.K. and Yoshiyama, K., 2010. Linking traits to species diversity and community structure in phytoplankton. In *Fifty years after the "Homage to Santa Rosalia": Old and new paradigms on biodiversity in aquatic ecosystems* (pp. 15-28). Springer, Dordrecht.

Litchman, E., Klausmeier, C.A., Schofield, O.M. and Falkowski, P.G., 2007. The role of functional traits and trade-offs in structuring phytoplankton communities: scaling from cellular to ecosystem level. *Ecology letters*, *10*(12), pp.1170-1181.

Madec, G., 2015. NEMO ocean engine.

Megann, A.P., Storkey, D., Aksenov, Y., Alderson, S., Calvert, D., Graham, T., Hyder, P., Siddorn, J. and Sinha, B., 2014. GO 5.0: The joint NERC-Met Office NEMO global ocean model for use in coupled and forced applications. *Geotechnical Model Development*, *7*(3), pp.1069-1092

Morel, A. and Maritorena, S., 2001. Bio-optical properties of oceanic waters: A reappraisal. *Journal of Geophysical Research: Oceans*, *106*(C4), pp.7163-7180.

Morel, A., 1988. Optical modeling of the upper ocean in relation to its biogenous matter content (case I waters). *Journal of geophysical research: oceans*, *93*(C9), pp.10749-10768.

O'Dea, E., Furner, R., Wakelin, S., Siddorn, J., While, J., Sykes, P., King, R., Holt, J. and Hewitt, H., 2017. The CO5 configuration of the 7 km Atlantic Margin Model: large-scale biases and sensitivity to forcing, physics options and vertical resolution. *Geoscientific Model Development*, *10*(8), p.2947.

O'Dea, E.J., Arnold, A.K., Edwards, K.P., Furner, R., Hyder, P., Martin, M.J., Siddorn, J.R., Storkey, D., While, J., Holt, J.T. and Liu, H., 2012. An operational ocean forecast system incorporating NEMO and SST data assimilation for the tidally driven European North-West shelf. *Journal of Operational Oceanography*, *5*(1), pp.3-17.

Platt, T., Harrison, W.G., Irwin, B., Horne, E.P. and Gallegos, C.L., 1982. Photosynthesis and photoadaptation of marine phytoplankton in the Arctic. *Deep Sea Research Part A. Oceanographic Research Papers*, *29*(10), pp.1159-1170.

Siddorn, J.R. and Furner, R., 2013. An analytical stretching function that combines the best attributes of geopotential and terrain-following vertical coordinates. *Ocean Modelling*, *66*, pp.1-13.

Varela, R.A., Cruzado, A. and Gabaldón, J.E., 1995. Modelling primary production in the North Sea using the European regional seas ecosystem model. *Netherlands Journal of Sea Research*, *33*(3-4), pp.337-361.

9. Appendix III: Assessing the nutrient behaviour in NEMO-ERSEM

This is initial work to quantify the changes in cross-shelf flux between contrasting climatological modes. Although the results remained inconclusive, they have been included as Appendix III for completeness

In temperate continental shelf seas, such as the Northwest (NW) European shelf, phytoplankton growth is controlled by the availability of light and nutrients. The winter period is characterised by a homogenised water column where phytoplankton are mixed entirely to depth, resulting in a low light environment that inhibits growth. A different regime occurs following the onset of seasonal stratification, as phytoplankton become primarily nutrient limited, with concentrations of nitrate (N), silicate (Si) and phosphate (P) directly impacting the rate of primary productivity and seasonal succession. Previous work in this thesis has highlighted that winter phytoplankton growth is modulated by changes in the Atlantic Multidecadal Oscillation (AMO), as changes in storm activity promote more favourable light environments through the formation of ephemeral stratification events. Yet, the influence of this climatic control on nutrient availability remains uncertain. Using a coupled hydrodynamic-biogeochemical model, we show evidence to suggest an increase in winter nutrient concentrations between negative and positive AMO phases. Winter windspeeds display a subtle decrease of 0.5 ± 0.7 ms^{-1} from negative to positive AMO phases, whereas summer wind speeds display a 0.3 ± 0.3 ms^{-1} increase over the same time period (with a $\pm 90\%$ confidence interval). This supports our hypothesis of an enhanced cross-shelf flux during positive AMO phases. However, a full quantitative assessment of the cross-shelf nutrient transport is currently beyond the scope of this work. Nevertheless, we speculate on the likely implications of an enhanced cross-shelf nutrient flux for primary productivity on the NW European shelf.

9.1. Introduction

Phytoplankton primary production in continental shelf seas contributes to 15-30% of total oceanic primary productivity (Hickman et al, 2012), forming the base of marine food webs and supporting 90% of the global fisheries (Pauly et al, 2002). Phytoplankton growth is limited by light and nutrients, where the relative importance of each changes throughout the seasonal cycle. During the mid and high latitude winter, light is the foremost limiting factor, with phytoplankton growth within a mixed layer only occurring once cells remain in the euphotic

zone for prolonged periods (Sverdrup, 1953; Townsend et al, 1992; Taylor and Ferrari, 2011). Meteorological controls, such as cloudiness (Hickman et al, 2012), elevated wind stress (Townsend et al, 1994; Sharples et al, 2006; Waniek, 2003), spring-neap tidal modulation (Sharples, 2007), and vertical stability from both rainfall (see Chapter 4 and 5) and riverine runoff (Labry et al, 2001; Gohin et al, 2015), can directly modulate the amount of light available to support winter phytoplankton growth.

Once light conditions are favourable, the spring bloom is initiated, which is a large-scale biological event that acts to resupply the marine ecosystem with organic matter (Sharples, 2007). During the spring bloom, the primary limiting factor for phytoplankton growth changes from light to nutrient availability. In particular, the relative stocks of key macronutrients (e.g. nitrate, N; phosphate, P; and silicate, Si) have a first order control on the spring bloom succession (Holligan, 1984; Kivi et al, 1993), as different phytoplankton cells have unique nutrient requirements for growth. One example are diatoms, as they utilise silicate for the formation of their frustules (e.g. Bernard et al, 2011).

The proportion of allochthonous (new) vs autochthonous (regenerated) forms of nitrogen (Dugdale and Goering, 1967) is also important for seasonal phytoplankton succession. The fraction of primary production from nitrate, as opposed to other nitrogen compounds such as ammonium, is known as the f-ratio (Eppley and Peterson, 1979; Eppley, 1981; Harrison et al, 1987), which changes across the spring bloom period (Rees et al, 1999). High f-ratios are associated with larger cells, such as diatoms, and dominate at the beginning of the spring bloom when new nutrients are replete (Rees et al, 1999; Needham and Fuhrman, 2016; Gilbert et al, 2016). These phytoplankton populations are then outcompeted and replaced by low f-ratio species such as dinoflagellates (Holligan, 1984; Sellner et al, 2001; Hickman et al, 2009; Gilbert, 2016; McQuatters-Gollop et al, 2007). As such, the proportion of nutrients and its origin (i.e. new vs regenerated) can directly influence seasonal phytoplankton growth and composition.

Through a combination of observational and model work, previous chapters (4 and 5) in this thesis have demonstrated that ephemeral stratification events throughout the winter period can promote phytoplankton growth, through the temporary formation of favourable light environments. Chapter 5 demonstrated that changes in meteorological (i.e. storm) variability in contrasting climatological phases resulted in increased phytoplankton growth from 1998 to 2015, consistent with the transition from a negative to positive phase of the Atlantic

Multidecadal Oscillation (AMO). However, the influence of this climatic variability on nutrient stocks, and thus phytoplankton succession and variability, remains uncertain. Using coupled hydrodynamic-biogeochemical modelling results from the AMM7 configuration of the coupled NEMO-ERSEM model, this Chapter aims to quantify the changes in nutrients across contrasting climatological regimes.

9.2. Methods and Model Validation

9.2.1. Study area

Modelled nutrient data (N, P, Si) was analysed from a virtual mooring in the Celtic Sea. Located on the western approaches of the Northwest (NW) European Shelf, the Celtic Sea is directly influenced by extratropical cyclones translating across the North Atlantic. The influence of riverine runoff in the open shelf region is likely to be low, as riverine outflow is constrained to the coastal currents (Fernand et al, 2006; Brown et al, 2003). Model output was set at 49.0005°N, -9.0001°E (Fig. 9.1), which is 78 km from the shelf break, and was consistent with the location of the observed onset of rain-induced stratification described in Chapter 3. Chapter 5, which focussed on the interannual winter phytoplankton variability as a result of these storm systems, also used this virtual mooring location.

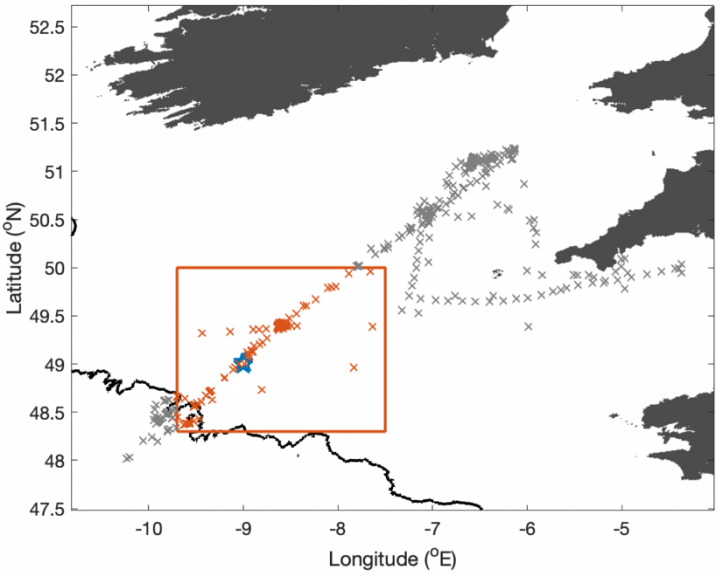

Fig. 9.1: Locations of all the Niskin samples collected as part of the Shelf Sea Biogeochemistry project in the Celtic Sea (grey crosses). The red crosses, identified by the red box, are the samples used to compare against the modelled virtual mooring (identified by the blue star). The shelf break is identified by the 200m black isobath (GEBCO, 2014).

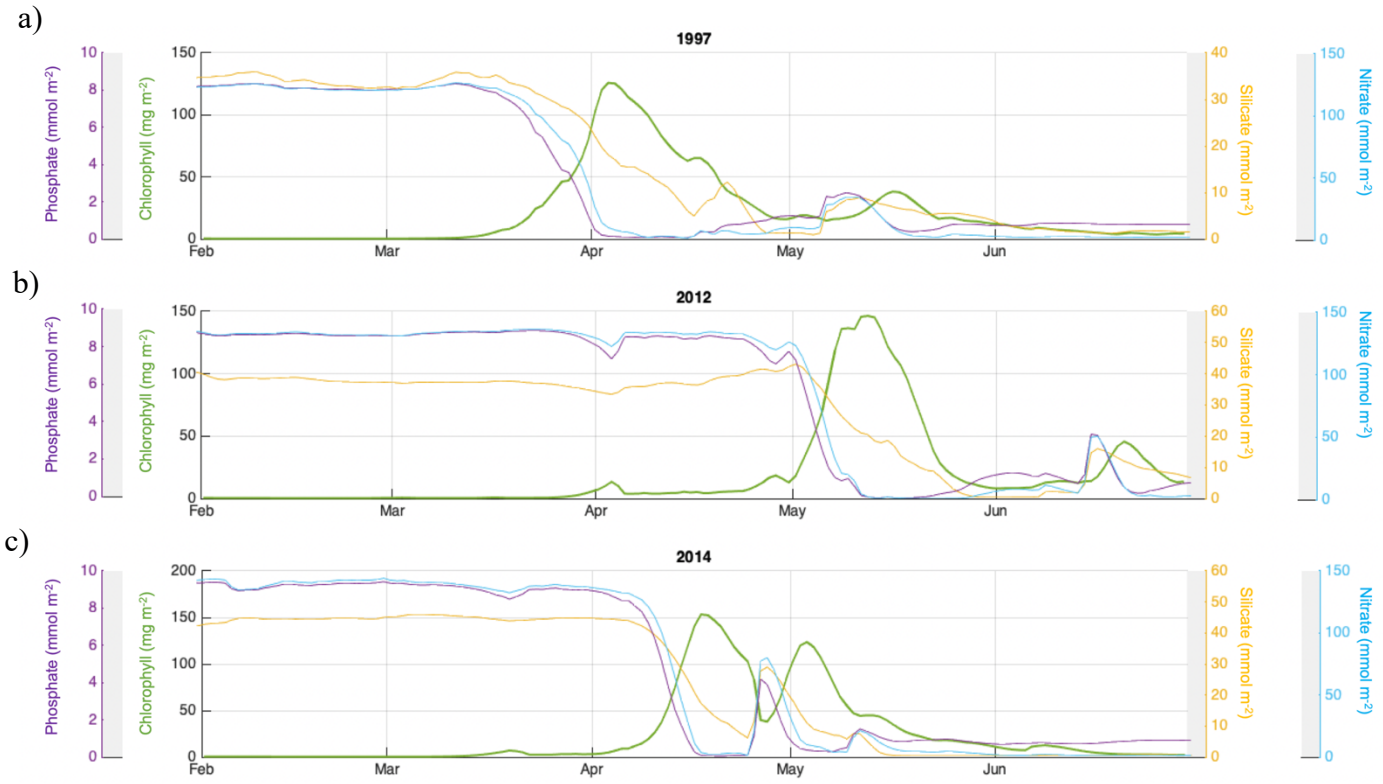

Fig 9.2: Depth-integrated concentrations, from the surface to 20m depth, of nitrate (blue), silicate (orange) and phosphate (purple) compared to depth-integrated total chlorophyll concentrations (green) from February to June for a) an early stratification event, 1997; b) a late stratification event, 2012; and c) a stormy spring bloom period, 2014

Modelled nutrients were validated against data collected from the Shelf Sea Biogeochemistry Project. Process cruises collected samples throughout 2014 and 2015, which were analysed for nitrate, silicate and phosphate concentrations (data available via the British Oceanographic Data Centre). To reduce any spatial variability when comparing the model and observational data, only samples taken shallower than 160m depth and within a bespoke 2° box (-9.7 °E to -7.5 °E, 48.3 °N to 50 °N) were compared to the model virtual mooring (Fig. 9.1).

9.2.2. Interannual variability of nutrients

The expected behaviour of nutrients with respect to phytoplankton growth and uptake is well simulated in the model (Fig 9.2). Surface (0-20m) nutrients are depleted with increasing chlorophyll concentrations across both early (e.g. 1997, Fig 9.2a) and late (e.g. 2012, Fig 9.2b) stratification onset dates. Winter nutrients are replete with little variability, however nutrient drawdown is still seen during prebloom periods of phytoplankton growth, such as the prebloom event in 2012 (Fig 9.2b). From the 25th March to the 3rd April 2012, total surface

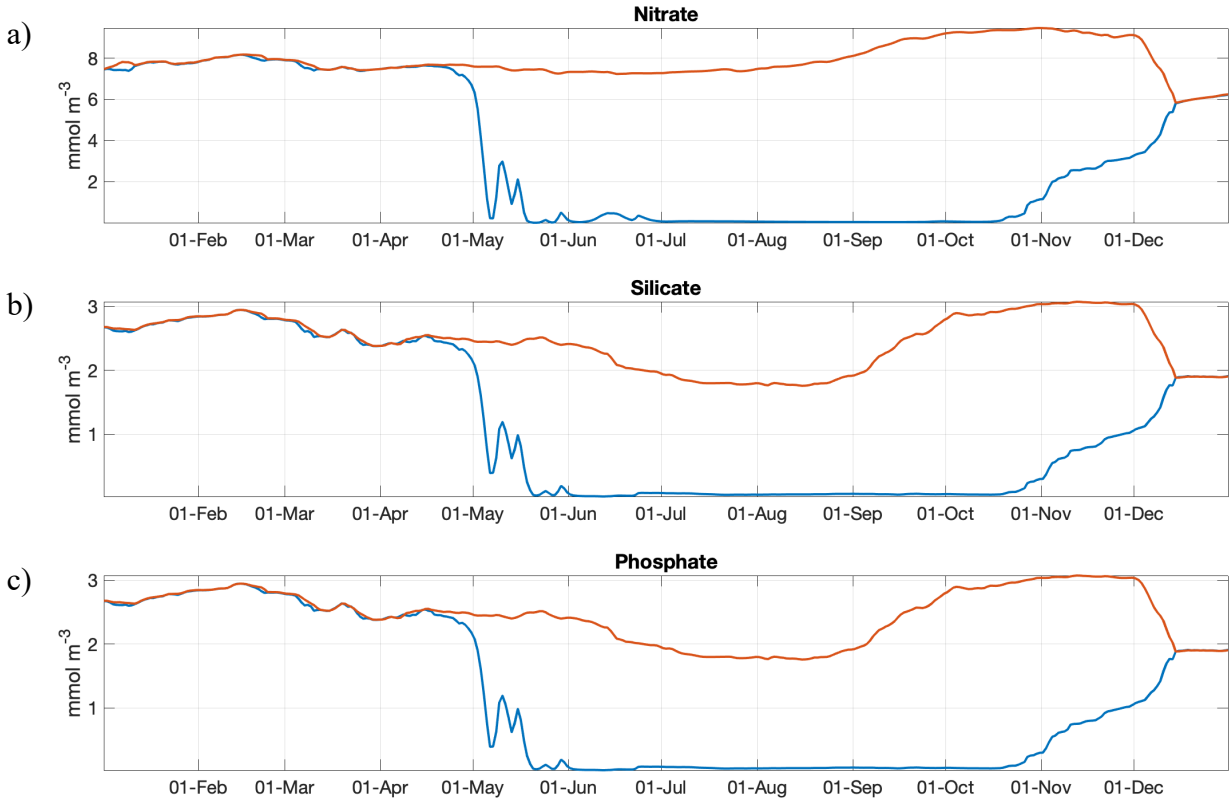

Fig 9.3: Average surface (blue, 0-10m) and bottom (red, 95-150m) concentrations for a) nitrate; b) silicate and c) phosphate, from January to December 2015

nitrate concentrations decreased from 135.6 mmol m^{-2} to 121.9 mmol m^{-2}, and total surface phosphate concentrations from 8.9 mmol m^{-2} to 7.6 mmol m^{-2}. Meteorological controls on modelled nutrient pulses are also well represented, demonstrated as a rapid increase in nitrate concentrations from 4.8 mmol m^{-2} to 49.9 mmol m^{-2} on the 14th June 2012, and 1.2 mmol m^{-2} to 80.1 mmol m^{-2} on the 24th April 2014. These pulses of nutrients, which occurred due to the passing of storms (Williams et al, 2013; Davis et al, 2014), promoted phytoplankton growth that resulted in secondary peaks of chlorophyll, similar to observed double pulses in surface productivity following spring tidal mixing (Sharples et al, 2006). While the surface nutrients are depleted, nutrients at depth displayed a gradual increase from September, due to enhanced remineralisation at depth (Fig. 9.3). For example, averaged bottom mixed layer nitrate concentrations in 2015 ranged from 7.7 mmol m^{-3} on the 15th April 2015, to 9.5 mmol m^{-3} on the 1st November 2015 (Fig. 9.3a). Both bottom and surface nitrate concentrations returned to 5.8 mmol m^{-3} following autumnal water column homogenisation on the 14th December 2015.

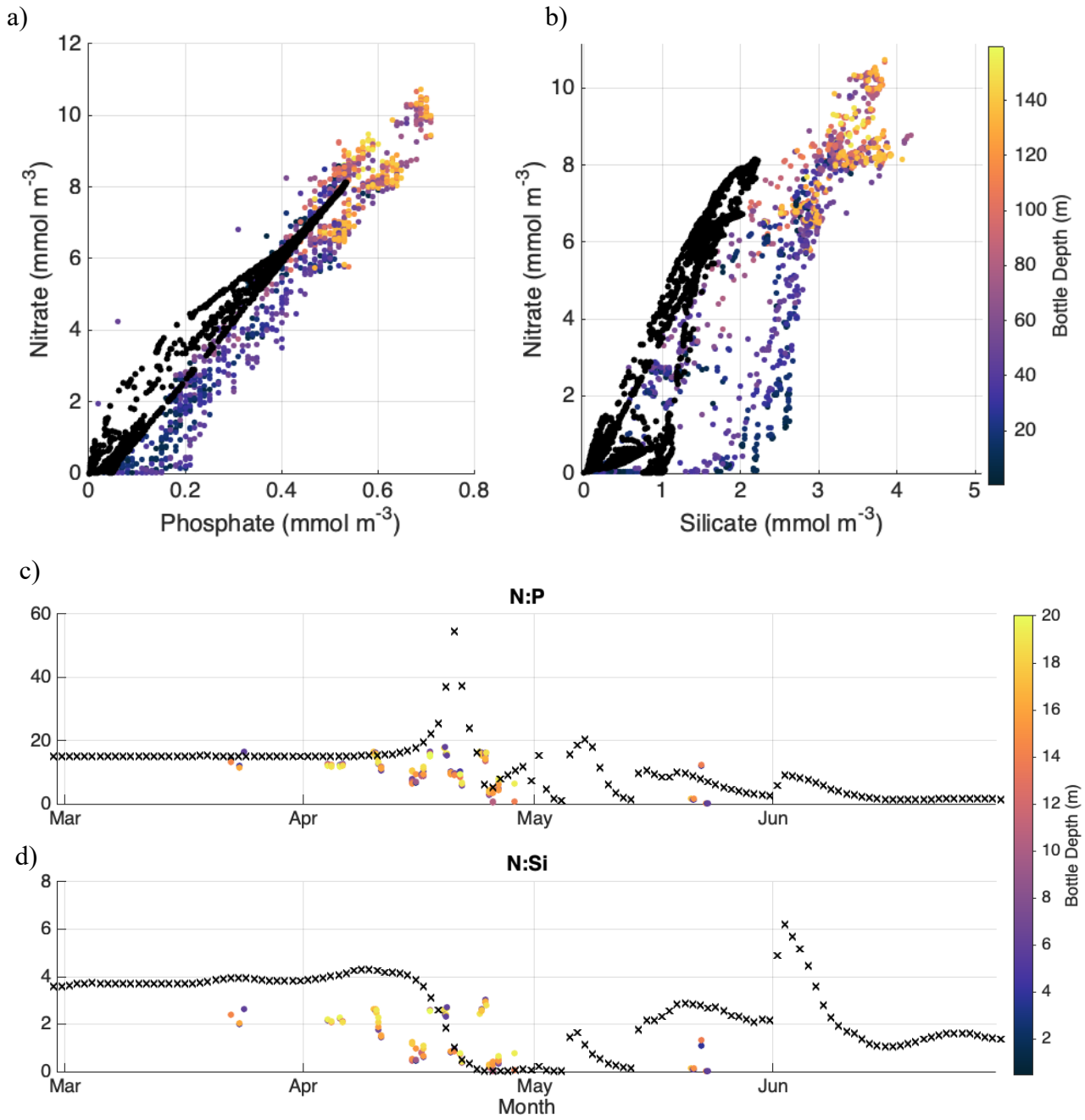

Fig. 9.4: Comparisons of modelled (black) to observed (coloured by bottle depth) nutrient concentrations. Direct comparisons between nitrate to a) phosphate and b) silicate are made using observations collected by the Shelf Sea Biogeochemistry Programme to 160m depth. The time-varying ratios of nitrate to c) phosphate and d) silicate are averaged from the surface to 20m depth.

9.2.3. Assessment of the stoichiometry

Comparisons with observational data suggested the model only partly represents the observed stoichiometry during the spring bloom initiation, with both N:P and N:Si being consistently

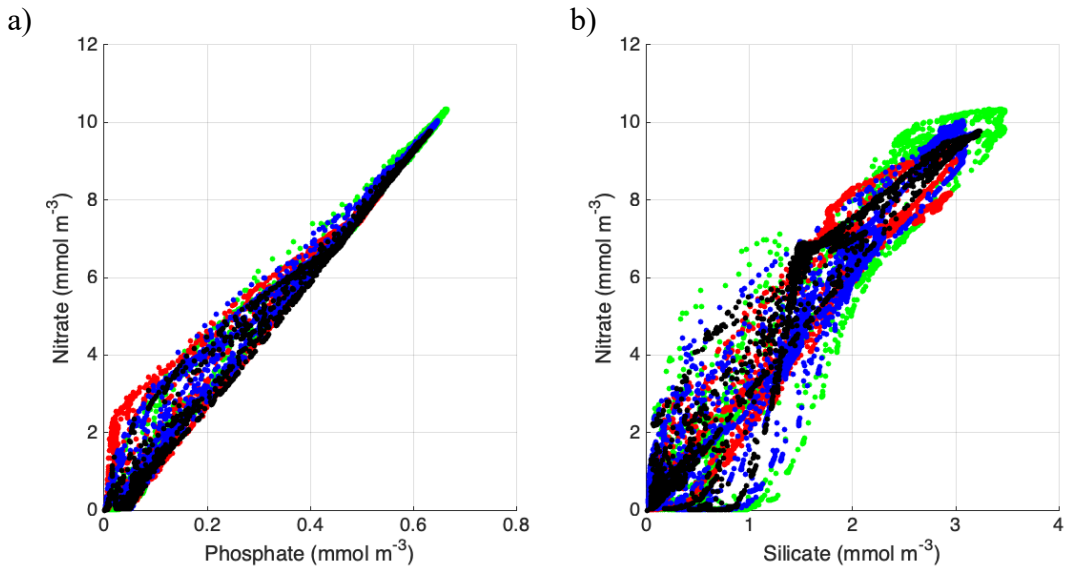

Fig. 9.5: Comparisons of the modelled nitrate concentrations to a) modelled phosphate and b) modelled silicate in 2012 (green), 2013 (red), 2014 (blue) and 2015 (black).

overestimated in 2015 (Fig. 9.4). At lower concentrations, modelled N:P ratios exceeded 33:1, which is over double the Redfield Ratio of 16:1 (Redfield et al, 1963) and indicates an excess in nitrate that is not captured in observations. Similar ratio analyses from 2012 to 2015 confirmed that this stochiometric irregularity was a consistent anomaly between years (Fig. 9.5). A similarly high stoichiometry of 4:1 is observed in the modelled N:Si ratios, and the variability seen in observations is also not captured in the model. This is likely due to the representation of a single diatom functional group within the model, insofar that natural variability in nutrient uptakes is not fully captured.

However, the time-varying N:P ratios across the winter period were consistent with nutrient samples taken from process cruises (Fig 9.4). Stoichiometry for modelled N:Si across March and April 2015 are nearly double (1.8) those of observations, implying an excess in Si uptake to N. However, both stoichiometry assessments remained relatively consistent throughout the winter until the spring bloom was initiated, suggesting that the winter nutrient stocks observed in the model are consistent with what is observed in reality.

9.3 Variability in winter nutrient concentrations

Total water-column nutrient concentrations were integrated over the January-February winter period from 1982 to 2015. This time frame was specifically chosen because the water column during this timeframe was consistently homogenised, and not influenced by late stratification

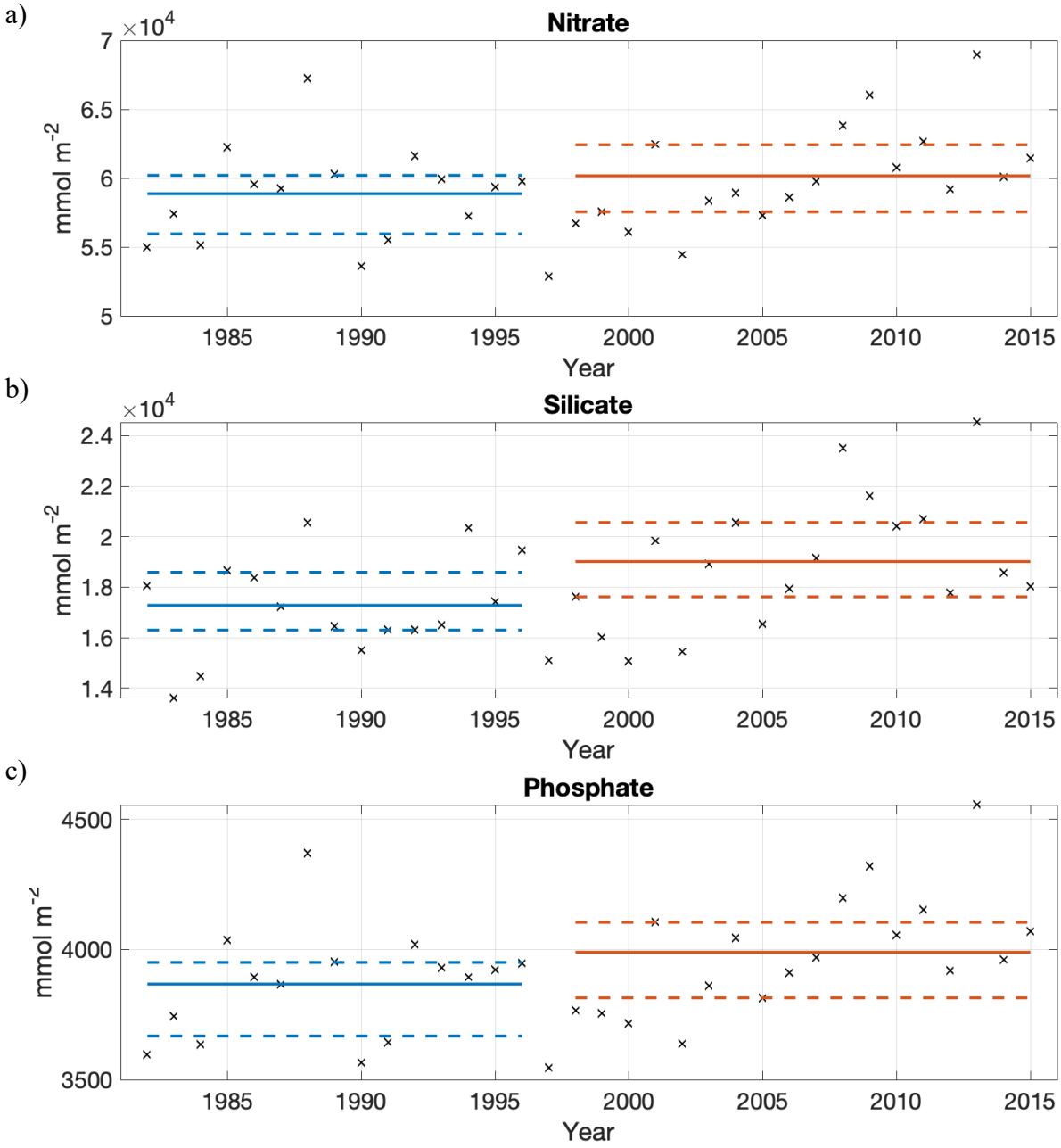

Fig. 9.6: Total depth-integrated a) nitrate, b) silicate and c) phosphate, from the model, for the January – February period from 1982 to 2015 (black crosses). The mean (solid) and the 25th and 75th percentiles (dashed lines) are also present for the negative (blue) and positive (red) AMO period

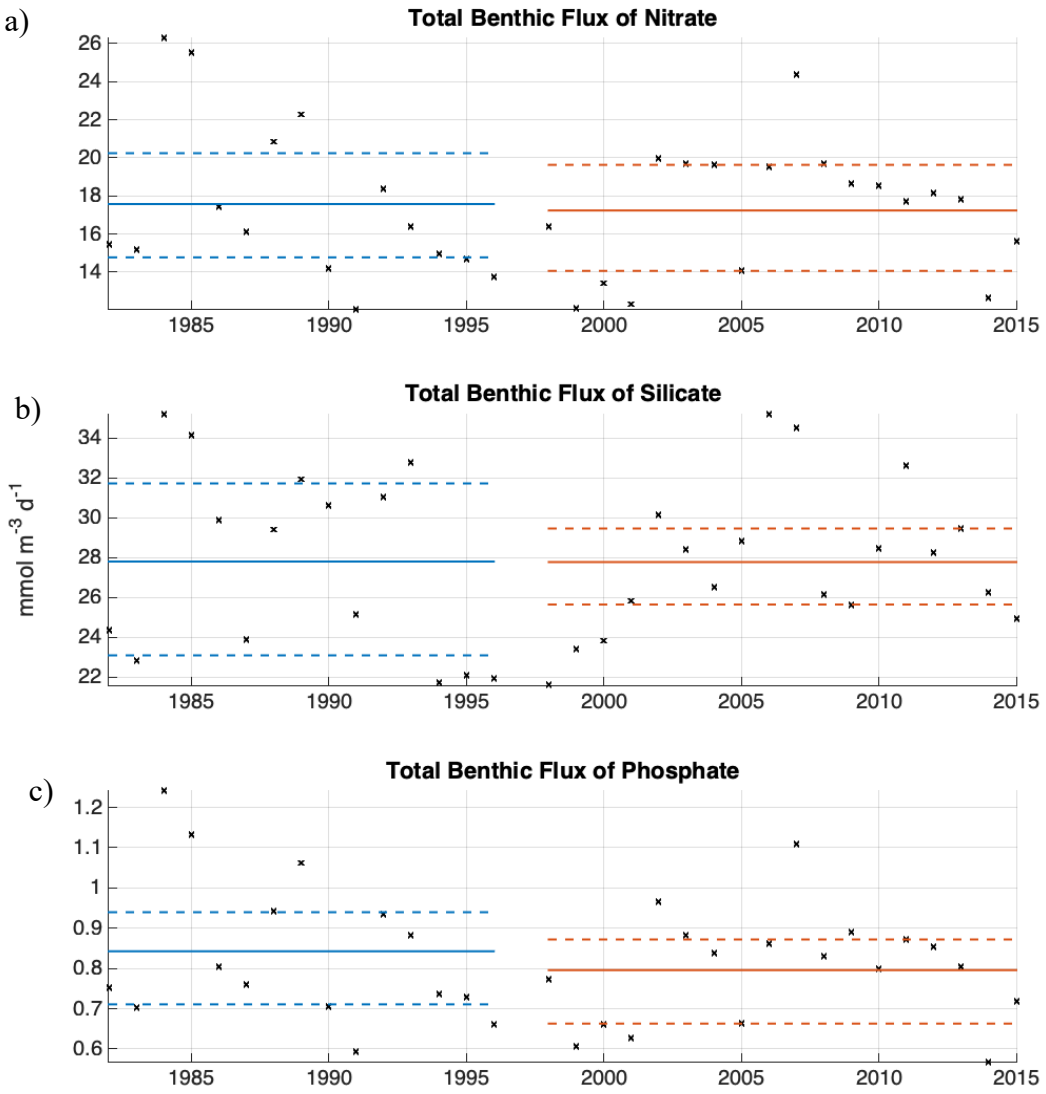

Fig. 9.7: Total benthic flux of a) nitrate, b) silicate and c) phosphate from the sediments for the January – February period, from 1982 to 2015 (black crosses). The mean (solid) and the 25th and 75th percentiles (dashed lines) are also present for the negative (blue) and positive (red) AMO period

breakdown in December, or early stratification events occurring in March. Results show a subtle increase in nitrate, silicate and phosphate in positive AMO phases as opposed to negative AMO phases (Fig 9.6). It is important to note that the relatively few datapoints in each phase (15 in negative phases and 17 in positive phases), combined with large variability of datapoints, results in relatively large uncertainties. However, as the variability (demonstrated by the bounds of the 25th and 75th percentiles in Fig. 9.6) remain consistent between each AMO phase, this is an indication that mean increase in nutrients, although subtle, are

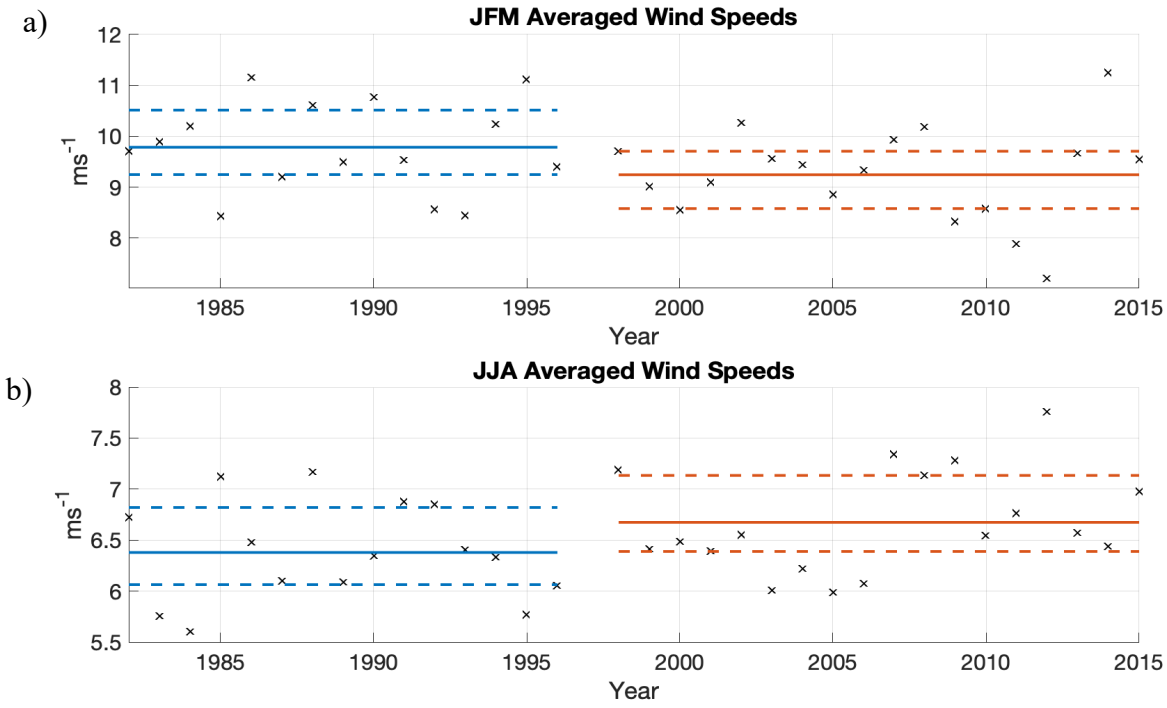

Fig. 9.8: The averaged 10m wind speeds (ms^{-1}) in winter (January to March) and summer (June to August) from 1982 to 2015 are shown by the black crosses. The negative (blue) and positive (red) phases of the AMO have been labelled, including the mean (solid) and 25th and 75th percentiles (dashed lines)

representative of the complex physical-biogeochemical interactions that occur within the model.

Now we step through some possible drivers of the observed nutrient change between AMO phases. Modelled benthic fluxes from the sediments are relatively consistent throughout both AMO phases (Fig 9.7), so this is an unlikely source. Ruiz-Castillo (2019a) demonstrated that only 10% of nutrients at the CCS site are riverine in origin, with riverine influence during the winter months being limited. Cross-shelf fluxes provide the most robust explanation for the observed nutrient increase, as previous research has already demonstrated that high-nutrient oceanic water can fuel productivity on shelf (e.g. Brion et al, 2004; Townsend et al, 2010). Enhanced mixing at the shelf break combined with wind-driven surface flow was shown to promote a steady exchange of oceanic-shelf waters (e.g. Huthnance et al, 2009, Simpson and Sharples, 2012), that was further supported by modelling studies (e.g. Holt et al, 2012). During the winter, lower nutrient concentrations on shelf would promote a nutrient gradient that would promote cross-shelf flux of nutrient-rich water onto the shelf (Hydes et al, 2004). However, Ruiz-Castillo (2019a, 2019b) demonstrated that the winter nutrient concentrations

are set during the summer months and are recirculated back on shelf during the winter. As both benthic fluxes and riverine outflow are unlikely to be the dominant source of the observed nutrient increase at this location, increasing cross-shelf flux of high-nutrient oceanic water appears to be the most suitable hypothesis for the observed nutrient changes in the model.

Whether the winter nutrient concentrations are set in winter (Hydes et al, 2004) or summer (Ruiz-Castillo et al, 2019a), any cross-shelf flux of nutrients could be enhanced by changing meteorological conditions between contrasting AMO phases, provided there is cross-shelf gradient in nutrients. Cross-shelf flux is dependent on wind speeds, with a stronger propagation of nutrients (via the slope current) during periods of higher wind stress (Hydes et al, 2004). Average winter windspeeds during winter (Fig 9.8) indicated a subtle decrease from 9.8 ms^{-1} to 9.2 ms^{-1} from negative to positive AMO periods. As such, the small decrease in winter wind speeds in positive AMO periods could have reduced the northward propagation of high-nutrient water and promoted a weak on-shelf flux. In summer, there was a small increase ($\pm$90% confidence interval) in average wind speeds of 0.3$\pm$0.3 ms^{-1} from negative to positive AMO phases (Fig 9.8). Assuming winter nutrient concentrations are set during summer (Ruiz-Castillo et al, 2019a), the increase in nutrient concentrations seen in the model could be a result of an increased Ekman transport of surface oceanic water off shelf, with a weak compensating on-shore flow in the bottom mixed layer (as outlined in Ruiz-Castillo et al, 2019a). This is reinforced by the JJA windspeed for 2012, which at 7.7 ms^{-1} was the largest value from 1982 to 2015 (Fig 9.8), and could have resulted in the exceptionally high nutrient concentrations recorded in winter 2013 (where N = $6.9x10^4$ mmol m^{-2}; Si = $2.4x10^4$ mmol m^{-2} and P = 4554 mmol m^{-2}). This could suggest that the high windspeeds during the summer of 2012 drove an enhanced cross-shelf flux, as described by Ruiz-Castillo et al (2019a), that resulted in increased nutrient concentrations the following winter.

Whether the increased nutrients seen in positive AMO phases are a consequence of an enhanced cross-shelf flux, either in winter and/or summer, remains uncertain. Due to the complicated bathymetry of the Celtic Sea, the relatively course 7km resolution of the model domain results in a slope current that is not well represented in this region (see Chapter 2 and Appendix 2). Cross-shelf transport mechanisms, such as from a propagating internal tide (Huthnance, 1995; Sharples et al, 2009; Ruiz-Castillo et al, 2019a) or high-salinity lenses (Hopkins et al, 2012), will not be captured by the model (Huthnance, 1995; Holt et al, 2012).

As such, while cross-shelf flux is a likely explanation for the increase in nutrients during positive AMO periods, we cannot confidently conclude any quantitative variations in cross-shelf flux between climatological phases.

9.4. Implications of enhanced cross-shelf nutrient flux

Although the cross-shelf flux has not been quantified in this thesis, an enhanced cross-shelf flux will still have profound implications for the ecological functioning in the Celtic Sea. These implications are discussed below.

9.4.1 Seasonal phytoplankton succession

In the winter, light is the primary limiting factor for phytoplankton growth and carbon fixation (Riley, 1957; Sverdrup, 1953; Smetacek and Passow, 1990; Siegal et al, 2002). As such, the increase in nutrients between AMO periods is not likely to influence winter phytoplankton growth that occurs before the onset of seasonal stratification (which are defined as the prebloom periods in Chapter 5.3.2). However, phytoplankton groups that have specific nutrient requirements will benefit from elevated nutrient concentrations. In the model, diatoms are the only phytoplankton group to utilise silicate (Butenshön et al, 2016) and so a combination of favourable light conditions and elevated nutrients, particularly silicate concentrations, could explain the observed increase in diatoms populations from negative to positive AMO phases (see Chapter 5.3.2).

During the spring bloom and towards summer, light limitation is overtaken by low nutrient concentrations to become the primary limiting factor for phytoplankton growth (Pingree et al, 1976). At this stage of the seasonal cycle, the relative concentrations of nutrients could directly influence phytoplankton succession (Holligan, 1984; Kivi et al, 1993; Gilbert et al, 2016). Species that utilise forms of new nitrogen (high f-ratio) would be well adapted for these elevated nitrate concentrations (Rees et al, 1999; Needham and Fuhrman, 2016). Increased nutrients stocks would support growth for these species for longer, before they were outcompeted by low f-ratio phytoplankton populations that utilised regenerated forms of nitrogen (Holligan, 1984; Sellner et al, 2001; Hickman et al, 2009; Gilbert, 2016).

9.4.2 Primary productivity

Relative concentrations of nutrients can directly influence the net community production (NCP). Previous modelling studies have already demonstrated that Celtic Sea primary production increased by 5-10% due to a maximum of 15% increase in dissolved inorganic nitrogen (Holt et al, 2012). A one-dimensional box model of the open ocean showed that nitrate delivery from rivers had no effect on productivity, yet elevated phosphate delivery increased productivity (Tyrrell, 1999), thus eluding to a phosphate-limited regime. In comparison, summer shelf sea regions are primarily nitrate limited (Kivi et al, 1993), with surface nutrient concentrations in the Celtic Sea displaying 98%, 85% and 75% reduction for nitrate, silicate and phosphate respectively (Pingree et al, 1976). Phytoplankton utilise different nutrients for different metabolic functions (Arrigo 2005): nitrate is used to sustain cells (the "survivalist" regime), while phosphate is needed for growth (the "bloomer" regime). As such, a combined increase in both nitrate and phosphate would lead to increased phytoplankton growth and longevity.

As phytoplankton in a summer shelf sea are primarily nutrient limited, they congregate at the base of pycnocline in a subsurface chlorophyll maximum (SCM; Pingree et al, 1982; Hickman et al, 2009; Hickman et al, 2012). In the Celtic Sea, the SCM can reach depths of 70m (Giering et al, 2018), and thus could result in a light limiting environment through phytoplankton self-shading (Huisman et al, 2004; Ross and Sharples, 2007; Ross and Sharples, 2008), the periodic deepening of the pycnocline due to spring-neap cycles (Sharples et al, 2007), or local variations in cloud cover (Hickman et al, 2012). This could mean more instances of light limitation, particularly during periods of high cloud cover (e.g. Hickman et al, 2012). Increased nutrients during positive AMO phases could therefore delay the development of the SCM, thus providing a stable, favourable light environment for phytoplankton growth and enhancing carbon fixation. The Celtic Sea has already been shown to be a net carbon sink (Frankignoulle and Borges, 2001), with the global contribution of shelf seas to anthropogenic carbon uptake amounting to 20% (Thomas et al, 2004).

9.5 Conclusions and key findings

Building upon previous chapters in this thesis, analysis of modelled winter nutrients concentrations in the Celtic Sea demonstrated a subtle increase in nitrate, phosphate and silicate concentrations between negative (1982 to 1996) and positive (1998 to 2015) AMO phases. Model validation against samples collected from 2014 and 2015 indicated variable stoichiometry, with winter N:P ratios adequately capturing observations. Winter stoichiometry for modelled N:Si ratios are higher than observed, though remain stable.

While the influence of enhanced nutrients during the winter will likely be small, as light is the primary limiter for phytoplankton growth, higher nutrient concentrations at the initiation of the spring bloom could determine the succession of the spring bloom community species. Phytoplankton adapted to a high f-ratio will benefit most from increased new nitrate supply with the transition to smaller, low f-ratio species consequently being delayed. Elevated silicate concentrations may result in increased diatom populations, while increased phosphate could lead to enhanced growth for all phytoplankton groups. Incorporating all the responses of such nutrient utilisations results in enhanced carbon fixation.

Positive AMO periods can be analogous for future ocean warming scenarios. As such, it can be inferred from this study that with future warming, nutrient concentrations on shelf may increase. However, a full quantitative assessment of the origin of these nutrients is yet to be completed. While it is hypothesised that positive AMO periods promoted enhanced cross-shelf nutrient flux, the fact that the slope current is poorly parameterised in the model for the Celtic Sea means that a full quantitative assessment would be inconclusive. Future work will aim to fully investigate the origin of this increased nutrients, and to fully quantify the cross-shelf nutrient flux in contrasting climatological phases.

9.6 References

Arrigo, K.R., 2005. Marine microorganisms and global nutrient cycles. *Nature*, *437*(7057), pp.349-355.

Bernard, C.Y., Dürr, H.H., Heinze, C., Segschneider, J. and Maier-Reimer, E., 2011. Contribution of riverine nutrients to the silicon biogeochemistry of the global ocean–a model study. *Biogeosciences*, *8*(3), pp.551-564.

Brion, N., Baeyens, W., De Galan, S., Elskens, M. and Laane, R.W., 2004. The North Sea: source or sink for nitrogen and phosphorus to the Atlantic Ocean?. *Biogeochemistry*, *68*(3), pp.277-296.

Davis, C.E., Mahaffey, C., Wolff, G.A. and Sharples, J., 2014. A storm in a shelf sea: Variation in phosphorus distribution and organic matter stoichiometry. *Geophysical Research Letters*, *41*(23), pp.8452-8459.

Dugdale, R.C. and Goering, J.J., 1967. Uptake of new and regenerated forms of nitrogen in primary productivity 1. *Limnology and oceanography*, *12*(2), pp.196-206.

Eppley, R.W. and Peterson, B.J., 1979. Particulate organic matter flux and planktonic new production in the deep ocean. *Nature*, *282*(5740), p.677.

Eppley, R.W., 1981. Relations between nutrient assimilation and growth in phytoplankton with a brief review of estimates of growth rate in the ocean. *Canadian bulletin of fisheries and aquatic sciences*.

Fernand, L., Nolan, G.D., Raine, R., Chambers, C.E., Dye, S.R., White, M. and Brown, J., 2006. The Irish coastal current: A seasonal jet-like circulation. *Continental Shelf Research*, *26*(15), pp.1775-1793.

Frankignoulle, M. and Borges, A.V., 2001. European continental shelf as a significant sink for atmospheric carbon dioxide. *Global biogeochemical cycles*, *15*(3), pp.569-576.

Giering, S.L., Wells, S.R., Mayers, K.M., Schuster, H., Cornwell, L., Fileman, E.S., Atkinson, A., Cook, K.B., Preece, C. and Mayor, D.J., 2019. Seasonal variation of zooplankton community structure and trophic position in the Celtic Sea: a stable isotope and biovolume spectrum approach. *Progress in Oceanography*, *177*, p.101943.

Glibert, P.M., 2016. Margalef revisited: a new phytoplankton mandala incorporating twelve dimensions, including nutritional physiology. *Harmful Algae*, *55*, pp.25-30.

Gohin, F., Bryère, P. and Griffiths, J.W., 2015. The exceptional surface turbidity of the North-West European shelf seas during the stormy 2013–2014 winter: Consequences for the initiation of the phytoplankton blooms?. *Journal of Marine Systems*, *148*, pp.70-85.

Harrison, W.G., Platt, T. and Lewis, M.R., 1987. f-Ratio and its relationship to ambient nitrate concentration in coastal waters. *Journal of Plankton Research*, *9*(1), pp.235-248.

Hickman, A.E., Holligan, P.M., Moore, C.M., Sharples, J., Krivtsov, V. and Palmer, M.R., 2009. Distribution and chromatic adaptation of phytoplankton within a shelf sea thermocline. *Limnology and Oceanography*, *54*(2), pp.525-536.

Hickman, A.E., Moore, C.M., Sharples, J., Lucas, M.I., Tilstone, G.H., Krivtsov, V. and Holligan, P.M., 2012. Primary production and nitrate uptake within the seasonal thermocline of a stratified shelf sea. *Marine Ecology Progress Series*, *463*, pp.39-57.

Holligan, P.M., leB. Williams, P.J., Purdie, D. and Harris, R.P., 1984. Photosynthesis, respiration and nitrogen supply of plankton populations in stratified, frontal and tidally mixed shelf waters. *Marine Ecology Progress Series*, pp.201-213.

Holt, J., Wakelin, S., Lowe, J. and Tinker, J., 2010. The potential impacts of climate change on the hydrography of the northwest European continental shelf. *Progress in Oceanography*, *86*(3-4), pp.361-379.

Holt, J.T., Butenschon, M., Wakelin, S.L., Artioli, Y. and Allen, J.I., 2012. Oceanic controls on the primary production of the northwest European continental shelf: model experiments under recent past conditions and a potential future scenario. *Biogeosciences*, *9*, pp.97-117.

Hopkins, J., Sharples, J. and Huthnance, J.M., 2012. On-shelf transport of slope water lenses within the seasonal pycnocline. *Geophysical Research Letters*, *39*(8).

Humphreys, M.P., Achterberg, E.P., Hopkins, J.E., Chowdhury, M.Z., Griffiths, A.M., Hartman, S.E., Hull, T., Smilenova, A., Wihsgott, J.U., Woodward, E.M.S. and Moore, C.M., 2019. Mechanisms for a nutrient-conserving carbon pump in a seasonally stratified, temperate continental shelf sea. *Progress in Oceanography*, *177*, p.101961.

Huthnance, J.M., 1995. Circulation, exchange and water masses at the ocean margin: the role of physical processes at the shelf edge. *Progress in Oceanography*, *35*(4), pp.353-431.

Huthnance, J.M., Holt, J.T. and Wakelin, S.L., 2009. Deep ocean exchange with west-European shelf seas. *Ocean Science*, *5*(4), pp.621-634.

Hydes, D.J., Gowen, R.J., Holliday, N.P., Shammon, T. and Mills, D., 2004. External and internal control of winter concentrations of nutrients (N, P and Si) in north-west European shelf seas. *Estuarine, Coastal and Shelf Science*, *59*(1), pp.151-161.

Kivi, K., Kaitala, S., Kuosa, H., Kuparinen, J., Leskinen, E., Lignell, R., Marcussen, B. and Tamminen, T., 1993. Nutrient limitation and grazing control of the Baltic plankton community during annual succession. *Limnology and Oceanography*, *38*(5), pp.893-905.

Labry, C., Herbland, A., Delmas, D., Laborde, P., Lazure, P., Froidefond, J.M., Jegou, A.M. and Sautour, B., 2001. Initiation of winter phytoplankton blooms within the Gironde plume waters in the Bay of Biscay. *Marine Ecology Progress Series*, *212*, pp.117-130.

McQuatters-Gollop, A., Raitsos, D.E., Edwards, M. and Attrill, M.J., 2007. Spatial patterns of diatom and dinoflagellate seasonal cycles in the NE Atlantic Ocean. *Marine Ecology Progress Series*, *339*, pp.301-306.

Needham, D.M. and Fuhrman, J.A., 2016. Pronounced daily succession of phytoplankton, archaea and bacteria following a spring bloom. *Nature microbiology*, *1*(4), p.16005.

Pauly, D., Christensen, V., Guénette, S., Pitcher, T.J., Sumaila, U.R., Walters, C.J., Watson, R. and Zeller, D., 2002. Towards sustainability in world fisheries. *Nature*, *418*(6898), p.689.

Pingree, R.D., Holligan, P.M., Mardell, G.T. and Head, R.N., 1976. The influence of physical stability on spring, summer and autumn phytoplankton blooms in the Celtic Sea. *Journal of the Marine Biological Association of the United Kingdom*, *56*(4), pp.845-873.

Pingree, R.D., Mardell, G.T., Holligan, P.M., Griffiths, D.K. and Smithers, J., 1982. Celtic Sea and Armorican current structure and the vertical distributions of temperature and chlorophyll. *Continental Shelf Research*, *1*(1), pp.99-116.

Platt, T., Fuentes-Yaco, C. and Frank, K.T., 2003. Marine ecology: spring algal bloom and larval fish survival. *Nature*, *423*(6938), p.398.

Rees, A.P., Joint, I. and Donald, K.M., 1999. Early spring bloom phytoplankton-nutrient dynamics at the Celtic Sea Shelf Edge. *Deep Sea Research Part I: Oceanographic Research Papers*, *46*(3), pp.483-510.

Riley, G.A., 1957. Phytoplankton of the North Central Sargasso Sea, 1950–52 1. *Limnology and Oceanography*, *2*(3), pp.252-270.

Ross, O.N. and Sharples, J., 2007. Phytoplankton motility and the competition for nutrients in the thermocline. *Marine Ecology Progress Series*, *347*, pp.21-38.

Ross, O.N. and Sharples, J., 2008. Swimming for survival: a role of phytoplankton motility in a stratified turbulent environment. *Journal of Marine Systems*, *70*(3-4), pp.248-262

Ruiz Castillo, E., 2019b. *Cross-shelf transport and exchange between a temperate shelf sea and the North Atlantic Ocean* (Doctoral dissertation, University of Liverpool).

Ruiz-Castillo, E., Sharples, J., Hopkins, J. and Woodward, M., 2019a. Seasonality in the cross-shelf physical structure of a temperate shelf sea and the implications for nitrate supply. *Progress in Oceanography*, *177*, p.101985.

Sellner, K.G., Sellner, S.G., Lacouture, R.V. and Magnien, R.E., 2001. Excessive nutrients select for dinoflagellates in the stratified Patapsco River estuary: Margalef reigns. *Marine Ecology Progress Series*, *220*, pp.93-102.

Sharples, J., 2007. Potential impacts of the spring-neap tidal cycle on shelf sea primary production. *Journal of Plankton Research*, *30*(2), pp.183-197.

Sharples, J., Moore, C.M., Hickman, A.E., Holligan, P.M., Tweddle, J.F., Palmer, M.R. and Simpson, J.H., 2009. Internal tidal mixing as a control on continental margin ecosystems. *Geophysical Research Letters*, *36*(23).

Sharples, J., Ross, O.N., Scott, B.E., Greenstreet, S.P. and Fraser, H., 2006. Inter-annual variability in the timing of stratification and the spring bloom in the North-western North Sea. *Continental Shelf Research*, *26*(6), pp.733-751.

Simpson, J.H. and Sharples, J., 2012. *Introduction to the physical and biological oceanography of shelf seas*. Cambridge University Press.

Smetacek, V. and Passow, U., 1990. Spring bloom initiation and Sverdrup's critical-depth model. *Limnology and oceanography*, *35*(1), pp.228-234.

Sverdrup, H.U., 1953. On conditions for the vernal blooming of phytoplankton. *J. Cons. Int. Explor. Mer*, *18*(3), pp.287-295.

Taylor, J.R. and Ferrari, R., 2011. Shutdown of turbulent convection as a new criterion for the onset of spring phytoplankton blooms. *Limnology and Oceanography*, *56*(6), pp.2293-2307.

Thomas, H., Bozec, Y., Elkalay, K. and De Baar, H.J., 2004. Enhanced open ocean storage of CO2 from shelf sea pumping. *Science*, *304*(5673), pp.1005-1008.

Townsend, D.W., Cammen, L.M., Holligan, P.M., Campbell, D.E. and Pettigrew, N.R., 1994. Causes and consequences of variability in the timing of spring phytoplankton blooms. *Deep Sea Research Part I: Oceanographic Research Papers*, *41*(5-6), pp.747-765.

Townsend, D.W., Keller, M.D., Sieracki, M.E. and Ackleson, S.G., 1992. Spring phytoplankton blooms in the absence of vertical water column stratification. *Nature*, *360*(6399), p.59.

Townsend, D.W., Rebuck, N.D., Thomas, M.A., Karp-Boss, L. and Gettings, R.M., 2010. A changing nutrient regime in the Gulf of Maine. *Continental Shelf Research*, *30*(7), pp.820-832.

Tyrrell, T., 1999. The relative influences of nitrogen and phosphorus on oceanic primary production. *Nature*, *400*(6744), p.525.

Waniek, J.J., 2003. The role of physical forcing in initiation of spring blooms in the northeast Atlantic. *Journal of Marine Systems*, *39*(1-2), pp.57-82.

Williams, C., Sharples, J., Mahaffey, C. and Rippeth, T., 2013. Wind-driven nutrient pulses to the subsurface chlorophyll maximum in seasonally stratified shelf seas. *Geophysical Research Letters*, *40*(20), pp.5467-5472